**UNIVERSIDADE DE BRASÍLIA**
**INSTITUTO DE GEOCIÊNCIAS**

**DISSERTAÇÃO DE MESTRADO**

**N° 235**

# "ESTUDO PETROGRÁFICO E GEOQUÍMICO DAS ROCHAS VULCÂNICAS AFLORANTES NO EMBASAMENTO (PROTEROZÓICO SUPERIOR-PALEOZÓICO INFERIOR) DA CORDILHEIRA ORIENTAL, NOROESTE ARGENTINO."

**Autora:**
**NATALIA HAUSER**

**Orientador:**
**Prof. Dr. Márcio Martins Pimentel**

**BRASILIA-DF**
**DEZEMBRO DE 2007**

**UNIVERSIDADE DE BRASÍLIA**
**INSTITUTO DE GEOCIÊNCIAS**

**DISSERTAÇÃO DE MESTRADO**

**N° 235**

# "ESTUDO PETROGRÁFICO E GEOQUÍMICO DAS ROCHAS VULCÂNICAS AFLORANTES NO EMBASAMENTO (PROTEROZÓICO SUPERIOR-PALEOZÓICO INFERIOR) DA CORDILHEIRA ORIENTAL, NOROESTE ARGENTINO."

**Autora:**
**NATALIA HAUSER**

**Orientador:**
**Prof. Dr. Márcio Martins Pimentel**

**BANCA EXAMINADORA:**
**Orientador: Prof. Dr. Márcio M. Pimentel (UnB/IG)**
**Examinador Interno: Prof. Dr. Affonso Brod (UnB)**
**Examinador Externo: Prof. Dr. Sérgio Castro Valente (UFRJ)**

**BRASILIA-DF**
**DEZEMBRO DE 2007**

*Toda porção de verdade deve encaixar em qualquer outra porção, porque todas elas formam parte do todo.*

*Atkinson Thomas Willian*

*Quando se sabe uma coisa, sustentar que se sabe; e, quando não se sabe, admitir que não sabe. Este é o verdadeiro conhecimento.*

*Confucio*

# Índice ..... **i**

**Lista de Figuras** ..... iv

**Lista de Tabelas** ..... ix

**Agradecimentos** ..... xi

**Resumo** ..... xiii
**Abstract** ..... xv

**CAPÍTULO I** ..... 1

**1.1.** Introdução ..... 1

**1.2.** Objetivos ..... 2

**1.3.** Localização e vias de acesso ..... 3

**1.4.** Marco geológico regional do noroeste Argentino ..... 4

Altiplano-Puna ..... 4

Cordilheira Oriental ..... 7

**1.5.** Metodologia geral do trabalho ..... 8

Etapa de Campo
Estudo da petrografia das rochas vulcânicas
Análises químicas de minerais-Microsonda Eletrônica
Preparação das amostras para análises químicas de rochas e análises isotópicas Sr-Nd
Seaparação de minerais
Montagem dos grãos de zircão
Anánlises químicas de rochas
Difratometría de raios-x
Geoquímica isotópica Sr-Nd
Geocronologia U-Pb, K-Ar
Confecção da disseração de mestrado e dos artigos

**1.6.** Escopo da dissertação ..... 11

**CAPÍTULO II** ..... 13

"K-Ar AGE AND Sr-Nd ISOTOPIC GEOCHEMISTRY OF ALKALINE LAMPROPHYRE DYKES, FROM THE RIO GRANDE VALLEY, EASTERN CORDILLERA, NW ARGENTINA: ORIGIN OF PARENTAL MAGMAS FROM A METASOMATIZED MANTLE"

*Abstract*
**1.** Introduction ..... 14

**2.** Geological Setting ..... 15

**2.1.** Local Geology ..... 18
*The Rio Grande Dykes and sill*

20

**3.** Petrography ..... 22

**3.1.** The Río Grande lamprophyres ..... 22
**3.2.** Globular structures ..... 24

**4.** Mineral Chemistry ..... 25

Olivine ..... 25
Clinopyroxene ..... 25
Amphibole ..... 30
Mica ..... 33
Apatite ..... 35
Analcime ..... 35
Carbonate ..... 36

**5.** Analitycal Procedures ..... 38

**6.** Geochemistry ..... 40

**7.** Geochronology ..... 43

**7.1.** K-Ar data ..... 43
**7.2.** Sr-Nd isotopic data ..... 44

**8.** Discussion and Conclusions ..... 46

*Acknowledgement*
References

**CAPÍTULO III** ..... 62

"LA-ICPMS U-PB GEOCHRONOLOGY AND PETROLOGY OF VOLCANIC ROCKS OF THE NEOPROTEROZOIC TO LOWER PALEOZOIC BASEMENT OF CENTRAL ANDES, NW ARGENTINA: INSIGHTS ON THE EVOLUTION OF WESTERN GONDWANA."

*Abstract*
**1.** Introduction ..... 64

**2.** Geological Setting ..... 65

**2.1.** Field Relationships ..... 67

**2.1.1.** El Niño Muerto Hill ..... 67

**2.2.2.** Río Blanco Valley ..... 69
*Sedimentary Sequence*
*Río Blanco volcanic rocks*
*Peperite deposits*

**3.** Petrography ..... 72

**3.1.** Subvolcanic rocks of the El Niño Muerto Hill ..... 72
**3.2.** Volcanic and subvolcanic rocks of the Río Blanco Valley ..... 73

**4.** Analitycal Procedures ..... 75

**5.** Geochemistry ..... 76

**5.1.** El Niño Muerto metadacites ..... 76
**5.2.** Río Blanco basalts ..... 77

**6.** Geochronology ..... 81

**6.1.** U-Pb data ..... 81

**6.1.1.** El Niño Muerto metadacites (sample BNM11) ..... 81
**6.1.2.** Río Blanco basalts (sample BRB43) ..... 84

**6.2.** Nd and Sr Isotopic Data ..... 87

**7.** Discussion and Conclusions ..... 89

**7.1.** El Niño Muerto metadacites ..... 89
**7.2.** Río Blanco basalts ..... 90
**7.3.** Age and tectonic evolution ..... 90

*Acknowledgements*
References

**CAPÍTULO IV** ..... 100

**4.1.** Conclusões ..... 100
*Setor Norte: Vale do Río Grande*
*Setor Central e Sul: Serra de El Niño Muerto e vale de Río Blanco*

References

ANEXOS
I ANALISES DE DIFRACTOMETRIA DE RAIOS-X
II. ANÁLISES DE MICROSONDA
III COORDENADAS DAS AMOSTRAS

**Lista de Figuras**

# CAPÍTULO I

**Introducção**

**Figura 1:** Mapa de localização e vias de acesso às áreas estudadas. 1, Vale de Rio Grande. 2, Serra de El Niño Muerto. 3, Vale de Rio Blanco.

**Figura 2:** localização e distribuição das províncias morfoestruturais no norte-centro de Argentina. (modificado de Pankhurst and Rapela, 1998).

**Figure 3:** afloramentos do embasamento Neoproterozoico-Paleozoico Inferior do noroeste de Argentina (modificado de Do Campo and Guevara, 2005 and Viramonte et al., 2007).

# CAPÍTULO II

**Paper 1:** "K-Ar AGE AND Sr-Nd ISOTOPIC GEOCHEMISTRY OF ALKALINE LAMPROPHYRE DYKES, FROM THE RIO GRANDE VALLEY, EASTERN CORDILLERA, NW ARGENTINA: ORIGIN OF PARENTAL MAGMAS FROM A METASOMATIZED MANTLE"

## *1*. Introduction

**Figure 1** Paleostructural sketch-map of the Jurassic-Cretaceous Rift of NW Argentina. The location of pre-rift plutonic rocks and the study area are shown. Modified from Salfity and Marquillas, (1981) and Viramonte et al., (1999).

## *2*. Local Geology

**Figure 2:** typical field features of the Río Grande dykes and sills. A) Typical aspect of the Río Grande dykes. They display chilled margin (Ch mg) and the host rocks appear blanked. B) Flow differentiation of mica, amphibole and xenoliths. C) Example of subvolcanic rocks from the Yacoraite Valley. They are partially concordant with the Puncoviscana Formation. D) Zoned internal structures by multiple intrusions. The $dyk_2$ occur inside the $dyk_1$, and the chilled margin (Ch mg) in the border of $dyk_2$, indicate that this was generated in a second time. E) Concordant dykes with thermometamorphic pelite (Pl) inside, from the Coraya locality. The scale has 25 cm.

## *3*. Petrography

**Figure 3:** Photomicrographs of several features exhibited by the Río Grande subvolcanic rocks. A) Euhedral and strongly zoned clinopyroxene crystals (Cpx) and minor amounts of euhedral olivine crystals (Ol). Note the high crystals/groundmass proportions. B) Euhedral olivine phenocrysts in a groundmass. These commonly show unstable features as embayment. The groundmass is composed by abundant clinopyroxene and biotite crystals.

In this photomicrograph is observed also the Type-III ocelli, completely formed by carbonate. C) Abundant zoned amphibole (Amp)/biotite (Bt) phenocrysts and apatite (Ap) as microphenocrysts characterized the dyke of sample p8. D) The two commonly amphibole types presented. Note the high carbonate and mica concentrations in the groundmass. E) Hornblendite-xenolith with slight mosaic texture. F) Carbonatite-like xenolith. G) Phenocrysts of diopside (Cpx) with inclusion of olivine crystals (Ol). H) Phenocrystal of augite enclosing poikilitically apatite (Ap) crystals. I) Characteristics of ***Type-I ocelli***, concentric zones of carbonate surrounded by radial diopside crystals. J) The ***Type-II ocelli*** and segregations. This ocelli type is marked by analcime forming the central pool surrounded by carbonate. The segregations are characterized by high concentrations of biotite microphenocrysts (Seg-bt) or by high concentrations of carbonate (Seg-Cb).

## 4. Mineral chemistry

**Figure 4:** Representative pyroxene and olivine compositions of the Río Grande subvolcanic rocks. Wollastonite (Wo)-Enstatite (En)-Ferrosilite (Fs) classification diagram after Morimoto et al., (1988). They are calcic clinopyroxene, almost all of them fall in the field of Fe-diopside but samples P8 and BYA 124a also fall in the Mg-augite field.

**Figure 5:** $Al_2O_3$/ mg# vs. $TiO_2$ diagram showing the compositions of clinopyroxene crystals. In this diagram are observed two groups of clinopyroxens, differentiated for the $TiO_2$ contents.

**Figure 6:** Classification diagram for amphiboles after Leake et al., 1997. All crystals are plotted in the calcic amphiboles field and are classified as Titanian-Pargasite.

**Figure 7:** $Al_2O_3$/mg# vs. $TiO_2$ diagram shows the lower $TiO_2$ compositions for some green cores and xenoliths crystals. Observed that the rims of crystals with green cores have similar compositions with the brown amphiboles.

**Figure 8:** Classification diagram for mica compositions after Rieder et al., 1998. Note the core-rim trend followed by singular grains.

**Figure 9:** A) $Al_2O_3$ vs. $TiO_2$ diagram and B) BaO vs. $TiO_2$ diagram for micas. The mica from ocelli (sample BHU131) and cores of phenocrysts are richer in $TiO_2$ (~7.5 wt. %) and BaO (~ 2 wt. %) compared with the rest.

**Figure 10:** Carbonate compositions of Río Grande lamprophyres. A) Ca-Mg-Fe system (moles %). All types of carbonate are dolomite in composition except for the carbonate segregations that is breunnerite. B) BaCO-$Sr_2CO2$ covariation (wt. %) diagram. Note that xenoliths carbonate have the highest contents in SrO wt. %.

## 6. Geochemistry

**Figure 11:** Rock classification diagram using Zr, Ti, Nb and Y immobile elements (Winchester and Floyd, 1977) for the Río Grande rocks.

**Figure 12:** A) Chondrite normalized abundance spidergrams (Thompson 1982) and B) REE normalized diagram after Nakamura 1974, for the Rio Grande rocks. For comparison monchiquite-alkaline lamprophyres after Rock (1991) and average ocean island basalt (OIB) after Sun and McDonough (1989) are shown.

## 8. Discussions and Conclusions

**Figure 13:** A) Discriminate diagram showing compositional field on pyroxene crystals to the different lamprophyres branches. The Rio Grande pyroxen crystals are plotted in the limit between Al/CAL-UML fields. B) Al2O3/TiO2 vs. CaO/Na2O discriminate diagram for amphibole compositions, after Rock, 1987, 1991. The

Rio Grande amphibole crystals are plotted in the UML-AL/CAL limits fields. **CAL:** calc-alkaline lamprophyres, **AL:** alkaline lamprophyres, **UML:** ultramafic lamprophyres and **LL:** lamproites.

**Figure 14:** Trace elements pattern of pré-rift stage and syn-rift stage rocks of Salta Rift. The Rio Grande lamprophyres and Tusaquillas plutonic complex belong to pre-rift stage. Note the high concentrations in LILE and HFSE of the Rio Grande lamprophyrescompared with the Tusaquillas complex. The syn rift volcanic rocks selected are Las Conchas, El Cadillal, Finca El Rodeo and Matancillas basanites. Date of Tusaquillas complex, from Cristiani et al., 2004. Data of Syn-Rift volcanic rocks from Lucassen et al., 2007. Normalized values from Thompson, 1982.

**Figure 15:** $^{87}Sr/^{86}Sr$ vs. $^{143}Nd/^{144}Nd$ diagram for the Río Grande lamprophyres. The isotopic compositions of xenoliths and mantle-derived rocks from the Central Andes are also shown. The data are recalculated to 160 Ma (Lucassen et al., 2005).

**Figure 16:** Ce/Yb vs. Ce diagram for the Rio Grande lamprophyres. Melting curves for amphibolite lherzolite of sample BD3438A from a metasomatised mantle of Pello Hill, Tanzania. Degree of partial melting (%) is indicated along the melting lines.

# CAPÍTULO III

**Paper II:** "LA-ICPMS U-PB GEOCHRONOLOGY AND PETROLOGY OF VOLCANIC ROCKS OF THE NEOPROTEROZOIC TO LOWER PALEOZOIC BASEMENT OF CENTRAL ANDES, NW ARGENTINA: INSIGHTS ON THE EVOLUTION OF WESTERN GONDWANA."

## 1. Introduction

**Figure. 1:** Geological map showing the distribution of Neoproterozoic to lower Paleozoic basement rock units of NW Argentina (modified after Do Campo and Guevara, 2005 and Viramonte et al., 2007).

## 2. Local Geology

**Figure 2:** A) Panoramic view of the El Niño Muerto sill (Dc) north sector. The dacites are intruded in the turbidite sequence (Tb) of the Puncoviscana Formatio. B) The contact, is marked by thermometamorphosed and bleached pelites (Pl) indicating the intrusive character. Note that sediment and dacite are intensely foliated. C) View of sill outcrop with prominent foliation. D) Aspect of dacites in fresh cut. They are characterized by porphiritic textures with plagioclase phenocrysts embedded in a gray groundmass of biotite, quartz and plagioclase crystals and abundant pelite enclaves (En). The scale has 25 centimeters long.

**Figure 3:** Contact between pillow lavas (Pw), red pelites (Pl) and the turbidite sequence (Tb) of the Neoproterozoic to Lower Paleozoic basement in the Rio Blanco Valley.

**Figure 4:** A) Panoramic view of the Rio Blanco volcanic rocks. They are intruded in a hemipelagitic? sequence made of red pelite (Pl) and limestone (Lm), that are enclosed by the turbidite sequence (Tb). B) Detail of pillow-like lava (Pw) intruded in yellowish pink limestone (Lm). Note the chilled margin and connection among the individual pillows. C) Aspect of the banded lava flow with abundant lensoidal limestone clasts. D) View of globular peperite deposit formed in the contact between lava flow and red pelite (Pl). The scale is 25 centimeters long.

## 3. Petrography

**Figure 5:** Photomicrographs of representative textures of the El Niño Muerto metadacites. A) Porphyritic metadacite with plagioclase, quartz and K-feldspar phenocrysts. The matrix is made of alternating quartz-rich and biotite-rich bands. B) Plagioclase crystal. The fractures perpendicular to the main stress are filled with mica. C) Quartz crystal showing embayment and D) plagioclase crystals showing pressure shadows. *Abbreviations*: Pl, plagioclase; Qtz, quartz; Kfs, feldspar; Ep, epidote.

**Figure 6:** Photomicrographs of the Rio Blanco volcanic rocks. A) A plagioclase laths with intergranular opaque oxides is the most common textural variety of these basaltic rocks B) A less common textural variety is characterized by plagioclase phenocrysts (up to 2 mm) partially altered to epidote. C) Example of porphyritic intergranular texture. Albite phenocrysts are set in a groundmass composed totally by microcrystals of the same composition. D) Carbonate- and hematite-filled vesicles. *Abbreviations*: Pl, plagioclase; Ep, epidote; Vs, vesicles.

## 4. Geochemistry

**Figure 7:** A) Chemical compositions of the El Niño Muerto subvolcanic rocks in the Total alkalis versus Silica diagram (Le Maitre et al., 1989) and in the Peccerilo and Taylor (1976) diagram for subalkaline rocks. B) The $Al_2O_3$/ (CaO + $Na_2O$ + $K_2O$) vs. $Al_2O_3$/($Na_2O$ + $K_2O$) diagram (Shand, 1929) shows the peraluminous nature of the original magmas. C) Spidergrams of Primordial Mantle-normalized trace elements distributions (Wood et al., 1979) for the El Niño Muerto dacites and sample PCS3 of "Faja Eruptiva de la Puna Oriental" (Viramonte et al., 2007). D) Chondrite-normalized diagram for representative samples of the El Niño Muerto metadacites. The normalizing factors are from Sun and McDonough (1989).

**Figure 8:** Rock classification diagram using Zr, Ti, Nb and Y immobile elements (Winchester and Floyd, 1977) for the Rio Blanco volcanic rocks.

**Figure 9:** A) Spidergrams of Primordial Mantle-normalized trace elements distributions (Wood et al., 1979) for the Rio Blanco rocks. B) Chondrite-normalized REE abundance diagram for representative samples of the Rio Blanco basalts. The normalizing factors are from Sun and McDonough (1989). E-MORB (average Pacific E-MORB from GEOROC) and OIB (Sun and McDonough 1989) are plotted for comparison.

## 5. Geochronology

**Figure 10** Zircon U-Pb data for the El Nino Muerto Hill. A) LA-ICPMS Concórdia Age. B) ID-TIMS.

**Figure 11:** LA ICPMS Zircon U-Pb data for the Rio Blanco basalt

**Figure 12:** $\varepsilon_{Nd}$ versus age diagram for the El Niño Muerto metadacites. The Nd isotopic compositions of these rocks are similar to the felsic metavolcanic samples of Faja Eruptiva Oriental and the metamorphic and granitoids rocks of the basement of Puna.

## 6. Discussion and Conclusions

**Figure 13*:*** Tectonic discriminant diagrams for the Rio Blanco basalts. A) Triangular discriminate Th-Hf/3-Ta diagram after Wood 1980. Abbreviations: N-MORB= normal mid-ocean ridge basalt, E-MORB and WPB= enriched mid-ocean ridge basalt and within plate basalt respectively, WPA= within plate alkali, VAB= volcanic arc basalt. B) Triangular discriminant diagram of Pearce and Cann (1973). Abbreviations: IAT= island-arc tholeiite, MORB= mid-ocean ridge basalt, CAB=calc-alkali basalt, WPB= within plate basalt. C) Triangular discriminant diagram of Meschede, 1986.

**Lista de Tabelas**

## CAPÍTULO II

**Paper I:** "K-Ar AGE AND Sr-Nd ISOTOPIC GEOCHEMISTRY OF ALKALINE LAMPROPHYRE DYKES, FROM THE RIO GRANDE VALLEY, EASTERN CORDILLERA, NW ARGENTINA: ORIGIN OF PARENTAL MAGMAS FROM A METASOMATIZED MANTLE"

## 3. Local Geology

**Table 1:** Summarized lithological and petrographic characteristics of the Rio Grande sills and dykes.

## 4. Mineral chemistry

**Table 2:** Representative electron microprobe analyses of olivine minerals from the Río Grande subvolcanic rocks.

**Table 3A:** Representative electron microprobe analyses of clinopyroxene minerals from samples BYA 123, 124, 127 and BHU 131 of the Río Grande subvolcanic rocks.

**Table 3B:** Representative electron microprobe analyses of clinopyroxene minerals from sample P8, Río Grande subvolcanic rocks.

**Table 4:** Representative electron microprobe analyses of amphibole minerals from the Río Grande subvolcanic rocks.

**Table 5:** Representative electron microprobe analyses of mica minerals from the Río Grande subvolcanic rocks.

**Table 6:** Representative electron microprobe analyses for apatite minerals from sample P8, Río Grande subvolcanic rocks.

**Table 7:** Representative electron microprobe analyses for analcime minerals from Río Grande subvolcanic rocks.

**Table 8:** Representative electron microprobe analyses for carbonate minerals from Río Grande subvolcanic rocks.

## 6. Geochemistry

**Table 9:** Representative major and trace elements analyses from the Rio Grande subvolcanic rocks.

## 7. Geochronology

### 7.1. K-Ar Data

**Table 10:** K-Ar biotite age data for the Rio Grande subvolcanic rocks.

### 7.2. Sr and Nd Isotopic Data

**Table 11:** Rb-Sr and Sm-Nd isotopic data for the Rio Grande subvolcanic rocks.

## CAPÍTULO III

**Paper II:** **"**LA-ICPMS U-PB GEOCHRONOLOGY AND PETROLOGY OF VOLCANIC ROCKS OF THE NEOPROTEROZOIC TO LOWER PALEOZOIC BASEMENT OF CENTRAL ANDES, NW ARGENTINA: INSIGHTS ON THE EVOLUTION OF WESTERN GONDWANA."

## 3. Analytical Procedures

**Table 1:** Operating data of LA-ICPMS

## 4. Geochemistry

**Table 2A:** Representative whole rock analyses of the El Niño Muerto Hill and Rio Blanco volcanic rocks.

**Table 2B:** Representative whole rock trace Elements and REE analyses of the El Niño Muerto Hill and Rio Blanco volcanic rocks.

## 6. Geochronology

### 6.1. U-Pb data

**Table 3:** LA-ICPMS U-Pb isotopic data from the El Niño Muerto metadacites.

**Table 4:** Summary of ID-TIMS U-Pb data from the El Niño Muerto metadacites

**Table 5:** LA -ICPMS U-Pb isotopic data from the Rio Blanco volcanic rocks.

### 6.2. Nd and Sr Isotopic data

**Table 6:** Sr-Nd isotopic data for volcanic rocks from the El Niño Muerto metadacites and Rio Blanco basalts.

**AGRADECIMENTOS**

**Ao Marcio, meu orientador**

Primeiramente eu quero agradecer profundamente ao meu orientador Marcio Martins Pimentel, ou Marcio.....por sua boa vontade de fazer que tudo seja possível, também o impossível !! ...muito obrigada per tudo Marcio de coração!!!.....obrigada por sua amizade, sinceridade e tranqüilidade sempre!... Por abrir as portas desta casa para min, por amostrar me a pesquisa desde um punto mais realístico e estimulante, por ajudar me sempre!

**Aos membros da banca**

Aos membros da banca, Dr. Affonso Broad, Dr. Sergio de Castro Valente e Dr. Marcio Martins Pimentel, muito obrigada pela sua assistência e pelas boas criticas que farão melhorar sem duvida o meu trabalho.

**Ao Instituto de Geociências**

Um agradecimento especial e para todo o Instituto, especialmente aos professores que de boa vontade me ajudaram quando precise, Nilson Francisquini Botelho, José Affonso Brod, Tete Junqueira, Reinhardt Fuck, Bernhard Buhn, Elton Dantas, Miguelito Basei, Sergio Valente, Edi Guimarães, Detlef Hans Gertwalde e Silvia de Araújo.

A todo o pessoal da secretaria do IG, especialmente a Francisca, Stella e Bubu, por tanta paciência e pela ajuda constante.

Ao pessoal dos laboratórios, pela ajuda que me brindaram, Francisca das Chagas Morais e Adalgisa de laminação, na preparação das lâminas. Ao Onesio da microsonda pela ajuda durante as análises.

**Ao pessoal do Laboratório de Geocronologia**

Ao pessoal do laboratório, Bárbara, Sandrine, Jorge Laux , Sergio Junges e Denilson pela ajuda com os dados isotópicos e a preparação das amostras...e agora também Giani. Ao Ravikant, obrigada!

**Aos Colegas do IG**

A minha amiga Ana Maria, Anita!!! por tantos momentos compartidos entre estudo, vida e incansáveis "charlas" entre capuccino e capuccino! Ao Reinaldo, muito obrigada!

A os colegas que se voltaram amigos e que conheci na universidade Elisa, Glorita, Osmar, Oscar, Carlos, Camila, Dhebora, Giana, Jô, Emilia, Christiano, Karin, Danielle, Carol....

**Ao pessoal da Universidad Nacional de Salta (UN.Sa)**

Ao prof. Ricardo Omarini da UNSa.....muito obrigada !.....pelo apoio nas campanas feitas na Argentina e as discussões mantidas.

Ao Negro Dominguez, Omar e ao Christian.....na valiosa ajuda durante a preparação das amostras entre mates e mates!!

**Aos colegas de Argentina**

..... aos amigos argentinos que conheci também aqui!! Caro, Silvy, Alfonso, Sonia.....a todos por tantos momentos compartidos entre geologia e amizade .....obrigada pela ajuda sobre todo nos últimos momentos da dissertação , Silvina, Giana, Ana Maria, Alfonso.....

Aos amigos da turma ARGEBRADE, com quantos “asados” de por medio, Gaby, Fer, Brenda, Guille, Ramon, e muitos mais.

Ao Massimo, GRACIAS POR TODO MI AMOR! ...por estar siempre conmigo y acompañarme en todo. Por ser mi compañero de aventura durante este viaje. Por tantas discusiones, (no siempre com final feliz), sobre geología, ayudándome a ver los errores que cometía... que me sirvieron para aprender, mejorarme y corregirlos…….a mi Manchuly!!

A minha mãe, Irmita, te quiero mucho mami!! a minhas irmãs Mada e Ceci, Javier, Gustavo, e sobrinos Nahuel, Abril, Aldana e o que esta em camino (ainda não se sabe o nome de ele), mais é um meninino. A meu pai, Roque, papi, gracias!!...A minha família italiana, Mario, Cosetta, Analisa, Mauro, Antonella, Giuseppe e meus sobrinos Marco, Rebecca e Sara. A TODOS POR ESTAR MUITO PERTO DO MEU CORAÇÃO!!!!.

Finalmente a TODOSSS!! Aos que agradeci e também aos que não lembre de agradecer.....muito obrigada!! Que de uma forma ou outra aportaram VALIOSAMENTE na minha vida!!

MUITO OBRIGADA!
MUCHISIMAS GRACIAS!
GRAZIE!!!!

## RESUMO

O embasamento da Cordilheira Andina no noroeste de Argentina registra pelo menos duas orogenias paleozóicas: a Orogênese Pampeana (~520 Ma) e a Orogênese Famatiniana (~ 460 Ma).

A orogênese Pampeana foi registrada mais extensivamente na parte noroeste das Sierras Pampeanas, na Cordilheira Oriental e no altiplano da Puna. Nas Sierras Pampeanas, a orogênese foi caracterizada pela formação de um arco magmático relacionado à subducção de litosfera oceânica durante o Cambriano Inferior, seguida de colisão continental (535-520 Ma) de um terreno semiautoctone (bloco Pampia ou o Craton Arequipa-Belen-Antofalla). O Ciclo orogenético Famatianiano, ocorrido desde 490 ate 400 Ma, foi documentado no Sistema de Famatina, na Cordilheira Oriental e no altiplano da Puna. Registra a subducção de litosfera oceânica durante o Paleozóico Inferior com a acreção de um terreno exótico, a Precordilheira, aos 460 Ma aproximadamente.

No noroeste argentino a orogênese Pampeana é documentada na Cordilheira Oriental e no setor leste do Altiplano da Puna como uma seqüência turbidítica de margem passiva denominada Formação Puncoviscana. Rochas plutônicas, com idades de ca. 530 Ma, intrudem a Formação já deformada, marcando o final da orogênese. Entanto a Orogênese Famatiniana no noroeste argentino é representada na Cordilheira Oriental por rochas siliciclasticas de plataforma e marinhas rasas e na Puna por rochas marinhas profundas. Durante este ciclo no Altiplano da Puna são gerados dois arcos magmáticos, denominados "*Faja Eruptiva de la Puna Occidental*" e "*Faja Eruptiva de la Puna Oriental*".

Rochas vulcânicas e sub-vulcânicas intercaladas na Formação Puncoviscana foram reconhecidas em diferentes localidades da Cordilheira Oriental e na borde leste do Altiplano da Puna: Vale do Río Grande, Serra de Niño Muerto e no Vale do Río Blanco. O presente trabalho reúne um conjunto de dados petrográficos, de química mineral, geoquímicos, e geocronológicos (idades U-Pb e K-Ar e relações isotópicas Sr-Nd) dessas rochas vulcânicas com o objetivo de classificá-las, conhecer o seu ambiente tectônico e vinculá-las por meio de suas idades à evolução da margem oeste da América do Sul.

No Vale do Río Grande, as rochas do embasamento Neoproterozoico-Paleozoico Inferior são intrudidas por diques basálticos. Os dados petrográficos, de química mineral assim como os dados geoquímicos e isotópicos permitiram classificá-las como "ocellar-analcima monchiquitos", uma variedade de lamprofiro alcalino sem feldspato. Dados K-Ar indicaram a idade de 163 Ma, as rochas exibem baixas a médias relações iniciais isotópicas $^{87}Sr/^{86}Sr$ (0.70377-0.70781) e relativamente altas relações iniciais de $^{143}Nd/^{144}Nd$ (0.512506-0.512716), correspondendo a valores positivos de $\varepsilon_{Nd}$ (t) (+1.5-+5.6) e idades modelos entre

0.25-0.64 Ga. Os novos dados permitem sugerir que os lamprofiros de Río Grande, foram gerados durante o estagio de pre-rift do Rift Intracontinental de Salta (Jurássico Superior-Eoceno Inferior). Os dados isotópicos e as evidências petrológicas e geoquímicas, junto com os dados da literatura referentes à composição do manto neste setor dos Andes Centrais, permitiram inferir que os magmas derivam de um manto metassomatizado, modificado provavelmente pela Orogênese Famatiniana durante o Paleozóico Inferior.

A área de El Niño Muerto, na borda leste do Altiplano da Puna, consiste em uma serra de direção nordeste-sudoeste, formada totalmente pelas rochas metassedimentares da Formação Puncoviscana. Rochas calci-alcalinos de alto K e composição dacitica intrudem na formação como um sill. Novos dados U-Pb por LA-ICPMS em zircões, bem como de isótopos de Sr-Nd indicam que os metadacitos de El Niño Muerto cristalizaram há 495 ± 4 Ma com altas relações iniciais de $^{87}Sr/^{86}Sr$ (0.71107-0.71180) e valores de $\varepsilon_{Nd}$ (t) negativos entre -9.7 e -5.9. O caráter peraluminoso apresentado por estas rochas sugerem que o magma do qual derivam os dacitos teve forte participação de material crustal seja por contaminação ou por fusão parcial de uma crosta continental com importante componente sedimentar. A idade e as características geoquímicas e isotópicas permitem localizar estas rochas no Arco Famatiniano desenvolvido durante o Ordoviciano no noroeste da Argentina.

No vale do Río Blanco, na Cordilheira Oriental, foram reconhecidas rochas subvulcânicas, lavas almofadadas e depósitos peperíticos que se intercalam às rochas sedimentares hemipelágicas e turbiditicas reconhecidas como parte da Formação Puncoviscana. A geoquímica de elementos traço e terras raras, permitiu classificar estas rochas como basaltos e determinar que elas têm semelhanças com E-MORBs, com razões Zr/Nb desde 6.8 ate 9.5. Os novos dados LA-ICPMS U-Pb obtidos em zircões indicam que os basaltos cristalizaram há 501 ± 9 Ma a partir de um magma primitivo, com valores positivos de $\varepsilon_{Nd}$ (T) . Eles são caracterizados por relações moderadamente altas $^{87}Sr/^{86}Sr$ (0.70713-0.70942), valores de $\varepsilon_{Nd}$ (T) positivos entre +2.47 e +4.46 e idades modelo entre 0.84 e 1.12 Ga. O ambiente tectônico de formação destas rochas permanece pouco claro e as características geoquímicas indicam que eles podem ser comparados com os basaltos tipo E-MORB ou com os basaltos anorogenicos de intraplaca.

Tendo em conta que os basaltos do Vale de Río Blanco e os metadacitos de arco de El Niño Muerto foram gerados no mesmo momento, sugere-se nesta dissertação que os basaltos podem representar os remanescentes de uma bacia de retroarco, em relação ao Arco Famatiniano desenvolvido mais para o oeste durante o Cambriano Superior-Ordoviciano Inferior no noroeste de Argentina.

## ABSTRACT

The basement of the Andean Cordillera in NW Argentina records at least two orogenetic episodes during the Paleozoic: the Pampean Orogeny, (~520 Ma) and the Famatinian Orogeny (~ 460 Ma)

The Pampean Orogeny was registered extensively in the northwestern Sierras Pampeanas and in the Eastern Cordillera and Puna Plateau. In northwestern Sierras Pampeanas this cicle was characterized by an early subduction-related magmatic arc followed by an Early Cambrian (535-520 Ma) continental collision of an semiautoctone terrane identified as the Pampia block or the Arequipa-Belen-Antofalla Craton. The Famatinian Orogenetic Cycle, documented in Famatina System, Eastern Cordillera and Puna Plateau, took place between 490 and 400 Ma. It records the subduction of oceanic lithosphere during the Early Paleozoic, followed by the an exotic terrane accretion, the so-called Precordillera terrane at ca. 460 Ma.

In NW Argentina the Pampean Orogeny is documented in Eastern Cordillera and eastern border of Puna Plateau as a passive margin turbidite sequence, named Puncoviscana Formation. Plutonic rocks intrude into the folded sedimentary sequence, with age ca. 530 Ma, marking the end of this cycle. The Famatinian Orogeny, in NW Argentina is represented by platformal siliciclastic, shallow-marine sedimentary succession in the Eastern Cordillera and by deeper marine sediments to the west, in the Puna Plateau. In the Puna Plateau, during this cycle, two magmatic arcs so-called "*Faja Eruptiva de la Puna Occidental*" and "*Faja Eruptiva de la Puna Oriental*" are generated.

Volcanic and subvolcanic rocks of uncertain age intercalated with detrital sediments of the Puncoviscana Formation have been recognized in several localities of the Eastern Cordillera and easternmost Puna Plateau: in the Río Grande Valley, in the El Niño Muerto Hill and in the Río Blanco Valley. The present study presents petrographic, geochemical and geochronological (U-Pb and K-Ar ages and Sr-Nd isotopic ratios) data for these volcanic/subvolcanic rocks. This study attempts to characterizations these rocks, identify their original tectonic setting and link them with the western margin evolution of South America.

In the Río Grande Valley, the Neoproterozoic to lower Paleozoic basement rock units are intruded by dikes of basaltic compositions. Petrochemical, mineral chemistry, geochemical and isotopic data for these dykes permitted to classify them as ocellar-analcime monchiquite, a feldspar-free variety of alkaline lamprophyre. Biotite K-Ar data indicate the age of 164 ± 8 Ma. They have low to medium $^{87}Sr/^{86}Sr$ initial ratios (0.70377-0.70781), and Nd isotopic compositions corresponding to positive $\varepsilon_{Nd}$ (t) values (+1.5-+5.6) and $T_{DM}$ model ages between 0.25-0.64 Ga. Taking in account the new data, we suggest that the Río Grande

lamprophyres are associated with pre-rift stage of Upper Jurassic to Lower Eocene Salta Intracontinental Rift. The isotopic date and petrochemical characteristics suggest together with the mantle compositions bibliography for this sector, that they derive from an old metasomatized lithospheric mantle, which has probably been chemically transformed during the Ordovician Famatinian Orogeny.

The El Niño Muerto area, localized in the easternmost part of Puna Plateau, consists of a NE-SW hill formed entirely by the Puncoviscana metasedimentary sequence. High-K calc-alkaline rocks of dacitic compositions constitute a sill which intruded into the sequence. New LA-ICPMC U-Pb zircon data and Sr-Nd isotopic ratios indicate that the metadacites crystallized at 495 ± 4 Ma with high initial $^{87}Sr/^{86}Sr$ (0.71107-0.71180) and negative $\varepsilon_{Nd}$ (t) values, between -9.7 to -5.9. Their peraluminous character suggests that the original magma was strongly contaminated with continental crust or that it derived from the partial melting of a crustal material with an important sedimentary component. The geochemical and isotopic data presented in this study indicate that the El Niño Muerto metadacites formed in the Famatinian calc-alkaline magmatic arc developed in Ordovician in NW Argentina.

In the Río Blanco Valley, in the eastern Cordillera, have been recognized subvolcanic rocks, pillow lavas and peperite deposits interbedded with metasedimentary rock units which are considered part of the Puncoviscana Formation. The geochemical data allows us to classification the Río Blanco rocks as basalts with geochemical characteristics similar to E-MORBs, with Zr/Nb ratios from 6.8 to 9.5. New LA-ICPMC U-Pb zircon data and Sr-Nd isotopic ratios indicate that the basalts crystallized at 501 ± 9 Ma from a primitive magma with positive $\varepsilon_{Nd}$ (t) values. The Río Blanco basalts have moderately high $^{87}Sr/^{86}Sr$ initial ratios (0.70713-0.70942), positive $\varepsilon_{Nd}$(t) values (+2.47 to +4.46) and $T_{DM}$ model ages between 0.84 to 1.12 Ga. The tectonic setting of formation of the Río Blanco basalts remains unclear and their geochemical characteristics indicate that they correspond either to an E-MORB or to within plate anorogenic basalts.

Taking in account that the Rio Blanco basalts and the El Niño Muerto Metadacites had been generated in the same moment, we suggest that the Rio Blanco basalts would be interpreted as a remnant of a back-arc basin, in relation to the Famantinian Arc developed more to west during the Late Cambrian /Early Ordovician in NW Argentina.

# CAPÍTULO I

## 1.1. Introdução

O embasamento do noroeste da Argentina, entre 22º e 33º S, registra ao menos duas orogenias durante tempos paleozóicos, as Orogenias Pampeana e Famatiniana (Aceñolaza and Toselli 1973).

O ciclo orogenético Pampeano, aproximadamente contemporâneo com o episódio Panafricano-Brasiliano (Miller and Sollner, 2005), ocorre entre 550 e 515 Ma (Sollner *et al.*, 2000b). Ele é documentado nas províncias morfoestruturais da Cordillera Oriental (CO), Puna e Serras Pampeanas Orientais (Aceñolaza *et al.*, 1990). Esta orogenia compreende etapas de subducção (arco magmático) e colisão de um terreno semiautoctone ao final do Cambriano, o terreno de Pampia (Rapela *et al.*, 2001 a, b) ou o cráton de Arequipa-Belén-Antofalla (Ramos 1988). Depois da acreção ortogonal do terreno, a protomargem de Gondwana se tornou uma margem passiva até os 499 Ma, quando se inicia o Ciclo Famatiniano.

O ciclo Famatiniano ocorre entre 499 e 400 Ma e é um ciclo completo que compreende dois arcos, um externo e o outro interno associados às etapas de subduccção e colisão de um terreno exótico a Gondwana durante tempos silurianos, o terreno Precordillera.

Em contraposição à teoria que postula duas orogêneses (Aceñolaza *et al.*, 1990; Rapela *et al.*, 2001 a, b; Ramos 1988), outros autores (Lucassen *et al.*, 2000, Lucassen *et al.*, 2006) acreditam na existência de uma única orogênese desenvolvida entre 600 e 400 Ma e propõem uma evolução em ambiente de cinturão móvel para o embasamento dos Andes Centrais (Lucassen *et al.*, 2000).

O Ciclo Pampeano está representado entre 22º e 27ºS por depósitos turbidíticos da Formação Puncoviscana, de idade proterozóica superior - cambriana inferior, e por granitóides cambrianos alojados durante esta orogenia (Bachmann *et al.*, 1987, Omarini *et al.*, 1999).

A Formação Puncoviscana aflora na província morfoestructural da Cordilheira Oriental (Turner 1960) e no limite entre esta e a província da Puna. É constituída por seqüências clásticas turbidíticas (pelitos e grauvacas) e inclui conglomerados e calcários subordinados (Omarini y Baldis, 1984, Jezek, 1990). A complexidade tectônica (Mon y Hongn, 1991) limita as avaliações estratigráficas e torna difíceis as correlações entre os distintos afloramentos.

O Ciclo Famatiniano é caracterizado no noroeste da Argentina por rochas sedimentares e magmáticas. Na Cordilheira Oriental as rochas sedimentares são seqüências marinhas pouco

profundas enquanto na Puna predominam as seqüências marinhas profundas. O magmatismo famatiniano desenvolvido na Puna compreende rochas básicas e ácidas associadas a importantes depósitos turbidíticos vulcanoclásticos. Durante este ciclo se desenvolveram dois arcos magmáticos, denominados pela posição geográfica "Faixa Eruptiva da Puna Oriental" (Mendez *et al.*, 1973) e "Faixa Eruptiva da Puna Ocidental" (Palma *et al.*, 1986).

Rochas vulcânicas de natureza calci-alcalina e alcalina (Toselli e Aceñolaza, 1984, Coira *et al.*, 1990; Omarini *et al.*, 1999) de idades incertas se intercalam na Formação Puncoviscana. Os afloramentos de rochas vulcânicas estão expostos em três setores: um setor norte, o Vale de Río Grande; um setor central, a Serra de El Niño Muerto e um setor sul, o Vale de Río Blanco (Fig. 1).

Estas rochas vulcânicas não foram estudadas em detalhe e pouco se sabe a respeito de sua relação com a Formação Puncoviscana e a margem de Gondwana. Os estudos propostos neste trabalho oferecem a possibilidade de definir a idade e o ambiente de alojamento das mesmas e a sua relação com a evolução da Plataforma Sulamericana.

## 1.2. Objetivos

*Objetivos gerais*

Os objetivos gerais desta dissertação são gerar novos dados petrográficos, geoquímicos e isotópicos das rochas vulcânicas que se intercalam na seqüência sedimentar da Formação Puncoviscana, no noroeste da Argentina. O estudo detalhado dessas rochas aportará melhor conhecimento dos ambientes de alojamento e permitirá vinculá-las com os orógenos da Plataforma Sul-americana.

*Objetivos específicos*

Os objetivos específicos desta dissertação são:

a) caracterizar petrograficamente as litologias vulcânicas com a finalidade de classificá-as;

b) caracterizar geoquimicamente as rochas vulcânicas mediante análises de elementos maiores, traço e Terras Raras com a finalidade de determinar o ambiente tectônico e os possíveis processos magmáticos envolvidos na sua geração e evolução;

c) determinar idades através de análises U-Pb em zircões por *laser ablation inductively coupled plasma mass spectometry*, (LA-ICPMS) e K-Ar em biotitas, além de estudos de isótopos de Sr-Nd. Estes dados em conjunto têm como finalidade determinar a fonte magmática das rochas vulcânicas e associá-las a um quadro tectônico apropriado.

### 1.3. Localização e vias de acesso

A área de trabalho está inserida nas unidades morfoestruturais da Cordilheira Oriental e no limite desta com o platô da Puna e coincide com afloramentos da Formação Puncoviscana. As áreas estudadas podem ser divididas geograficamente em três setores.

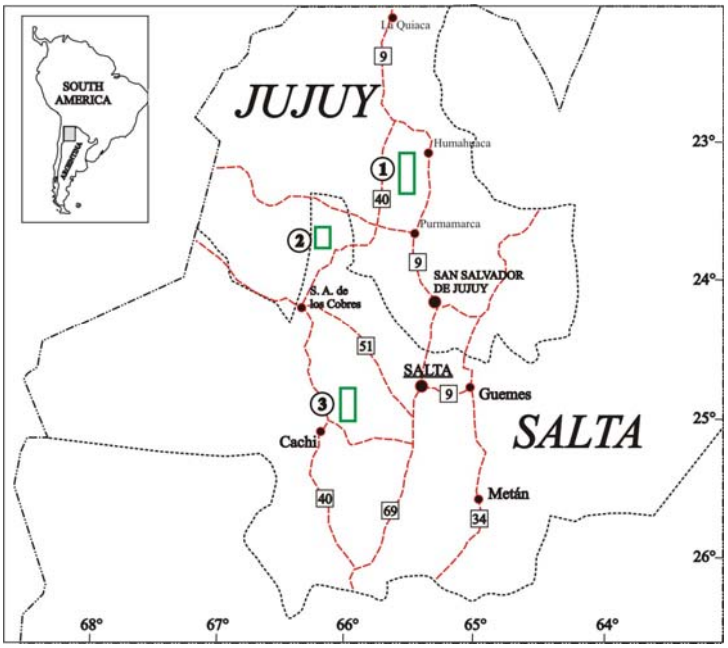


**Figura 1:** Mapa de localização e vias de acesso às áreas estudadas. 1, Vale de Río Grande. 2, Serra de El Niño Muerto. 3, Vale de Río Blanco.

***1) Setor norte:*** está localizado no departamento de Humahuaca, na província de Jujuy. A área de estudo compreende a localidade de Coraya e as Quebradas de Yacoraite e Huichaira, as quais são delimitadas pelos paralelos 23º 35' 00.01" e 23º 09' 13.00" S e meridianos 65º 27' 27.00" e 65º 22' 00.01" W (Fig. 1). Essa área se encontra 150 km a norte da cidade de Salta (capital da província de Salta) e 30 km a norte da cidade de San Salvador de Jujuy (capital da província de Jujuy), sendo a principal via de acesso para a área estudada a Rodovia Nacional N° 9. Neste setor foram reconhecidos diferentes diques alcalinos que intrudem a Formação Puncoviscana.

Tanto Coraya quanto as duas quebradas fazem parte de vales secundários relacionados ao Vale de Río Grande ou Quebrada de Humahuaca. Este vale foi um importante centro de assentamento de povoados pré-históricos.

***2) Setor Central:*** o acampamento de El Niño Muerto está no setor sul do Salar de Salinas Grandes, no limite entre as províncias morfoestruturais da Cordilheira Oriental e da Puna. Localiza-se no departamento de Susques, na província de Jujuy e é limitado pelos

paralelos 23º 46' 34.73" e 23º 44' 07.68" S e meridianos 66º 14' 50.52" e 66º 12' 48.88" W (Fig. 1). A principal via de acesso é a Rodovia Nacional N° 51, que parte da cidade de Salta e leva até a localidade de San Antonio de los Cobres, de onde se segue por 30 Km para norte por estradas não asfaltadas até o acampamento de El Niño Muerto. Neste setor foi identificado um sill de composição dacítica que instrude turbiditos finos da Formação Puncoviscana.

***3) Setor sul:*** no setor sul foram agrupadas as localidades de Las Cuevas e Vale do Río Blanco.

O Vale de Río Blanco se localiza no setor leste dos Vales Calchaquíes, no departamento de Cachi (província de Salta), a aproximadamente 160 km a oeste da cidade de Salta-capital. A área de estudo é limitada pelos paralelos 24º 58' 08.73" e 24º 57' 05.43" S e meridianos 65º 58' 03.41" e 65º 57' 35.71" W (Fig. 1). Partindo da cidade de Salta pela Rodovia Nacional N° 78 se chega até a localidade de Guachipas, onde se encontra a Rodovia Nacional N° 40, principal via de acesso aos Vales Calchaquíes para leste. Após a Cuesta del Obispo, na entrada dos povoados de Payogasta e Cachi, se encontra uma rodovia não asfaltada que, para leste, conduz à Chácara de Colomé. Segue-se aproximadamente 15 km por esta estrada até a entrada do Vale do Río Blanco. Neste setor foram reconhecidas rochas vulcânicas submarinas contemporâneas com a deposição de seqüências hemipelágicas e turbiditos, reconhecidos como parte da Formação Puncoviscana.

## 1.4. Marco geológico regional do noroeste Argentino

Os Andes Centrais entre 22º e 26º S (Fig. 2) estão caracterizados por diferentes províncias morfoestruturais que de oeste para leste são: Cordilheira de la Costa, Precordilheira Chilena, Valle Longitudinal, Depressão Preandina, Cordilheira Ocidental, Altiplano/Puna, Cordilheira Oriental, Serras Subandinas e Planície Chaqueña.

Tanto os afloramentos da Formação Puncoviscana quanto as rochas vulcânicas estudadas estão expostas na Cordilheira Oriental e no limite entre esta e o Altiplano-Puna, portanto estas duas províncias morfoestruturais serão brevemente descritas a seguir:

### Altiplano-Puna

O Platô Altiplano-Puna foi chamado inicialmente Puna de Atacama por Brachkebusch (1883). Os investigadores que o seguiram a chamaram simplesmente de Puna (Bonarelli, 1913, 1915; Keidel, 1927). É caracterizado por altitudes acima de 3.700 m.s.n.m. Apresenta limites bem definidos com a Cordilheira Oriental (Fig. 2) a leste e com a Cordilheira

Occidental a oeste, já em território chileno. Para sul é limitado pela Cordilheira Frontal e Sistema de Famatina. Suas características foram bem definidas por Turner em 1970.

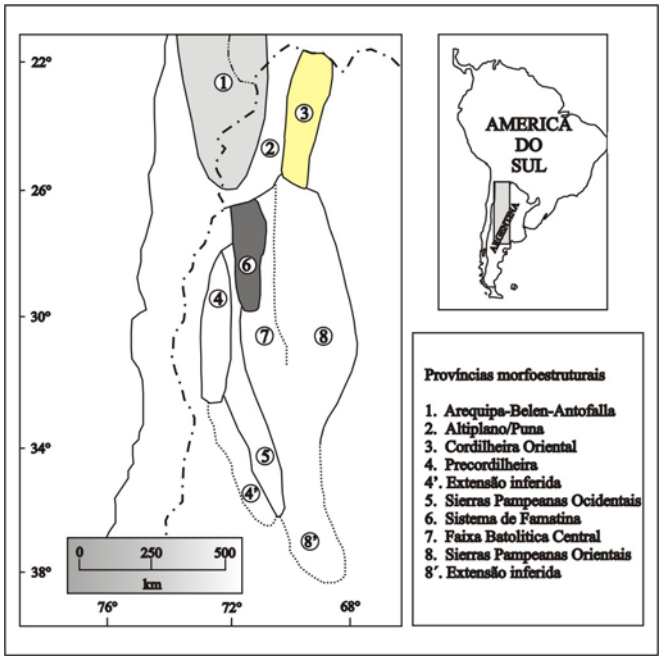


**Figura 2:** localização e distribuição das províncias morfoestruturais no centro-norte da Argentina. (modificado de Pankhurst and Rapela, 1998)

Sua estrutura está caracterizada por grandes falhas de empurrão de idade paleógena a miocênica que estruturaram esta altiplanície. Alguns autores (Alonso *et al.*, 1984) propuseram dividir a Puna em dois setores com base em suas características geológicas regionais: Puna Setentrional ou Jujeña, e a Puna Austral ou Saltocatamarqueña. O limite entre essas províncias corresponde ao lineamento Calama-Olacapato-El Toro (COT) (Salfity *et al.*, 1975, 1984).

A Puna setentrional ou Jujeña é caracterizada pela presença de rochas ordovicianas enquanto a Puna Austral é caracterizada por afloramentos de rochas de baixo grau metamórfico pré-cambrianas, uma faixa eruptiva ordoviciana com granodioritos, granitos e extenso magmatismo basáltico pleistoceno associado a um regime extensional.

As rochas mais antigas que afloram são sedimentos e rochas ordovicianas de baixo grau metamórfico sem base exposta, as quais no setor ocidental se encontram fortemente deformadas. Elas se associam a dois arcos magmáticos, a Faixa Eruptiva da Puna Oriental (Mendez *et al.*, 1973) e a Faixa Eruptiva da Puna Ocidental. (Palma *et al.*, 1986). No limite com o Chile, rochas marinhas silurianas e devonianas encontram-se sobre os sedimentos ordovicianos, que são sobrepostos por depósitos continentais de idade neopaleózoica.

Os depósitos mesozóicos a eoterciários correspondem à bacia do rift do Grupo Salta, que no setor norte da Puna apresentam um importante depocentro de sedimentação. Os depósitos que preenchem o rift são em suas maioria continentais, porém há uma breve transgressão marinha que corresponde à Formação Yacoraite, de idade campaniana-maestrichtiana (Salfity y Marquillas, 1981, 1994).

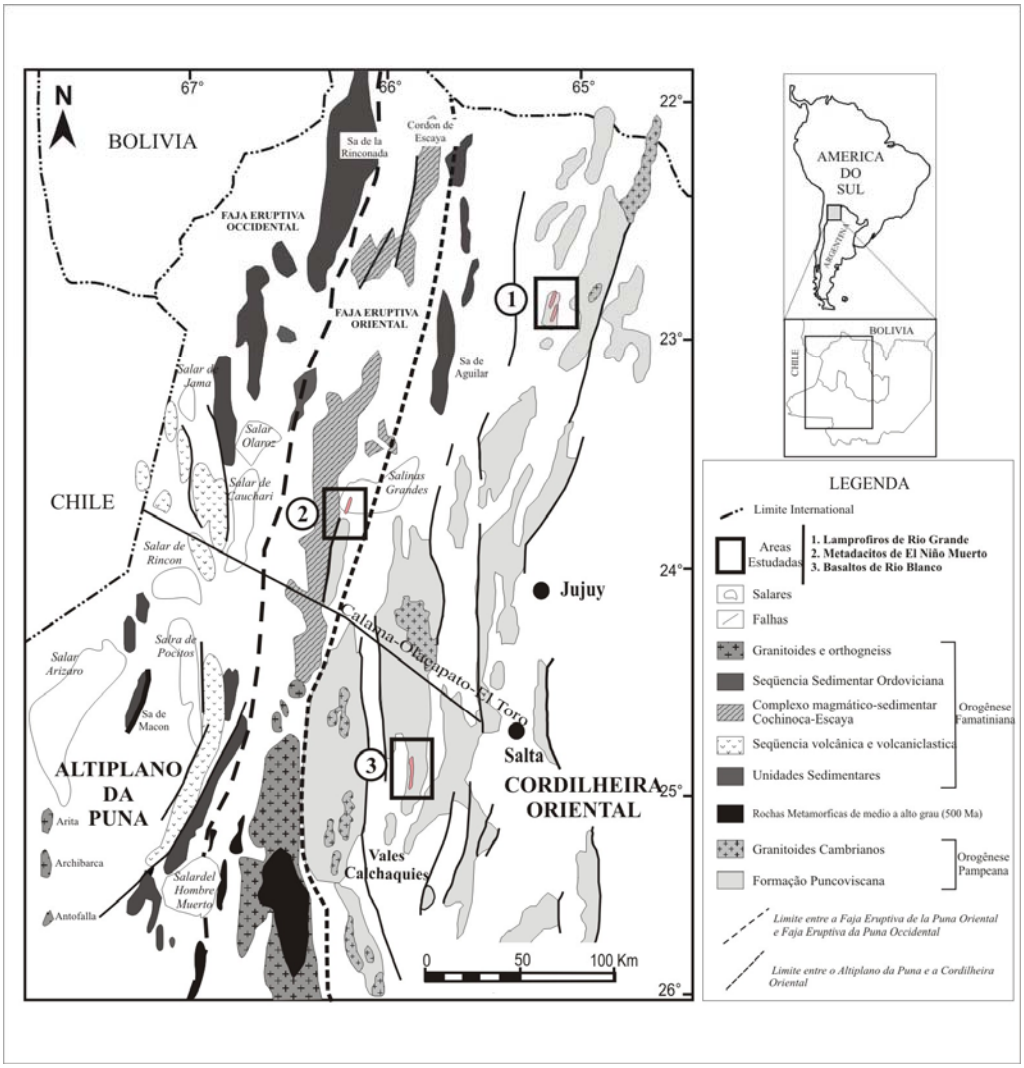


**Figure 3:** afloramentos do embasamento Neoproterozóico - Paleozóico-Inferior do noroeste da Argentina (modificado de Do Campo and Guevara, 2005 and Viramonte et al., 2007)

O Platô Altiplano-Puna apresenta como característica principal o vulcanismo orogenético cenozóico, representado por estrato vulcões de composição andesítica-dacítica, caldeiras vulcânicas associadas a fluxos ignimbríticos e cones basálticos monogenéticos. Eles se intercalam com depósitos terciários continentais desenvolvidos em bacias endorréicas que culminam com depósitos evaporíticos. Estes últimos constituem os grandes salares da Puna, outra características marcante.

**Cordilheira Oriental**

A Cordilheira Oriental foi definida por Brackebusch (1892) para o território argentino, entretanto Keidel (1925) e Groeber (1938) restringiram o uso do termo para as províncias de Salta e Jujuy. É limitada a oeste pelo Platô da Puna, que corresponde ao limite da antiga plataforma eo-paleozoica. Para sul é limitada pelas Serras Pampeanas Orientais (Fig. 2). Para leste o limite com as Serras Subandinas é tectônico, representado pela falha de empurrão Andina Principal (*main Andean Thrust*, Roeder, 1988). Esta falha foi responsável pelo soerguimento do embasamento neoproterozóico e das seqüências cambro-ordovicianas

O soerguimento da Cordilheira Oriental ocorreu durante o Mioceno superior com importantes movimentos neotectônicos que prosseguem até os dias atuais. Sua estrutura está caracterizada por imbricações de escamas de direção norte-noroeste que envolvem o embasamento granítico e sedimentar. As escamas têm uma estrutura complexa, resultado das orogenias Pampeana (limite Neoproterozóico-Cambriano), Oclóyica (Ordoviciano médio-superior) e Chánica (final do Devoniano).

A característica principal da Cordilheira Oriental é o desenvolvimento de grandes lascas de empurrão descritas por Keidel (1943). Estas lascas são compostas por um bloco neoproterozóico caracterizado por sedimentos pouco metamorfisados da Formação Puncoviscana. Rochas plutônicas do Cambriano, como os Granitos de Tastil, Cañani, Nevado de Cachi e Nevado de Palermo alojam-se nesta unidade e sedimentos clásticos de ambiente de plataforma dos Grupos Mesón (Cambriano) e Santa Victoria (Ordoviciano Inferior a Médio) depositam-se em discordância angular sobre ela (Fig. 3). Depósitos marinhos silurianos e devonianos estão em suave discordância angular sobre os depósitos anteriores. Essa discordância é resultante dos movimentos da fase Oclóyica, que ocasionou a ascensão da protoPuna (Bonarelli, 1915) ou, alternativamente, da Protocordilheira Oriental (Ramos y Palma, 1996).

As diferentes unidades da bacia do rift do Grupo Salta, desenvolvido entre o Cretáceo e o Eoceno, se depositaram em discordância sobre os depósitos paleozóicos e mais antigos. Escasso vulcanismo cenozóico se aloja no Abra de Pives e Diego de Almagro.

No extremo austral da Cordilheira Oriental (Turner 1970) está a subprovíncia de Cumbres Calchaquíes (Baldis *et al.*, 1976), que compreende o extremo norte das Serras Pampeanas Norocidentales (Caminos, 1979). Esta não apresenta variações estratigráficas tão marcantes para separá-la da Cordilheira Oriental. A subprovíncia de Cumbres Calchaquíes é formada por um embasamento neoproterozoico de baixo grau metamórfico, a Formação Puncoviscana, e seu equivalente de maior grau metamórfico, a Formação La Paya. O embasamento também está constituído por granitóides eopaleózoicos como a Formação Cachi

e ordovicianos como os Granitos Angostura, Pucará, Complexo Eruptivo Oire. Sobre estes se depositam os sedimentos continentais do Subgrupo Pirgua (Cretáceo superior) e os depósitos continentais com registro de transgressões marinhas, os Subgrupos Balbuena e Santa Bárbara (Paleógeno). Os depósitos do Grupo Salta são característicos da região oriental. Sobre eles estão os depósitos da Formação Luracatao e do Grupo Payogastilla. Durante este período (Neógeno) se registrou um episódio vulcânico (Ignimbritas Pucarilla) que representaria uma conexão com o vulcanismo da Puna.

### 1.5. Metodologia geral do trabalho

O trabalho de pesquisa foi dividido em 8 etapas:

**(i)** *Etapa de campo:* foi dividida em três partes e consiste no reconhecimento e amostragem das rochas vulcânicas, objeto deste estudo nas diferentes localidades. Posteriormente as amostras foram enviadas para o Brasil, para continuar com as etapas seguintes.

**(ii)** *Estudo da Petrografia das rochas vulcânicas:* as lâminas correspondentes à primeira campanha foram realizadas no *Laboratório de Petrotomia de la Universidad Nacional de Salta-Argentina*. As lâminas das amostras recolhidas nas duas etapas subseqüentes foram confeccionadas no Laboratório de Laminação do Instituto de Geociências da Universidade de Brasília-UnB. Foram descritas 110 lâminas em microscópios petrográficos de luz transmitida do Laboratório de Microscopia do Instituto de Geociências da UnB. A partir do estudo petrográfico, foram selecionadas amostras para as análises geoquímicas realizadas no Laboratório Acme, no Canadá.

**(iii)** *Análises químicas de minerais - Microsonda Eletrônica (ANEXO II):* a composição química do de olivina, clinopiroxênio, anfibólio, mica, analcima, apatita e carbonato foi obtida no Laboratório de Microsonda Eletrônica do Instituto de Geociências da UnB. O modelo da microssonda utilizada é CAMECABAX SX 50. As condições analíticas foram 10 nÅ de transmissão de corrente e 15 KeV de transmissão de energia. O tempo de aquisição foi de 10 segundos e o diâmetro do feixe foi de 1 μm.

**(iv)** *Preparação das amostras para análises químicas de rochas e análises isotópicas Sr-Nd:* Superfícies de alteração e veios de quartzo e carbonato foram cuidadosamente retirados das amostras. Posteriormente as rochas não alteradas foram pulverizadas a uma granulometria

inferior a 200 mesh utilizando-se um moínho de bola de carbeto de tungstênio no Laboratório de preparação de amostras do Laboratório de Geocronologia do Instituto de Geociências - UnB.

**(v)** *Separação de minerais:* a separação dos minerais pesados (zircão) foi realizada no Laboratório de Concentração de amostras do Laboratório de Geocronologia - UnB. Utiliza-se como método de pré-concentração o método da batéia e posteriormente o separador magnético Frantz. A última etapa de concentração foi realizada por seleção no microscópio binocular.

**(vi)** *Montagem dos grãos de zircão*: foram selecionados aproximadamente 30 zircões euédricos e limpos para cada amostra. Posteriormente cada grupo foi montado sobre uma lâmina de vidro e colocado sobre um molde cilíndrico onde se colocou duas partes de resina (Struer, Epo Fix Resin) e uma parte de endurecedor (Struer, Epo Fix Hardener). Cada amostra foi deixada em repouso aproximadamente 12 horas para permitir que a resina e o endurecedor se solidificassem. Em seguida, retira-se o molde cilíndrico e obtém-se os "mount" de zircões. Cada mount foi polido com pasta diamantada e lavado com $HNO_3$ 3% junto com zircões padrões durante 5 minutos para remover da superfície possíveis contaminações com Pb. Este último passo foi realizado imediatamente antes de serem efetuadas as análises no LA ICP-MS.

**(vii)** *Análises químicas de rochas:* as análises químicas de elementos maiores, traços e terras raras foram realizadas em 24 amostras. A preparação das amostras para análises dos elementos maiores e parte dos traços foi feita por fusão com $LiBO_2$ e para a obtenção dos metais base e preciosos por digestão com água régia. As análises dos elementos maiores, Ni e Sc (ppm) foram efetuadas por espectrometria de emissão com ICP-OES e dos elementos traços por espectrometria de massa com ICP-MS.

**(viii)** *Difratometría de raios-x (ANEXO I):* Foram realizadas duas análises por difração de Raios-X. As análises foram feitas no Laboratório de Difração de Raios-X do IG-UnB. O difratômetro usado é um Rigaku-D/MAX-2 A/C com fonte de cobre e filtro de Ni, operando com 40 Kv e 20 mA. A interpretação dos difratogramas foi feita pela professora Edi Mendes Guimarães, usando o Software JADE 3-0 da MDI, com banco de dados PC-PDF (Power Diffraction File-PDF para PC) produzido pelo International Center for Diffraction.

**(ix)** Geoquímica isotópica Sr-Nd: Análises de Sm-Nd e Rb-Sr foram realizadas em amostras de rocha total (25 exemplares e 11 exemplares, respectivamente) no Laboratório de Geocronologia da UnB. As amostras selecionadas foram: dacitos, lamprófiros e basaltos. As análises Sm-Nd foram feitas segundo o método descrito por Gioia & Pimentel (2000). Entre 70 e 100mg de pó de amostra foram misturados com uma solução traçadora mista (spike) de $^{149}Sm$-$^{150}Nd$ e dissolvidos em cápsulas Savillex. A extração dos elementos lantanídeos foi feita através de técnicas convencionais de troca iônica em colunas de quartzo, usando resina BIO-RAD AG-50W-X8. As extrações de Sm e Nd foram realizadas em colunas de teflon empacotadas com resina LN-Spec (resina líquida HDEHP-ácido di-ethylhexil fosfórico impregnada em pó de teflon). As frações de Sr, Sm e Nd foram depositadas em arranjos duplos de filamentos de rênio. As razões isotópicas foram determinadas em espectrômetro de massa multi-coletor Finnigan MAT 262 em modo estático. As incertezas para $^{87}Sr/^{86}Sr$ são menores do que 0.01% (2σ) e para as razões $^{147}Sm/^{144}Nd$ e $^{143}Nd/^{144}Nd$ são melhores do que ±0.2% (1σ) e ±0.005% (1σ) respectivamente, baseadas em análises repetidas dos padrões BHVO-1 e BCR-1. As razões $^{143}Nd/^{144}Nd$ são normalizadas para o valor de $^{146}Nd/^{144}Nd$ de 0.7219 e a constante de desintegração (λ) usada é $6.54 \times 10^{-12}$ $a^{-1}$. Os resultados foram processados utilizando-se o programa ISOPLOT/Ex 3 (Ludwig 2007). Os valores de $T_{DM}$ foram calculados utilizando o modelo DePaolo (1981).

**(viii)** *Geocronologia U-Pb, K-Ar:* as determinações isotópicas U-Pb sobre zircões foram realizadas no Laboratório de Geocronologia da Universidade de Brasília-UnB. O equipamento utilizado foi o Laser Ablation (LA)-ICP MS multi-colector. O Laser Ablation usa um laser de corrente concentrada para vaporizar pequenas quantidades de amostra de zircão contidas numa cela fechada. O material evaporado é transportado em gás Helio (gás transportador), desde a cela até o ICP-MS para a quantificação isotópica. O instrumento tem incorporado um microscópio que permite obter uma imagem de alta resolução, o que facilita a localização dos diferentes grãos de zircão da amostra.

*As condições analíticas foram as seguintes:*
Padrão usado: **GJ 1**
Método de varredura: linear (2x)/ pré-ablation
Diâmetro do laser: 30 μm.
Energia (%): 32%
Energia J/$cm^3$): 0.15
Freqüência: 12 Hz.

Tempo de aquisição: 10 segundos
Fluxo de Argônio: 0.903
Fluxo de Helio: 0.4

**(ix)** *Confecção da dissertação de mestrado e dos artigos:* esta etapa consistiu na redação do texto da dissertação, elaboração dos artigos, preparação, apresentação de defesa de dissertação.

### 1.6. Escopo da dissertação

Os resultados obtidos nesta dissertação são referentes às rochas vulcânicas do embasamento sedimentar do noroeste argentino. Os dados são apresentados em forma de dois artigos.

***No Capitulo 2***, são apresentados os dados obtidos no Vale de Río Grande. A razão da escolha foi a idade jurássica obtida para os diques da região o que permitiria ligá-los à abertura do Rift de Salta, desenvolvido durante o Cretáceo no noroeste da Argentina. O título do artigo é: **"K-Ar AGE AND Sr-Nd ISOTOPIC GEOCHEMISTRY OF ALKALINE LAMPROPHYRE DYKES, FROM THE RIO GRANDE VALLEY, EASTERN CORDILLERA, NW ARGENTINA: ORIGIN OF PARENTAL MAGMAS FROM A METASOMATIZED MANTLE."**

O artigo se inicia com uma introdução e contexto geológico sobre o Jurássico nos Andes Centrais e sobre o desenvolvimento do rift Cretáceo tanto na Argentina como no sul da Bolívia. Seguem, nos capítulos de geologia de campo e Petrografia, a descrição de campo, tipos de contato com o embasamento e caracterização petrográfica das rochas. A caracterização química dos minerais destas rochas é apresentada no capítulo química mineral. Posteriormente há uma breve descrição dos métodos analíticos usados para a obtenção dos dados de elementos maiores, traços e terras raras e para os dados isotópicos Sr-Nd. Nos capítulos de geoquímica e geocronologia as rochas são caracterizadas e classificadas. Finalmente os dados são tratados no capítulo de Discussões

***No Capitulo 3***, são apresentados os dados obtidos na Serra de El Niño Muerto e no Vale do Río Blanco. Os motivos da escolha foram as idades semelhantes obtidas para estes dois grupos de rochas que permitiram relacioná-los com a margem de Gondwana durante o Paleozóico Inferior.

O título do artigo é: **"LA-ICPMS U-PB GEOCHRONOLOGY AND PETROLOGY OF VOLCANIC ROCKS OF THE NEOPROTEROZOIC**

**TO LOWER PALEOZOIC BASEMENT OF THE CENTRAL ANDES, NW ARGENTINA: INSIGHTS ON THE EVOLUTION OF WESTERN GONDWANA."**

O artigo começa com uma introdução e contexto geológico sobre as orogenias registradas no embasamento do noroeste, desde o Neoproterozoico até o Paleozóico Médio-Superior. Seguem, nos capítulos de Relações de campo e Petrografia, a descrição de campo, tipo de contatos com o embasamento e caracterização petrográfica das rochas. Posteriormente segue uma breve descrição dos métodos analíticos usados para a obtenção dos dados de elementos maiores, traços e terras raras, alem de dados isotópicos Sr-Nd e idades U-Pb sobre zircões. Nos capítulos de geoquímica e geocronologia as rochas são caracterizadas e classificadas. Finalmente os dados são tratados no capítulo de Discussões.

# CAPÍTULO II

Este Capítulo apresenta os resultados petrológicos, geoquímicos e isotópicos, referentes às rochas subvolcânicas do Vale de Río Grande. As informações serão apresentadas na forma de artigo completo, que será submetido ao periódico ***Journal of South American Earth Sciences,*** com o título:

"K-Ar AGE AND Sr-Nd ISOTOPIC GEOCHEMISTRY OF ALKALINE LAMPROPHYRE DYKES, FROM THE RIO GRANDE VALLEY, EASTERN CORDILLERA, NW ARGENTINA: ORIGIN OF PARENTAL MAGMAS FROM A METASOMATIZED MANTLE."

# K-Ar AGE AND Sr-Nd ISOTOPIC GEOCHEMISTRY OF ALKALINE LAMPROPHYRE DYKES, FROM THE RIO GRANDE VALLEY, EASTERN CORDILLERA, NW ARGENTINA: ORIGIN OF PARENTAL MAGMAS FROM A METASOMATIZED MANTLE

Natalia Hauser [a, b], Massimo Matteini [a], Marcio Martins Pimentel [a], Ricardo H. Omarini [b].

[(a)] Laboratorio de Geocronología. Instituto de Geosciências, Universidade de Brasilia. Brasília-DF 70910-900 Brasil. E-mail address: (Natalia Hauser) hausernatalia@yahoo.com.ar

[(b)] Universidad Nacional de Salta-CONICET. Buenos Aires 177, Salta 4400. Argentina

***Abstract***

In the Río Grande Valley, NW Argentina, several dykes intrude the Neoproterozoic to lower Paleozoic basement. In this study new petrographic, geochemical and isotopic data allowed to classify these rocks as ocellar-analcime monchiquite, a feldspar-free variety of alkaline lamprophyre composed mainly of Ti-rich-diopside or augite, Ti-rich biotite/phlogopite, forsteritic olivine, titanian-pargasite and analcime with abundant ocelli filled with analcime and carbonate. High LOI, Cr, Ni, Sc, Co and V and variable contents in Ba, Sr, Rb and Nb are observed. They show distinct enrichment in LILE and LREE compared to HFSE and HREE, and the lack of Eu anomaly indicates the absence of plagioclase fractionation. Trace element contents suggest that they were formed in a within plate setting. K-Ar analyses of biotite indicates an age of 164 ± 8 Ma. They present variable $^{87}Sr/^{86}Sr$ initial ratios, ranging from 0.70377 to 0.70781, and initial $^{143}Nd/^{144}Nd$ ratio between 0.512506 and 0.512716), corresponding to positive $\varepsilon_{Nd}$ (t) values (+1.5 to +5.6) and $T_{DM}$ model ages between 0.25-0.64 Ga. Taking into account their age, petrography, geochemical and isotopic data, we suggest that the Río Grande lamprophyres originated during the Jurassic by partial melting of old metasomatized lithospheric mantle, during the pre-rift stage in NW Argentina.

## 1. Introduction

Lamprophyres comprise an important group of rocks since they are considered to represent primary mantle-derived magmas generated at considerable depths (100-150 km) (*e.g.* Rock, 1991, Bernard-Griffiths et al., 1991, Bédard, 1994). Generally they carry mantle and crustal xenoliths, yielding crucial information on the mantle source and also on geodynamic processes involved in the origin of these magmas. Similarly to other alkaline rocks, lamprophyres are abundant in continental rifts, failed arms of triple junctions (Brooks & Platt 1975) as well as in some oceanic islands (Almeida 1955, 1961, Mitchell and Thom, 1976).

However they also occur in orogenic zones and their peripheries (Richey 1939, Barrab 1952, Viterbo and Zanettin 1959, Rock 1982, Knill 1982), in island arcs (Yagi et al., 1975, Nixon et al., 1980), in passive to destructive continental margins (Snaveley and Wagner 1961), in anomalous uplifted fragments of oceanic crust (Aumento and Ade-Hall 1973, Aumento et al., 1974, Cornen 1981, 1982,) and near major transcurrent faults (Cooper 1979). Therefore, lamprophyres are associated not only with intra plate settings, but also with divergent, passive and even convergent plate margin settings (Rock, 1987).

In the Río Grande Valley in northwestern Argentina (Eastern Cordillera) subvolcanic alkaline rocks, which are the subject of the present study, are emplaced into Upper Neoproterozoic to Lower Paleozoic basement rock units of uncertain age. Originally these rocks have been classified as ankaramites, piroxenitic horblendites, picrites and basalts with alkaline affinities (Toselli and Aceñolaza, 1984, Manca et al., 1987 and Chayle et al., 1987) (Fig. 1). Toselli and Aceñolaza (1984) and Omarini et al. (1999) suggested a Neoproterozoic age for these dykes based on field evidence, whereas other authors proposed an uncertain post- Ordovician age (Manca et al., 1987 and Chayle et al., 1987, Coira et al., 1990). Due to the lack of detailed field and petrological data as well as of accurate geochronology, little is known about their tectonic setting of emplacement.

In this paper new field, petrographic, geochemical and isotopic data for the subvolcanic rocks of the Río Grande Valley are discussed. The new data show that these rocks are alkaline lamprophyres and they also allowed us to place constraints on their petrogenesis. We show and discuss, for the first time, their mineral chemistry, geochemical data and a K-Ar radiometric age on biotite. Additionally, a new set of whole rock Sr-Nd isotopic data is presented and helped to better understand the magmatic evolution, nature of the mantle source and tectonic setting of emplacement of these lamprophyres. Finally, we attempt to clarify the geodynamic significance of these dyke swarm and integrate the new results into the geodynamic evolution of NW Argentina.

## 2. Geological Setting

Since the Early Mesozoic, the geodynamic evolution of the Andean margin was characterized by a complex interaction of the Aluk-Phoenix, Farallon and Pacific oceanic plates with the South American Continental plate (Zonenshayn et al., 1984, Jaillard et al., 1990, 2000, Scheuber et al., 1994). During the Lower Jurassic (Sinemurian-Pleinsbachian times) the subduction of the Aluk (Phoenix) plate developed a large magmatic arc along the western margin of South America. This magmatic activity is represented by the emplacement of subalkaline plutonic and volcanic rocks exposed, for instance, in northern Chile (Mpodoziz

and Ramos, 1990, Romeuf et al., 1995, Jaillard et al., 2000). At that time, the whole region, including southeastern Bolivia and northwestern Argentina, was affected by extensive tectonic and magmatic activity, which produced abundant alkaline-subalkaline plutonic and volcanic rocks (e.g. Galliski and Viramonte, 1988, Rubiolo, 1992, Viramonte et al., 1999, Menegatti, 2001, Cristiani, 2004, Comin-Chiaramonte et al., 2005, Cristiani et al., 2005). To the east, in northwestern Argentina and eastern Bolivia the magmatism was clearly associated with the formation and evolution of a continental rift system (Fig. 1) (Salfity and Marquillas, 1981, Galliski and Viramonte, 1988, Avila Salinas, 1986 and Omarini et al., 1989) in a back-arc position with respect to the Jurassic-Cretaceous volcanic arc. This structure was filled with a sedimentary sequence represented by the Salta Group in Argentina (Moreno, 1970, Reyes and Salfity, 1973, Salfity and Marquillas, 1981, Salfity, 1982, Gomez Omil et al., 1989) and the Puca Group in Bolivia (Russo and Rodrigo, 1965, Reyes and Salfity, 1973, Cherroni, 1977). The Salta Group comprises three units: the Pirgua, Balbuena and Santa Barbara subgroups in which three major magmatic phases have been recognized and are briefly described below (Salfity and Marquillas, 1981, Avila Salinas, 1986, Galliski and Viramonte, 1988, and Omarini et al., 1989).

During the Early Jurassic and Cretaceous the *pre-rift* phase (Fig. 1) was dominated by regional doming produced by the rise of plume-related asthenospheric masses, with associated crustal thinning and an intricate pattern of extensional faults. This stage was characterized by

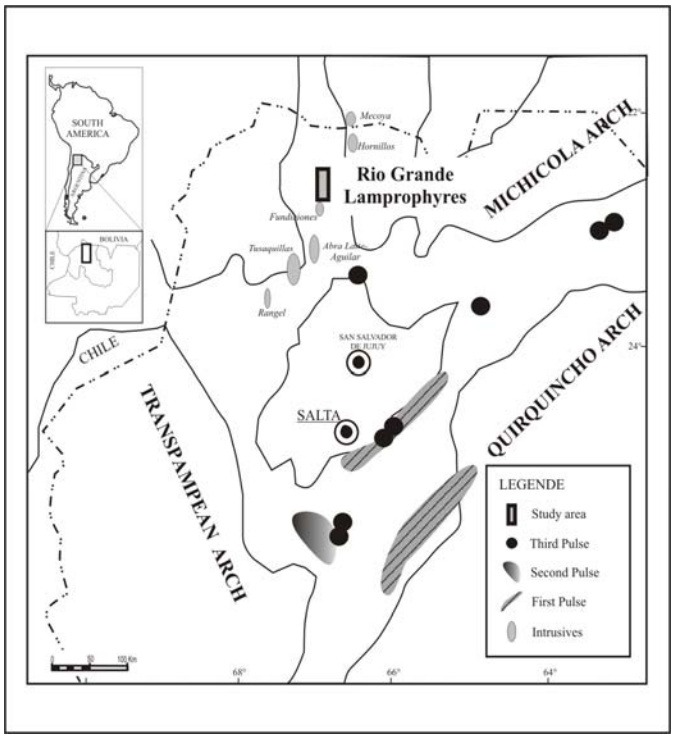


**Figure 1:** Map of the Jurassic-Cretaceous Rift of NW Argentina. The location of pre-rift plutonic rocks and the study area are shown. Modified from Salfity and Marquillas, (1981) and Viramonte et al., (1999).

the emplacement of anorogenic igneous complexes along the major extensive tectonic structures striking NNE (e.g. Cobres Salinas Grandes fault). The Agua Del Desierto, Rangel, Tusaquillas, Abra Laite, Aguilar, Fundiciones, Hornillos and Mecoya plutonic complexes characterize this ***first magmatic phase (at ca. 150-100 Ma)*** in NW Argentina, consisting of plutonic rocks which intruded into Late Precambrian/Lower Paleozoic metasedimentary sequences (Lanfranco, 1972, Rubiolo, 1992, Menegatti, 2001, Cristiani, 2004).

The *syn-rift phase* was marked by thermal subsidence, with continental red beds infilling the intracontinental rift, with minor marine transgressions registered in the Pirgua Subgroup. The Balbuena Subgroup is the main representative of the syn-rift sequence and is the most characteristic lithostratigraphic unit of the Cretaceous-Paleocene basins in central-western South America. During this stage the two other magmatic phases took place. ***The second magmatic phase (80-75 Ma)*** is marked by alkaline volcanism (basanites and mugearites) developed along the axis of the main tectonic structures. The ***third and late igneous phase (65-60 Ma)*** comprises lamproitic sills intruded into the Blanquitos Formation of the Pirgua Subgroup (Omarini et al., 1989), basanites interbedded in the Balbuena and Santa Barbara Subgroups in Argentina as well as basanites, phonotephrites (Vargas Gil, 1965, Galliski and Viramonte, 1988) and lava flows (Castaño and Rodrigo, 1978) associated with equivalent sedimentary successions in Bolivia. This late igneous phase marks the onset of the thermal subsidence and collapse of the basin during the *post-rift stage*, just before the closure of the Cretaceous-Paleocene rift basin due to the dramatic change in the geodynamic style of the region caused by the Incaic compressive phase during the Upper Paleocene.

The origin of this important extensional geological structure, which played a major role in the Central Andean Cordillera evolution, still remains controversial. Galliski and Viramonte (1988) related this magmatism to the back-arc zone in relation to the Jurassic subduction of the Aluk plate under South America, whereas Cristiani et al. (2000) associated the Upper Jurassic-Cretaceous magmatism in NW Argentina with the break-up of Gondwana. We are in agreement with the second hypothesis.

The pre-rift magmatic phase was characterized by the emplacement of intrusive rocks located in central and southeastern Bolivia (Velasco and Ayopaya region) and in NW Argentina (Puna Plateau and Eastern Cordillera). Close to the Argentina-Bolivia border alkaline and ultramafic lamprophyres of uncertain affinity have been described by Rubiolo et al. (1997). These authors recognized aillikite dykes with K-Ar age of 224 ± 08 Ma intruding into the Puncoviscana Formation. Towards the south, Rubiolo et al. (1997) identified sannaites associated with the cretaceous alkaline complex of Hornillos (59±04 and 71±09 K-Ar age) intruding into the Neoproterozoic-Lower Paleozoic basement rock units. They have

been interpreted as representative of igneous activity associated with extensional processes related with the formation of the intracontinental rift (Galliski and Viramonte, 1988, Rubiolo, 1992, 1997, Rubiolo et al., 1996). Two lamprophyre dykes of this complex were dated with the K-Ar method at 71 ± 9 and 59 ± 4 Ma (Rubiolo et al., 2003). Approximately 100 km east of the Río Grande Valley, in Sierras Subandinas, in the Los Alisos locality, ultramafic dykes dated at 303± 10 Ma K-Ar age have been recognized (Mendez and Villar, 1979, Barbieri et al., 1997), apparently not related to the Salta rift development.

In the Río Grande Valley several alkaline dykes, object of the present study, outcrop in the Coraya, Yacoraite and Huichaira secondary valleys (Manca et al., 1987 and Chayle et al., 1987, Coira et al., 1990) between 23º 35' 00.01" and 23º 09' 13.00" S from 65º 27' 27.00" to 65º 22' 00.01" W (Fig. 1). These dykes intrude into the Neoproterozoic-Lower Paleozoic basement of the Eastern Cordillera, formed by the Puncoviscana Formation, together with the Meson and Santa Victoria Groups.

## 2.1. Local Geology

The study area is characterized by Neoproterozoic to Lower Paleozoic sedimentary basement rock units. The lower unit is the Puncoviscana Formation which, according to available geochronological (e.g. Do Campo, 1999b, Do Campo et al., 1999), and paleontological data (Buatois and Mangano, 2003), has been interpreted as Vendian to Nemakitian-Daldynian age. It is represented by a turbidite sequence consisting of centimetric to decimetric beds of grey and grayish-red to green greywacke and pelite which have been intensely folded. Their tectonic settings of deposition remain a subject of debate. Models vary from passive margin (Ramos, 1988, Jezek, 1990, Sims et al., 1998, Rapela et al., 1998) and foreland basin settings (Kraemer et al., 1995, Keppie and Bahlburg, 1999) to intracontinental rift which might have evolved into an active plate margin (Omarini et al., 1999a, b). This unit was affected by polyphase deformation during the evolution of western South America, however the main deformational event took place during the Tilcaric Orogeny in late Neoproterozoic to early Cambrian times (Ramos and Basei, 1997, Do Campo, 1999b). The sequence is unconformably overlain by pink sandstones of the Middle to Upper Cambrian Meson Group which is interpreted as a shallow-marine passive margin system (Aceñolaza et al., 1982, Kumpa and Sanchez, 1988). This is overlain by the greywacke and pelites of Santa Victoria Group (Turner, 1960, Salfity et al., 1984) which represent the Famatinian Cycle in the Eastern Cordillera.

*Table 1: Summarized lithological and petrographic characteristics of the Río Grande sills and dykes.*

| *Locality* | *Sample N°* | *Lithology* | *Host rock* | *Texture* | *Phenocrysts* | *Microphenocrysts and groundmass* | *Ocelli* | *Mantle xenoliths* |
|---|---|---|---|---|---|---|---|---|
| ***Coraya*** | BCO 49 | dyke, 30 cm thick | Turbidites of Puncoviscana Formation | porphyritic- strongly panidiomorphic | Ol, Cpx (altered to Cc, Serp) | Abundant Fe-ti oxides, Cpx, Bt | Scarce. Carbonate compositions | Not observed |
| | BCO 51 | sill, 40 cm thick | | | | | | |
| | BCO 52 | dyke, 50 cm thick | | | | | | |
| ***Yacoraite*** | P8 | sill | Turbidites of Puncoviscana Formation | porphyritic; panidiomorphic, flow differentation | Amph, Bt, Cpx, Ap | Amph, Cpx, Phlog, Ap | Scarce. Carbonate compositions | Abundant, 0.5-5 cm large. Carbonatitic and Horblendite compositions |
| | BYA 122 | sill | | porphyritic | Cpx completly altered to carbonate | Carbonate, Fe-Ti oxides | Not observed | Not observed |
| | BYA 123 | sill | | porphyritic, panidiomorphic, crystals rich | Cpx, scarce Ol altered to talc | Cpx, Bt, Fe-Ti oxides | Scarce. Carbonate-analcime compositions | Not observed |
| | BYA 124a | sill-multiple intrusions | | porphyritic, panidiomorphic, crystals rich | Strongly zoned titanian Cpx, Bt, scarce Ol | Cpx, Bt | Scarce. Carbonate compositions | Not observed |
| | BYA 125 | sill | | porphyritic | Not observed. Completely altered to Fe-Ti oxides | Not observed. Completely altered to Fe-Ti oxides | Not observed | Not observed |
| | BYA 126 | dyke | | porphyritic, panidiomorphic | Amph, Cpx, Bt | Amph, Bt | Not observed | Abundant. Horblendite compositions |
| | BYA 127 | dyke | | porphyritic, panidiomorphic, cpx glomeroporphyritic | Ol, Cpx | Cpx, Bt | Abundant. Carbonate compositions | Not observed |
| ***Huichaira*** | BHU 131 | sill | Turbidites of Puncoviscana Formation | porphyritic-panidiomorphic-glomeroporphyritic | Cpx, Ol (altered to carbonate and talc), Bt | Bt, Fe-Ti oxides | Abundant. Carbonate-analcime, carbonate and cpx compositions. Segregations | Not observed |

## The Río Grande Dykes and Sills

The rocks investigated here are 30-40 cm-thick concordant to discordant in relation with the host Puncoviscana rocks and are folded (Fig. 2) according to the regional structures. Detailed lithological and petrographic characteristics are described in Table 1.

The best exposures of sills and dykes are in the ***Yacoraite Valley***, where two textural varieties have been identified: (i) dykes with aphanitic to porphiritic textures with clinopyroxene phenocrysts (Fig. 2 A) and (ii) dykes with mica flakes and amphibole macrocrysts up to 1 cm together with abundant xenoliths (Fig. 2 B, C) concentrated along bands, (e.g. sample P8), indicating flow differentiation (Currie and Ferguson, 1970, Rock, 1987, Rock, 1991). Almost all dykes display a well developed 5-10 cm thick chilled margin and produce thermal metamorphism and bleaching of the host pelites (Fig. 2 A). This suggests that these rocks were emplaced into a relatively cool basement at upper- to medium- crustal levels (Delor and Rock, 1991). The presence of chilled margin inside the BYA 124 dyke, indicate multiple intrusions (Fig. 2 D) or flow differentiation. The multiple intrusions are a typical feature associated with distensive settings.

In the ***Coraya Valley*** the length/width ratios of dykes are smaller than that of the *Yacoraite valley*. Some dykes display chilled margins and contain fragments of thermometamorphosed pelite (Fig. 2 E). The dykes are strongly altered and their mineralogy is only recognized by crystals habit; the most common rock type is formed by euhedral olivine and pyroxene phenocrysts up to 2 mm in size in a fine-grained green groundmass.

In the ***Huichaira Valley***, the sedimentary sequence is completely fractured making it difficult to follow up and characterize individual dykes. Columnar joints and the spotted appearance of rocks, due to red glomeroporphyritic aggregates or individual crystals of altered olivine, are very common.

**Figure 2:** typical field features of the Río Grande dykes and sills. A) Typical aspect of the Río Grande dykes. They display chilled margin (Ch mg) and the host rocks appear blanked. B) Flow differentiation of mica, amphibole and xenoliths. C) Example of subvolcanic rocks from the Yacoraite Valley. They are partially concordant with the Puncoviscana Formation. D) Zoned internal structures by multiple intrusions. The $dyk_2$ occur inside the $dyk_1$, and the chilled margin (Ch mg) in the border of $dyk_2$; indicate that this was generated in a second time. E) Concordant dykes with thermometamorphic pelite (Pl) inside, from the Coraya locality. The scale has 25 cm.

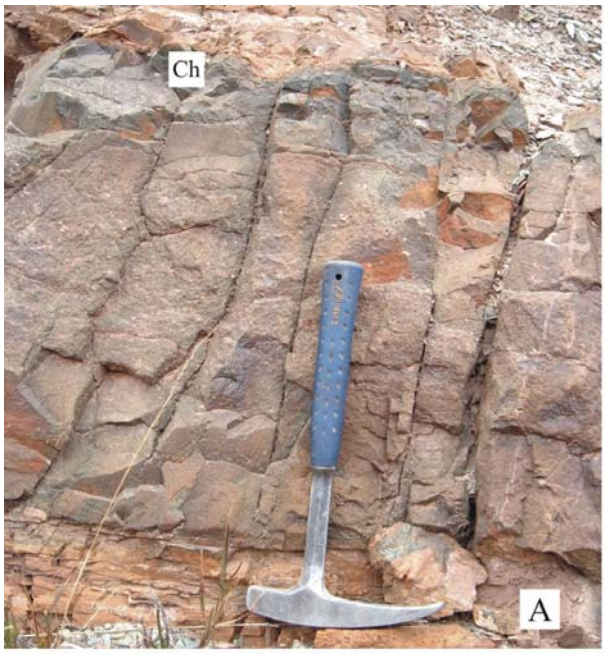
Ch
A


B

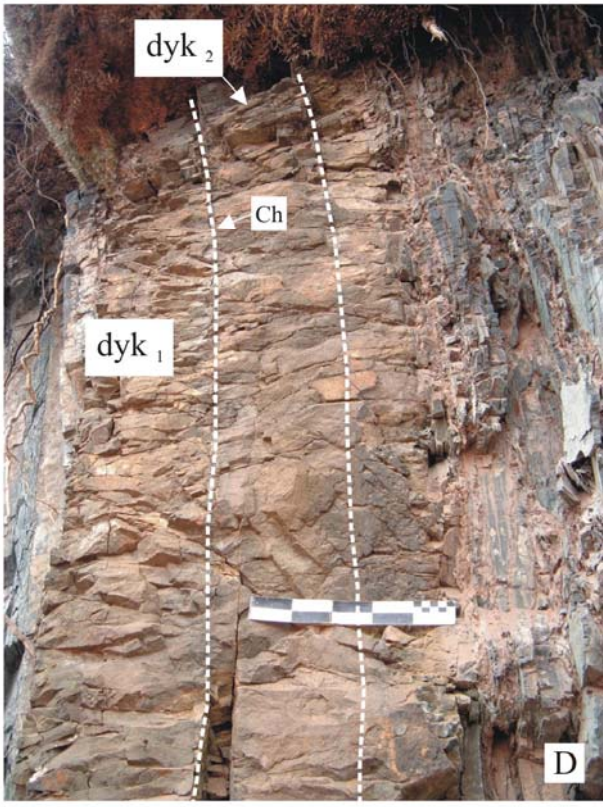
dyk 2
Ch
dyk 1
D


C

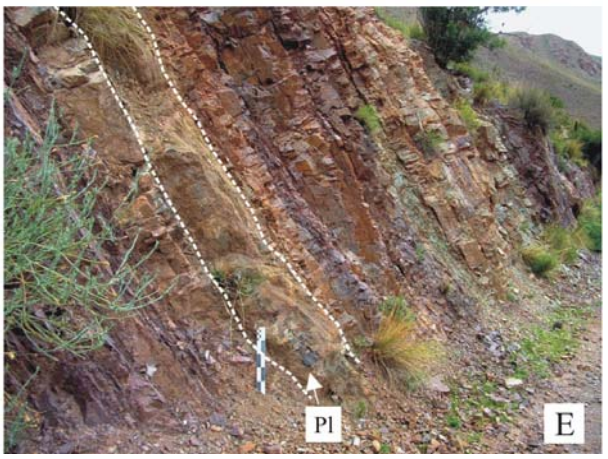
Pl
E

# 3. Petrography

## 3.1. The Río Grande Lamprophyres

The ***Coraya Valley*** rocks are characterized by porphyritic, panidiomorphic texture with phenocrysts of olivine and pyroxene, almost completely replaced by calcite and serpentine, with pseudo-hexagonal and pseudo-octagonal outlines. The phenocrysts represent approximately 25% of the rock. The groundmass is altered to carbonate and is characterized by the presence of abundant biotite and minor Fe-Ti oxide crystals. These latter also occur as poikilitic inclusions in the rims of olivine and pyroxene phenocrysts.

The ***Yacoraite and Huichaira Valleys*** rocks display porphyritic to seriate, panidiomorphic textures, globular structures and crustal-mantle xenoliths. Two groups of rocks are recognized.

The first group, represented by samples BYA 123, 124, 127 and BHU 131 (Table 1)**,** is characterized by the presence of zoned Ti-rich clinopyroxene and olivine phenocrysts (Fig. 3 A). Samples BYA 127 and BHU 131 show abundant olivine phenocrysts (Fig. 3 B) whereas samples BYA 123, 124 exhibit predominant clinopyroxene phenocrysts, in both cases they are immersed in a groundmass made of small prismatic crystals of diopside and abundant phlogopite (Fig. 3 B). Globular structures made of carbonate and analcime are common (Fig. 3 I, J). In this group poikilitic phenocrysts of *clinopyroxene with olivine inclusions* are observed (Fig. 3G)**.**

The second group is represented by samples P8 and BYA 126 (Table 1), from the Yacoraite Valley. This group is characterized by zoned amphibole, clinopyroxene and phogopite phenocrysts together with apatite microphenocrysts (Fig. 3 C, D). Abundant xenoliths also occur. The groundmass is made of carbonate enclosing abundant microliths of biotite, amphibole and apatite (Fig. 3 D). In sample P8, two types of clinopyroxene are present: the first is euhedral to subhedral, has green cores, pale pink rims and is often surrounded by analcime; the second type is anhedral, colourless. Similarly, two distinct varieties of amphibole phenocrysts are recognized (Fig. 3 D). One shows zonating from brown core to pale brown rim and the other displays zonating from green core to pale brown rim. Phlogopite phenocrysts exhibit strong zonating with dark brown core and pale brown rims.

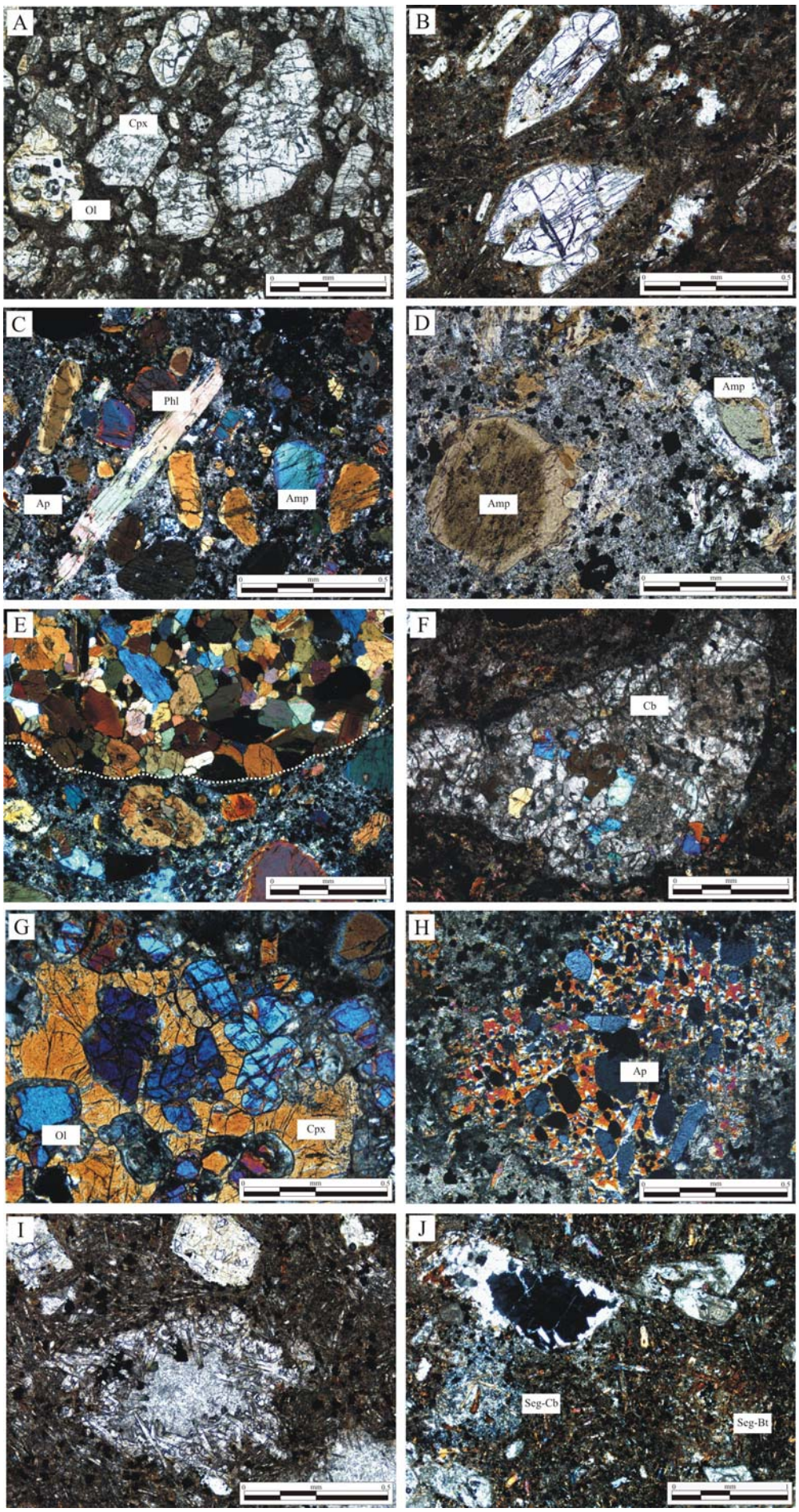
A
Cpx
Ol
B
C
Phl
Ap
Amp
D
Amp
Amp
E
F
Cb
G
Ol
Cpx
H
Ap
I
J
Seg-Cb
Seg-Bt

**Figure 3:** Photomicrographs of several features exhibited by the Río Grande subvolcanic rocks. A) Euhedral and strongly zoned clinopyroxene crystals (Cpx) and minor amounts of euhedral olivine crystals (Ol). Note the high crystals/groundmass proportions. B) Euhedral olivine phenocrysts in a groundmass. These commonly show unstable features as embayment. The groundmass is composed by abundant clinopyroxene and biotite crystals. In this photomicrograph is observed also the Type-III ocelli, completely formed by carbonate. C) Abundant zoned amphibole (Amp)/biotite (Bt) phenocrysts and apatite (Ap) as microphenocrysts characterized the dyke of sample p8. D) The two commonly amphibole types presented. Note the high carbonate and mica concentrations in the groundmass. E) Hornblendite-xenolith with slight mosaic texture. F) Carbonatite-like xenolith. G) Phenocrysts of diopside (Cpx) with inclusion of olivine crystals (Ol). H) Phenocrystal of augite enclosing poikilitically apatite (Ap) crystals. I) Characteristics of ***Type-I ocelli***, concentric zones of carbonate surrounded by radial diopside crystals. J) The ***Type-II ocelli*** and segregations. This ocelli type is marked by analcime forming the central pool surrounded by carbonate. The segregations are characterized by high concentrations of biotite microphenocrysts (Seg-bt) or by high concentrations of carbonate (Seg-Cb).

This group also contains large amounts of varied types of macrocrysts and minor carbonatite-like and hornblendite xenoliths. The *hornblendite xenolith*s (Fig. 3 E) are of variable size (2 mm to 6 cm), rounded to planar. They consist mainly of brown unzoned amphibole and minor brown biotite and clinopyroxene. They display (crystaloblastic polygonal) textures. The *clinopyroxene-bearing carbonate xenoliths* (Fig. 3 F) are small (5 mm in diameter) and dolomite-rich. Minor clinopyroxene and Fe-Ti oxide crystals are also present. Triple junctions between crystals of clinopyroxene and carbonate are observed. The *clinopyroxene phenocrysts with apatite inclusions* (Fig. 3 H) range from 0.5 to 1 mm.

## 3.2 Globular structures

One characteristic feature of the Río Grande subvolcanic rocks is the presence of ocelli and segregations (Rock, 1991, Fareeddudin, 2001, Azbej, 2006). In the sense of Rock (1991), ocelli are sub-rounded; leucocratic structures and whenever they show no clear limits and grade into their host they may be called “segregations” (Rock 1979, 1991). The ocelli, show globular shapes, display rounded to elongated forms and are approximately 1.0 mm in diameter. Three types of ocelli have been recognized according to their mineral compositions. (i) *Type-I ocelli* have globular to elongated carbonate cores surrounded by radial clinopyroxene and some acicular apatite crystals. The contact between this and their host is invariably sharp Fig. 3 I. (ii) *Type-II* (Fig. 3 J) *ocelli* is more abundant and characterized by analcime surrounded by carbonate crystals and occasionally biotite crystals occur in the rim or inside of ocelli. The contact between this type of ocelli and the host groundmass is marked by carbonate-rich and biotite-poor segregations. The *Type-III ocelli* (Fig. 3 B) are very common

and made of carbonate occasionally surrounded by biotite or Ti-Fe oxide. Besides these three ocelli types, two varieties of segregations have been identified. One type is characterized by the red colour and conspicuous presence of Ti-rich biotite (Seg-Bt) (Fig. 3 J). The other type is richer in carbonate (Seg-Cb) (Fig. 3 J) and also includes biotite crystals. This type is commonly in contact with the ocelli.

Ocelli and segregations have been described in a variety of rock type including basalt (Upton and Wadsworth, 1971), spilite (Smith, 1967), picrite (Drever, 1960) and tholeiitic dolerite (Nakamura and Coombs, 1973), but they are most commonly found in lamprophyres (e.g. Ferguson and Currie, 1971, Cooper, 1979; Phillips, 1968; Philpotts, 1972, 1976, Strong and Harris, 1974; Foley, 1984; Rock, 1991). The large amount of ocelli in the studied rocks suggests high volatile content of the original magma. In the three types of ocelli identified, the predominance of carbonate minerals over biotite or amphibole in some samples, suggests that $CO_2$ dominate over $H_2O$ in the gas phase (Nedli and Tóth, 2007).

## 4. Mineral chemistry

The chemical composition of minerals of the Río Grande lamprophyres was obtained with an electron microprobe CAMECABAX SX 50 at the Electron Probe Laboratory of the Universidade de Brasilia. Analytical conditions include beam current of 10 nÅ, beam energy of 15 KeV and a spot size of 1 μm. Acquisition time was 10s. Each element was standardized using either synthetic or natural minerals. Mineral chemistry studies were carried out for olivine, clinopyroxene, amphibole, mica, analcime, apatite and carbonate minerals.

### *Olivine*

Representative chemical analyses of olivine crystals of samples 124a and 127 from the Yacoraite Valley are given in Table 2. The analyses were carried out both on phenocrysts and xenoliths. All analyzed olivine crystals contain 76 to 86 % of forsterite.

Phenocrysts in sample BYA 127 show a slight decrease in forsterite content from cores (86 %) to rims (84 %) however; in general, all phenocrysts, microphenocrysts and xenolith crystals have rather homogeneous compositions.

### *Clinopyroxene*

The analyses of clinopyroxene crystals from the Río Grande rocks are shown in Tables 3 A, B. The analyzed crystals are phenocrysts-microphenocrysts, groundmass crystals, as well as microinclusions in amphibole. Crystals present in the clinopyroxene-bearing carbonate

*Table 2: Representative electron microprobe analyses of olivine minerals from the Rio Grande subvolcanic rocks*

| | *Phenocrysts* | | | | | | | | | | | *Microph* | *in poikilitic clinopyroxene phenocryst* |
|---|---|---|---|---|---|---|---|---|---|---|---|---|---|
| | Rim | | | Intermediate | | | Core | | | | | | |
| | 1 | 2 | 3 | 1 | 2 | 3 | 1 | 2 | 3 | ***4*** | ***5*** | 6 | ***7*** |
| $SiO_2$ | 40.32 | 39.47 | 39.52 | 40.21 | 39.59 | 38.87 | 40.22 | 39.66 | 39.38 | 39.49 | 38.06 | 40.42 | 39.60 |
| $TiO_2$ | 0.05 | 0.07 | 0.00 | 0.01 | 0.01 | 0.03 | 0.02 | 0.01 | 0.05 | 0.02 | 0.03 | 0.03 | 0.03 |
| $Al_2O_3$ | 0.08 | 0.01 | 0.02 | 0.02 | 0.03 | 0.03 | 0.05 | 0.05 | 0.06 | 0.01 | 0.02 | 0.03 | 0.07 |
| $FeO_{(t)}$ | 15.00 | 15.08 | 15.03 | 13.05 | 14.11 | 18.94 | 13.20 | 13.10 | 19.14 | 17.04 | 21.96 | 14.97 | 14.28 |
| *MnO* | 0.22 | 0.25 | 0.26 | 0.15 | 0.12 | 0.24 | 0.18 | 0.12 | 0.24 | 0.22 | 0.31 | 0.18 | 0.19 |
| *MgO* | 44.02 | 44.12 | 43.70 | 45.56 | 44.79 | 41.14 | 45.21 | 45.68 | 41.16 | 42.86 | 39.05 | 44.36 | 44.50 |
| *CaO* | 0.42 | 0.40 | 0.38 | 0.21 | 0.26 | 0.15 | 0.24 | 0.23 | 0.11 | 0.31 | 0.13 | 0.33 | 0.21 |
| $Cr_2O_3$ | 0.08 | 0.09 | 0.05 | 0.04 | 0.04 | 0.03 | 0.03 | 0.07 | 0.01 | 0.01 | 0.01 | 0.00 | 0.03 |
| *NiO* | 0.19 | 0.15 | 0.20 | 0.32 | 0.21 | 0.21 | 0.31 | 0.20 | 0.16 | 0.29 | 0.18 | 0.24 | 0.30 |
| $K_2O$ | 0.00 | 0.00 | 0.01 | 0.01 | 0.01 | 0.01 | 0.01 | 0.01 | 0.00 | 0.01 | 0.00 | 0.01 | 0.00 |
| *Total* | 100.38 | 99.63 | 99.16 | 99.58 | 99.17 | 99.64 | 99.46 | 99.13 | 100.30 | 100.25 | 99.75 | 100.56 | 99.20 |
| ***FO*** | ***84.24*** | ***84.14*** | ***84.03*** | ***86.27*** | ***85.18*** | ***79.44*** | ***86.04*** | ***86.30*** | ***79.22*** | ***81.92*** | ***75.89*** | ***84.30*** | ***84.82*** |
| ***FA*** | ***16.11*** | ***16.13*** | ***16.21*** | ***13.86*** | ***15.05*** | ***20.52*** | ***14.10*** | ***13.88*** | ***20.67*** | ***18.28*** | ***23.94*** | ***15.95*** | ***15.27*** |
| ***mg#*** | ***0.75*** | ***0.75*** | ***0.74*** | ***0.78*** | ***0.76*** | ***0.68*** | ***0.77*** | ***0.78*** | ***0.68*** | ***0.72*** | ***0.64*** | ***0.75*** | ***0.76*** |

xenolith have been also analyzed. According to the nomenclature proposed by Morimoto et al., (1988), all the analyzed crystals belong to the calcic series.

Most of them fall in the Fe-diopside field but some macrocrysts and those in clinopyroxene-bearing carbonate xenoliths plot in the Mg-augite field (Fig. 4 A). The diopside grains are characterized by wollastonite contents of 45-52%, whereas the augite grains have wollastonite contents of 39-45%.

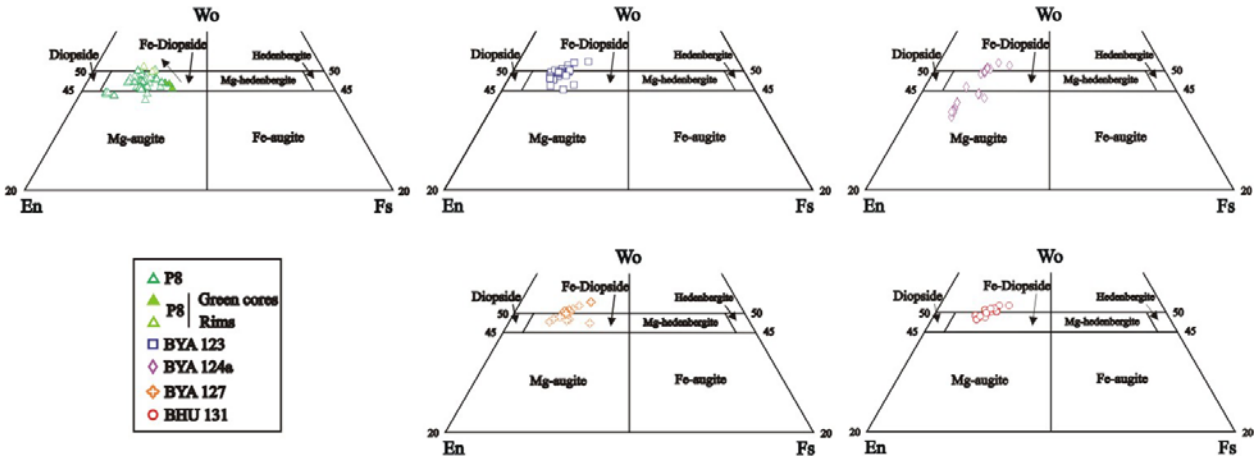


**Figure 4:** Representative pyroxene and olivine compositions of the Río Grande subvolcanic rocks. Wollastonite (Wo)-Enstatite (En)-Ferrosilite (Fs) classification diagram after Morimoto et al., (1988). They are calcic clinopyroxene, almost all of them fall in the field of Fe-diopside but samples P8 and BYA 124a also fall in the Mg-augite field.

Zoned phenocrysts with green cores and white rims have been recognized only in sample P8. They are characterized by lowest Ti and highest Na contents compared with the diopside crystals from other samples. The cores (green) of these crystals are characterized by the highest $Na_2O$ contents (~2.5 wt. %), and the lowest mg# (~67) showing reverse zoning (increasing mg#, decreasing Na from core to rim). The cores of white diopside are less sodic (<2.5 wt. %), present higher mg# (~78) (Table 3 B) and show normal zoning (decreasing mg#, increasing Na from core to rim). Both groups show similar rim compositions with intermediate $Na_2O$ and mg# (~74) values. In the rest of samples, clinopyroxene have increasing Ti content from the core to the rim and some crystal rims are classified as Titanian-

*Table 3 A: Representative electron microprobe analyses of clinopyroxene minerals from samples BYA 123, 124, 127 and BHU 131 of the Rio Grande subvolcanic rocks*

| | *Phenocrysts* | | | | | | *Mesophenocrysts* | | | | | | | | | | *Poikilitic cpx with olv inclusions* | *Glomer* | *Ocelli* |
|---|---|---|---|---|---|---|---|---|---|---|---|---|---|---|---|---|---|---|---|
| | Rim | | Inter | | Core | | Rim | | Inter | Core | | Rim | | Inter | Core | | | | |
| | 1 | 2 | 1 | 2 | 1 | 2 | 3 | 4 | 4 | 3 | 4 | 5 | 6 | 5 | 5 | 6 | 7 | 8 | 9 |
| $SiO_2$ | 46.36 | 51.47 | 49.45 | 46.90 | 47.12 | 52.21 | 47.44 | 47.98 | 44.97 | 46.38 | 48.17 | 43.65 | 40.55 | 50.03 | 49.42 | 46.37 | 51.40 | 47.62 | 52.05 |
| $TiO_2$ | 2.76 | 0.70 | 1.41 | 2.68 | 2.16 | 0.34 | 2.81 | 2.78 | 3.49 | 3.01 | 2.73 | 4.79 | 5.51 | 1.86 | 1.75 | 3.20 | 0.85 | 2.42 | 1.44 |
| $Al_2O_3$ | 6.06 | 4.61 | 5.25 | 5.39 | 8.45 | 4.32 | 5.56 | 4.63 | 6.97 | 5.85 | 4.59 | 7.99 | 9.92 | 3.36 | 3.45 | 5.88 | 5.69 | 5.03 | 2.06 |
| $FeO_{(t)}$ | 7.36 | 5.36 | 5.07 | 6.67 | 6.02 | 5.47 | 6.55 | 6.79 | 7.14 | 7.15 | 6.81 | 7.52 | 8.46 | 5.56 | 5.91 | 6.50 | 5.17 | 6.77 | 6.41 |
| $MnO$ | 0.08 | 0.09 | 0.09 | 0.13 | 0.10 | 0.15 | 0.14 | 0.08 | 0.10 | 0.10 | 0.10 | 0.13 | 0.09 | 0.11 | 0.07 | 0.09 | 0.07 | 0.15 | 0.15 |
| $MgO$ | 12.82 | 16.44 | 14.14 | 12.75 | 12.67 | 17.02 | 13.37 | 13.42 | 12.08 | 13.06 | 13.76 | 11.58 | 10.51 | 14.41 | 14.36 | 12.98 | 15.87 | 13.39 | 14.03 |
| $CaO$ | 23.65 | 19.51 | 23.25 | 23.50 | 22.71 | 18.42 | 24.13 | 23.91 | 23.35 | 23.61 | 23.63 | 23.59 | 22.75 | 23.59 | 22.94 | 23.10 | 18.92 | 22.75 | 23.56 |
| $Cr_2O_3$ | 0.08 | 0.35 | 0.79 | 0.00 | 0.21 | 0.52 | 0.00 | 0.01 | 0.18 | 0.03 | 0.13 | 0.01 | 0.02 | 0.47 | 0.24 | 0.39 | 0.72 | 0.11 | 0.67 |
| $Na_2O$ | 0.16 | 0.76 | 0.74 | 0.30 | 0.56 | 0.90 | 0.26 | 0.72 | 0.25 | 0.26 | 0.39 | 0.54 | 0.80 | 0.40 | 0.48 | 0.42 | 0.94 | 0.49 | 0.01 |
| $K_2O$ | 0.01 | 0.02 | 0.01 | 0.00 | 0.00 | 0.02 | 0.01 | 0.01 | 0.01 | 0.02 | 0.01 | 0.01 | 0.01 | 0.00 | 0.02 | 0.00 | 0.02 | 0.05 | 0.02 |
| *Total* | 99.73 | 99.50 | 100.60 | 98.59 | 100.21 | 99.55 | 100.65 | 100.90 | 98.88 | 99.96 | 100.72 | 100.33 | 99.37 | 100.02 | 98.95 | 99.26 | 99.70 | 99.16 | 100.55 |
| | | | | | | | | | | | | | | | | | | | |
| ***FeO*** | 3.92 | 4.17 | 1.82 | 4.15 | 3.93 | 4.37 | 3.13 | 1.87 | 4.20 | 3.20 | 3.30 | 2.98 | 1.73 | 3.60 | 3.30 | 3.57 | 5.15 | 3.52 | 5.05 |
| $Fe_2O_3$ | 3.82 | 1.32 | 3.60 | 2.80 | 2.32 | 1.22 | 3.80 | 5.47 | 3.27 | 4.38 | 3.90 | 5.06 | 7.47 | 2.18 | 2.90 | 3.26 | 0.02 | 3.61 | 1.51 |
| **Structural formula based on 6 oxygens** | | | | | | | | | | | | | | | | | | | |
| **Si** | 1.74 | 1.89 | 1.81 | 1.77 | 1.74 | 1.91 | 1.76 | 1.77 | 1.70 | 1.73 | 1.78 | 1.64 | 1.54 | 1.85 | 1.85 | 1.74 | 1.88 | 1.79 | 1.92 |
| **Al z** | 0.26 | 0.11 | 0.19 | 0.23 | 0.26 | 0.09 | 0.24 | 0.20 | 0.30 | 0.26 | 0.20 | 0.35 | 0.44 | 0.15 | 0.15 | 0.26 | 0.12 | 0.21 | 0.08 |
| **Fe3+** | 0.00 | 0.00 | 0.00 | 0.00 | 0.00 | 0.00 | 0.00 | 0.03 | 0.00 | 0.01 | 0.02 | 0.01 | 0.01 | 0.00 | 0.00 | 0.00 | 0.00 | 0.00 | 0.00 |
| ***Sitio T*** | **2.00** | **2.00** | **2.00** | **2.00** | **2.00** | **2.00** | **2.00** | **2.00** | **2.00** | **2.00** | **2.00** | **2.00** | **2.00** | **2.00** | **2.00** | **2.00** | **2.00** | **2.00** | **2.00** |
| **Al $^{VI}$** | 0.01 | 0.08 | 0.04 | 0.01 | 0.11 | 0.09 | 0.00 | 0.00 | 0.02 | 0.00 | 0.00 | 0.00 | 0.00 | 0.00 | 0.00 | 0.00 | 0.12 | 0.01 | 0.01 |
| **Ti** | 0.08 | 0.02 | 0.04 | 0.08 | 0.06 | 0.01 | 0.08 | 0.08 | 0.10 | 0.08 | 0.08 | 0.14 | 0.16 | 0.05 | 0.05 | 0.09 | 0.02 | 0.07 | 0.04 |
| **Fe3+** | 0.11 | 0.03 | 0.10 | 0.08 | 0.07 | 0.03 | 0.11 | 0.12 | 0.09 | 0.11 | 0.09 | 0.13 | 0.20 | 0.06 | 0.08 | 0.09 | 0.00 | 0.10 | 0.04 |
| **Fe2+** | 0.12 | 0.13 | 0.06 | 0.13 | 0.12 | 0.13 | 0.10 | 0.06 | 0.13 | 0.10 | 0.10 | 0.09 | 0.05 | 0.11 | 0.10 | 0.11 | 0.16 | 0.11 | 0.16 |
| **Mn** | 0.00 | 0.00 | 0.00 | 0.00 | 0.00 | 0.00 | 0.00 | 0.00 | 0.00 | 0.00 | 0.00 | 0.00 | 0.00 | 0.00 | 0.00 | 0.00 | 0.00 | 0.00 | 0.00 |
| **Mg** | 0.72 | 0.90 | 0.77 | 0.72 | 0.70 | 0.93 | 0.74 | 0.74 | 0.68 | 0.73 | 0.76 | 0.65 | 0.60 | 0.80 | 0.80 | 0.73 | 0.86 | 0.75 | 0.77 |
| **Cr** | 0.00 | 0.01 | 0.02 | 0.00 | 0.01 | 0.02 | 0.00 | 0.00 | 0.01 | 0.00 | 0.00 | 0.00 | 0.00 | 0.01 | 0.01 | 0.01 | 0.02 | 0.00 | 0.00 |
| ***Sitio O*** | **1.04** | **1.18** | **1.03** | **1.03** | **1.06** | **1.21** | **1.02** | **1.00** | **1.03** | **1.03** | **1.03** | **1.01** | **1.01** | **1.04** | **1.05** | **1.04** | **1.19** | **1.05** | **1.02** |
| **Ca** | 0.95 | 0.77 | 0.91 | 0.95 | 0.90 | 0.72 | 0.96 | 0.95 | 0.95 | 0.95 | 0.94 | 0.95 | 0.93 | 0.94 | 0.92 | 0.93 | 0.74 | 0.91 | 0.93 |
| **Na** | 0.01 | 0.05 | 0.05 | 0.02 | 0.04 | 0.06 | 0.02 | 0.05 | 0.02 | 0.02 | 0.03 | 0.04 | 0.06 | 0.03 | 0.03 | 0.03 | 0.07 | 0.04 | 0.05 |
| **K** | 0.00 | 0.00 | 0.00 | 0.00 | 0.00 | 0.00 | 0.00 | 0.00 | 0.00 | 0.00 | 0.00 | 0.00 | 0.00 | 0.00 | 0.00 | 0.00 | 0.00 | 0.00 | 0.00 |
| ***Sitio C*** | **0.96** | **0.82** | **0.97** | **0.97** | **0.94** | **0.79** | **0.98** | **1.00** | **0.97** | **0.97** | **0.97** | **0.99** | **0.99** | **0.96** | **0.95** | **0.96** | **0.81** | **0.95** | **0.98** |
| | | | | | | | | | | | | | | | | | | | |
| ***Wo*** | **50.06** | **41.89** | **49.59** | **50.59** | **50.42** | **39.72** | **49.86** | **49.93** | **51.06** | **50.44** | **49.12** | **51.76** | **51.73** | **49.16** | **48.25** | **49.95** | **42.00** | **48.75** | **49.00** |
| ***En*** | **37.77** | **49.13** | **41.98** | **38.20** | **39.14** | **51.07** | **38.87** | **39.00** | **36.76** | **38.37** | **39.82** | **35.36** | **33.25** | **41.79** | **42.04** | **39.07** | **49.05** | **39.93** | **40.60** |
| ***Fs*** | **12.17** | **8.98** | **8.43** | **11.20** | **10.43** | **9.21** | **10.69** | **11.07** | **12.18** | **11.78** | **11.06** | **12.89** | **15.01** | **9.05** | **9.71** | **10.97** | **8.96** | **11.33** | **10.41** |
| **mg#*** | **75.63** | **84.54** | **83.27** | **77.32** | **78.96** | **84.72** | **78.44** | **77.90** | **75.11** | **76.51** | **78.27** | **73.29** | **68.90** | **82.20** | **81.24** | **78.07** | **84.56** | **77.90** | **79.59** |

*mg# =100*Mg/(Mg+Fetot)

*Table 3B: Representative electron microprobe analyses of clinopyroxene minerals from sample P8, Río Grande subvolcanic rocks.*

| | **Phenocryst** | | | | | | | | **Microph** | | **Incl** | **Xenoliths**** | | | **Poikilitic phenocryst***** |
|---|---|---|---|---|---|---|---|---|---|---|---|---|---|---|---|
| | *Green cpx* | | | | *White cpx* | | | | | | | | | | |
| | Rim | | Core | | Rim | | Core | | | | | | | | |
| | 1 | 2 | 1 | 2 | 3 | 4 | 3 | 4 | 5 | 6 | 7 | 8 | 9 | 10 | 11 |
| $SiO_2$ | 48.00 | 46.44 | 51.91 | 51.34 | 48.26 | 46.85 | 52.10 | 50.81 | 53.27 | 51.41 | 53.11 | 53.64 | 53.50 | 53.03 | 52.18 |
| $TiO_2$ | 1.52 | 3.06 | 0.54 | 0.80 | 1.60 | 2.34 | 0.87 | 1.09 | 0.25 | 0.42 | 0.37 | 0.15 | 0.48 | 0.19 | 0.23 |
| $Al_2O_3$ | 5.50 | 6.84 | 3.27 | 3.21 | 4.80 | 6.73 | 3.96 | 5.68 | 1.36 | 4.54 | 1.30 | 4.00 | 4.23 | 0.95 | 1.88 |
| $FeO_{(t)}$ | 7.67 | 6.37 | 9.53 | 10.24 | 7.79 | 7.82 | 6.80 | 6.73 | 7.63 | 7.89 | 7.35 | 3.31 | 4.38 | 7.37 | 8.89 |
| *MnO* | 0.14 | 0.06 | 0.19 | 0.22 | 0.16 | 0.20 | 0.15 | 0.12 | 0.21 | 0.16 | 0.31 | 0.06 | 0.14 | 0.19 | 0.23 |
| *MgO* | 12.46 | 13.13 | 11.21 | 11.12 | 12.73 | 11.95 | 14.15 | 13.53 | 13.43 | 12.65 | 13.78 | 16.07 | 15.50 | 14.01 | 14.08 |
| *CaO* | 22.81 | 23.92 | 20.06 | 20.30 | 22.64 | 22.66 | 20.94 | 20.71 | 20.90 | 21.60 | 21.06 | 19.33 | 19.20 | 20.95 | 19.47 |
| $Cr_2O_3$ | 0.02 | 0.00 | 0.00 | 0.03 | 0.01 | 0.05 | 0.55 | 0.30 | 0.20 | 0.00 | 0.07 | 1.11 | 0.84 | 0.15 | 0.01 |
| *NiO* | 0.00 | 0.03 | 0.08 | 0.00 | 0.00 | 0.05 | 0.00 | 0.00 | 0.00 | 0.03 | 0.05 | 0.06 | 0.03 | 0.01 | 0.02 |
| $Na_2O$ | 0.82 | 0.44 | 2.51 | 2.35 | 0.53 | 0.89 | 1.24 | 1.37 | 2.06 | 1.15 | 1.65 | 1.71 | 2.09 | 1.50 | 1.72 |
| $K_2O$ | 0.00 | 0.01 | 0.00 | 0.02 | 0.00 | 0.02 | 0.00 | 0.02 | 0.02 | 0.00 | 0.02 | 0.01 | 0.02 | 0.02 | 0.01 |
| *Total* | 99.41 | 100.77 | 99.80 | 100.19 | 98.83 | 100.07 | 100.95 | 100.58 | 99.81 | 100.02 | 99.40 | 99.52 | 100.64 | 98.68 | 99.21 |
| ***FeO*** | 3.40 | 2.14 | 5.08 | 5.11 | 4.85 | 3.34 | 5.13 | 4.59 | 3.38 | 6.10 | 4.25 | 2.86 | 2.25 | 4.57 | 4.32 |
| ***$Fe_2O_3$*** | 4.75 | 4.70 | 4.97 | 5.70 | 3.27 | 4.98 | 1.85 | 2.38 | 4.73 | 1.95 | 3.45 | 0.50 | 2.37 | 3.11 | 5.08 |
| **Structural formula based on 6 oxygens** | | | | | | | | | | | | | | | |
| **Si** | 1.80 | 1.72 | 1.93 | 1.91 | 1.82 | 1.75 | 1.90 | 1.86 | 1.97 | 1.90 | 1.97 | 1.95 | 1.93 | 1.98 | 1.94 |
| **Al $^{IV}$** | 0.20 | 0.28 | 0.07 | 0.09 | 0.18 | 0.25 | 0.10 | 0.14 | 0.03 | 0.10 | 0.03 | 0.05 | 0.07 | 0.02 | 0.06 |
| **$Fe^{3+}$** | 0.00 | 0.00 | 0.00 | 0.00 | 0.00 | 0.00 | 0.00 | 0.00 | 0.00 | 0.00 | 0.00 | 0.00 | 0.00 | 0.00 | 0.00 |
| ***Sitio T*** | **2.00** | **2.00** | **2.00** | **2.00** | **2.00** | **2.00** | **2.00** | **2.00** | **2.00** | **2.00** | **2.00** | **2.00** | **2.00** | **2.00** | **2.00** |
| **Al $^{VI}$** | 0.04 | 0.01 | 0.08 | 0.05 | 0.03 | 0.05 | 0.07 | 0.10 | 0.03 | 0.10 | 0.03 | 0.12 | 0.11 | 0.02 | 0.03 |
| **Ti** | 0.04 | 0.09 | 0.02 | 0.02 | 0.05 | 0.07 | 0.02 | 0.03 | 0.01 | 0.01 | 0.01 | 0.00 | 0.01 | 0.01 | 0.01 |
| **$Fe^{3+}$** | 0.13 | 0.13 | 0.14 | 0.16 | 0.09 | 0.14 | 0.05 | 0.07 | 0.13 | 0.05 | 0.10 | 0.01 | 0.06 | 0.09 | 0.14 |
| **$Fe^{2+}$** | 0.11 | 0.07 | 0.16 | 0.16 | 0.15 | 0.11 | 0.16 | 0.14 | 0.10 | 0.19 | 0.13 | 0.09 | 0.07 | 0.14 | 0.13 |
| **Mn** | 0.00 | 0.00 | 0.01 | 0.01 | 0.01 | 0.01 | 0.00 | 0.00 | 0.01 | 0.00 | 0.01 | 0.00 | 0.00 | 0.01 | 0.01 |
| **Mg** | 0.70 | 0.72 | 0.62 | 0.62 | 0.72 | 0.67 | 0.77 | 0.74 | 0.74 | 0.70 | 0.76 | 0.87 | 0.83 | 0.78 | 0.78 |
| **Cr** | 0.00 | 0.00 | 0.00 | 0.00 | 0.00 | 0.00 | 0.02 | 0.01 | 0.01 | 0.00 | 0.00 | 0.03 | 0.02 | 0.00 | 0.00 |
| ***Sitio O*** | **1.03** | **1.02** | **1.02** | **1.02** | **1.05** | **1.03** | **1.09** | **1.09** | **1.02** | **1.06** | **1.04** | **1.13** | **1.11** | **1.05** | **1.10** |
| **Ca** | 0.92 | 0.95 | 0.80 | 0.81 | 0.92 | 0.91 | 0.82 | 0.81 | 0.83 | 0.86 | 0.84 | 0.75 | 0.74 | 0.84 | 0.78 |
| **Na** | 0.06 | 0.03 | 0.18 | 0.17 | 0.04 | 0.06 | 0.09 | 0.10 | 0.15 | 0.08 | 0.12 | 0.12 | 0.15 | 0.11 | 0.12 |
| **K** | 0.00 | 0.00 | 0.00 | 0.00 | 0.00 | 0.00 | 0.00 | 0.00 | 0.00 | 0.00 | 0.00 | 0.00 | 0.00 | 0.00 | 0.00 |
| ***Sitio C*** | **0.97** | **0.98** | **0.98** | **0.98** | **0.95** | **0.97** | **0.91** | **0.91** | **0.98** | **0.94** | **0.96** | **0.87** | **0.89** | **0.95** | **0.90** |
| ***Wo*** | **49.44** | **50.72** | **46.54** | **46.38** | **48.76** | **49.92** | **45.58** | **46.23** | **45.89** | **47.65** | **45.81** | **43.66** | **43.45** | **45.35** | **42.32** |
| ***En*** | **37.59** | **38.74** | **36.19** | **35.37** | **38.15** | **36.63** | **42.86** | **42.04** | **41.04** | **38.82** | **41.70** | **50.50** | **48.82** | **42.20** | **42.60** |
| ***Fs*** | **12.97** | **10.55** | **17.27** | **18.26** | **13.09** | **13.45** | **11.56** | **11.72** | **13.08** | **13.53** | **12.49** | **5.84** | **7.74** | **12.45** | **15.08** |
| **mg#*** | **74.35** | **78.60** | **67.70** | **65.95** | **74.45** | **73.14** | **78.76** | **78.20** | **75.83** | **74.15** | **76.96** | **89.64** | **86.32** | **77.22** | **73.86** |

*mg# =100*Mg/(Mg+Fetot)

**Xenoliths: 8 and 9, from cpx-bearing carbonate xenolith and 10, amphibole-cpx xenolith and *** Poikilitic phenocrytal with apatite inclusions.

diopside (> 0.10 Ti apfu). In the clinopyroxene-bearing carbonate xenolith, augite crystals are classified as chromian-sodian augite, they have the highest $Cr_2O_3$ content (up 1.1 wt. %) and mg# (~90) (Table 3B). In the $Al_2O_3$/mg# vs. $TiO_2$ diagram (Fig. 5 A) clinopyroxene crystals from samples BYA127 and BHU131 display higher $TiO_2$ contents, compared to pyroxenes in sample P8. Clinopyroxenes of samples BYA123 and 124 seem to be intermediate in composition between the two trends above.

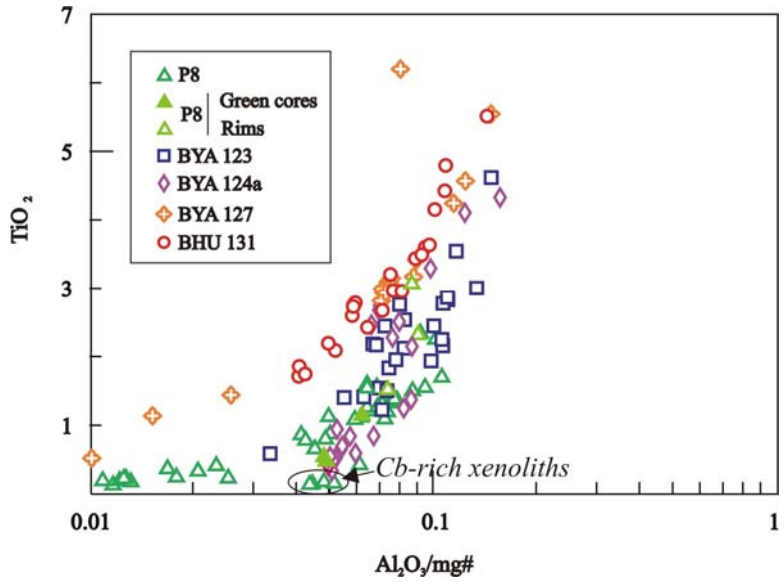


**Figure 5:** $Al_2O_3$/ mg# vs. $TiO_2$ diagram showing the compositions of clinopyroxene crystals. In this diagram are observed two groups of clinopyroxens, differentiated for the $TiO_2$ contents.

### *Amphibole*

Representative analyses of amphibole crystals are presented in Table 4. This mineral was recognized only in sample P8. The analyses were carried out on brown and green amphibole phenocrysts and xenolith crystals. According to the classification proposed by

*Table 4: Representative electron microprobe analyses of amphibole minerals from the Rio Grande subvolcanic rocks*

| | *Phenocrysts* | | | | | | | | | *Xenoliths* | |
|---|---|---|---|---|---|---|---|---|---|---|---|
| | *Brown amphibole* | | | | *Green amphibole* | | | | | | |
| | Rim | | Core | | Rim | | Core | | Inter | | |
| | 1 | 2 | 1 | 2 | 3 | 4 | 3 | 4 | 4 | 5 | 6 |
| $SiO_2$ | 41.22 | 40.30 | 40.75 | 40.99 | 40.13 | 41.49 | 41.01 | 42.77 | 41.30 | 43.53 | 44.24 |
| $TiO_2$ | 2.84 | 3.90 | 3.99 | 4.15 | 3.96 | 3.46 | 1.24 | 1.40 | 1.22 | 2.97 | 2.33 |
| $Al_2O_3$ | 12.07 | 13.16 | 12.62 | 12.45 | 12.97 | 11.28 | 14.45 | 13.38 | 14.12 | 11.57 | 10.11 |
| $Fe_2O_3$ | 1.33 | 0.06 | 0.47 | 0.82 | 0.56 | 0.31 | 3.07 | 2.52 | 3.12 | 0.19 | 2.04 |
| $FeO$ | 8.84 | 10.38 | 11.74 | 12.61 | 10.09 | 13.37 | 10.70 | 9.46 | 8.92 | 8.47 | 10.45 |
| $Cr_2O_3$ | 0.00 | 0.03 | 0.07 | 0.00 | 0.01 | 0.07 | 0.00 | 0.00 | 0.01 | 0.47 | 0.21 |
| $MnO$ | 0.17 | 0.14 | 0.13 | 0.17 | 0.14 | 0.24 | 0.25 | 0.30 | 0.23 | 0.10 | 0.20 |
| $MgO$ | 14.57 | 13.41 | 12.19 | 11.67 | 13.69 | 11.48 | 11.13 | 12.80 | 12.54 | 15.27 | 13.79 |
| $CaO$ | 11.90 | 11.99 | 10.64 | 10.58 | 11.94 | 11.24 | 9.63 | 9.76 | 10.14 | 11.39 | 10.10 |
| $Na_2O$ | 2.74 | 2.29 | 2.80 | 2.70 | 2.50 | 3.13 | 4.02 | 3.98 | 3.74 | 3.29 | 4.20 |
| $K_2O$ | 1.42 | 1.99 | 2.11 | 2.00 | 1.90 | 1.86 | 1.06 | 1.33 | 1.29 | 1.25 | 1.15 |
| *Total* | 97.08 | 97.65 | 97.50 | 98.15 | 97.89 | 97.94 | 96.55 | 97.69 | 96.60 | 98.51 | 98.82 |
| **Structural formula based on 23 oxygens** | | | | | | | | | | | |
| **Si** | 6.11 | 5.98 | 6.09 | 6.10 | 5.95 | 6.22 | 6.14 | 6.28 | 6.15 | 6.30 | 6.46 |
| **$Al^{IV}$** | 1.89 | 2.02 | 1.91 | 1.90 | 2.05 | 1.78 | 1.86 | 1.72 | 1.85 | 1.70 | 1.54 |
| **Sum T** | **8.00** | **8.00** | **8.00** | **8.00** | **8.00** | **8.00** | **8.00** | **8.00** | **8.00** | **8.00** | **8.00** |
| **$Al^{VI}$** | 0.22 | 0.28 | 0.31 | 0.29 | 0.21 | 0.22 | 0.69 | 0.60 | 0.62 | 0.28 | 0.20 |
| **$Fe^{3+}$** | 0.15 | 0.01 | 0.05 | 0.09 | 0.06 | 0.04 | 0.35 | 0.28 | 0.35 | 0.02 | 0.22 |
| **Ti** | 0.32 | 0.44 | 0.45 | 0.46 | 0.44 | 0.39 | 0.14 | 0.15 | 0.14 | 0.32 | 0.26 |
| **Cr** | 0.00 | 0.00 | 0.01 | 0.00 | 0.00 | 0.01 | 0.00 | 0.00 | 0.00 | 0.05 | 0.02 |
| **Mg** | 3.22 | 2.97 | 2.72 | 2.59 | 3.03 | 2.57 | 2.49 | 2.80 | 2.78 | 3.29 | 3.00 |
| **$Fe^{2+}$** | 1.09 | 1.29 | 1.47 | 1.57 | 1.25 | 1.68 | 1.33 | 1.16 | 1.11 | 1.03 | 1.28 |
| **Zn** | 0.00 | 0.00 | 0.00 | 0.00 | 0.00 | 0.00 | 0.00 | 0.00 | 0.00 | 0.00 | 0.00 |
| **Mn** | 0.00 | 0.02 | 0.00 | 0.00 | 0.01 | 0.03 | 0.00 | 0.00 | 0.00 | 0.01 | 0.02 |
| **Sum C** | **5.00** | **5.00** | **5.00** | **5.00** | **5.00** | **4.93** | **5.00** | **5.00** | **5.00** | **5.00** | **5.00** |
| **Mg** | 0.00 | 0.00 | 0.00 | 0.00 | 0.00 | 0.00 | 0.00 | 0.00 | 0.00 | 0.00 | 0.00 |
| **$Fe^{2+}$** | 0.00 | 0.00 | 0.00 | 0.00 | 0.00 | 0.00 | 0.01 | 0.00 | 0.00 | 0.00 | 0.00 |
| **Zn** | 0.00 | 0.00 | 0.00 | 0.00 | 0.00 | 0.00 | 0.00 | 0.00 | 0.00 | 0.00 | 0.00 |
| **Mn** | 0.02 | 0.00 | 0.01 | 0.02 | 0.01 | 0.00 | 0.03 | 0.04 | 0.03 | 0.01 | 0.01 |
| **Ca** | 1.89 | 1.91 | 1.70 | 1.69 | 1.90 | 1.81 | 1.54 | 1.54 | 1.62 | 1.77 | 1.58 |
| **Na** | 0.09 | 0.09 | 0.28 | 0.29 | 0.09 | 0.19 | 0.42 | 0.43 | 0.36 | 0.23 | 0.41 |
| **Sum B** | **2.00** | **2.00** | **2.00** | **2.00** | **2.00** | **2.00** | **2.00** | **2.00** | **2.00** | **2.00** | **2.00** |
| **Na** | 0.70 | 0.57 | 0.53 | 0.49 | 0.63 | 0.72 | 0.75 | 0.71 | 0.72 | 0.70 | 0.78 |
| **K** | 0.27 | 0.38 | 0.40 | 0.38 | 0.36 | 0.36 | 0.20 | 0.25 | 0.24 | 0.23 | 0.21 |
| **Sum A** | **0.97** | **0.95** | **0.93** | **0.87** | **0.99** | **1.07** | **0.95** | **0.96** | **0.97** | **0.93** | **0.99** |
| ***$(Ca+Na)_B$*** | ***1.98*** | ***2.00*** | ***1.99*** | ***1.97*** | ***1.99*** | ***2.00*** | ***1.96*** | ***1.96*** | ***1.97*** | ***1.99*** | ***1.99*** |
| ***$Na_B$*** | ***0.09*** | ***0.09*** | ***0.28*** | ***0.29*** | ***0.09*** | ***0.19*** | ***0.42*** | ***0.43*** | ***0.36*** | ***0.23*** | ***0.41*** |
| ***$Ca_B$*** | ***1.89*** | ***1.91*** | ***1.70*** | ***1.69*** | ***1.90*** | ***1.81*** | ***1.54*** | ***1.54*** | ***1.62*** | ***1.77*** | ***1.58*** |
| ***$(Na+K)_A$*** | ***0.97*** | ***0.95*** | ***0.93*** | ***0.87*** | ***0.99*** | ***1.07*** | ***0.95*** | ***0.96*** | ***0.97*** | ***0.93*** | ***0.99*** |
| ***Si*** | ***6.11*** | ***5.98*** | ***6.09*** | ***6.10*** | ***5.95*** | ***6.22*** | ***6.14*** | ***6.28*** | ***6.15*** | ***6.30*** | ***6.46*** |
| ***$Mg/(Mg+Fe^{2+})$*** | ***0.75*** | ***0.70*** | ***0.65*** | ***0.62*** | ***0.71*** | ***0.60*** | ***0.65*** | ***0.71*** | ***0.71*** | ***0.76*** | ***0.70*** |

Leake et al., (1997), the amphibole compositions of sample P8 belong to the calcic group (Fig. 6) with $(Ca+Na)_B > 1.00$ and $Na_B < 0.50$ (fig). All crystals have pargasitic compositions (AlIV>Fe+3) and due to their Ti apfu content (0.25 < Ti < 0.49) these amphiboles are classified as ***"titanian pargasite"***. Only one macrophenocryst is edenite in composition (Si in formula > 6.5).

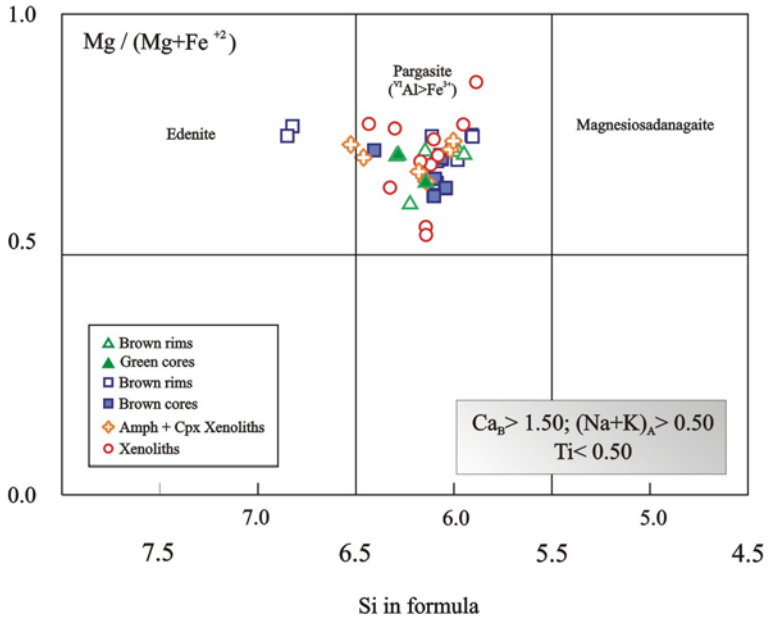


**Figure 6:** Classification diagram for amphiboles after Leake et al., 1997. All crystals are plotted in the calcic amphiboles field and are classified as Titanian-Pargasite.

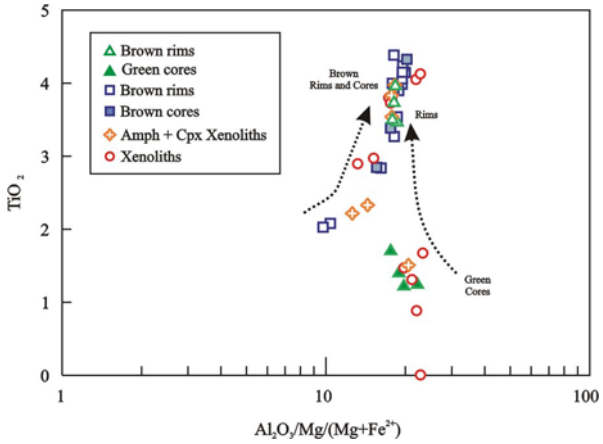


**Figure 7:** $Al_2O_3$/mg# vs. $TiO_2$ diagram shows the lower $TiO_2$ compositions for some green cores and xenoliths crystals. Observed that the rims of crystals with green cores have similar compositions with the brown amphiboles.

Green and brown amphibole show compositional differences in their cores. Green amphibole cores have *mg*# around 0.68, $TiO_2$ contents of approximately 2 % and show higher $Al_2O_3$ (13.0 wt. %), whereas cores of brown amphibole have mg# between 0.63-0.70, $TiO_2$ of 4

% and are less rich in $Al_2O_3$ (12.5 wt. %). Rims of green and brown amphiboles have light brown colour and show higher mg# (0.70) compared to their cores and are more homogeneous in $TiO_2$ and $Al_2O_3$ contents (3.5% and 12.0% respectively)**.** These differences are evident in $Al_2O_3$/mg# vs. $TiO_2$ diagram (Fig. 7A).

Amphibole compositions are plotted in the $Al_2O_3/TiO_2$ vs. $CaO/Na_2O$ diagram of Rock, 1987 (Fig. 7B). All titanian-pargasite fall in the intersection of Ultramafic lamprophyres-Alkaline lamprophyres with Calcio-alkaline lamprophyres (UML-AL from CAL lamprophyres) fields.

***Mica***

Representative analyses of mica crystals from the Río Grande rocks appear in Table 5. The analyzed crystals are represented by phenocrysts, mesophenocrysts and groundmass crystals. Microinclusions in amphibole and clinopyroxene as well as their presence in the globular structures (ocelli and segregations) have also been analyzed. Mica compositions of phenocrysts, microphenocrysts, groundmass crystals and inclusions belong to the phlogopite field (Fig. 8), whereas biotite composition is observed in microphenocrysts inside and around the globular structures (ocelli and segregations).

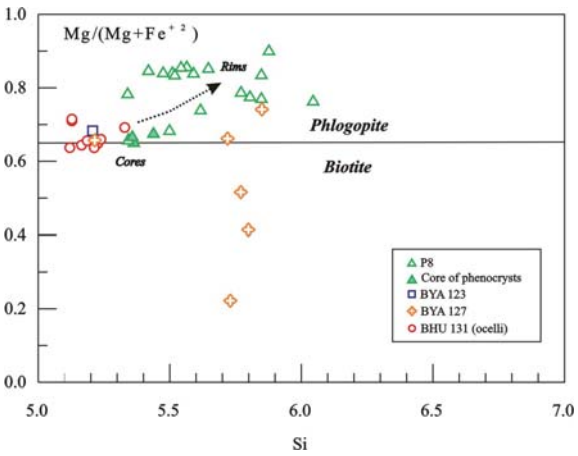


**Figure 8:** Classification diagram for mica ompositions after Rieder et al., 1998. Note the ore-rim trend followed by singular grains.

The phlogopite crystals have $Mg/Mg+Fe^{+2}$ ratios from 0.66 to 0.89; whereas biotite shows values ranging between 0.61 and 0.66. The cores of phenocrysts have similar compositions to microphenocrysts located in ocelli and segregations, showing the highest $TiO_2$ contents (~8 % wt.), whereas the rims of phenocrysts have similar compositions to mesophenocrysts and microphenocrysts with $TiO_2$ about 4 % (Fig. 8).

*Table 5: Representative electron microprobe analyses of mica minerals from the Rio Grande subvolcanic rocks*

| | *Phenocrysts* | | | | *Microphenocrysts* | | | *Incl* | *Amp rim* | *In segregations* | | | | | *Ocelli* |
|---|---|---|---|---|---|---|---|---|---|---|---|---|---|---|---|
| | | | | | | | | | | *bt-rich* | | | *cb-rich* | | |
| | *Rim* | | *Core* | | | | | | | *Rim* | *Core* | *Core* | | | |
| | 1 | 2 | 1 | 2 | 3 | 4 | 5 | 6 | 7 | 8 | | 9 | 10 | 11 | 13 |
| ***$SiO_2$*** | 37.61 | 35.80 | 36.57 | 36.17 | 37.47 | 39.27 | 38.24 | 38.89 | 37.41 | 35.49 | 34.25 | 34.25 | 34.67 | 33.61 | 36.96 |
| ***$TiO_2$*** | 3.24 | 6.06 | 5.23 | 6.29 | 3.19 | 2.68 | 2.87 | 3.13 | 3.16 | 6.82 | 7.88 | 7.85 | 5.76 | 5.59 | 3.68 |
| ***$Al_2O_3$*** | 14.99 | 15.24 | 14.83 | 15.27 | 14.30 | 14.76 | 14.06 | 14.16 | 14.86 | 14.79 | 15.51 | 15.33 | 15.52 | 14.51 | 10.11 |
| ***FeO*** | 7.06 | 13.62 | 13.21 | 13.82 | 7.42 | 6.61 | 7.29 | 11.90 | 7.16 | 11.43 | 10.23 | 11.90 | 12.94 | 12.39 | 22.30 |
| ***$Fe_2O_3$*** | 0.00 | 0.00 | 0.00 | 0.00 | 0.00 | 0.00 | 0.00 | 0.00 | 0.00 | 1.06 | 2.08 | 1.49 | 0.48 | 2.19 | 4.83 |
| ***$Cr_2O_3$*** | 0.00 | 0.00 | 0.00 | 0.00 | 0.00 | 0.00 | 0.00 | 0.00 | 0.00 | 0.00 | 0.00 | 0.00 | 0.00 | 0.00 | 0.00 |
| ***MnO*** | 0.22 | 0.10 | 0.04 | 0.11 | 0.15 | 0.19 | 0.17 | 0.12 | 0.16 | 0.10 | 0.10 | 0.06 | 0.11 | 0.25 | 0.43 |
| ***MgO*** | 20.67 | 14.62 | 15.29 | 14.30 | 20.80 | 21.21 | 21.12 | 18.85 | 20.97 | 14.96 | 14.86 | 13.38 | 15.63 | 14.14 | 9.37 |
| ***CaO*** | 0.04 | 0.00 | 0.03 | 0.01 | 0.04 | 0.11 | 0.08 | 0.01 | 0.07 | 0.11 | 0.05 | 0.12 | 0.08 | 0.29 | 0.21 |
| ***$Na_2O$*** | 0.40 | 0.60 | 0.82 | 0.72 | 0.68 | 0.89 | 0.61 | 1.36 | 0.74 | 0.38 | 0.46 | 0.75 | 0.35 | 0.27 | 0.00 |
| ***$K_2O$*** | 9.12 | 9.16 | 9.23 | 9.19 | 9.26 | 9.04 | 9.37 | 8.31 | 8.92 | 8.64 | 8.71 | 8.47 | 9.22 | 9.10 | 9.49 |
| ***BaO*** | 1.14 | 0.00 | 0.28 | 0.00 | 1.03 | 0.74 | 1.17 | 0.00 | 1.57 | 0.98 | 2.00 | 1.39 | 0.43 | 2.08 | 0.00 |
| ***Cl*** | 0.00 | 0.02 | 0.03 | 0.02 | 0.01 | 0.00 | 0.00 | 0.02 | 0.00 | 0.02 | 0.00 | 0.02 | 0.02 | 0.01 | 0.02 |
| ***$H_2O$*** | 4.09 | 4.01 | 4.02 | 4.03 | 4.06 | 4.16 | 4.09 | 4.14 | 4.01 | 3.99 | 4.02 | 3.96 | 3.99 | 3.88 | 3.86 |
| ***Total*** | 98.57 | 99.24 | 99.58 | 99.92 | 98.38 | 99.67 | 99.07 | 100.90 | 99.03 | 98.75 | 100.14 | 98.95 | 99.18 | 98.29 | 101.25 |
| **Structural formula based on 22 oxygens** | | | | | | | | | | | | | | | |
| **Si** | 5.51 | 5.34 | 5.44 | 5.36 | 5.52 | 5.65 | 5.59 | 5.62 | 5.48 | 5.33 | 5.13 | 5.19 | 5.21 | 5.22 | 5.80 |
| **$Al^{IV}$** | 2.49 | 2.66 | 2.56 | 2.64 | 2.48 | 2.35 | 2.41 | 2.38 | 2.52 | 2.62 | 2.74 | 2.74 | 2.75 | 2.65 | 1.87 |
| **$Fe^{+3}$** | 0.00 | 0.00 | 0.00 | 0.00 | 0.00 | 0.00 | 0.00 | 0.00 | 0.00 | 0.05 | 0.14 | 0.08 | 0.05 | 0.13 | 0.33 |
| **Sum T** | **8.00** | **8.00** | **8.00** | **8.00** | **8.00** | **8.00** | **8.00** | **8.00** | **8.00** | **8.00** | **8.00** | **8.00** | **8.00** | **8.00** | **8.00** |
| **$Al^{VI}$** | 0.10 | 0.03 | 0.04 | 0.03 | 0.00 | 0.15 | 0.01 | 0.03 | 0.04 | 0.00 | 0.00 | 0.00 | 0.00 | 0.00 | 0.00 |
| **$Fe^{+2}$** | 0.86 | 1.70 | 1.64 | 1.71 | 0.91 | 0.79 | 0.89 | 1.44 | 0.88 | 1.38 | 1.14 | 1.43 | 1.58 | 1.48 | 2.59 |
| **$Fe^{+3}$** | 0.00 | 0.00 | 0.00 | 0.00 | 0.00 | 0.00 | 0.00 | 0.00 | 0.00 | 0.07 | 0.10 | 0.09 | 0.01 | 0.12 | 0.24 |
| **Ti** | 0.36 | 0.68 | 0.59 | 0.70 | 0.35 | 0.29 | 0.32 | 0.34 | 0.35 | 0.77 | 0.89 | 0.89 | 0.65 | 0.65 | 0.43 |
| **Mg** | 4.51 | 3.25 | 3.39 | 3.16 | 4.57 | 4.55 | 4.60 | 4.06 | 4.57 | 3.35 | 3.32 | 3.02 | 3.50 | 3.27 | 2.19 |
| **Mn** | 0.03 | 0.01 | 0.01 | 0.01 | 0.02 | 0.02 | 0.02 | 0.01 | 0.02 | 0.01 | 0.01 | 0.01 | 0.01 | 0.03 | 0.06 |
| **Sum O** | **5.86** | **5.67** | **5.66** | **5.62** | **5.85** | **5.80** | **5.84** | **5.88** | **5.86** | 5.58 | 5.46 | 5.44 | 5.75 | 5.56 | 5.51 |
| **Ca** | 0.01 | 0.00 | 0.00 | 0.00 | 0.01 | 0.02 | 0.01 | 0.00 | 0.01 | 0.02 | 0.01 | 0.02 | 0.01 | 0.05 | 0.04 |
| **Na** | 0.11 | 0.17 | 0.24 | 0.21 | 0.19 | 0.25 | 0.17 | 0.38 | 0.21 | 0.11 | 0.13 | 0.22 | 0.10 | 0.08 | 0.00 |
| **K** | 0.85 | 0.87 | 0.88 | 0.87 | 0.87 | 0.83 | 0.87 | 0.77 | 0.83 | 1.66 | 1.66 | 1.64 | 1.77 | 1.80 | 1.90 |
| **Ba** | 0.13 | 0.00 | 0.03 | 0.00 | 0.12 | 0.08 | 0.13 | 0.00 | 0.18 | 0.06 | 0.12 | 0.08 | 0.03 | 0.13 | 0.00 |
| **Sum A** | **1.10** | **1.05** | **1.15** | **1.08** | **1.19** | **1.18** | **1.19** | **1.15** | **1.23** | **1.78** | **1.80** | **1.88** | **1.88** | **1.93** | **1.93** |
| ***Cations*** | **14.96** | **14.72** | **14.81** | **14.70** | **15.04** | **14.98** | **15.04** | **15.03** | **15.09** | **15.36** | **15.26** | **15.32** | **15.63** | **15.49** | **15.45** |
| ***Mg/(Mg+$Fe^{+2}$)*** | ***0.84*** | ***0.66*** | ***0.67*** | ***0.65*** | ***0.83*** | ***0.85*** | ***0.84*** | ***0.74*** | ***0.84*** | ***0.69*** | ***0.71*** | ***0.66*** | ***0.68*** | ***0.66*** | ***0.41*** |
| ***$Fe^{+2}$/($Fe^{+2}$+Mg)*** | ***0.16*** | ***0.34*** | ***0.33*** | ***0.35*** | ***0.17*** | ***0.15*** | ***0.16*** | ***0.26*** | ***0.16*** | ***0.31*** | ***0.29*** | ***0.34*** | ***0.32*** | ***0.34*** | ***0.59*** |

*Obs: H2O recalculated by stequiometrie. Fe2O3 recalculated for samples with deficiency in tetraedric site*

The compositions of groundmass phlogopite and some phenocrysts and microphenocrysts rims is marked by higher Mg concentrations compared to cores of phenocrysts and microphenocrysts. This variation is accompanied by decrease in $TiO_2$ and $Al_2O_3$ contents. On the other hand, biotite crystals are characterized by lower Mg and higher $TiO_2$ and $Al_2O_3$ contents (Fig. 9 A, B) The biotite crystals in segregations, display higher $TiO_2$ (from 5.59 to 7.88 wt. %) and BaO (from 0.43 to 2.08 wt. %) values (Fig. 9 B).

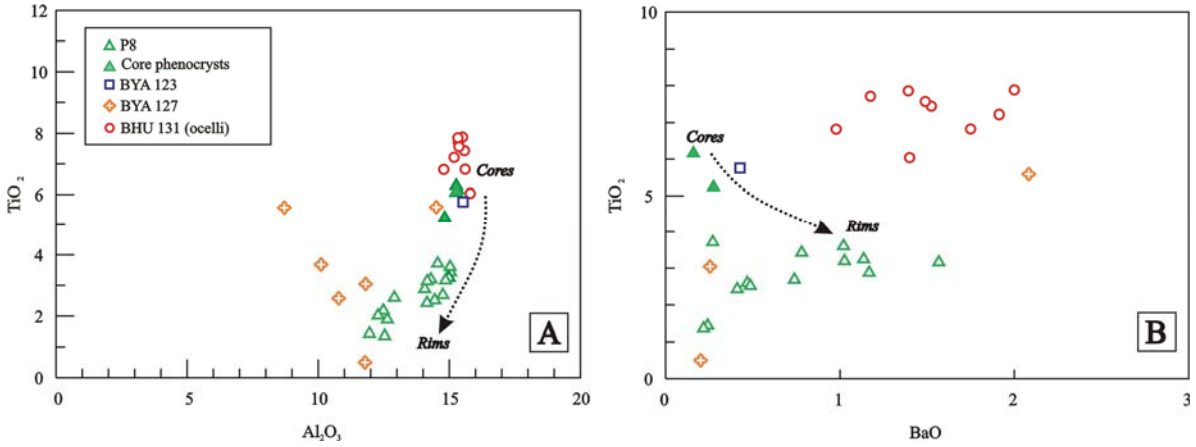


**Figure 9:** A) $Al_2O_3$ vs. $TiO_2$ diagram and B) BaO vs. $TiO_2$ diagram for micas. The mica from ocelli (samples BHU 131) and cores of phenocrysts are richer in $TiO_2$ (~7.5 wt. %) and BaO (~2 wt. %) compared with the rest. Note the core-rim trend (arrows) followed by singular grains.

### *Apatite*

Chemical analyses for two apatite crystals are given in Table 6. This phase was only recognized in sample P8 and one corresponds to a phenocryst and the other corresponds to a crystal from a *clinopyroxene phenocrysts with apatite inclusions*. The phenocryst is characterized by the higher SrO content (1.075 wt. %), whereas the apatite in a nodule have SrO values between 0.30 to 0.43 wt. %.

### *Analcime*

Chemical analyses of analcime are given in Table 7. This constitutes a subordinate phase in the groundmass and an important mineral in ocelli and segregations. They are compositionally identical and have 57 wt. % $SiO_2$, 24 wt. % $Al_2O_3$ and 13 wt. % $Na_2O$ and very low CaO and $K_2O$ contents. In the ocelli, analcime crystals show slight increases in Ba content from 0 to 0.11 wt. % BaO from core to rim.

*Table 6: Representative analyses microprobe for apatite minerals from sample P8, Rio Grande subvolcanic rocks*

| | *Phenocryst* | *In augite phenocrysts* | |
|---|---|---|---|
| | *1* | 2 | 3 |
| $SiO_2$ | 0.00 | 0.13 | 0.12 |
| $Al_2O_3$ | 0.00 | 0.00 | 0.01 |
| $MgO$ | 0.14 | 0.38 | 0.34 |
| $Fe_2O_3$ | 0.34 | 0.34 | 0.32 |
| $CaO$ | 53.31 | 53.83 | 54.50 |
| $Na_2O$ | 0.35 | 0.06 | 0.12 |
| $K_2O$ | 0.00 | 0.01 | 0.03 |
| $P_2O_5$ | 41.67 | 40.14 | 40.51 |
| $Cl$ | 0.24 | 0.13 | 0.11 |
| $SrO$ | 1.08 | 0.43 | 0.31 |
| $BaO$ | 0.01 | 0.00 | 0.00 |
| $H_2O$ | 1.70 | 1.69 | 1.72 |
| *Total* | 98.83 | 97.14 | 98.07 |
| **Cations per fórmula unit** | | | |
| Na | 0.12 | 0.02 | 0.04 |
| Si | 0.00 | 0.02 | 0.02 |
| Al | 0.00 | 0.00 | 0.00 |
| Mg | 0.04 | 0.10 | 0.09 |
| K | 0.00 | 0.00 | 0.01 |
| P | 6.02 | 5.90 | 5.90 |
| Ca | 9.74 | 10.02 | 10.04 |
| Cl | -0.05 | -0.03 | -0.02 |
| Sr | 0.11 | 0.04 | 0.03 |
| Fe | 0.05 | 0.05 | 0.05 |
| Ba | 0.00 | 0.00 | 0.00 |
| H | 0.56 | 0.57 | 0.57 |
| ***Cations*** | ***16.57*** | ***16.69*** | ***16.71*** |

### *Carbonate*

This mineral phase has been analyzed in smaller crystals in the groundmass, in xenoliths, in globular structures (ocelli and segregations) and in carbonate rims of one amphibole phenocryst (sample P8). Their results are shown in Table 8.

Dolomite is the principal composition (Fig. 10 A) observed in Río Grande lamprophyres. Only one carbonate mineral, which occurs in segregations, is breunnerite in composition. The breunnerite mineral seems to occur only in ultramafic lamprophyres (UML) and lamproites (LL) (Rock, 1987).

*Table 7: Representative electron microprobe analyses of analcime minerals from the Rio Grande subvolcanic rocks*

| | *Rim to amphibole* | *in Ocelli* | | | | | | | *in Bt-rich segreg* | *Microphenocrysts* | | |
|---|---|---|---|---|---|---|---|---|---|---|---|---|
| | 1 | 2 | 3 | 4 | 5 | 6 | 7 | 8 | 9 | 10 | 11 | 12 |
| $SiO_2$ | 55.51 | 57.23 | 53.20 | 55.76 | 52.18 | 54.66 | 59.20 | 61.92 | 58.02 | 62.77 | 50.61 | 52.08 |
| $Al_2O_3$ | 24.57 | 24.63 | 23.73 | 21.17 | 24.92 | 25.46 | 24.85 | 22.71 | 24.91 | 22.47 | 22.72 | 23.19 |
| $FeO$ | 0.14 | 0.01 | 0.07 | 0.09 | 0.63 | 0.51 | 0.13 | 0.18 | 0.16 | 0.26 | 0.04 | 1.23 |
| $CaO$ | 0.16 | 0.00 | 0.30 | 0.11 | 0.63 | 0.69 | 0.05 | 0.01 | 0.13 | 0.08 | 0.29 | 0.32 |
| $Na_2O$ | 12.94 | 13.26 | 12.93 | 13.96 | 10.92 | 10.46 | 13.58 | 12.18 | 12.24 | 10.91 | 11.46 | 11.85 |
| $K_2O$ | 0.12 | 0.04 | 0.25 | 0.12 | 0.34 | 0.20 | 0.08 | 0.08 | 0.05 | 0.09 | 0.27 | 0.55 |
| *Total* | 93.43 | 95.28 | 90.49 | 91.30 | 89.62 | 91.99 | 97.90 | 97.08 | 95.50 | 96.69 | 85.42 | 89.23 |
| **Recalculate cations in basis of 7 (O)** | | | | | | | | | | | | |
| **Si** | 2.20 | 2.39 | 2.23 | 2.33 | 2.18 | 2.29 | 2.48 | 2.59 | 2.43 | 2.63 | 2.12 | 2.18 |
| **Al** | 1.15 | 1.21 | 1.17 | 1.04 | 1.23 | 1.26 | 1.22 | 1.12 | 1.23 | 1.11 | 1.12 | 1.14 |
| **Sum T** | **3.35** | **3.61** | **3.39** | **3.38** | **3.41** | **3.54** | **3.70** | **3.71** | **3.65** | **3.73** | **3.24** | **3.32** |
| **$Fe^{+2}_t$** | 0.00 | 0.00 | 0.00 | 0.00 | 0.02 | 0.02 | 0.00 | 0.01 | 0.01 | 0.01 | 0.00 | 0.04 |
| **Ca** | 0.01 | 0.00 | 0.01 | 0.01 | 0.03 | 0.03 | 0.00 | 0.00 | 0.01 | 0.00 | 0.01 | 0.01 |
| **Na** | 1.00 | 1.08 | 1.05 | 1.13 | 0.89 | 0.85 | 1.10 | 0.99 | 0.99 | 0.88 | 0.93 | 0.96 |
| **K** | 0.01 | 0.00 | 0.01 | 0.01 | 0.02 | 0.01 | 0.00 | 0.00 | 0.00 | 0.00 | 0.01 | 0.03 |
| **Sum A** | **1.01** | **1.08** | **1.08** | **1.15** | **0.95** | **0.91** | **1.11** | **1.00** | **1.01** | **0.90** | **0.96** | **1.05** |
| ***Cations*** | *4.36* | *4.69* | *4.47* | *4.52* | *4.37* | *4.45* | *4.81* | *4.71* | *4.66* | *4.64* | *4.20* | *4.37* |

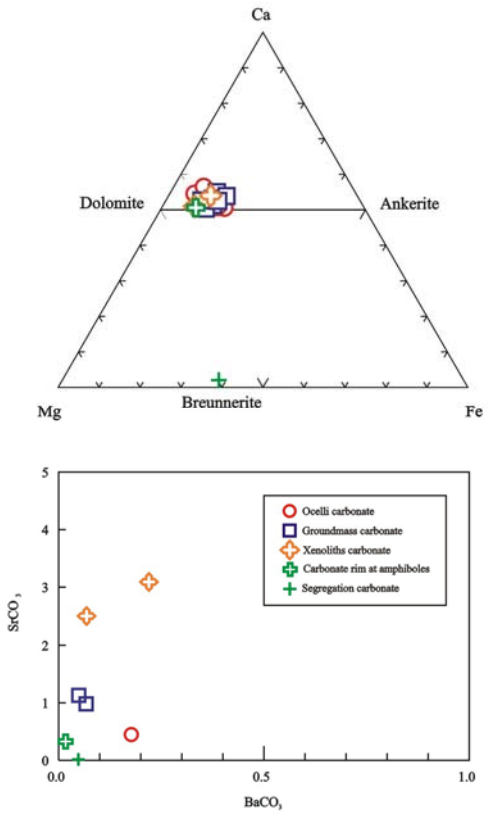


**Figure 10:** Carbonate compositions of Río Grande lamprophyres. A) Ca-Mg-Fe system (moles %). All types of carbonate are dolomite in composition except for the carbonate segregations that is breunnerite. B) BaCO-$SrCO_3$ covariation diagram. Note that xenoliths carbonate have the highest contents in $SrCO_3$.

The dolomite compositions from the clinopyroxene-bearing carbonate xenolith are Sr rich (2.5-3.0 wt. % $SrCO_3$) and moderately Ba rich (0.2 wt. % $BaCO_3$) (Fig. 10 B).

## 5. Analytical Procedures

Samples for geochemical analyses were washed and weathered and veined surfaces were cut off. The rocks were crushed and milled to a very fine powder. Major elements and Ni and Sc (ppm) were analyzed by ICP-OES and trace element analyses were carried out by ICP-MS at ACME Laboratories in Canada.

*Table 8: Representative electron microprobe analyses of carbonate minerals from the Rio Grande subvolcanic rocks*

| | *In Type-I ocelli* | | | | | | | | *In segregations (Breunnerite)* | *Groundmass* | | | | | *Cpx-bearing carbonate xenoliths* | | *Rim to amphibole* |
|---|---|---|---|---|---|---|---|---|---|---|---|---|---|---|---|---|---|
| | *1* | *2* | *3* | *4* | *5* | *6* | *7* | | | 1 | 2 | 3 | 4 | 5 | 1 | 2 | |
| *$FeCO_3$* | 12.70 | 9.69 | 7.08 | 12.12 | 8.62 | 15.77 | 17.70 | 15.87 | 45.15 | 13.02 | 16.01 | 14.05 | 12.85 | 14.68 | 11.77 | 9.21 | 9.84 |
| *$MnCO_3$* | 0.56 | 0.68 | 0.75 | 0.57 | 1.12 | 0.91 | 0.96 | 1.16 | 0.13 | 1.09 | 1.36 | 1.10 | 0.73 | 1.82 | 0.22 | 0.37 | 0.80 |
| *$MgCO_3$* | 30.73 | 34.43 | 33.91 | 33.86 | 30.92 | 30.07 | 28.63 | 30.19 | 51.40 | 28.35 | 26.32 | 30.73 | 33.19 | 28.74 | 29.77 | 35.41 | 35.26 |
| *$CaCO_3$* | 51.20 | 52.15 | 55.63 | 52.19 | 57.30 | 50.81 | 50.39 | 51.67 | 2.07 | 54.75 | 52.64 | 51.35 | 51.11 | 51.77 | 53.32 | 51.89 | 51.58 |
| *$SrCO_3$* | 2.06 | 0.80 | 0.45 | 0.15 | 0.04 | 0.45 | 0.47 | 0.62 | 0.02 | 0.96 | 0.71 | 0.48 | 0.39 | 1.13 | 3.09 | 2.50 | 0.33 |
| *$BaCO_3$* | 0.00 | 0.00 | 0.18 | 0.00 | 0.00 | 0.00 | 0.00 | 0.00 | 0.05 | 0.00 | 0.00 | 0.00 | 0.00 | 0.05 | 0.22 | 0.07 | 0.02 |
| *TOTAL* | 98.57 | 99.10 | 99.34 | 100.25 | 99.35 | 99.35 | 99.47 | 100.88 | 100.16 | 99.50 | 98.35 | 99.05 | 99.61 | 99.52 | 99.72 | 100.80 | 99.18 |
| **Cations per fórmula unit** | | | | | | | | | | | | | | | | | |
| Ca | 1.02 | 1.02 | 1.08 | 0.95 | 1.07 | 1.00 | 1.00 | 1.01 | 0.04 | 1.05 | 1.05 | 0.52 | 1.00 | 1.03 | 1.05 | 1.00 | 0.97 |
| Mg | 0.73 | 0.80 | 0.78 | 0.73 | 0.68 | 0.71 | 0.67 | 0.70 | 1.09 | 0.65 | 0.63 | 0.37 | 0.77 | 0.68 | 0.70 | 0.81 | 0.79 |
| Fe | 0.22 | 0.16 | 0.12 | 0.19 | 0.14 | 0.27 | 0.30 | 0.27 | 0.70 | 0.22 | 0.28 | 0.12 | 0.22 | 0.25 | 0.20 | 0.15 | 0.16 |
| Ba | 0.00 | 0.00 | 0.00 | 0.00 | 0.00 | 0.00 | 0.00 | 0.00 | 0.00 | 0.00 | 0.00 | 0.00 | 0.00 | 0.00 | 0.00 | 0.00 | 0.00 |
| Sr | 0.03 | 0.01 | 0.01 | 0.00 | 0.00 | 0.01 | 0.01 | 0.01 | 0.00 | 0.01 | 0.01 | 0.00 | 0.01 | 0.02 | 0.04 | 0.03 | 0.00 |
| Mn | 0.01 | 0.01 | 0.01 | 0.01 | 0.02 | 0.02 | 0.02 | 0.02 | 0.00 | 0.02 | 0.02 | 0.01 | 0.01 | 0.03 | 0.00 | 0.01 | 0.01 |
| ***Cations*** | 2.00 | 2.00 | 2.00 | 2.00 | 2.00 | 2.00 | 2.00 | 2.00 | 2.00 | 2.00 | 2.00 | 2.00 | 2.00 | 2.00 | 2.00 | 2.00 | 2.00 |

Sm-Nd and Rb-Sr isotopic date analyses followed the method described by Gioia and Pimentel (2000) and were carried out at the Geochronology Laboratory of the University of Brasilia, Brazil. Whole-rock powers (~100 mg) were mixed with $^{149}Sm$-$^{150}Nd$ spike solution and dissolved in savillex capsules. Sr, Sm and Nd extraction of whole rock samples followed conventional cation exchange techniques, with Teflon columns containing LN-Spec resin (HDEHP-diethylhexil phosphoric acid supported on PTFE powder). Sr, Sm and Nd samples were loaded on Re evaporation filaments of double filament assemblies, and the isotopic measurements were carried out on a multicollector Finnigan MAT 262 mass spectrometer in static mode. Uncertainties of $^{87}Sr/^{86}Sr$ ratios were better than ±0.01% (σ2) and of Sm/Nd and $^{143}Nd/^{144}Nd$ ratios were better than ±0.2% (σ2) and ±0.005% (σ2), respectively, according to repeated analyses of international rock standards BHVO-1 and BCR-1. $^{143}Nd/^{144}Nd$ ratios were normalized to $^{146}Nd/^{144}Nd$ of 0.7219, and the decay constant used was $6.54x10^{-12}$ $y^{-1}$. The $T_{DM}$ values were calculated using DePaolo's model (1981).

## 6. Geochemistry

Major and trace elements analyses were carried out on eleven selected samples (Table 9). In all bulk chemical analyses, the loss on ignition (LOI) values are high, varying from 5.9 to 22.8 %. The analyzed samples show high $TiO_2$ (up to 4.83 %) and MgO (~ 10 %) in contrast, the variable concentrations of $Na_2O$ (0.09-3.65) and $K_2O$ (0.87-1.9 wt. %) are probably due to subsequent alteration processes.

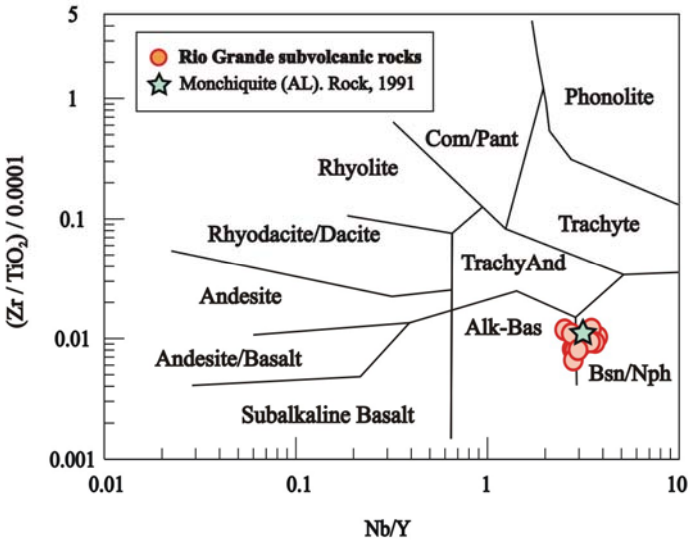


**Figure 11:** Rock classification diagram using Zr, Ti, Nb and Y immobile elements (Winchester and Floyd, 1977) for the Río Grande rocks.

*Table 9: Representative major and trace elements analyses from the Río Grande subvolcanic rocks*

| | ***Coraya*** | | | ***Yacoraite*** | | | | | | | ***Huichaira*** |
|---|---|---|---|---|---|---|---|---|---|---|---|
| *Sample* | BCO 49 | BCO 51 | BCO 52 | P8 | BYA 122 | BYA 123 | BYA 124a | BYA 125 | BYA 126 | BYA 127 | BHU 131 |
| *Major oxides (wt%)* | | | | | | | | | | | |
| $SiO_2$ | 33.55 | 52.71 | 33.50 | 26.48 | 38.54 | 38.05 | 38.03 | 28.53 | 28.80 | 35.24 | 37.45 |
| $TiO_2$ | 2.72 | 3.54 | 4.83 | 2.52 | 2.56 | 2.71 | 2.73 | 3.68 | 4.22 | 3.35 | 3.93 |
| $Al_2O_3$ | 8.72 | 9.43 | 14.05 | 7.11 | 14.20 | 9.71 | 9.24 | 10.63 | 9.72 | 9.27 | 10.32 |
| $Fe_2O_{3\,(t)}$ | 14.12 | 14.81 | 25.81 | 12.09 | 11.73 | 13.15 | 11.40 | 8.22 | 17.94 | 13.44 | 12.85 |
| $MnO$ | 0.20 | 0.29 | 0.08 | 0.34 | 0.20 | 0.17 | 0.15 | 0.43 | 0.35 | 0.21 | 0.16 |
| $MgO$ | 12.67 | 1.77 | 6.91 | 10.99 | 7.26 | 12.19 | 9.97 | 8.48 | 9.46 | 11.43 | 9.96 |
| $CaO$ | 9.48 | 6.06 | 3.26 | 16.76 | 7.05 | 11.60 | 9.43 | 14.18 | 10.01 | 13.15 | 10.96 |
| $Na_2O$ | 0.17 | 0.06 | 2.32 | 2.89 | 3.65 | 1.50 | 1.42 | 0.09 | 0.11 | 2.12 | 2.90 |
| $K_2O$ | 0.54 | 1.90 | 0.71 | 0.89 | 1.63 | 1.78 | 1.56 | 1.21 | 1.07 | 1.71 | 0.87 |
| $P_2O_5$ | 1.14 | 0.98 | 2.28 | 1.99 | 1.33 | 1.04 | 0.58 | 1.42 | 1.68 | 1.32 | 0.97 |
| *L.O.I* | 16.40 | 8.20 | 5.90 | 17.50 | 11.50 | 7.60 | 15.20 | 22.80 | 16.30 | 8.30 | 9.30 |
| *Total* | 99.71 | 99.75 | 99.65 | 99.61 | 99.65 | 99.50 | 99.71 | 99.67 | 99.66 | 99.54 | 99.67 |
| *Trace elements (ppm)* | | | | | | | | | | | |
| Be | 3.00 | 4.00 | 4.00 | 4.00 | 4.00 | 2.00 | 3.00 | 2.00 | 4.00 | 3.00 | 3.00 |
| Sc | 24.00 | 17.00 | 24.00 | 16.00 | 19.00 | 20.00 | 23.00 | 22.00 | 19.00 | 19.00 | 18.00 |
| Ti | 16306 | 21222 | 28956 | 15120 | 15347 | 16246 | 16366 | 22062 | 25299 | 20083 | 23560 |
| V | 202.00 | 242.00 | 400.00 | 190.00 | 234.00 | 219.00 | 218.00 | 218.00 | 269.00 | 256.00 | 263.00 |
| Cr | 249.74 | 225.79 | 253.16 | 109.47 | 75.26 | 164.21 | 225.79 | 177.89 | 112.89 | 171.05 | 164.21 |
| Co | 84.00 | 47.00 | 69.00 | 73.30 | 44.40 | 62.70 | 67.80 | 73.40 | 94.80 | 68.70 | 59.20 |
| Ni | 423.00 | 243.90 | 350.40 | 141.10 | 94.70 | 176.70 | 323.50 | 256.80 | 239.50 | 193.40 | 152.40 |
| Cu | 30.50 | 165.30 | 47.40 | 56.30 | 108.40 | 84.80 | 88.80 | 85.60 | 65.50 | 70.90 | 76.50 |
| Zn | 157.00 | 70.00 | 156.00 | 104.00 | 122.00 | 73.00 | 89.00 | 127.00 | 400.00 | 105.00 | 56.00 |
| Ga | 14.00 | 9.80 | 24.80 | 14.30 | 25.70 | 17.10 | 15.90 | 20.00 | 26.50 | 18.60 | 20.80 |
| As | 7.60 | 27.90 | 13.70 | 11.90 | 8.70 | 6.30 | 9.60 | 11.60 | 3.90 | 3.50 | 16.60 |
| Se | b.d.l | 0.80 | 0.70 | b.d.l | 0.50 | 0.50 | b.d.l | 0.70 | b.d.l | b.d.l | 0.70 |
| Rb | 22.00 | 75.10 | 25.80 | 27.30 | 63.20 | 62.00 | 52.10 | 57.10 | 56.20 | 71.20 | 35.20 |
| Sr | 355.70 | 275.30 | 412.60 | 2589.20 | 753.80 | 1040.60 | 712.30 | 828.40 | 436.50 | 1657.40 | 812.40 |
| Y | 29.00 | 31.40 | 55.90 | 66.70 | 45.40 | 29.00 | 20.50 | 47.10 | 55.50 | 37.90 | 30.70 |
| Zr | 222.60 | 282.70 | 415.50 | 259.20 | 302.90 | 253.90 | 180.40 | 403.90 | 506.80 | 310.60 | 316.10 |
| Nb | 80.10 | 89.30 | 171.30 | 251.30 | 114.70 | 100.10 | 57.50 | 128.80 | 193.30 | 138.00 | 91.20 |
| Mo | 1.10 | 0.70 | 0.50 | 15.70 | 2.60 | 3.50 | 2.30 | 0.40 | 0.60 | 0.30 | 1.50 |
| Ag | b.d.l | b.d.l | b.d.l | b.d.l | 0.10 | b.d.l | 0.10 | 0.10 | b.d.l | b.d.l | b.d.l |
| Cd | 0.20 | 0.10 | b.d.l | 0.20 | 0.10 | 0.10 | 0.10 | 0.30 | 0.20 | 0.10 | 0.10 |
| Sn | 1.00 | 2.00 | 3.00 | 2.00 | 3.00 | 2.00 | 1.00 | 2.00 | 2.00 | 2.00 | 2.00 |
| Sb | 0.60 | 1.80 | 1.90 | 0.20 | 0.20 | 0.10 | 0.40 | 0.20 | 0.30 | b.d.l | 0.20 |
| Cs | 4.30 | 6.30 | 6.60 | 38.90 | 4.50 | 12.20 | 8.10 | 40.70 | 26.50 | 35.50 | 87.30 |
| Ba | 318 | 315 | 283 | 1666 | 394 | 1008 | 466 | 229 | 324 | 1016 | 881 |
| Hf | 5.80 | 7.30 | 8.70 | 5.10 | 7.40 | 5.50 | 4.80 | 9.30 | 11.80 | 6.70 | 7.20 |
| Ta | 4.20 | 5.50 | 9.40 | 8.20 | 6.40 | 5.60 | 3.70 | 8.00 | 12.60 | 7.50 | 5.90 |
| W | 16.20 | 34.80 | 19.50 | 55.20 | 38.60 | 39.90 | 38.20 | 47.10 | 10.10 | 58.10 | 48.80 |
| Au* | 7.10 | 17.30 | 11.20 | 8.70 | 14.30 | b.d.l | 31.20 | 14.40 | 9.70 | 51.00 | b.d.l |
| Hg | b.d.l | b.d.l | b.d.l | 0.01 | b.d.l | 0.01 | 0.02 | 0.05 | 0.04 | b.d.l | 0.02 |
| Tl | 0.10 | 0.10 | 0.10 | 0.10 | 0.20 | 0.30 | 0.10 | 0.20 | 0.10 | 0.20 | 0.10 |
| Pb | 32.70 | 73.90 | 38.10 | 21.70 | 11.10 | 6.70 | 64.70 | 25.50 | 19.50 | 4.80 | 2.60 |
| Bi | b.d.l | 0.50 | 0.10 | 0.10 | 0.10 | b.d.l | b.d.l | 0.10 | b.d.l | b.d.l | b.d.l |
| Th | 9.50 | 10.40 | 26.90 | 56.90 | 21.40 | 12.70 | 7.40 | 16.50 | 19.40 | 15.10 | 10.70 |
| U | 2.60 | 13.10 | 6.50 | 11.00 | 5.10 | 3.10 | 2.10 | 6.40 | 6.70 | 4.30 | 2.10 |
| *Rare earth elements (ppm)* | | | | | | | | | | | |
| La | 87.80 | 82.80 | 181.80 | 297.70 | 117.20 | 96.90 | 55.50 | 134.00 | 138.50 | 132.20 | 80.80 |
| Ce | 180.00 | 175.10 | 370.50 | 570.30 | 243.50 | 198.00 | 111.80 | 287.60 | 283.50 | 261.90 | 169.80 |
| Pr | 17.82 | 17.09 | 35.40 | 56.99 | 23.69 | 18.95 | 11.26 | 27.79 | 27.09 | 24.91 | 17.68 |
| Nd | 66.00 | 65.70 | 134.20 | 189.90 | 88.50 | 69.80 | 44.10 | 105.50 | 103.20 | 92.50 | 68.40 |
| Sm | 11.60 | 12.30 | 22.80 | 27.95 | 14.90 | 11.80 | 7.80 | 18.00 | 18.20 | 16.10 | 11.90 |
| Eu | 3.57 | 3.77 | 7.21 | 7.35 | 4.27 | 3.33 | 2.08 | 5.62 | 5.73 | 4.61 | 3.83 |
| Gd | 8.94 | 10.33 | 18.86 | 18.77 | 11.92 | 9.04 | 6.29 | 14.84 | 15.24 | 11.72 | 9.65 |
| Tb | 1.40 | 1.36 | 2.59 | 3.02 | 1.73 | 1.20 | 0.86 | 2.04 | 2.13 | 1.62 | 1.49 |
| Dy | 6.04 | 7.19 | 12.66 | 13.21 | 8.86 | 5.89 | 4.31 | 9.43 | 11.12 | 7.90 | 6.55 |
| Ho | 0.98 | 1.07 | 1.98 | 1.94 | 1.50 | 0.99 | 0.69 | 1.60 | 1.86 | 1.34 | 1.01 |
| Er | 2.52 | 2.71 | 4.97 | 4.94 | 4.16 | 2.51 | 1.76 | 3.92 | 4.88 | 3.48 | 2.63 |
| Tm | 0.30 | 0.40 | 0.61 | 0.61 | 0.57 | 0.33 | 0.23 | 0.50 | 0.61 | 0.37 | 0.38 |
| Yb | 2.01 | 2.20 | 3.77 | 3.75 | 3.40 | 1.76 | 1.34 | 2.71 | 3.70 | 2.53 | 2.01 |
| Lu | 0.23 | 0.27 | 0.49 | 0.52 | 0.54 | 0.26 | 0.18 | 0.32 | 0.46 | 0.31 | 0.28 |
| ***$La/Yb_n$*** | ***29.2*** | ***25.2*** | ***32.2*** | ***53.08*** | ***23.1*** | ***36.8*** | ***27.7*** | ***33.1*** | ***25.0*** | ***34.9*** | ***26.9*** |
| ***$La/Sm_n$*** | ***4.7*** | ***4.2*** | ***4.9*** | ***6.57*** | ***4.9*** | ***5.1*** | ***4.4*** | ***4.6*** | ***4.7*** | ***5.1*** | ***4.2*** |
| ***$Gd/Yb_n$*** | ***3.5*** | ***3.7*** | ***4.0*** | ***3.99*** | ***2.8*** | ***4.1*** | ***3.7*** | ***4.4*** | ***3.3*** | ***3.7*** | ***3.8*** |

(*) concentrations of Au element in ppb

The high LOI values observed are the result of alteration; although high volatile content is a common feature of lamprophyres (up to 5-6%, Rock, 1991). If we consider that the LOI represent in part magmatic $CaCO_2$, the major elements cannot be used in discrimination diagrams; whereas if we assume that the LOI represent $CaCO_2$ produced by later alteration, recalculation of the major element contents to an anhydrous basis is justifiable. The petrographic and mineral chemistry indicate that some xenoliths and ocelli have dolomite with features that resemble carbonatitic rocks. Therefore the carbonate in the groundmass of these rocks has probably a similar origin, suggesting that the high LOI represent original magmatic volatiles.

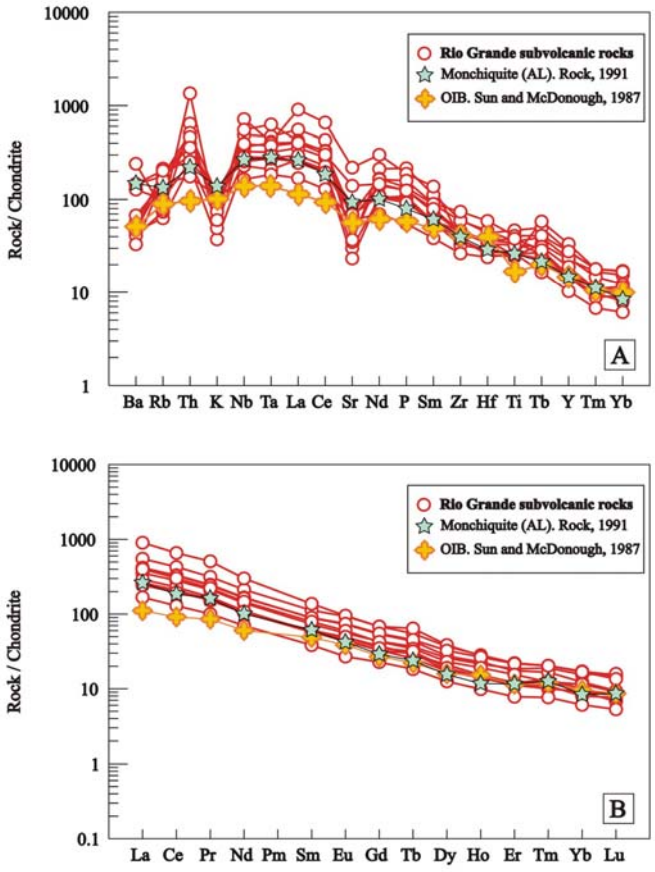


**Figure 12:** A) Chondrite normalized abundance spidergrams (Thompson 1982) and B) REE normalized diagram after Nakamura 1974, for the Rio Grande rocks. For comparison monchiquite-alkaline lamprophyres after Rock (1991) and average ocean island basalt (OIB) after Sun and McDonough (1989) are shown.

High contents in compatible trace elements (164-253.3 ppm for Cr, 152.4-423 ppm for Ni, 17-24 ppm for Sc, 44.4-94.8 ppm for Co and 202.2-400 ppm for V); indicate moderate degrees of fractionation (Table 9). The wide range in some incompatible trace elements (229-1666 ppm Ba, 356-2590 ppm Sr and 22-75 ppm Rb, 57-251 ppm Nb) may also be due to alteration, although similarly high concentrations and wide variations of LIL elements have been described for several lamprophyres (e.g. Rock, 1991, Azambre et al., 1992, Szabo et al., 1993, Dostal, Owen, 1998, Nedli and Tóth, 2007). Sample P8 displays the highest contents in Ba, Sr and Nb elements.

The Nb/Y vs. $Zr/TiO_2$ diagram (Fig. 11) show that the Río Grande rocks are transitional between alkali basalts and Basanites/Nephelinites. For comparison, a monchiquite (alkaline lamprophyre) sample is also shown (Rock, 1991). The analyzed samples normalized to the chondrite values from Thompson, (1982) (Fig. 12 A) show enrichments in LILE and LREE with values from 50 to approximately 800 time greater than the chondrite values, whereas the HREE and HFSE contents are lower. Evident negative K and Sr anomalies together with a small negative Ti anomaly are observed. A monchiquite sample (Rock, 1991) and an ocean island basalt (Sun and McDonough, 1987) are also shown for comparison.

Total REE concentrations range from 376 to 798 ppm (Table 9). Chondrite-normalized trace element patterns (Fig. 12 B) are characterized by strong (LREE) enrichment and distinctive REE fractionation with $(La/Yb)_n$ ratio varying from 23.1 to 36.8 for all samples, except for sample P8, which has a higher $(La/Yb)_n$ ratio (53.08). The $(La/Sm)_n$ and $(Gd/Yb)_n$ values from 4.15 to 5.06 and from 2.79 to 4.36 respectively, indicate that garnet was not an important phase in the source. The lack of Eu anomaly suggests that plagioclase fractionation (either by crystal settling or crustal melting) was not important during the origin and differentiation of the original magma. Normally negative Sr and Eu anomalies indicate plagioclase fractionation, but as in the present case no Eu anomaly is observed, the observed negative Sr anomaly is interpreted to indicate source characteristics that could be related to the presence of residual amphibole and clinopyroxene crystals in the source. The depletion of mantle source in Sr during a previous phase of melt extraction is unlikely.

# 7. Geochronology

## 7.1. K-Ar data

Some of the samples investigated in the present study have biotite macrocrysts (up to 2 cm). Biotite was separated from two samples (BYA 126 and P8) for K-Ar geochronology at the Center of Geochronological Research of the University of São Paulo. The analyses resulted

(Table 10) in K-Ar ages of ***190 ± 11 Ma*** (sample BYA 126) and ***163 ± 9 Ma*** (sample P8). Due to the older age corresponds with the altered sample, we prefer to use the ***163 ± 9 Ma*** as representative age.

*Table 10: K-Ar biotite age data for the Río Grande subvolcanic rocks*

| *Sample* | Rock type | Mineral | Age (Ma) | Max. Error | $Ar^{40}$ rad ccSTP/g ($*10^{-6}$) | $Ar^{40}$ atm (%) | % K | K error (%) |
|---|---|---|---|---|---|---|---|---|
| ***BYA 126*** | alkaline-lamprophyres | bt | ***190*** | 11 | 44.60 | 15.01 | 5.73 | 3.93 |
| ***P8*** | alkaline-lamprophyres | bt | ***163*** | 9 | 33.05 | 17.16 | 4.99 | 3.10 |

## 7.2. Sr and Nd Isotopic Data

Eight whole rock samples were selected for Nd isotopic analyses and five samples were selected for Sr isotope analyses. Sm and Nd concentration were calculated by isotopic dilution, whereas Rb and Sr contents were taken from ICP-MS analyses. The results are listed in Table 11. Initial Sr and Nd isotopic ratios have been re-calculated to the ***163 Ma*** *K-Ar* age.

The Río Grande rocks display, in general, moderately high initial $^{87}Sr/^{86}Sr$ isotopic ratios, ranging from 0.70724 to 0.70781. Samples P8 and BYA 127, however, present much lower Sr initial ratios, of 0.70377 and 0.70455, respectively. $\varepsilon_{Nd}$ (t) values are positive, ranging between + 1.5 (BHU 131) and + 5.6 (BYA 124a). $T_{DM}$ model ages vary between 0.25-0.64 Ga (Table 11).

*Table 11: Rb-Sr and Sm-Nd isotopic data for the Río Grande subvolcanic rocks.*

.

| *Locality* | Sample | Rb (**) (ppm) | Sr (**) (ppm) | $^{87}Rb/^{86}Sr$ | $(^{87}Sr/^{86}Sr)_{meas}$ | $(^{87}Sr/^{86}Sr)$ t | Sm (ppm) | Nd (ppm) | $^{147}Sm/^{144}Nd$ | $(^{143}Nd/^{144}Nd)_{meas}$ | $(^{143}Nd/^{144}Nd)$ t | $\varepsilon_{Nd\ (t)}$ | $T_{DM\ (Ga)}$ |
|---|---|---|---|---|---|---|---|---|---|---|---|---|---|
| ***Coraya*** | BCO 49 | 22.00 | 356.00 | 0.01 | 0.70756 (±02) | 0.70715 | 13.38 | 66.10 | 0.12 | 0.512752 (±06) | 0.512621 | 3.77 | 0.51 |
| | BCO 52 | | | | | | 25.38 | 136.21 | 0.11 | 0.512753 (±06) | 0.512633 | 4.00 | 0.46 |
| ***Yacoraite*** | P8* | 8.87* | 825.60* | 0.03* | *0.70373 (±02) | 0.70377 | 25.07* | 159.24* | 0.09* | 0.512635 (±05)* | 0.512533 | 2.06* | 0.54 |
| | BYA 123 | | | | | | 12.73 | 74.40 | 0.10 | 0.512752 (±06) | 0.512642 | 4.17 | 0.42 |
| | BYA 124a | 52.10 | 712.30 | 0.36 | 0.70829 (±02) | 0.70781 | 7.94 | 41.21 | 0.12 | 0.512716 (±11) | 0.512716 | 5.62 | 0.25 |
| | BYA 125 | 57.10 | 828.40 | 0.54 | 0.70783 (±01) | 0.70737 | 18.24 | 100.84 | 0.11 | 0.512747 (±16) | 0.512630 | 3.95 | 0.45 |
| | BYA 126 | | | | | | 18.23 | 100.73 | 0.11 | 0.512743 (±15) | 0.512626 | 3.87 | 0.46 |
| | BYA 127 | 71.20 | 1657.40 | 0.31 | 0.70484 (±01) | 0.70455 | 15.78 | 90.19 | 0.11 | 0.512735 (±07) | 0.512622 | 3.79 | 0.46 |
| ***Huichaira*** | BHU 131 | 35.20 | 812.40 | 0.13 | 0.70753 (±03) | 0.70724 | 13.21 | 71.68 | 0.11 | 0.512625 (±06) | 0.512506 | 1.52 | 0.64 |

*Obs:*

Errors on measured isotope ratios are given in parenthesis as uncertainty in last digits (2s)
$\varepsilon_{Nd}$ (T) calculated relative to CHUR with present-day value of $^{143}Nd/^{144}Nd= 0.512638$. $T_{DM}$ values were calculated using De Paolo' model (1981).

$^{87}Sr/^{86}Sr$ and $^{143}Nd/^{144}Nd$ and $\varepsilon_{Nd(t)}$ calculate with an age of 163 Ma.

(*) Data from *Omarini et al., 2005*.

(**) Elemental abundances of Rb and Sr are taken from ICP-MS analyses

## 8. Discussion and Conclusions

The Río Grande subvolcanic rocks have been classified previously as ankaramites, piroxenitic horblendites, picrites or basalts with alkaline affinities (Toselli and Aceñolaza, 1984, Manca et al., 1987 and Chayle et al., 1987). The field relationships and the new petrochemical, geochemical, and isotope data, permitted us to classify these rocks as alkaline lamprophyres. The presence of (i) porphyritic panidiomorphic textures, (ii) leucocratic carbonate-analcime rich ocelli and (iii) volatile mineralogical compositions (amphibole, phlogopite) are important characteristics for distinguish lamprophyres rocks from others basic rocks and these characteristics are present in the Rio Grande subvolcanic rocks. According to Rock (1991), the alkaline lamprophyres (AL) are volatile ($H_2O \pm CO_2$)-rich rocks, characterized by high LOI values. On the other hand there is a complete gradation (Rock, 1991) between them and alkali basalts, one can consider AL as volatile-enriched equivalents of alkali basalts (Wimmenauer 1973b).

We plotted the pyroxene and amphibole crystals compositions of the Rio Grande lamprophyres in the classification diagrams proposed by Rock, 1987 for lamprophyres (Fig. 13). In the pyroxene diagram (Fig. 13 A), the diopside and augite crystals fall in the Alkaline lamprophyres (AL) field, close to straddling the boundary separating Calc-alkaline (CAL) and Alkaline lamprophyres (AL) from Ultramafic lamprophyres (UML). In the amphibole diagram ($Al_2O_3/TiO_2$ vs. $CaO/Na_2O$) the titanian-pargasite crystals (Fig. 13 B) are plotted at the intersection of Ultramafic lamprophyres-Alkaline lamprophyres with Calcio-alkaline lamprophyres (UML-AL from CAL lamprophyres) fields.

Among the alkaline lamprophyres three major varieties, camptonites, monchiquites and sannaites, are distinguished. On the bases of paragenesis, the Río Grande rocks can be classified as monchiquite, a feldspar-free alkaline lamprophyre composed of diopside, Ti-rich biotite/phlogopite, Ti-pargasite, forsteritic olivine phenocrysts in a groundmass made of the same minerals except olivine, with analcime or glass and abundant globular structures. Since analcime is an important phase in the ocelli, the rock is identified here as ***ocellar analcime monchiquite***.

The origin of globular structures is much debated (Rock, 1991). They are believed to represent either: (i) magmatic crystallization involving liquid immiscibility (Philpotts 1976, Eby, 1980) or (ii) segregations of late stage liquids (Cooper, 1979) or amygdales. Those originated by liquid immiscibility have high $TiO_2$ contents (Philpotts, 1976) and are characterized by distinctive chemistry and different rim compositions between the minerals of globules and groundmass (Foley, 1984), whereas those originated by late stage segregations

have low $TiO_2$ contents (Philpotts, 1976) and are zoned, with inner analcime-carbonate zone and outer ground-mass mineral zones (Foley, 1984). The similar chemistry between the ocelli and groundmass minerals and the lack of early differentiates (as olivine, clinopyroxene, etc.) within the structures suggest that the ocelli in the Río Grande lamprophyres can be explained by late stage-segregations.

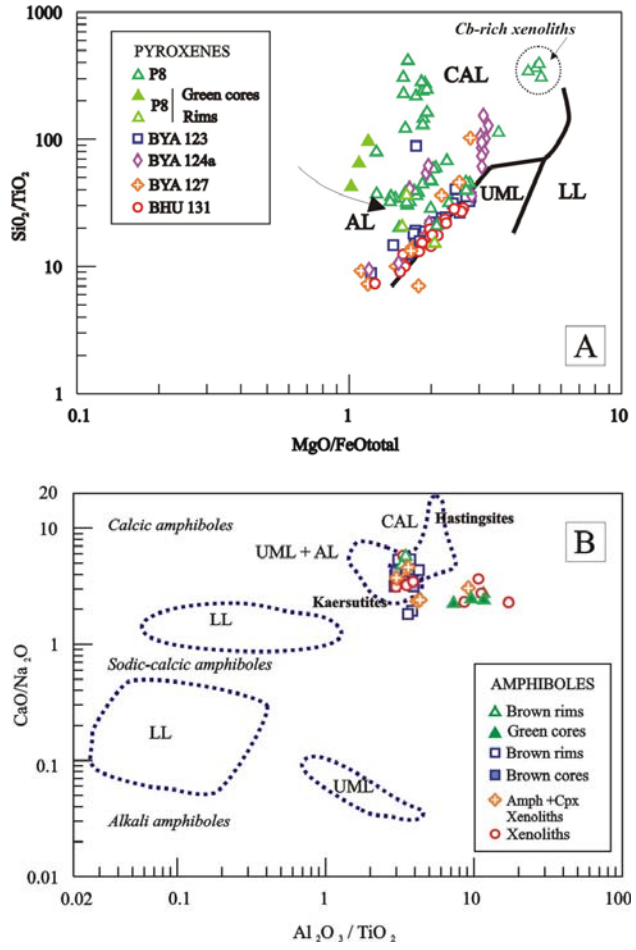


**Figure 13:** A) Discriminate diagram showing compositional field on pyroxene crystals to the different lamprophyres branches. The Rio Grande pyroxen crystals are plotted in the limit between Al/CAL-UML fields. B) Al2O3/TiO2 vs. CaO/Na2O discriminate diagram for amphibole compositions, after Rock, 1987, 1991. The Rio Grande amphibole crystals are plotted in the UML-AL/CAL limits fields. **CAL:** calc-alkaline lamprophyres, **AL:** alkaline lamprophyres, **UML:** ultramafic lamprophyres and **LL:** lamproites.

The 163 Ma K-Ar ages allow to associate the Rio Grande monchiquites with the pre-rift stage of the Salta rift (Jurassic-Eocene) evolution. They were placed in the centre of the future rift structure. For the pre-rift phase the older rocks known were emplaced at ca. 154 Ma (Cristiani et al. 2004, Cristiani et al., 2008) as anorogenic plutonic complexes (Castro Tolay-

Tusaquillas, Abra-Laite-Aguilar and Fundiciones, plutonic complexes) along the Cobres-Salinas Grandes and Tres Cruces branches. The basic magmas of Castro Tolay and Aguilar intrusives have OIB affinity indicating that they were generated in the asthenospheric mantle (Cristiani et al., 2005). At 100 Ma, during the syn-rift phase, rocks with basanite (Matancillas, Finca El Rodeo and Las Conchas, Lucassen et al., 2007) and phonotephrite (Cadillal) compositions have been recognized. For comparison rocks from the different stages of the Salta Rift are plotted in the spiderdiagram of figure 14. The Rio Grande rocks are characterized by the highest contents of LILE, HFSE and REE and by a pronounced K and Sr negative anomaly.

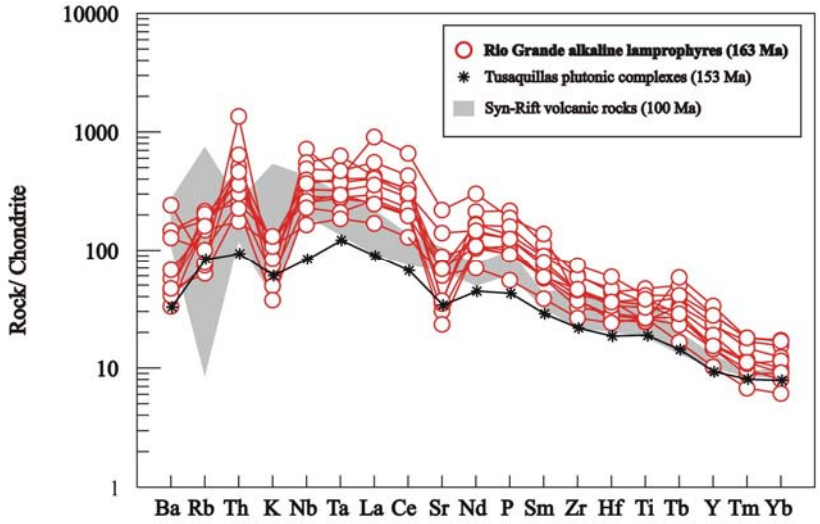


**Figure 14:** Trace elements pattern of pré-rift stage and syn-rift stage rocks of Salta Rift. The Rio Grande lamprophyres and Tusaquillas plutonic complex belong to pre-rift stage. Note the high concentrations in LILE and HFSE of the Rio Grande lamprophyrescompared with the Tusaquillas complex. The syn rift volcanic rocks selected are Las Conchas, El Cadillal, Finca El Rodeo and Matancillas basanites. Date of Tusaquillas complex, from Cristiani et al., 2004. Data of Syn-Rift volcanic rocks from Lucassen et al., 2007. Normalized values from Thompson, 1982.

Lucassen et al., (2005) propose that the lithospheric mantle composition under the Central Andes has been modified periodically by subduction processes since the Paleozoic. Therefore, according to these authors, at present day there are three possible mantle sources under the Central Andes: (i) an early Paleozoic mantle, which formed, or was modified, during the late Cambrian early Ordovician Famatinian orogeny , (ii) a Proterozoic sub-continental lithospheric mantle (SCLM), belonging to the Brazilian shield, which is thought to be progressively underthrusted beneath the present Central Andes during Miocene shortening

(e.g., McQuarrie et al., 2005) and (iii) mantle modified by magmatic activity during Mesozoic extension (e.g., Viramonte et al., 1999; Sempere et al., 2002).

In order to constrain isotopically their mantle source(s), the Río Grande monchiquites are plotted in the $^{87}Sr/^{86}Sr$ vs. $^{143}Nd/^{144}Nd$ isotope diagram (Fig. 15). The samples plot within the high $^{87}Sr/^{86}Sr$ peridotite field and close to two Sr-enriched basanite shown by Lucassen et al. (2005). In order to explain the presence of high $^{87}Sr/^{86}Sr$ peridotite and the Sr-enriched basanite in this area, these authors propose, the separation of Rb-bearing hydrous minerals, such as phlogopite and amphibole, or the long-term separation of the respective parent/daughter element pairs in the pre-cretaceous metasomatized mantle. The isotopic data point to a metasomatized mantle as a source also for the Río Grande lamprophyres.

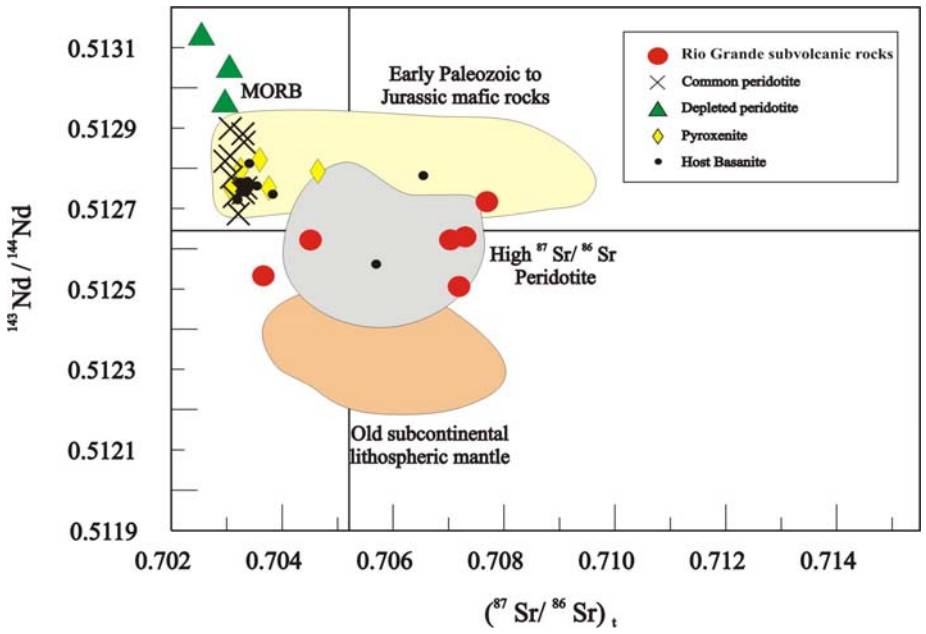


**Figure 15:** $^{87}Sr/^{86}Sr$ vs. $^{143}Nd/^{144}Nd$ diagram for the Río Grande lamprophyres. The isotopic compositions of xenoliths and mantle-derived rocks from the Central Andes are also shown. The data are recalculated to 160 Ma (Lucassen et al., 2005).

The Nd and Sr isotopic characteristics also suggest a heterogeneous mantle source, with one end-member formed by high $^{87}Sr/^{86}Sr$ ratios and other which show low values for this ratio.

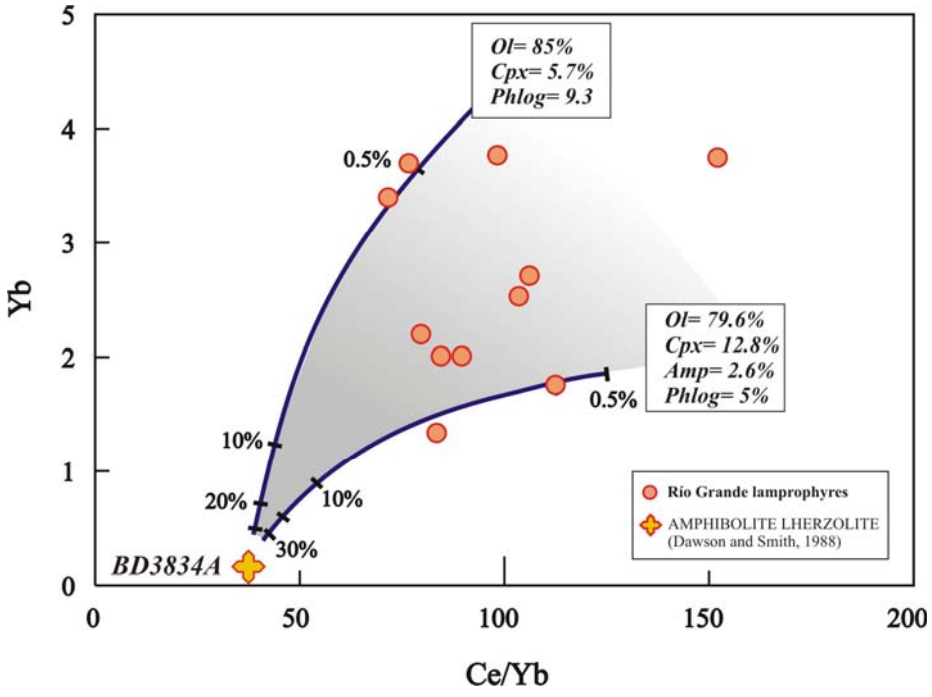


**Figure 16:** Ce/Yb vs. Ce diagram for the Rio Grande lamprophyres. Melting curves for amphibolite lherzolite of sample BD3438A from a metasomatised mantle of Pello Hill, Tanzania, are shown. Degree of partial melting (%) is indicated along the melting lines.

In figure 16 partial melting modeling of a metasomatized mantle is shown. Modal bach-melting calculation have been carried out on a metasomatized mantle. We select an amphibolite lherzolite (BD3848A) from the Pello Hill in Tanzania (Dawson and Smith, 1988). It is characterized by 6.0 ppm of Ce and 0.16 ppm of Yb. For the clinopyroxene and phlogopite we used the partition coefficient proposed by Foley, 1996 for alkaline lamprophyres. For the rest of minerals we used the partition coefficient shown in Rollinson, 1993 for basaltic liquids. Partial melting trajectories suggest that the Rio Grande lamprophyres could be generated from an enriched amphibolite lherzolite mantle source by less than 2 % partial melting (Fig. 16). The different lamprophyres were formed by nearly the same degree of melting of the same source with slightly different parageneses. The BYA123 and 124, are explained by a partial melting of a amphibolite lherzolite with Ol (79.6%), Cpx (12.8%), Amp (2.6%) and Phlo (5%), whereas samples BYA123 and 122 could be explained by a partial melting around 0.5% of a amphibolite lherzolite with Ol (85%), Cpx (5.7%) and Phlo (9.3%). The rest of samples could be modeled using a source with intermediate mineral compositions.

Several types of metasomatism have been identified in mantle xenoliths around the world on the basis of chemical, isotopical and mineralogical compositions. Proposed metasomatic agents include alkali-rich silicate and $CO_2 \pm H_2O$-rich fluids or carbonatite melts (e.g. Frey and Green, 1974; Roden et al., 1984, Coltorti et al., 1999). The REE patterns of the studied rocks show strong enrichment in LREE, while HREE are depleted. The presumed introduction of a $CO_2$ rich fluid in the depleted mantle source might have increased LREE with respect to HREE (Barbieri et al., 1997). The anomalous $SrCO_3$ content of carbonate (e.g. ocelli, cpx-bearing carbonate xenoliths and groundmass in sample P8) (Table 8), may suggest the involvement of carbonatitic liquids during the evolution of the Río Grande monchiquites and the presence of apatite may also be suggestive of metasomatism by carbonatite melts or $CO_2$ rich fluids. The hypothesis that the mantle where the Rio Grande lamprophyres derived is metasomatized by carbonatite fluids is also supported by the occurrence of carbonatite rocks associated with the Salta rift in NW Argentina such as the Santa Julia Complex (Zappettini, 1998 ) and the Ayopaya carbonatite complex (Schultz et al., 2004, Lucassen et al., 2007)

Considering that the Río Grande lamprophyre original magmas derived from to the metasomatized mantle, their $T_{DM}$ model ages might record a metasomatic event at approximately 0.45 Ga, coincident with the Ordovician Famatinian Orogeny (Lucassen et al., 2005).

***Acknowledgements***

The authors are CNPq and CONICET researchers and grateful for the research grant that allowed field and laboratory work and financing from the PROSUL programme. Sérgio Junges, Jorge Laux, Bárbara Lima and Sandrine Ferreira are acknowledged for technical assistance. Dr. Miguel Based is grateful for the K-Ar age.

## References

**Aceñolaza, E. G., Fernandez, R. I., Manca, N., 1982**. Caracteres bioestratigráficos y paleoambientales del Grupo Mesón (Cámbrico Medio-Superior), centro-oeste de América del Sur. Estudios Geológicos, 38, 385-392.

**Adams, Ch., Miller, H., Toselli., A. J., 1990.** Nuevas Edades de Metamorfismo por el método k-Ar de la Formación Puncoviscana y equivalentes, NW Argentina. In: Aceñolaza, F. G;

Millar, H; Toselli, A. J; (Eds.), El Ciclo Pampeano en el Noroeste Argentino. Serie de Correlación Geológica N 4. Universidad Nacional de Tucumán, 209-219.

**Adams, Ch.; Miller, H.; Toselli, A. J., 2006.** Maximum age and provenance area of the Puncoviscana Fm. Sediments (NW Argentina), based on detrital zircon geochronology-a pilot study. XI Congreso Geológico Chileno, 2006 Antofagasta, Chile. Actas, Vol. 1, 11-14.

**Aumento, F., Ade-Hall, J. M., 1973**. Deep-drill-1972. Petrology of the Bermuda drill core. *EOS,* 54, 485

**Aumento, F., Ade-Hall, J. M., Reynolds, P. M., Gunn, B. M., 1974.** The Bermuda seamount: a reactivated section of an older ocean crust. *EOS,* 55, 455.

**Avila Salinas, W. A., 1986.** El magmatismo Cretácico en Bolivia. Symposium IGCP Project 242, La Paz, Proceedings, 52-66.

**Azambre B., Rossy M., Albarede, F., 1992.** Petrology of the alkaline magmatism from the Cretaceous Norht-Pyrenean Rift Zone (France and Spain). Eur. J. Mineral, 4, 813-834.

**Azbej, T., Szabó C., Bodnár R. J., Dobosi, G., 2006.** Genesis of carbonate aggregates in lamprophyres from the northeastern Transdanubian Central Range, Hungary: magmatic or hydrothermal origin? Mineral Petrol, 88, 479-497.

**Bahlburg, H., 1998.** The geochemistry and provenance of Ordovician turbidites in the Argentina Puna. In: Pankhurst, R. J. & Rapela, C. W. (Eds.), The Proto-Andean margin of Gondwana. Geological Society Special Publication, London N 142, 127-142.

**Barbieri, M., Ghiara, M. R., Stanzione, M., Villar, L. M., Pezzutti, N. E., Segal., S., 1997.** Trace-Element and Isotope constraints on the origin of Ultramafic Lamprophyres from Los Alisos (Sierras Subandinas, Northern Argentina). Journal of South American Earth Sciences, 10, 39-47.

**Barrabé, L. C., 1952**. Les roches intrusives à hornblende brune des Pyrenées. 19th Int. Geol. Cong, vi, 9-22.

**Bédard, J. H., 1994.** Mesozoic east North American alkaline magmatism: Part 1. Evolution of Monteregian lamprophyres, Québec, Canada. Geochim. Cosmochim Acta, 58, 95–112.

**Bernard-Griffiths, J., Fourcade, S., Dupuy, C., 1991.** Isotopic study (Sr, Nd, O and C) of lamprophyres and associated dykes from Tamazert (Morocco): crustal contamination processes and source characteristics. Earth Planet Sci Lett. 103, 190–199.

**Bordonaro, O. L., 1992.** El Cámbrico de Sudamerica In: Gutiererz-Marco, J. G. Saavedra, J. and Rabano, I. (Eds.), Paleozoico Inferior de IberoAmerica. Universidad de Extremadura, Spain, 23-68.

**Brooks, C., Platt, R. C., 1975.** Kaersutite-bearing gabbroic inclusions and the late dike swarm of Kangerdlugssuaq, E. Greenland. *Mineral. Mag.,* 40, 258-83.

**Buatois, L. A., Mángano, M. G. 2003.** La icnofauna de la formación Puncoviscana en el noroeste argentino: La colonización de fondos oceánicos y reconstrucción de paleoambientes y paleoecosistemas de la transición precámbrica-cámbrica. Ameghiniana 40 (1), 103–117.

**Castaño, A. Rodrigo, L. A., 1978.** Sinopsis estratigráfica de Bolívia Parte 1: Paleozóico. Publicaciones Academia Nacional de Ciencias Boliviana 146 pp.

**Coira, B., Manca, N. y Chayle, W., 1990.** Registros volcánicos en la Formación Puncoviscana. In: Aceñolaza, F. G; Millar, H; Toselli, A. J; (Eds.), El Ciclo Pampeano en el Noroeste Argentino. Serie de Correlación Geológica N 4. Universidad de Tucumán, 53-60.

**Coltorti, M., Bonadiman, C., HintonR. W, , Siena, F., Upton B. G. J., 1999.** Carbonatite metasomatism of the oceanic upper mantle: evidence for clinopyroxenes and glasses in ultramafic xenoliths of Grande Comoro, Indian Ocean. J. Petrology,40, 133-165.

**Comin-Chiaramonti, P., Gomes, C. B., Velázques V. F., Censi, P., Antonini, P., Comin-Chiaramonti, F., Punturo, R., 2005.** Alkaline complexes from southeastern Bolivia. In: Comin-Chiaramonti, P., Gomes, C. B. (Eds.) Mesozoic to Cenozoic Magmatism in the Brazilian Platform. EDUSP/FAPESP, São Paulo, 71-148.

**Cooper, A. F., 1979.** Petrology of ocellar lamprophyres from western Otago, New Zealand. J. Petrology, 20, 139-164.

**Cornen, G., 1981.** . Des complexes alcalins similaires en domaines oceániques et continental: le banc de Gorringe comparé à la Serra de Monchique. C. R. *Acad. Sci. Paris,* 292, 463-466.

**Cornen, G., 1982.** Petrology of the alkaline volcanism of Gorringe bank (SW Portugal). *Marine Geol,*. 47, 101-130.

**Cristiani, C., Del Moro, A., Matteini, M., Mazzuoli, R., Menegatti, N., Omarini, R. H., 2000.** The Jurassic-Cretaceous plutonism of NW Argentina (central Andes): age, geochemical characters and geological setting. 31 st International Geological Congress, rio de Janeiro, Symposium Volcanism and Associated Regime, (CD-ROM).

**Cristiani, C., 2004.** Il plutonismo anorogenico Mesozoico nell'Altiplano della Puna (Argentina Nord occidentale, Ande Centrali): implicazioni petrogenetiche e geodinamiche. Ph.D Thesis, Universita de Pisa, 229 pp.

**Cristiani, C., Matteini, M., Mazzuoli, R., Omarini, R. H., Villa, I. M., 2005**. Petrology of late Jurassic-early Cretaceous Tusaquillas and Abra Laite-Aguilar Plutonic Complexes (Central Andes, 23º 05' S-66º 05' W): a comparison with rift-related magmatism of NW Argentina and E Bolivia. In: Comin-Chiaramonti, P., Gomes, C. B. (Eds.) Mesozoic to Cenozoic Magmatism in the Brazilian Platform. EDUSP/FAPESP, São Paulo, 213-240.

**Currie, K. L., Ferguson, J., 1970.** The mechanism of intrusión of lamprophyre dikes as indicated by “offsetting” of dikes. Tectonophysics, 9, 525-535.

**Chayle, W., Coira, B., 1987**. Vulcanitas básicas a ultrabásicas y mesosilíceas de la Formación Puncovicana en el área del Cerro Alto de Minas-Departamento Tilcara-Jujuy, Argentina. X. Congr. Geol. Argentino, Tucumán, Actas 4**,** 292-295.

**Cherroni, C., 1977.** El sistema Cretácico em la parte boliviana de la cuenca cretácica andina. Revista Técnica YPFB 6 (12), 5-46.

**Dawson, J. B., and Smith, J. V., 1988**. Metasomatized and veined upper-mantle xenoliths from Pello Hill, Tanzania: evidence for anomalously-high mantle beneath the Tanzania sector of the East African Rift Valley. Contrib. Mineral. Petrol. 100, 510-527.

**De Almeida, M. A., 1955**. Geologia e Petrología do arquipé1ago de Fernando de Noronha. Monogr. Div. Geol. Mineral. Brazil, 13.

**Delor, C. P., Rock, N. M. S., 1991.** Alkaline-ultramafic lamprophyre dykes from the Vestfold Hills, Princess Elizabeth Land, E. Antarctica. Antarctic Science, 3 (4) 419-432.

**DePaolo, D.J., 1981.** A neodymium and strontium isotopic study of Mesozoic calc-alkaline granitic batholith of the Sierra Nevada and Peninsular Ranges. California. Journal Geophysical Research 86, 10470-10488.

**Do Campo, M., Nieto, F., Omarini, R., Ostera, H., 1999.** Neoproterozoic K–Ar ages for the metamorphism of the Puncoviscana formation, Northwestern Argentina, 2 Simposio Sudamericano de Geología Isotópica, V. Carlos Paz, Argentina, Actas I, 48–53.

**Do Campo, M., 1999b.** Mineralogía, geoquímica y geocronología de la Formación Puncoviscana (Neoproterozoico) entre los 23° 30' y 25° 50' de Latitud Sur, Noroeste de Argentina. PhD thesis, Universidad de Buenos Aires, Argentina, 287 pp.

**Dostal J, Owen J. V., 1998.** Cretaceous alkaline lamprophyres from northeastern Czech Republic: geochemistry and petrogenesis. Geol. Rundsch 87, 67-77.

**Drever, H. I., 1960.** Immiscibility in the picritic intrusión at Igdlorssuit, West Greenland. 21 st Int. Geol. Congr., 13, 47-58.

**Durant, F. R.; Aceñolaza, F. G. 1990.** Caracteres biofaunísticos, paleoecológicos y paleogeográficos de la Formación Puncoviscana (Precámbrico Superior-Cámbrico Inferior) del Noroeste Argentino. In: Aceñolaza, F. G; Millar, H; Toselli, A. J; (Eds.), El Ciclo Pampeano en el Noroeste Argentino. Serie de Correlación Geológica N 12. Universidad de Tucumán, 71-112.

**Durant, F. R., 1996.** La transición Precámbrico-Cámbrico en el sur de Sudamérica. In: Baldis, B., Aceñolaza, F. G. (Eds.), Early Paleozoic Evolution in NW Gondwana. Serie de Correlación Geológica, N **12.** Universidad Nacional de Tucumán, 195-205.

**Eby, G. N., 1980.** Minor and trace elements partitioning between immiscible ocelli groundmass pairs from lamprophyres dykes and sills, Monteregian Hills petrographic province, Quebec. Contri. Mineral Petrlology, 75, 269-278.

**Fareeduddin, I., Kirmani, R.,Basavalingu, B., 2001.** Petrology of ocellar lamprophyres in South Delhi Fold Belt, Danva, Sirohi District, Rajasthan, India. Gondwana Research, 3, 497-508.

**Ferguson, J., Currie, K. L., 1971**. Evidence of liquid immiscibility in alkaline ultrabasic dykes at Callander bay, Ontario. J. Petrology, 12, 561-585.

**Foley, S. F., 1984.** Liquid immiscibility and melt segregations in alkaline lamprophyres from Labrador. Lithos, 17, 127-137.

**Foley, S. F., Jackson, S. E., Fryer, B. J., Greenough, J. D., Genner, G. A., 1996.** Trace element partition coefficients for clinopyroxene and phlogopite in an alkaline lamprophyre from Newfoudland by La-ICP-MS.Geochim Cosmochim Acta, 60, 229–238.

**Frey, F. A., and Green, D. H., 1974.** The mineralogy, geochemistry and origin of lherzolite inclusions in Victorian basanites. Geochim Cosmochim Acta, 38, 1023–1059.

**Galliski, M. A., Viramonte, J. G., 1988.** The Cretaceous paleo-rift in northwestern Argentina: a petrologic approach. Journal of South American Earth Sciences, 1, 329-242.

**Gioia, S.M.C., Pimentel, M., 2000.** The Sm-Nd isotopic method in the Geochronology Laboratory of University of Brasilia. Anais da Academia Brasileira de Ciências, 72, 219-245.

**Gohrbrandt K. H. A., 1992.** Paleozoic paleogeographic and depositional developments on the proto-margin of Gondwana: their importance to hydrocarbon accumulation. Journal of South American Earth Sciences, 6, 267-287.

**Gomez Omil, R., Boll, A., Hernandez, R., 1989.** Cuenca Cretácico-Terciaria del noroeste argentino (Grupo Salta). In: Chebli, G., Spalleti, L. (Eds.) Cuencas Sedimentarias de la República Argentina. Serie de Correlación Geológica N 4 Universidad Nacional de Tucumán

**Jaillard, E., Soler, P., Carlier, G., Mourier, T., 1990.** Geodynamic evolution of the northern and central Andes during early to middle Mesozoic time: a Tethyan model. Journal of the Geological Society of London, 147, 1009-1022.

**Jaillard, E., Hérail, G., Monfret, T., Díaz-Martínez, E., Baby, P., Lavenu, A., Mumont, J. F., 2000.** Tectonic evolution of the Andes of Ecuador, Peru, Bolivia and Northernmost Chile. In: Cordani, U. G., Dilani, E. J., Thomaz Filho, A., Campos, D. A. (Eds.) Tectonic evolution of South America 31st International Geological Congress, rio de Janeiro, 481-559.

**Jezek, P. 1990.** Análisis sedimentológico de la Formación Puncoviscana entre Tucumán y Salta. In: Aceñolaza, F. G; Millar, H; Toselli, A. J; (Eds.), El Ciclo Pampeano en el Noroeste Argentino. Serie de Correlación Geológica N 4. Universidad Nacional de Tucumán, 9-35.

**Keppie, J. D., Bahlburg, H. 1999.** Puncoviscana Formation of northwestern and central Argentina: Passive margin or foreland basin deposits? In*:* Ramos, V.A. & Keppie, J.D. (Eds.), Laurentia-Gondwana Connections before Pangaea. Geological Society of America Special Publications, 336, 139-144.

**Knill, D. C., 1982**. Permian volcanism in SW England. In: Sutherland, D. S. (Ed.) Igneous Rocks of the British Isles, Wiley, New York. 329-332.

**Kraemer, P. E., Escayola, M. P., Martino, R. D., 1995**. Hipótesis sobre la evolución neoproterozoica de las Sierras Pampeanas de Córdoba (30º40'–32º40' S) Argentina. Revista de la Asociación Geológica Argentina 50 (1–4), 47–59.

**Kumpa, M., Sanchez, T. M., 1988.** Geology and sedimentology of the Cambrian Grupo Mesón (NW Argentina). In: Bahlbur, G., H., Breitkreuz, C., Giese, P. (Eds.), The southern Central Andes: Contributions to Structure and Evolution of an Active Continental Margin. Lecturer Notes on Earth Sciences, 17, Springer Verlag, Berlín, 39-53.

**Lanfranco, J. J., 1972.** Estudio de las intrusiones en la falda oriental de la Sierra de Aguilar y metamorfitas del área de contacto. Ph.D Thesis, Universidad Nacional de Córdoba, 68 pp.

**Leake, B.E., Wooley, A.R., Arps, C.E.S., Birch, W.D., Gilbert, M.C., Grice, J.D., Hawthorne, F.C., Kato, A., Kisch, H.J., Krivovichev, V.G., Linthout, K., Laird, J., Mandarino, J.A´ ., Maresch, W.V., Nickel, E.H., Rock, N.M.S., Schumacher, J.C., Smith, D.C., Stephenson, N.C.N., Ungaretti, L., Whittaker, E.J.W., Youzhi, G., 1997.** Nomenclature of amphiboles: report of the Subcommittee on Amphiboles of the International Mineralogical Association, Commission on New Minerals and Mineral Names. Am. Mineral. 82, 1019–1037.

**Lork, A., Miller, H. Kramm, U., Grauert, B., 1990**. Sistemática U-Pb de circones detríticos de la Fm. Puncoviscana y su significado para la edad máxima de sedimentación en la Sierra de Cachy (prov. De Salta, Argentina). In: Aceñolaza, F. G; Millar, H; Toselli, A. J; (Eds.), El Ciclo Pampeano en el Noroeste Argentino. Serie de Correlación Geológica N 4. Universidad de Tucumán, 199-208.

**Lucassen, F., Escayola, M., Franz, G., Romer, R. L., Koch, K., 2002a.** Isotopic composition of Late Mesozoic basic and ultrabasic rocks from the Andes (23º-32º)-implications for the Andean mantle. Contrib. Mineral. Petrol. 143, 336-349.

**Lucassen, F., Franz, G., Viramonte, J. G., Romer, R. L., Dulski, P., Lang, A., 2005.** The late Cretaceous lithospheric mantle beneath the central Andes: evidence from phase equilibrium and composition of mantle xenoliths. Lithos, 82, 379-406.

**Lucassen, F., Franz, G., Romer, R. L., Schultz, F., Dulski, P., Wemmer, K., 2007.** Precenozoic intra'plate magmatism along the Central Andes (17º-34ºS): Composition of the mantle at an active margin. Lithos, 99, 312-338.

**Manca, N., Coira, B., Barber, E., Pérez, A., 1987**. Episodios magmáticos de los ciclos Pampeano y Famatiniano en el rio Yacoraite, Jujuy. X. Congr. Geol. Argentino, Tucumán, Actas 4, 299-301.

**Mendez, V., Villar, L. M., 1979.** Los filones ultrabásicos del rio Piedras, Sierras Subandinas de Salta y Jujuy. VII Congreso Geológico Argentino, Actas, 2, 16-29.

**Menegatti, N., 2001.** El complejo alcalino Sierra de Rangel, provincia de Salta, Argentina. PH.D. Thesis, Universidad Nacional de Salta, Argentina, 157 pp.

**Mitchell-Thomé, R. C., 1976**. Geology of the Middle Atlantic Islands. Gebruder Borntraeger, Berlin. 382 pp.

**Moreno, J. A., 1970.** Estratigrafía y paleogeografía del Cretácico superior de la Cuenca del Noroeste Argentino, con especial mención de los Subgrupos Balbuena y Santa Bárbara. Revista de la Asociación Geológica Argentina XXV (1), 9-44.

**Morimoto, C.N., 1988.** Nomenclature of pyroxenes. Mineral. Mag. 52, 535–550.

**Moya, M. C., Malanca, S., Hongn, F. D., Bahlburg, H., 1993.** El Tremadoc temprano en la Puna Occidental argentina. XII Congreso de Exploración de Hidrocarburos, Mendoza, Actas, 11, 20-30.

**MPodoziz, C. Ramos, V. A., 1990.** The Andes of Chile and Argentina. In: Ericksen, G. E., Cañas, Pinochet, M. T., Reinemuf, J. A. (Eds.) Geology of the Andes and its relation to Hydrocarbon and Mineral Resources. Circumpacific Council for Energy and Mineral Resources, Earth Sciences Series, 11, 59-90.

**McQuarrie, N., Horton, B. K., Zandt, G., Beck, S., DeCelles P. G., 2005.** Lithospheric evolution of the Andean fold-thrust belt, Bolivia, and the origin of the Central Andean Plateou. Tectonophysics, 399, 15-37.

**Nakamura, R., Coombs, D. S., 1973.** Clinopyroxene in the Tawhiroko tholeiitic dolerite at Moeraki, northeastern Otago, New Zealand. Contrib. Mineral Petrol., 42, 213-228.

**Nedli, Zs., Tóth, T. M., 2007.** Origin and geodynamic significance of Upper Cretaceous lamprophyres from de Villany Mts. (S Hungary). Mineralogy and Petrology, 90, 73-107.

**Nixon, P. H., Mitchell, R. H., Rogers, N. W., 1980.** Petrogenesis of alnoitic rocks from Malaita, Solomon Islands. Mineral. Mag., 43, 587-596.

**Omarini, R.H., Salfity, J. A., Linares, E., Viramonte, J. G., Gorustovich, S. A., 1989.** Petrología geoquímica de un filon lamprofírico en el Subgrupo Pirgua (Alemanía-Salta). Revista del Instituto de Geología y Minería, Universidad Nacional de Jujuy, 7.

**Omarini, R.H., Sureda, R.J., Götze, H.J., Seilacher, A., Plüger, F., 1999**. The Puncoviscana folded belt: a testimony of Late Proterozoic Rodinia fragmentation and the collisional pre-Gondwanic episodes. Int Journ. Earth Sciences 88 (1), 76-97.

**Omarini R.H., Sureda R.J., Escayola M.P., Pimentel, M., Matteini M., 2005.** Datos preliminares (Sm-Nd) en lavas de la fm. Puncoviscana, Provincias de Salta y Jujuy, Republica Argentina. XVI Congreso geológico Argentino, La Plata

**Phillips, W. J., 1968.** The crystallization of the teschenite from the Lugar Sill, Ayrshire. Geol. Mag. , 105, 23-34.

**Philpotts, A. R., 1972.** Density, surface tension and viscosity of the immiscible phase in a basic alkaline magma. Lithos, 5, 1-18.

**Philpotts, A. R., 1976.** Silicate liquid immiscibility: its probable extent and petrogenetic significance. Am. J. Sci., 276, 1147-1177.

**Ramos, V.A., 1988**. Late Proterozoic–early Paleozoic of South America: a collisional history. Episodes 2, 168–174.

**Ramos, V. A., Basei, M., 1997.** The basement of Chilenia: an exotic continental terrane to Gondwana during the early Paleozoic. In: Bradshaw, J. D., Weaver, S. D. (Eds.) Terrane Dynamics International Conference on Terrane Geology, Christchurch, New Zealand, Abstracts, 140-143.

**Rapela, C. W., Pankhurst, R. J., Casquet, C., Baldo, E., Saavedra, J., Galindo, C., Fanning, C. M., 1998.** The Pampean Orogeny of the southern proto-Andes: Cambrian continental collision in the Sierras de Cordoba. In: Pankhurst, R.J. & Rapela, C.W. (Eds.), The Proto-Andean Margin of Gondwana. Geological Society, London, Special Publications, 142, 181-217.

**Reyes, F. C., Salfity, J. A., 1973**. Consideraciones sobre la estratigrafía del Cretácico (Subgrupo Pirgua) del norte Argentino. VI Congreso Geológico Argentino, Buenos Aires, Actas, 1, 205-223.

**Richey, J. E., 1939**. The dykes of Scotland. Trans. Edinb. geol. Soc., 13, 393-435.

**Rieder, M., Cavazzini, G., D'Yaconov Y., Frank-Kamenetskii, V., Gottardi, G., Guggenhein, S., Koval, P., Muller, G., Neiva, A., Radoslovich, E., Robert, J-L., Sassi, F., Takeda, H., Weiss, Z., Wones, D., 1998.** Nomenclature of mica. Can. Mineral. 36, 905.

**Rock, N. M. S., 1979.** Petrology and origin of the type monchiquites and associated lamprophyres of the Serra de Monchique, Portugal. Tr. R. Soc. Edinburgh, 70, 149-170.

**Rock, N. M. S., 1982.** The Late Cretaceous alkaline igneous province in the Iberian Peninsula, and its tectonic significance. Lithos, 15, 111-131.

**Rock, N. M. S., 1984.** Nature and origin of cal-alkaline lamprophyres: minettes, vogesites, kersantites and spessartites. Tr. R. Soc. Edinburgh, Earth Scienc, 74, 193-227.

**Rock, N. M. S., 1986.** The nature and origin of ultramafic lamprophyres: alnoites and allied rocks. J. Petrol. 27, 155-196.

**Rock, N. M. S., 1987.** The nature and origin of lamprophyres: an overview. In: Fitton, J.G., Upton, B.G.J. (Eds.), Alkaline Igneous Rocks. Geological Society of London, Special Publications, 30, 191–226.

**Rock, N. M. S., 1991.** Lamprophyres. Blackie-Van Norstrand Reinhold,New York, USA, 285 pp.

**Roden, M. F., Frey, F. A., Francis, D. M., 1984.** An exemplo of consequent mantle metasomatims in peridotite inclusions in Nunivak Island, Alaska. J.Petrology. 25, 546-577.

**Rollinson, H. R., 1993.** Using geochemical data: evaluation, presentation, interpretation. Burntmill: Longman, 335 p.

**Romeuf, N., Aguirre, L., Soler, P., Féraud, G. Jillard, E., Ruffet, G., 1995.** Middle Jurassic volcanism in the Northern and Central Andes. Revista Geológica de Chile, 22, 245-259.

**Rossi, J. N., Toselli, A. J., Durand, F. R., 1992.** Metamorfismo de baja presion, su relación con el desarrollo de la cuenca Puncoviscana, plutonismo y regimen tectónico. Estudios geológicos, **48**, 279-287.

**Rubiolo D.G., 1992.** Zur geologie, Petrographie und Geochemie der Alcali Magmatite der Sierra de Santa Victoria (E-Kordillere, NW-Argentinien). Clausthaler Geowissenschaftliche Dissertationen, 41, 145 pp.

**Rubiolo, D., Schwab, K., Sureda, R., Viramonte, J. G., 1994.** Relación petrogenética entre Sannaitas y Tinguaitas em la comarca de Maiguasi (Departamento de Iruya, província de Salta, Argentina). VII Congreso Geológico Chileno 2, 1189-1193.

**Rubiolo D., Seggiaro R., Gallardo E., Disalvo A., Sanchez M., Turel A., Ramallo E., Sandruss A., Godeas M., 1997.** Hoja Geológica 2366-II / 2166-IV. La Quiaca, Provincias de Jujuy y Salta. Instituto de Geologia y Recursos Minerales, Servicio Geológico Minero Argentino. Buenos Aires. Boletín, 113 pp.

**Rubiolo D., Gallardo E., Disalvo A., Sanchez M., Turel A.,Seggiaro R., Ramallo E., Sandruss A., Godeas M., Gonzalés, O., 2003.** Hoja Geológica 2366-II / 2166-IV La Quiaca, Provincias de Jujuy y Salta. Instituto de Geología y Recursos Minerales, Servicio Geológico Minero Argentino. Buenos Aires. Boletín 246, 123 pp.

**Russo, A., Rodrigo, L. A., 1965.** Estratigrafía y paleogeografía del grupo Puca em Bolívia. Boletín del Instituto Boliviano del Petróleo, 5 (34), 5-53.

**Salfity J. A., Omarini, R. H., Baldis, B., Gutierrez, W. 1975.** Consideraciones sobre la evolución geológica del Precámbrico y Paleozoico del norte argentino. 2nd Congreso Iberoamericano de Geología Económica, Buenos Aires, 4, 341-361.

**Salfity, J. A., Marquillas, R. A., 1981.** Las unidades estratigráficas cretácicas del Norte de la República Argentina. In: Volkheimer, W., Musacchio, E. (Eds.) Cuencas sedimentarias del Jurásico y Cretácico de América del Sur. Comité del Jurásico y Cretácico, 1, 303-317.

**Salfity, J. A., 1982.** Evolución paleogeográfica del Grupo Salta (Cretácico-Eogénico), Argentina. V Congreso Latinoamericano de Geología, Buenos Aires, 1, 11-26.

**Scheuber, E., Bogdanic, T., Lensen, A., Reutter, K. J., 1994.** Tectonic development of north Chilean Andes in relation to plate convergence and magmatism since the Jurassic. In: Reutter, k. J., Scheuber, E., Wigger, P. J., (Eds.) Tectonic of the Southern Central Andes. Berlin: Springer, 121-139.

**Sempere, T., Carlier, G., Soler, P., Fornari, M., Carlotto, V., Jacay, J., Arispe, O., Néraudeau, D., cárdenas, J., Rosas, S., Jimenéz, N., 2002.** Late Permian-Middle Jurassic lithospheric thinning in Perú and Bolivia, and its bearing on Andean-age tectonics. Tectonophysics 345, 153-181.

**Schultz, F., Lehmann, B., Tawackoli, S., Rosseling R., Belyatsky B., Dulski, P., 2004.** Carbonatite diversity in the Central Andes: the Ayopaya alkaline province, Bolivia. Contrib. Mineral. Petrol. 148, 391-408.

**Smith, R. E., 1967.** Segregations vesicles in basaltic lava. Am. J. Sci., 265, 696-713.

**Snaveley, P. D., Wagner, H. C., 1961**. Differentiated gabbroic sills and associated alkalic rocks in the central part of the Oregon coast range, Oregon. Res. U.S. Geol. Surv. Short Pap. geol. hydrol. Sci. Artic., 293-435.

**Strong, D. F., Harris, A., 1974.** The petrology of Mesozoic alkaline intrusives of Central Newfoundland. Can. J. Earth Sci., 11, 1208-1219.

**Sun, S., McDonough, W. F., 1989**. Chemical and isotopic systematic of ocean basalts: implication for mantle, composition and processes. In: Sounders A. D., Norry, M.J. (Eds.), Magmatism in ocean basins. Geol. Soc. London. Spec. Pub. 42, 313-345.

**Szabó, Cs., Kubovics, I., Molnár Zs. 1993.** Alkaline lamprophyre and related dyke rock in NE Transdanubia, Hungary: The Alcsútdoboz-2 (AD-2) borehole. Mineral Petrol, 47, 127-148.

**Thompson, R. N., 1982.** Magmatism of the Britsh Tertiary volcanic propvince. Scott. J. Geol. 18, 49-107.

**Toselli, A.J., Aceñolaza, F.G., 1984.** Presencia de eruptivas basálticas en los afloramientos de la Formación Puncoviscana, en Coraya, departamento Humahuaca, Jujuy. Revista de la Asociación Geológica Argentina, 39 (1-2), 158-159.

**Turner, J. C. M. 1960.** Estratigrafía de la Sierra de Santa Victoria y adyacencias Academia Nacional de Ciencias Boletín 41, Córdoba, 163-196.

**Upton, B. G. J., Wadsworth, W. J., 1971.** Rhyodacite glass in Reunion basalt. Mineral. Mag., 38, 152-159.

**Vargas Gil, J. R., 1965.** Contribución al conocimiento geológico de los alrededores de Tupiza (Republica de Bolivia). Unpublished Thesis, Facultad de Ciencias Naturales, Universidad de La Plata, 93 pp.

**Viramonte J. G., Kay, S. M., Becchio, R., Escayola, M., Novitski, I., 1999.** Cretaceous rift related magmatism in central-western South America. Journal of South Americam Earth Sciences, 12, 109-121.

**Viterbo, C., Zanettin, B., 1959.** I filoni lamprofirici dell'Alto Baltoro. Atti Mem. Acad. Patavina Class Sci. Mat. Nat. 71, 3-39.

**Wimmenauer, W., 1973b.** Lamprophyre, Semilamprophyre und anchibasaltische, Ganggesteine. Fortschr. Mineral. 51, 3-67.

**Winchester, J. A.,Floyd, P. A., 1977.** Geochemical discrimination of different magma series and their differentiation products using immobile elements. Chemical Geology, 20: 325–343.

**Yagi, K., Ishikawa, H., Kojima, M., 1975.** Petrologyof a lamprophyre sheet in Tanegashima Island, Kagoshima prefecture, Japan. J. Jap. Assoc. Mineral. Petrol. Econ. Geol., 70, 213-24.

**Zappettini, E. O., 1998.** El Complejo Alcalino Santa Julia, provincial de Jujuy, República Argentina. X Congreso Latinoamericano de Geología y VI Congreso nacional de Geología Económica, Buenos Aires, 2, 289-294.

**Zonenshayn, L. P., Savotin, L. A., Sedov, A. P., 1984.** Global paleogeodynamic reconstructions for the last 160 million years. Geotectonics 18, 181-195.

# CAPÍTULO III

Este Capítulo apresenta os resultados petrológicos, geoquímicos e isotópicos, referentes às rochas subvulcânicas da Serra de El Niño Muerto e do Vale de Río Blanco. As informações serão apresentadas na forma de artigo completo, que será submetido ao periódico ***Journal of South American Earth Sciences,*** com o título:

LA-ICPMS U-PB GEOCHRONOLOGY AND PETROLOGY OF VOLCANIC ROCKS OF THE NEOPROTEROZOIC TO LOWER PALEOZOIC BASEMENT OF THE CENTRAL ANDES, NW ARGENTINA: INSIGHTS ON THE EVOLUTION OF WESTERN GONDWANA."

# LA-ICPMS U-PB GEOCHRONOLOGY AND PETROLOGY OF VOLCANIC ROCKS OF THE NEOPROTEROZOIC TO LOWER PALEOZOIC BASEMENT OF THE CENTRAL ANDES, NW ARGENTINA: INSIGHTS ON THE EVOLUTION OF WESTERN GONDWANA."

Natalia Hauser[a, b], Massimo Matteini[a], Márcio Pimentel[a], Ricardo Omarini[b]

[a] Laboratorio de Geocronología. Instituto de Geosciências, Univesidade de Brasilia. Brasília-DF 70910-900 Brasil.

[b] Universidad Nacional de Salta-CONICET. Buenos Aires 177, Salta 4400. Argentina

E-mail address: hausernatalia@yahoo.com.ar (Natalia Hauser)

## *Abstract*

In situ LA-ICPMS U-Pb zircon analyses and Sr-Nd isotopic data combined with major, trace and rare earth elements (REE) contents for the El Niño Muerto and Rio Blanco volcanic rocks of the Neoproterozoic to Lower Paleozoic basement of the Central Andes in NW Argentina are discussed. They are associated with sediments which have been traditionally attributed to the Puncoviscana Formation. The new data helped to investigate the tectonic setting of emplacement of the original magmas, and contribute to the better understanding of the tectonic evolution of Western Gondwana during the Early Paleozoic.

The El Niño Muerto metadacites have high-K calc-alkaline nature characterized by intermediate $SiO_2$ contents, high $Al_2O_3$ and low MgO, Cr and Ni. They are peraluminous with up to 5 % normative corundum. Contents of large ion lithophyle elements (LILE) are high and high field strength element (HFSE) contents are comparatively low, typical of arc rocks. ∑REE abundances vary from 186 to 206 ppm and chondrite-normalized REE patterns are moderately fractionated, with $(La/Yb)_n$ ratios between 5.9 to 8.6. The Rio Blanco basalts have geochemical characteristics which are similar to E-MORB, with Zr/Nb ratios from 6.8 to 9.5. Contents

of large ion lithophyle elements (LILE) are variable (10-100 ppm) and high field strength element (HFSE) are low (8-50 ppm). ∑REE vary from 76 to 196 ppm and chondrite-normalized REE patterns are weakly fractionated, with $(La/Yb)_n$ ratios between 2.6 to 4.5. Both rock units were dated using laser ablation ICPMS on zircon crystals. The data yielded the ages of 495 ± 4 Ma for the El Niño Muerto metadacites and of 501 ± 9 Ma for the Rio Blanco basalts. The El Niño Muerto metadacites have high initial $^{87}Sr/^{86}Sr$ (0.71107-0.71180) and low initial $^{143}Nd/^{144}Nd$ (0.511506-0.511697) corresponding to negative $\varepsilon_{Nd}$ (t) values, between -9.7 to -5.9, and $T_{DM}$ model ages between 1.62-1.79 Ga. The Rio Blanco basalts have moderately high $^{87}Sr/^{86}Sr$ initial ratios (0.70713-0.70942), positive $\varepsilon_{Nd}$(t) values (+2.47 to +4.46) and $T_{DM}$ model ages between 0.84 to 1.12 Ga.

The geochemical and isotopic data presented in this study indicate that the El Niño Muerto metadacites formed in the Famatinian calc-alkaline magmatic arc and that the original magmas are strongly contaminated with Precambrian (Mesoproterozoic) continental crust. The tectonic setting of formation of the Rio Blanco basalts remain unclear and their geochemical characteristics indicate that they may correspond either to an E-MORB or to within-plate anorogenic basalts. Trace element contents show compositions which are intermediate between typical Pacific E-MORB and OIB. The geochemical characteristics and geological setting of the Rio Blanco

basalts suggest that they may also be interpreted as a remnant of a back-arc basin developed during the Late Cambrian /Early Ordovician in NW Argentina.

## 1. Introduction

The rock units comprising the basement of the Central Andes, between 22º and 33º S record at least two Paleozoic orogenetic episodes: the Pampean, at ca. 520 Ma (Aceñolaza and Toselli 1973) and the Famatinian, at ca. 460 Ma (Aceñolaza and Toselli 1973).

The pampean basement in NW Argentina includes mainly Neoproterozoic to Lower Paleozoic metasedimentary sequences; the Puncoviscana Formation (Turner 1960, Omarini, 1983, Omarini, 1983, Aceñolaza et al., 1988, Jezek, 1985, 1986, Willner et al., 1990, Do Campo and Guevara, 2005, Zimmermann, 2005) is the main and oldest representative of the basement in the Eastern Cordillera. It is characterized by a thick sequence (> 2000 m) of very low to low grade metapelite and turbidites with few intercalations of carbonates and volcanic rocks (Jezek 1990, Omarini et al., 1999). Do Campo et al., (1998), Do Campo, (1999b) and Do Campo et al., (1999), on the basis of K-Ar analyses on clay minerals, defined a Late Neoproterozoic age for the Puncoviscana Formation. Its ichnofauna, whose chronostratigraphic significance has been recently reinterpreted (Buatois and Mángano, 2003), indicates a Vendian-Nemakitian-Daldynian age.

Volcanic rocks of uncertain age intercalated with the Puncoviscana Formation in NW Argentina have been recognized in several localities of the Eastern Cordillera and easternmost Puna (Toselli and Aceñolaza, 1984; Coira et al., 1990, Manca et al., 1987, Chayle et al., 1987; Omarini y Alonso, 1987, Omarini et al., 1999, Omarini et al., 2005). Due to the lack of detailed field data as well as accurate geochronology, little is known about their tectonic setting of emplacement. Two of these volcanic rocks occurrences are the subject of this study.

In this paper we present new field, petrographic and geochemical data for volcanic rocks intercalated in the Puncoviscana Formation, exposed in the El Niño Muerto Hill and in the Rio Blanco Valley. We also show, for the first time, in situ LA-ICPMS U-Pb zircon ages and Sr-Nd isotopic data for these rocks. This study attempts to investigate the relationships between the volcanic rocks and the Paleozoic orogenic cycles, to date the sedimentary sequences which are associated with them, as well as to identify their original tectonic setting. The new results are discussed, in combination with data available from the literature, in order to clarify the geodynamic significance of these volcanic rocks in the tectonic evolution of the western margin of Gondwana in NW Argentina during the Late Neoproterozoic and Early Paleozoic.

## 2. Geological Setting

The basement of NW Argentina records at least two main orogenic cycles between the break-up of the Rodinia supercontinent (~750 Ma) and the continental amalgamation of Pangea (Upper Carboniferous): the Pampean and the Famatinian orogenies.

The *Pampean Cycle* (Aceñolaza and Toselli 1973), occurred between ca. 550 and 520 Ma (Rapela, et al., 2001a, Sollner et al., 2000b, Ramos and Basei, 1997). It has been documented in the Eastern Cordillera (EC), Puna and more extensively in northwestern Sierras Pampeanas Orientales (Aceñolaza et al., 1990, Toselli, 1990, Rapela, et al., 1992, Kraemer et al., 1995,

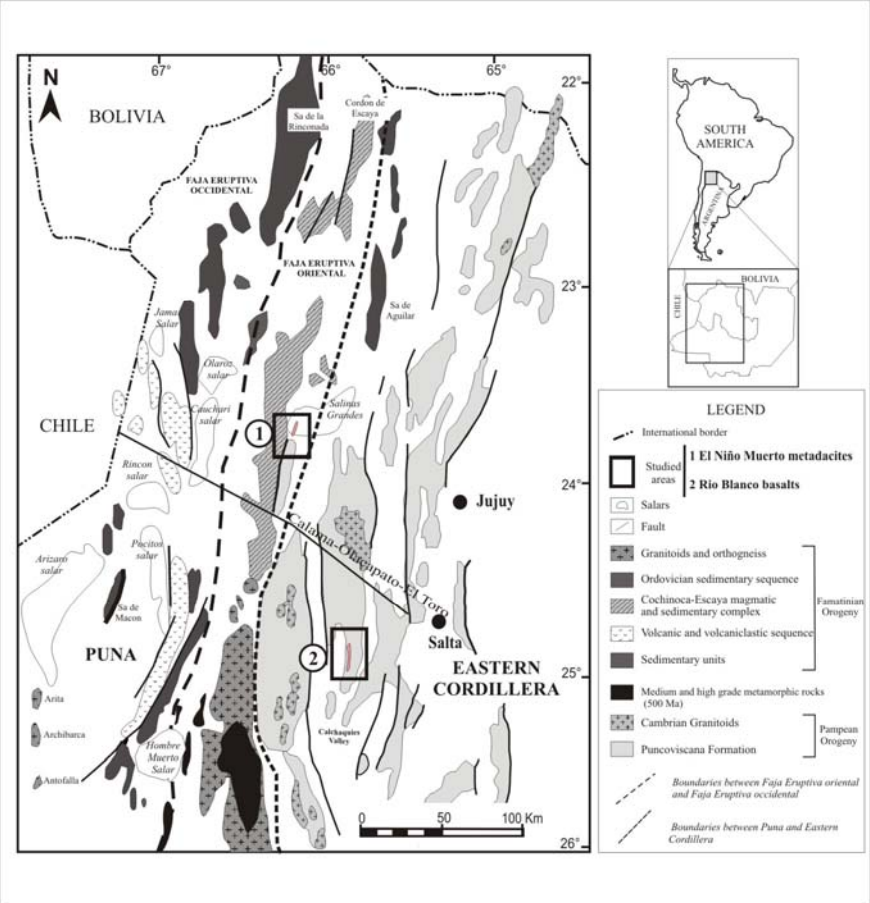


**Figure. 1:** Geological map showing the distribution of Neoproterozoic to lower Paleozoic basement rock units of NW Argentina (modified after Do Campo and Guevara, 2005 and Viramonte et al., 2007).

Llambías et al., 1998). It was characterized by an early subduction-related magmatic arc followed by the Early Cambrian (535-520 Ma) accretion of an exotic terrane, identified either as the Pampia block (Rapela et al., 2001a) or as the Arequipa-Belen-Antofalla Craton (Ramos 1988). After this accretion, the protomargin of Gondwana became a passive margin between 520 and 499 Ma (Keppie and Bahlburg, 1999, Rapela et al., 2001) until the Ordovician, when the Famatinian orogeny took place.

In NW Argentina (EC and Puna), the Pampean Cycle is represented by a passive margin sequence composed of a low- to very low-grade metamorphic sedimentary succession (Hongn et al., 1985, Mon and Hongn, 1991) made of thick turbiditic deposits with scarce associated limestones and volcanic rocks (Jezek 1990, Omarini et al., 1999).

This succession named by Turner (1960) as the Puncoviscana Formation has Neoproterozoic to lower Cambrian age, according to paleontological and gechronological data (Aceñolaza et al., 1982, Kumpa & Sanchez, 1988, Durand and Aceñolaza, 1990, Adams et al., 1990, Lork et al., 1990, Rossi et al., 1992, Bordonaro 1992, Durand 1996, Do Campo et al., 1999, Do Campo, 1999b, Buatois and Mángano 2003, Adams et al., 2006). Several volcanic rocks of uncertain age are interbedded in the sequence in different localities.

The *Famatinian Cycle* (Aceñolaza and Toselli 1973) took place between 490 to 400 Ma and records the subduction of oceanic lithosphere along the western margin of Gondwana during the Early Paleozoic. The tectonic reconstructions are supported by interpretation of the sedimentary faunal record, the tectonic-magmatic evolution of the basins, and paleomagnetic evidence (Aceñolaza and Toselli 1973, Dalziel, 1997, Rapela et al., 1992, Kraemer et at., 1995, Llambías et al., 1998, Rapela et al., 2001b). The final stage of this cycle was marked by the accretion of an exotic terrane, the Precordillera.

In NW Argentina, the *Famatinian Cycle* (490-400 Ma) is represented by: (i) platformal siliciclastic, shallow-marine sedimentary succession in the Eastern Cordillera and deeper marine sediments to the west, in the Puna plateau (Turner 1960, Salfity et al., 1975, Gohrbrandt, 1992, Moya et al., 1994, Balbhurg 1998), and (ii) basic and acid lavas and associated volcaniclastic turbidites exposed in the eastern Puna extending southwards to the Famatina magmatic arc. Two parallel N-S trending ordovician arcs are recognized in the Puna. The eastern arc known as “Faja Eruptiva de la Puna Oriental” (Mendez et al., 1973), and the western arc known as “Faja Eruptiva de la Puna Occidental” (Palma et al., 1986) (Fig. 1). The eastern arc is characterized by the alignment of small intrusion of Al-rich trondhjemites, tonalites and granodiorites as well as metadacites and metarhyolites (Omarini et al., 1984, Viramonte et al., 1984, Lorck and Balbhurg 1993, Palma et al., 1986, Blasco et al., 1996, Koukharsky et al., 2002, Kleine et al., 2004, Viramonte et al., 2007), with ages ranging from 499 to 478 Ma (Rapela et al., 2001a). The main features of the western arc is the presence of Al-poor granodioritic and monzogranitic cordilleran I-type bodies emplaced between 485 and 465 Ma (Rapela et al., 1998b, Pankhurst et al., 2000). At 460 Ma, the collision of an exotic terrane with Laurentian affinities, the Precordillera terrane, marks the final stage of this orogenic cycle (Rapela et al., 2001a).

Several studies recognized intercalations of volcanic rocks in the Neoproterozoic sedimentary successions of NW Argentina in three main localities: the Rio Blanco Valley, the El Niño Muerto Hill and the Rio Grande Valley (Toselli and Aceñolaza, 1984; Chayle and Coira, 1987; Manca et al., 1987; Do Campo and Riveiro Guevara 2005; Omarini and Alonso, 1987). In this paper we focus on the El Niño Muerto Hill and the Rio Blanco valley outcrops (Fig. 1).

The El Niño Muerto Hill is located at the eastern portion of the Puna, close to the limit with the Eastern Cordillera, between 23º 46' 34.73" and 23º 44' 07.68" S and 66º 14' 50.52" and 66º 12' 48.88" W (Fig. 1), at the southern margin of Salinas Grandes salar. A previous study of the El Niño Muerto Hill investigated the geochemistry of Puncoviscana Formation (Do Campo and Riveiro Guevara 2005) but did not focus on the associated subvolcanic rocks. The authors have recognized a conspicuous slaty cleavage (s1) in both the volcanic and sedimentary rocks (Fig. 2)**.** Kubler index (0.36; 0.24° 2θ) values for clay mineral as well as TEM (Transmission Electron Microscopy) and SEM (Scanner Electron Microscopy) data indicate a high-anchizonal to epizonal grade for the metamorphism of the Puncoviscana slates in that locality (Do Campo et al., 1998; Do Campo et al., 1999, Do Campo, 1999a, b, Do Campo and Nieto, 2003).

The Rio Blanco Valley is located in the Eastern Cordillera, approximately 60 Km west of Salta, between 24º 58' 08.73" and 24º 57' 05.43" S and from 65º 58' 03.41" to 65º 57' 35.71" W. In this area, submarine basaltic lavas and hialoclastites are associated with the Puncoviscana red pelites and turbidites (Omarini and Alonso, 1987) (Fig. 3).

## 2.1 Field relationships

### 2.1.1. El Niño Muerto Hill (ENM)

The ENM consists of a NE-SW hill formed entirely by the Puncoviscana metasedimentary sequence. Acid subvolcanic rocks constitute a sill intruded into the sequence (Fig. 2). The Puncoviscana Formation consists of fine-grained turbidites with alternating centimetric greywacke and pelite beds (Fig. 2 A) which commonly display cross-bedding and parallel stratification.

A felsic subvolcanic body forms a large (~ 6 kilometers long and 30 m thick) NE-SW tabular intrusion, which is intensely foliated in some localities (Fig. 2 A, B, and C). Enclaves of the host metasedimentary rocks, (Fig. 2 D) and thermal aureoles (Fig. 2 C) recognized by bleaching of the metasediments are evidence of the intrusive relationship.

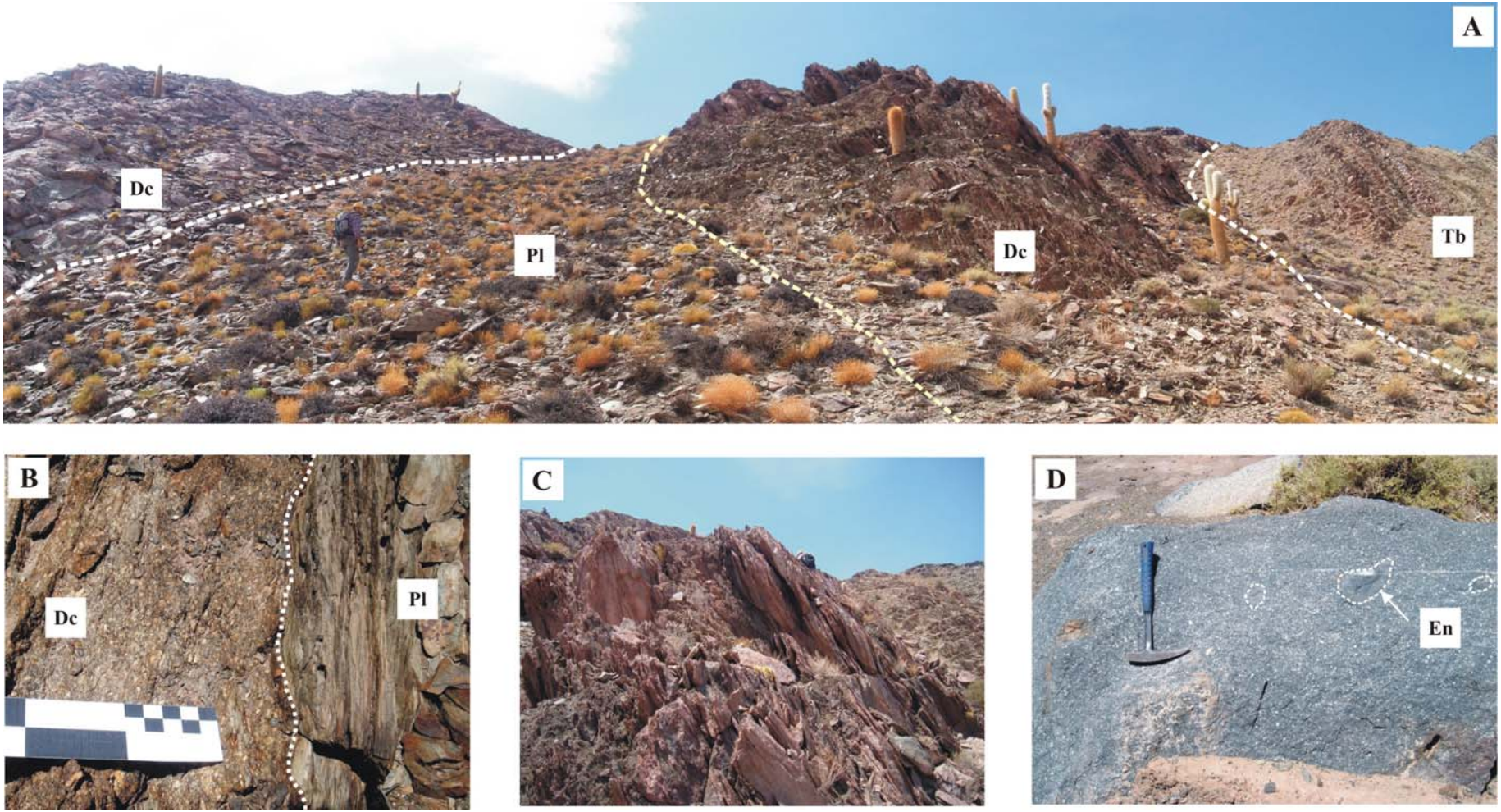


**Figure 2:** A) Panoramic view of the El Niño Muerto sill (Dc) north sector. The dacites are intruded in the turbidite sequence (Tb) of the Puncoviscana Formatio. B) The contact, is marked by thermometamorphosed and bleached pelites (Pl) indicating the intrusive character. Note that sediment and dacite are intensely foliated. C) View of sill outcrop with prominent foliation. D) Aspect of dacites in fresh cut. They are characterized by porphiritic textures with plagioclase phenocrysts embedded in a gray groundmass of biotite, quartz and plagioclase crystals and abundant pelite enclaves (En). The scale has 25 centimeters long.

The El Niño Muerto metadacites are dark grey, very homogeneous, and fine- to medium-grained. They are characterized by porphyritic textures with abundant plagioclase, K-feldspar and quartz phenocrysts up to 1 cm in size (Fig. 2 D).

### 2.1.2. Río Blanco Valley

The sedimentary succession in this area consists of a 2000 m-thick turbidite sequence, with a 200 m-thick intercalation of hemipelagic sediments represented by red pelites and minor pink limestone (Fig. 3). Excellent exposures of the Rio Blanco mafic volcanic rocks are associated with the hemipelagic level.

#### *Sedimentary sequence*

The turbidite sequence (Tb) is characterized by dominant pale-grey greywacke with minor gray pelites that pass to red pelites (Fig. 3). The greywacke beds exhibit typical sedimentary structures of turbidite, such as flute casts, current waves, cross bedding, erosion surfaces and water-escape structures.

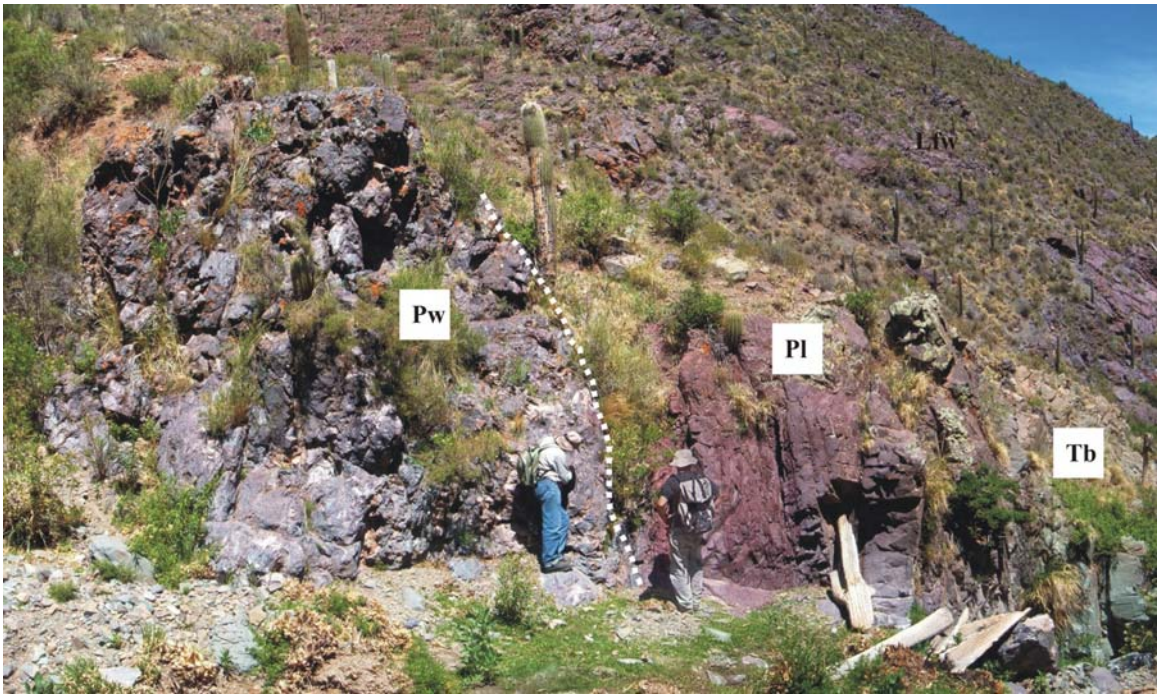


**Figure 3:** Contact between pillow lavas (Pw), red pelites (Pl) and the turbidite sequence (Tb) of the Neoproterozoic to Lower Paleozoic basement in the Rio Blanco Valley.

The turbidite sequence is interrupted by a hemipelagic sequence constituted by yellowish pink limestone (Lm) interbedded with red pelites (Pl). Parallel lamination and slump structures are observed in the pelites.

### *Río Blanco volcanic rocks*

The volcanic rocks are exposed in a tributary valley of the Río Blanco river forming a 5-km long N-S trending structure. They occur as hydrothermally altered basalt interbedded with red pelites and limestones (Fig. 4 A), including both subvolcanic and extrusive bodies. The subvolcanic bodies are characterized by massive to flow banded lavas (SbLv), whereas the extrusive bodies are formed essentially by pillowed lava flows (Pw). Important peperite deposits are associated with the subvolcanic bodies that intrude limestone and red pelites, indicating the synchronicity between the magmatic event and the deposition of these sediments.

Reddish to gray subvolcanic rocks outcrop extensively in the study area (Fig. 4 A) reaching thicknesses of up to 100 meters. They are massive to flow banded bodies characterized by porphyritic textures with variable amounts of plagioclase phenocrysts (up to 6 mm) immersed in an aphanitic greenish to red groundmass with abundant vesicles which have been partially filled with carbonate. Abundant centimetrics to decimetric yellow limestone enclaves are found. These enclaves, in the banded lava flows, are strongly deformed parallel to the lava flow displaying lensoidal shape (Fig. 4 C) indicating high velocity and low viscosity of lava flow and suggesting that the limestone was not consolidated at the time of extrusion.

Pillowed lavas are exposed in several outcrops (Fig. 4 A, B) forming beds with variable thicknesses. They are found mainly associated with limestone and red pelites. The pillow structures are commonly tightly packed; when this is not the case, limestone or crushed glass fill the spaces between the pillows. The individual pillows show chilled margins up to 1 cm thick and radial joints up to 10 cm in length, are typically 0.5-1 m across and in their interior plagioclase phenocrysts (up to 3 mm) and carbonate-filled vesicles are common.

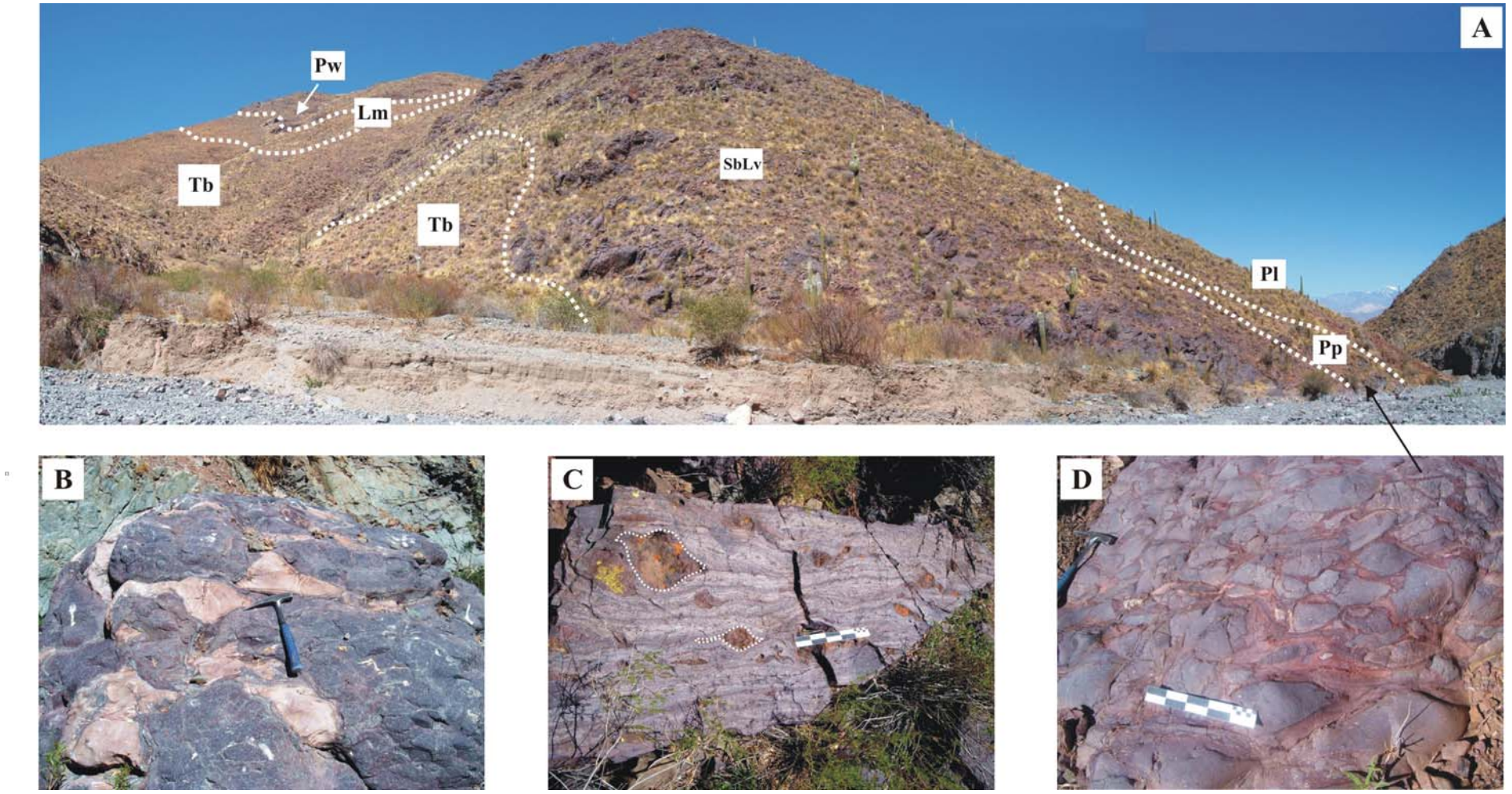


**Figure 4:** A) Panoramic view of the Rio Blanco volcanic rocks. They are intruded in a hemipelagitic? sequence made of red pelite (Pl) and limestone (Lm), that are enclosed by the turbidite sequence (Tb). B) Detail of pillow-like lava (Pw) intruded in yellowish pink limestone (Lm). Note the chilled margin and connection among the individual pillows. C) Aspect of the banded lava flow with abundant lensoidal limestone clasts. D) View of globular peperite deposit formed in the contact between lava flow and red pelite (Pl). The scale is 25 centimeters long.

### *Peperite deposits*

Reddish-gray peperite forming approximately 20 m-thick deposits (Pp) are located where subvolcanic bodies intruded the red pelites (Fig. 4 A, D). Peperite grades from closely packed, (high juvenile clasts/sediment ratios), close to the intrusion contact, to disperse peperites, (low juvenile clasts/sediment ratios)away from the contact with the igneous rocks (Hanson and Wilson, 1993). According to Busby-Spera and White (1987), they were divided into two textural end-members: blocky peperite and globular peperites. The juvenile clasts in both types have compositions and textures similar to the mafic lavas. Angular to pillow-like juvenile clasts characterize the blocky peperite (Fig. 4 D) whereas elongated lobe-like fluidal clasts with complex outlines are the main feature of the globular peperite

## 3. Petrography

### 3.1. Subvolcanic rocks of the El Niño Muerto Hill

The El Niño Muerto rocks are characterized by porphyritic textures with approximately 40% phenocrysts. These are quartz (~30%), corundum (~8%), alkali feldspar (~22%), anortite (± 1%), albite (~19%), enstatite (~5%) ferrosilite (~4%) and hypersthene (~12%) crystals (Table 2A) set in a fine-grained altered groundmass made of quartz, biotite and sericite/muscovite (Fig. 5). Fe-Ti oxides (~1.6%) and abundant zircon grains are important accessory phases.

The schistose fabric marked by the alternation of quartz- and mica-rich bands is the common feature of the groundmass. Polycrystalline aggregates of quartz grains elongated parallel to the regional cleavage characterize the quartz-rich bands, whereas fine-grained biotite and muscovite crystals elongated along the cleavage characterize the others bands (Fig. 5 A).

Plagioclase (albite-oligoclase $An_{10-30}$) phenocrysts and microphenocrysts commonly exhibit subhedral outlines and some crystals have disequilibrium features, such as sieve textures and rounded edges (Fig. 5 B). They show incipient alteration to white mica. Subhedral K-feldspar crystals are also observed but not common.

Quartz phenocrysts display rounded outlines and frequent disequilibrium textures such as embayments (Fig. 5 C). Eye-shaped deformation of groundmass fabrics is more common around quartz phenocrysts (Fig. 5 D). Some phenocrysts present poikilitic textures formed by

inclusions of biotite. Quartz in the fine groundmass has anhedral outlines and is strongly elongated.

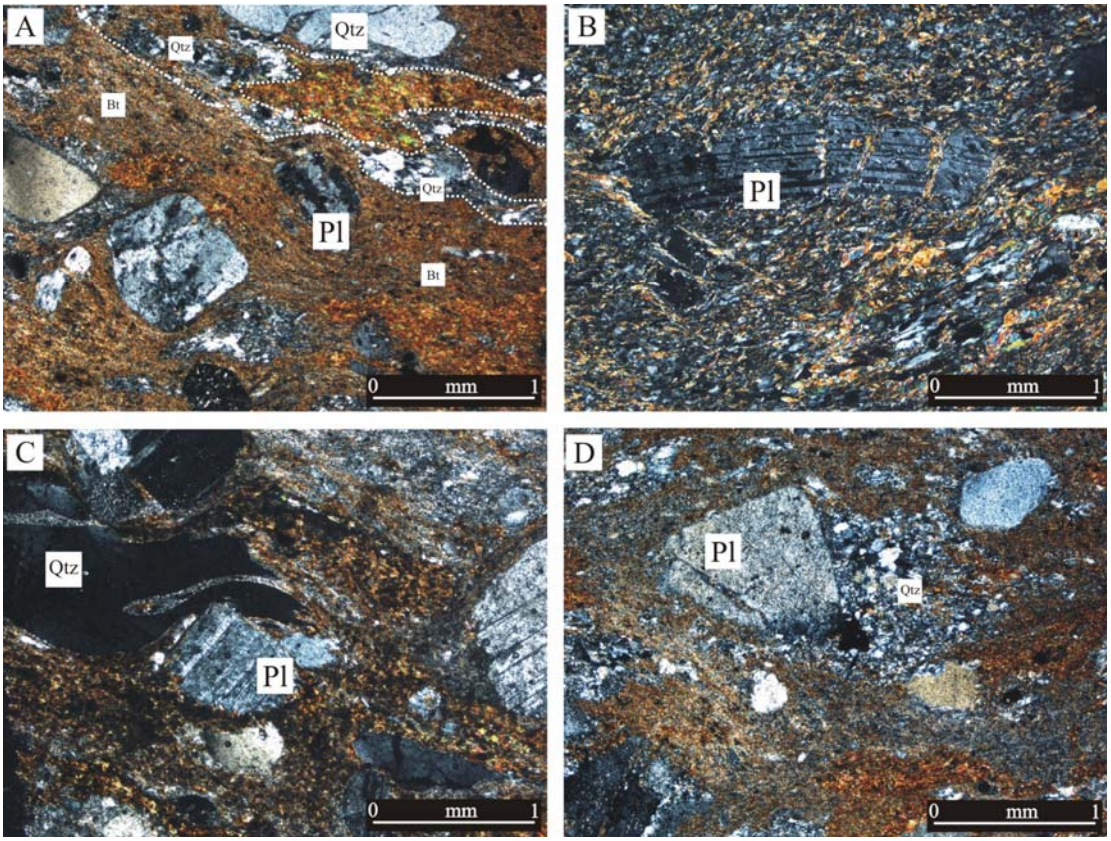


**Figure 5:** Photomicrographs of representative textures of the El Niño Muerto metadacites. A) Porphyritic metadacite with plagioclase, quartz and K-feldspar phenocrysts. The matrix is made of alternating quartz-rich and biotite-rich bands. B) Plagioclase crystal. The fractures perpendicular to the main stress are filled with mica. C) Quartz crystal showing embayment and D) plagioclase crystals showing pressure shadows. *Abbreviations*: Pl, plagioclase; Qtz, quartz; Kfs, feldspar; Ep, epidote.

Biotite is commonly present either as microphenocrysts or in the groundmass forming the dark-coloured layers. Muscovite is found as very small crystals in the groundmass together with biotite. (Fig. 5 A, C, D). The fine grained sericite is the most common alteration mineral in these rocks; they are found as small crystals in the groundmass as well as inside the plagioclase and sanidine crystals.

## 3.2. Subvolcanic and Volcanic rocks of the Rio Blanco Valley

Porphyritic to intergranular textures characterize the basaltic subvolcanic bodies and pillowed lava flows of the Rio Blanco Valley. Albite-oligoclase phenocrysts (up to 2 cm

across) and microphenocrysts, are set in a groundmass comprising albite, Fe-Ti oxides (hematite and ilmenite), calcite and quartz (Fig. 6 A). A less common textural type, characterized by large albite phenocrysts partially altered to epidote, is also recognized (Fig. 6 B). Albite phenocrysts (Fig. 6 C) and microphenocrysts display subhedral outlines and commonly show sieve textures. The groundmass albite is generally more altered, compared with the phenocrysts. Their major alteration products include sericite, calcite and epidote. Calcite commonly fills vesicles and also replaces plagioclase. Epidote recognized in samples BRB 64 and 65 (Fig. 6 B) occur as alteration products of calcic plagioclase, whereas chlorite constitutes a minor phase filling vesicles together with carbonate and hematite. Distinguishing features of the Rio Blanco volcanic rocks are the abundant vesicles (Fig. 6 D), present in different sizes and shapes being normally filled with hematite, calcite and minor chlorite

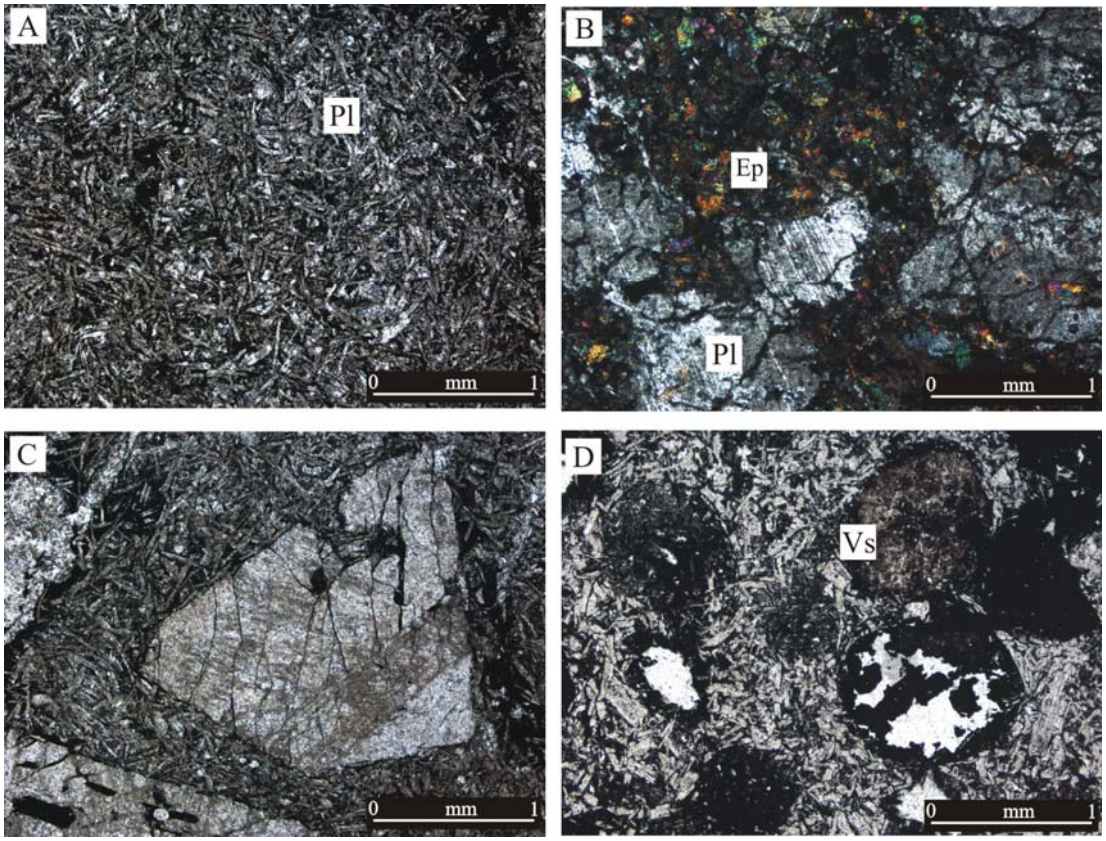


**Figure 6:** Photomicrographs of the Rio Blanco volcanic rocks. A) A plagioclase laths with intergranular opaque oxides is the most common textural variety of these basaltic rocks B) A less common textural variety is characterized by plagioclase phenocrysts (up to 2 mm) partially altered to epidote. C) Example of porphyritic intergranular texture. Albite phenocrysts are set in a groundmass composed totally by microcrystals of the same composition. D) Carbonate- and hematite-filled vesicles. *Abbreviations*: Pl, plagioclase; Ep, epidote; Vs, vesicles.

## 4. Analytical Procedures

Samples selected for geochemical analyses were washed and had weathered and veined portions cut off. The rocks were crushed and milled in a vídea mill to a very fine powder. Major elements and Ni and Sc (ppm) were analyzed by ICP-OES and trace element analyses were carried out by ICP-MS at the ACME Laboratories in Canada.

Zircon separation and analyses were carried out at the Geochronology Laboratory of the Universidade de Brasilia. Heavy mineral concentrates were obtained using conventional gravimetric and magnetic techniques (panning , Densitest$^{R}$ separator and Franz isodynamic separator). Final purification was achieved by hand picking using a binocular microscope and selected zircon grains were mounted on a polished epoxy section. Two parts of Resin (Struer, Epo Fix Resin) and one part of Hardener (Struer, Epo Fix Hardener) were poured into the cast with zircons inside and let to rest for twelve hours. The grain mounts containing the samples and standards were polished and cleaned in $HNO_3$ 3% during five minutes immediately prior to analysis to remove surface Pb contamination. Finally they were dried and mounted together with the standard in a Laser Ablation cell. The operating data are listed in Table 1. During analytical session GJ-1 standard zircon was used for correcting isotopic ratios using a standard-sample-standard "bracketing" technique.

Sm-Nd and Rb-Sr isotopic analyses followed the method described in Gioia and Pimentel (2000) and were carried out at the Geochronology Laboratory of the University of Brasilia. Whole-rock powders (~100 mg) were mixed with a $^{149}$Sm-$^{150}$Nd spike solution and dissolved in Savillex$^{R}$ capsules. Sr, Sm and Nd extraction from whole-rock samples followed conventional cation exchange techniques, with Teflon columns containing LN-Spec

| | |
|---|---|
| Instrument | MC-ICP-MS Neptune |
| Scan Mode | Static |
| Scanned masses | 238, 208, 207, 206, 204, 202 |
| Laser | UP213 New Wave, 213 nm, Nd:YAG |
| Integration time | 1 secs |
| Ablation time | 40 secs |
| Spot size | 30 μm |
| Laser settings | 10 Hz, ~2J/cm$^2$ |
| Auxiliary gas (He) | 0.38-0.41 l/min |
| Sample gas (Ar) | 0.903-0.995 l/min |

*Table 1: Operating data of LA-ICPMS*

resin (HDEHP-diethylhexil phosphoric acid supported on PTFE powder). Sr, Sm and Nd samples were loaded onto Re evaporation filaments of double filament assemblies, and the isotopic measurements were carried out on a multicollector Finnigan MAT 262 mass spectrometer in static mode. Uncertainties of $^{87}Sr/^{86}Sr$ ratios were better than ±0.01% (2σ) and of Sm/Nd and $^{143}Nd/^{144}Nd$ ratios were better than ±0.2% (2σ) and ±0.005% (2σ), respectively, according to repeated analyses of international rock standards BHVO-1 and BCR-1. $^{143}Nd/^{144}Nd$ ratios were normalized to $^{146}Nd/^{144}Nd$ of 0.7219, and the decay constant used was $6.54x10^{-12}$ $y^{-1}$. The $T_{DM}$ values were calculated using DePaolo's model (1981).

## 5. Geochemistry

### 5.1. El Niño Muerto metadacites

Major and trace element analyses were carried out on three samples of the ENM dacites (results are in Table 2A, B). They have $SiO_2$ contents between 65.0 and 67.3 wt.% and

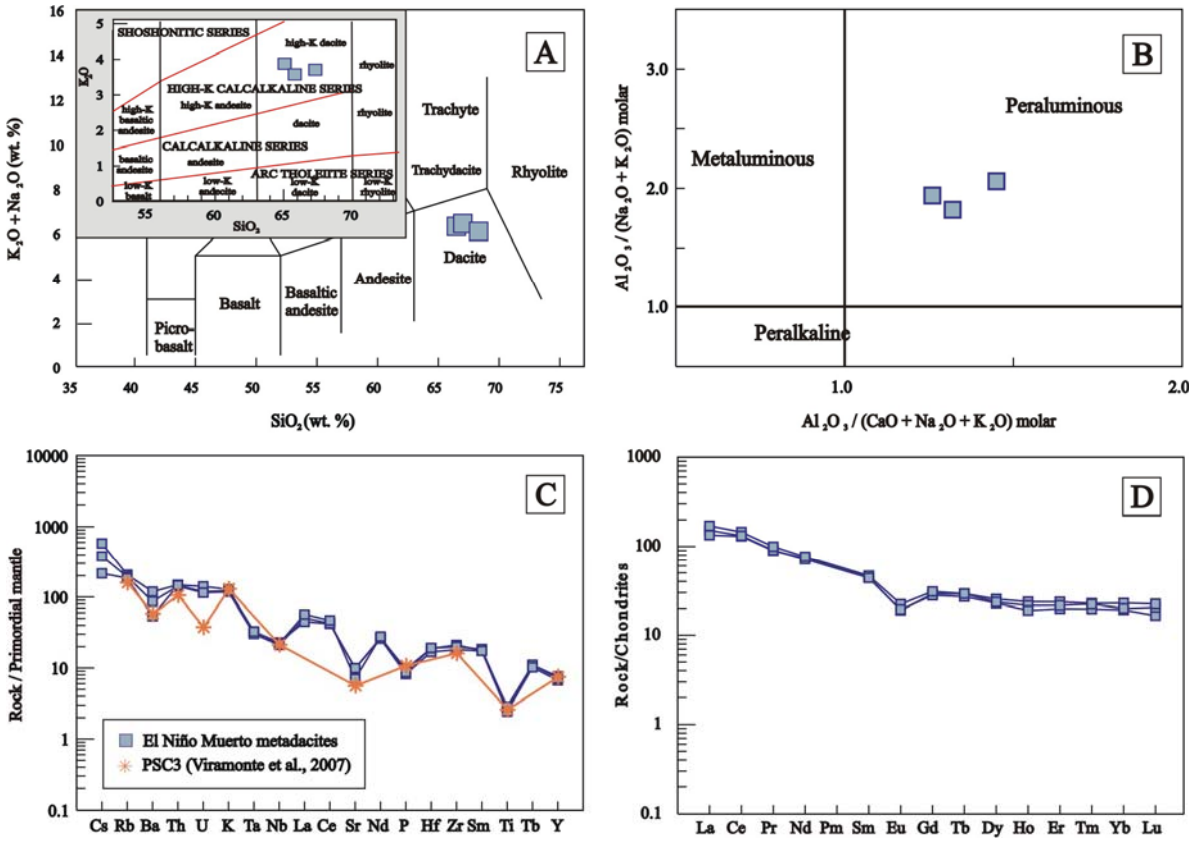


**Figure 7:** A) Chemical compositions of the El Niño Muerto subvolcanic rocks in the Total alkalis versus Silica diagram (Le Maitre et al., 1989) and in the Peccerilo and Taylor (1976) diagram for subalkaline rocks. B) The $Al_2O_3$/ (CaO + $Na_2O$ + $K_2O$) vs. $Al_2O_3$/($Na_2O$ + $K_2O$) diagram (Shand, 1929) shows the peraluminous nature of the original magmas. C) Spidergrams of Primordial Mantle-normalized trace elements distributions (Wood et al., 1979) for the El Niño Muerto dacites and sample PCS3 of "Faja Eruptiva de la Puna Oriental" (Viramonte et al., 2007). D) Chondrite-normalized diagram for representative samples of the El Niño Muerto metadacites. The normalizing factors are from Sun and McDonough (1989).

$Al_2O_3$contents from 15.09 to 16.4 wt. %. In the Total Alkali Silica (TAS) diagram (Fig. 7 A) these metavolcanic rocks fall in the dacite field, and in the Peccerilo and Taylor (1979) diagram for subalkalic rocks, they are classified as high-K dacites (Fig. 7A). They show peraluminous composition (Fig. 7 B) with normative corundum greater than 5 % (Table 2).

The concentrations in compatible elements is low (~ 27 ppm of Cr, ~ 30 ppm of V and ~ 22 ppm of Ni) and these rocks show relative enrichment in Ba (up to 897 ppm of Ba), Sr (161-226 ppm), Rb ( up to 177 ppm) and Nb (~ 27 ppm). In the normalized diagram of Wood et al. (1979) (Fig. 7 C) the subvolcanic rocks show enrichment in LILE elements between 100 and 800 times greater than the primordial mantle and depletion in the HFSE (~ 10 times) with negative anomalies in Ba, Ta, Nb, Sr, P and Ti elements. The negative anomalies in Nb and Ta, are characteristic of continental crust (subduction-signature) and depletion in P, Ti and Eu, indicate that apatite, ilmenite, and plagioclase crystalized in early stages of the magma evolution. Negative anomalies in Ba and Sr are consistent with plagioclase removal. Metacites of the El Niño Muerto Hill and a metadacite from the Faja Eruptiva de la Puna Oriental in the Puna (Viramonte et al., 2007) have very similar trace element distribution patterns (Fig. 7 C).

∑REE (Fig. 7 D) varies from 186 to 206 ppm, with a distinctive enrichment in the LREE ($La/Sm_N$ = 3.2-3.6). The $(La/Yb)_n$ ratio between 5.9 to 8.6 indicates that they are moderately fractionated, with $(La/Sm)_n$ values greater than $(Gd/Yb)_n$ (3.3 and 1.4 respectively). The negative Eu anomaly, from -0.53 to -0.59, indicates plagioclase fractionation.

## 5.2. Rio Blanco basalts

In all bulk chemical analyses of the Rio Blanco rocks (results are in Table 2A, B) the loss on ignition values are high, varying from 2.5 to 13.8 %, indicating significant alteration.

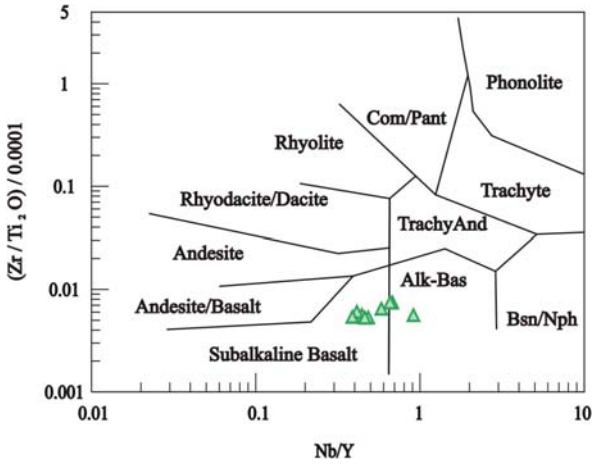


**Figure 8:** Rock classification diagram using Zr, Ti, Nb and Y immobile elements (Winchester and Floyd, 1977) for the Rio Blanco volcanic rocks.

*Table 2A: Representative whole rock analyses of the El Niño Muerto and Río Blanco volcanic rocks.*

| | ***El Niño Muerto*** | | | ***Río Blanco*** | | | | | | | | |
|---|---|---|---|---|---|---|---|---|---|---|---|---|
| *SAMPLE* | BNM 11 | BNM 14 | BNM 16 | BRB 22 | BRB 25 | BRB 30 | BRB 37 | BRB 43 | BRB 44 | BRB 64 | BRB 65 | BRB 66 |
| *Major oxides (wt%)* | | | | | | | | | | | | |
| $SiO_2$ | 65.07 | 65.81 | 67.31 | 41.37 | 46.94 | 36.56 | 38.60 | 45.78 | 36.47 | 45.63 | 44.75 | 42.00 |
| $TiO_2$ | 0.73 | 0.62 | 0.67 | 3.37 | 4.20 | 2.81 | 2.01 | 3.98 | 1.88 | 2.53 | 1.98 | 1.68 |
| $Al_2O_3$ | 16.44 | 15.23 | 15.09 | 15.85 | 17.39 | 22.53 | 14.97 | 16.41 | 14.55 | 16.43 | 19.79 | 18.01 |
| $Fe_2O_{3\,(t)}$ | 4.97 | 5.65 | 4.98 | 17.49 | 16.69 | 14.03 | 11.62 | 17.24 | 9.33 | 11.08 | 8.97 | 8.56 |
| *MnO* | 0.08 | 0.07 | 0.08 | 0.25 | 0.10 | 0.06 | 0.32 | 0.17 | 0.17 | 0.16 | 0.12 | 0.11 |
| *MgO* | 2.38 | 2.58 | 1.89 | 3.59 | 2.35 | 11.27 | 4.48 | 3.15 | 6.41 | 7.46 | 4.52 | 4.22 |
| *CaO* | 1.83 | 1.75 | 2.33 | 4.75 | 1.68 | 1.06 | 11.69 | 2.78 | 12.64 | 7.37 | 5.55 | 8.72 |
| $Na_2O$ | 2.29 | 2.73 | 2.28 | 5.06 | 5.98 | 0.34 | 4.96 | 3.60 | 3.99 | 2.23 | 2.07 | 5.13 |
| $K_2O$ | 3.88 | 3.58 | 3.71 | 1.35 | 1.24 | 3.33 | 0.15 | 2.23 | 0.48 | 0.04 | 3.31 | 1.25 |
| $P_2O_5$ | 0.20 | 0.17 | 0.18 | 0.44 | 0.85 | 0.34 | 0.21 | 0.38 | 0.25 | 0.33 | 0.29 | 0.24 |
| *L.O.I* | 2.00 | 1.70 | 1.40 | 6.40 | 2.50 | 7.60 | 10.90 | 4.20 | 13.80 | 6.70 | 8.60 | 9.90 |
| *Total* | 99.87 | 99.89 | 99.92 | 99.92 | 99.92 | 99.93 | 99.91 | 99.92 | 99.97 | 99.96 | 99.95 | 99.82 |
| | | | | | | | | | | | | |
| *Q* | 32.10 | 30.59 | 34.91 | - | - | - | - | - | - | - | - | - |
| *C* | 8.69 | 7.02 | 6.89 | - | - | - | - | - | - | - | - | - |
| *Or* | 23.52 | 21.64 | 22.34 | - | - | - | - | - | - | - | - | - |
| *Ab* | 19.88 | 23.63 | 19.66 | - | - | - | - | - | - | - | - | - |
| *An* | 0.00 | 0.00 | 1.56 | - | - | - | - | - | - | - | - | - |
| *En* | 6.08 | 6.57 | 4.80 | - | - | - | - | - | - | - | - | - |
| *Fs* | 4.65 | 5.59 | 4.74 | - | - | - | - | - | - | - | - | - |
| *Hy* | 10.73 | 12.16 | 9.53 | - | - | - | - | - | - | - | - | - |
| *Mt* | 1.57 | 1.78 | 1.56 | - | - | - | - | - | - | - | - | - |
| *Il* | 1.42 | 1.20 | 1.30 | - | - | - | - | - | - | - | - | - |
| *Ap* | 0.00 | 0.00 | 0.43 | - | - | - | - | - | - | - | - | - |
| *Cc* | 3.35 | 3.20 | 3.24 | - | - | - | - | - | - | - | - | - |
| Total | 101.27 | 101.23 | 101.43 | - | - | - | - | - | - | - | - | - |

*Table 2B: Representative whole rock Trace Elements and REE analyses of the El Niño Muerto and Rio Blanco volcanic rocks*

| | ***El Niño Muerto*** | | | ***Río Blanco*** | | | | | | | | |
|---|---|---|---|---|---|---|---|---|---|---|---|---|
| *SAMPLE* | BNM 11 | BNM 14 | BNM 16 | BRB 22 | BRB 25 | BRB 30 | BRB 37 | BRB 43 | BRB 44 | BRB 64 | BRB 65 | BRB 66 |
| *Trace elements (ppm)* | | | | | | | | | | | | |
| Be | 2.00 | 3.00 | 2.00 | 1.00 | 2.00 | 1.00 | b.d.l | 1.00 | 1.00 | 2.00 | 2.00 | 1.00 |
| Sc | 13.00 | 12.00 | 13.00 | 40.00 | 25.00 | 40.00 | 32.00 | 35.00 | 29.00 | 31.00 | 24.00 | 22.00 |
| V | 91.00 | 81.00 | 81.00 | 327.00 | 281.00 | 224.00 | 227.00 | 330.00 | 160.00 | 245.00 | 165.00 | 185.00 |
| Cr | 27.37 | 30.79 | 27.37 | 10.26 | 23.95 | 95.79 | 147.11 | 23.95 | 34.21 | 71.84 | 30.79 | 27.37 |
| Co | 29.10 | 30.50 | 30.30 | 65.00 | 49.30 | 33.40 | 63.10 | 54.10 | 46.90 | 49.10 | 34.90 | 36.80 |
| Ni | 25.50 | 22.80 | 24.70 | 45.50 | 48.60 | 45.80 | 61.30 | 37.30 | 48.50 | 57.10 | 39.50 | 32.00 |
| Cu | 16.10 | 18.60 | 3.50 | 52.60 | 22.50 | 5.70 | 9.50 | 28.00 | 12.20 | 49.80 | 2.70 | 6.10 |
| Zn | 57.00 | 62.00 | 66.00 | 151.00 | 112.00 | 106.00 | 93.00 | 127.00 | 94.00 | 107.00 | 85.00 | 70.00 |
| Ga | 21.80 | 19.80 | 18.40 | 23.40 | 20.30 | 26.10 | 15.50 | 26.10 | 20.50 | 22.00 | 23.90 | 20.30 |
| As | 9.30 | 4.20 | 2.00 | 7.10 | 38.60 | 6.90 | 30.60 | 21.40 | 6.00 | 7.20 | 2.20 | 6.80 |
| Se | b.d.l | b.d.l | 0.80 | b.d.l | 0.80 | b.d.l | 0.90 | 0.50 | b.d.l | b.d.l | b.d.l | b.d.l |
| Rb | 177.50 | 166.10 | 158.40 | 51.00 | 37.50 | 112.70 | 2.80 | 73.40 | 10.70 | b.d.l | 70.30 | 28.00 |
| Sr | 226.80 | 227.80 | 161.70 | 249.40 | 373.80 | 139.00 | 445.40 | 223.60 | 201.00 | 302.10 | 162.30 | 368.80 |
| Y | 37.00 | 32.50 | 34.70 | 41.60 | 66.00 | 49.60 | 32.50 | 34.30 | 27.40 | 32.70 | 29.20 | 22.30 |
| Zr | 231.90 | 199.60 | 219.10 | 185.70 | 218.50 | 165.00 | 106.20 | 218.30 | 98.40 | 179.50 | 123.30 | 118.40 |
| Nb | 14.20 | 13.10 | 13.60 | 19.50 | 32.10 | 21.80 | 13.50 | 30.80 | 13.90 | 22.50 | 17.50 | 14.90 |
| Mo | 0.20 | 0.20 | 0.10 | 0.40 | 0.20 | 0.10 | 0.30 | 0.20 | 0.20 | 0.10 | 0.10 | b.d.l |
| Ag | b.d.l | b.d.l | b.d.l | b.d.l | b.d.l | b.d.l | b.d.l | b.d.l | b.d.l | b.d.l | b.d.l | b.d.l |
| Cd | b.d.l | b.d.l | 0.10 | 0.10 | b.d.l | b.d.l | 0.10 | b.d.l | 0.30 | 0.10 | 0.10 | 0.20 |
| Sn | 4.00 | 3.00 | 3.00 | 2.00 | 2.00 | 1.00 | b.d.l | 2.00 | b.d.l | 1.00 | 1.00 | 1.00 |
| Sb | 0.30 | 0.30 | 0.30 | 1.90 | 0.30 | 0.20 | 0.70 | 0.50 | 0.90 | 0.30 | 0.10 | 1.30 |
| Cs | 11.00 | 7.20 | 4.10 | 3.80 | 3.40 | 9.70 | 1.60 | 6.20 | 1.30 | 0.20 | 5.90 | 3.90 |
| Ba | 897.60 | 653.30 | 405.70 | 227.00 | 147.40 | 176.30 | 80.90 | 193.90 | 34.30 | 13.40 | 364.00 | 160.10 |
| Hf | 6.60 | 5.90 | 6.70 | 5.40 | 5.80 | 4.40 | 3.20 | 7.00 | 2.90 | 4.00 | 3.50 | 3.00 |
| Ta | 1.40 | 1.30 | 1.40 | 1.40 | 2.30 | 1.40 | 0.90 | 2.30 | 1.00 | 1.60 | 1.20 | 1.00 |
| W | 180.20 | 192.80 | 199.60 | 34.90 | 55.70 | 3.40 | 38.60 | 44.40 | 25.20 | 33.40 | 11.60 | 21.10 |
| Au | 5.50 | b.d.l | b.d.l | 2.20 | b.d.l | b.d.l | 1.30 | 1.90 | b.d.l | 2.30 | b.d.l | b.d.l |
| Hg | b.d.l | b.d.l | b.d.l | b.d.l | b.d.l | b.d.l | b.d.l | b.d.l | b.d.l | b.d.l | b.d.l | b.d.l |
| Tl | 0.90 | 1.00 | 0.70 | 0.10 | b.d.l | b.d.l | b.d.l | 0.10 | b.d.l | b.d.l | b.d.l | b.d.l |
| Pb | 9.40 | 10.60 | 6.20 | 6.10 | 5.80 | 7.00 | 1.80 | 3.60 | 0.90 | 0.50 | 0.50 | 1.20 |
| Bi | 0.30 | 0.40 | 0.10 | 0.10 | 0.10 | 0.10 | b.d.l | b.d.l | b.d.l | b.d.l | b.d.l | b.d.l |
| Th | 14.20 | 13.60 | 14.00 | 1.20 | 3.20 | 1.10 | 1.20 | 3.30 | 1.20 | 1.90 | 1.20 | 1.90 |
| U | 3.80 | 3.10 | 3.20 | 0.30 | 0.90 | 0.40 | 0.20 | 0.30 | 0.20 | 0.60 | 0.20 | 0.30 |
| *Rare earth Elements (ppm)* | | | | | | | | | | | | |
| La | 31.80 | 36.00 | 40.40 | 17.50 | 27.30 | 16.60 | 10.20 | 21.30 | 13.20 | 17.10 | 13.50 | 11.70 |
| Ce | 79.70 | 80.80 | 89.00 | 44.40 | 63.70 | 35.60 | 24.50 | 59.10 | 31.70 | 42.40 | 29.40 | 26.60 |
| Pr | 8.51 | 8.61 | 9.44 | 5.68 | 8.52 | 4.84 | 3.47 | 7.87 | 3.99 | 5.28 | 3.73 | 3.34 |
| Nd | 34.30 | 33.40 | 35.70 | 26.50 | 39.40 | 23.60 | 16.00 | 33.80 | 18.80 | 22.90 | 16.50 | 15.40 |
| Sm | 6.80 | 6.70 | 7.10 | 6.40 | 10.60 | 5.90 | 4.40 | 8.20 | 4.30 | 5.90 | 4.30 | 3.80 |
| Eu | 1.10 | 1.12 | 1.29 | 2.42 | 3.50 | 2.07 | 1.61 | 2.99 | 1.48 | 1.96 | 1.47 | 1.41 |
| Gd | 5.97 | 5.75 | 6.33 | 7.55 | 12.06 | 6.85 | 5.15 | 8.28 | 4.30 | 6.75 | 4.57 | 4.36 |
| Tb | 1.09 | 1.01 | 1.09 | 1.29 | 2.04 | 1.24 | 0.87 | 1.35 | 0.76 | 1.05 | 0.82 | 0.79 |
| Dy | 6.44 | 5.80 | 5.97 | 7.24 | 12.02 | 7.33 | 5.23 | 7.11 | 4.52 | 6.04 | 4.69 | 4.05 |
| Ho | 1.34 | 1.07 | 1.22 | 1.35 | 2.35 | 1.53 | 1.05 | 1.30 | 0.90 | 1.10 | 0.94 | 0.78 |
| Er | 3.91 | 3.27 | 3.57 | 3.96 | 6.59 | 4.92 | 3.07 | 3.39 | 2.76 | 3.39 | 2.67 | 2.20 |
| Tm | 0.58 | 0.50 | 0.57 | 0.58 | 0.97 | 0.75 | 0.41 | 0.45 | 0.35 | 0.50 | 0.39 | 0.32 |
| Yb | 3.89 | 3.26 | 3.38 | 3.47 | 5.98 | 4.26 | 2.74 | 2.95 | 2.55 | 2.74 | 2.49 | 1.74 |
| Lu | 0.57 | 0.42 | 0.52 | 0.50 | 0.94 | 0.59 | 0.39 | 0.41 | 0.37 | 0.42 | 0.35 | 0.29 |
| **$(La/Yb)_N$** | **5.86** | **7.92** | **8.57** | **3.62** | **3.27** | **2.80** | **2.67** | **5.18** | **3.71** | **4.48** | **3.89** | **4.82** |
| **$(La/Sm)_N$** | **3.02** | **3.47** | **3.67** | **1.77** | **1.66** | **1.82** | **1.50** | **1.68** | **1.98** | **1.87** | **2.03** | **1.99** |
| **$(Gd/Yb)_N$** | **1.27** | **1.46** | **1.55** | **1.80** | **1.67** | **1.33** | **1.55** | **2.32** | **1.39** | **2.04** | **1.52** | **2.07** |

Therefore, major elements oxides and large ion lithophile elements cannot be used to chemically classify or discriminate the tectonic setting of these rocks, immobile elements and REE have been used. Using the diagram of Winchester and Floyd, (1977) the Rio Blanco volcanic rocks fall between subalkaline basalts and alkaline basalts fields (Fig. 8).They show low Cr (mostly between 10 and 147 ppm) and Ni (32-61 ppm) contents and display variable range in incompatible elements (13-364 ppm Ba; 139-445 ppm Sr; 2.8-112 ppm Rb; 13.5-22.5 ppm Nb). The Rio Blanco basalts display Zr/Nb ratios from 6.8 to 9.5 which are characteristic of E-MORB's.

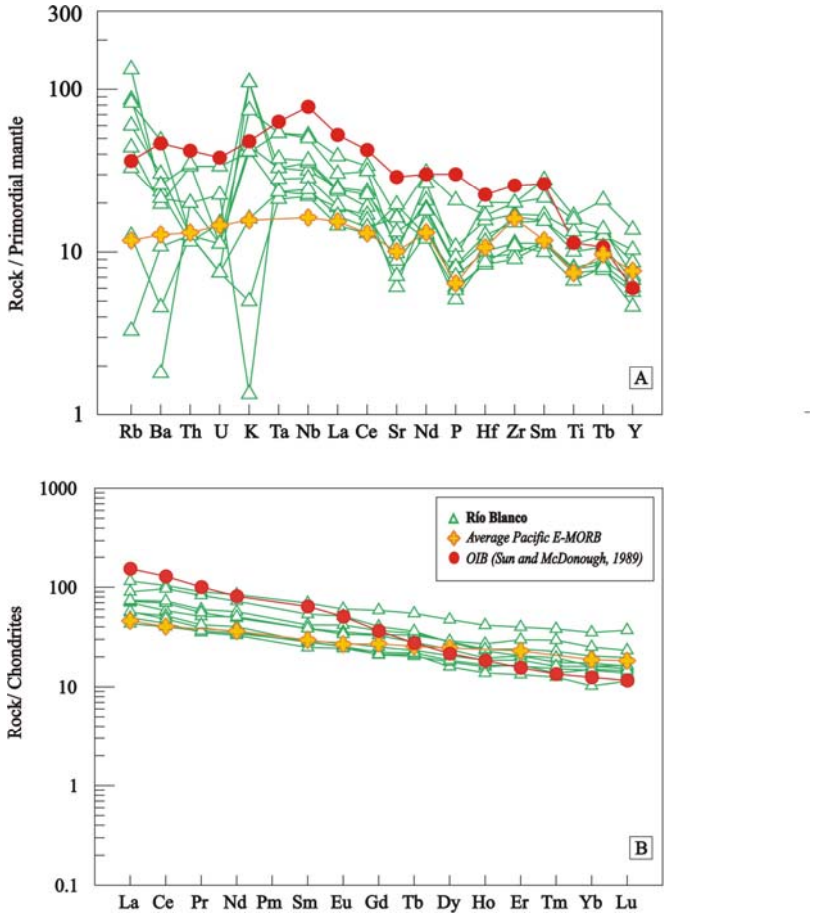


**Figure 9:** A) Spidergrams of Primordial Mantle-normalized trace elements distributions (Wood et al., 1979) for the Rio Blanco rocks. B) Chondrite-normalized REE abundance diagram for representative samples of the Rio Blanco basalts. The normalizing factors are from Sun and McDonough (1989). E-MORB (average Pacific E-MORB from GEOROC) and OIB (Sun and McDonough 1989) are plotted for comparison.

In the modified Wood et al., (1979) diagram (Fig. 8 A), normalized to the Primordial Mantle, the Rio Blanco (RB) samples show variable enrichment in large-ion lithophile elements (LILE) from 10 to approximately 100 times higher than the Primordial Mantle. It is noteworthy that the Rio Blanco samples do not show Ta and Nb anomalies. Strongly negative or positive anomalies in Th, K, Sr and Ti are observed. Trace elements abundances form a

moderate curvilinear pattern with large ion lithophile element (LILE) enrichment plotting between the OIB and E-MORB typical patterns.

The REE concentrations of the Rio Blanco rocks were normalized to the average C1 chondrite (Sun & McDonough 1989)**.** The Rio Blanco samples exhibit ∑REE values between 76 and 129 ppm. The $(La/Yb)_n$ ratios are between 2.6 and 4.5 indicating slight LREE enrichment (Fig. 8 B). The Eu anomalies (Eu/Eu*) vary between -0.9 and +0.9, suggesting that crystallization and fractionation of plagioclase was not very important. For comparison, the average Pacific E-MORB (from GEOROC.com) and the OIB of Sun and McDonough (1989) were also plotted in Fig. 9 A and B.

# 6. Geochronology

## 6.1. U-Pb data

Samples BNM 11 from the El Niño Muerto Hill and BRB 43 from the Rio Blanco Valley were dated by the U-Pb zircon method using Laser Ablation ICP-MS.

### 6.1.1. El Niño Muerto metadacites (sample BNM 11)

Two groups of zircons up to 200 μm are recognized in this sample. One is characterized by needle-shape acicular pink zircon crystals. In agreement with the "Pupin Diagram" this type of zircon is classified as prismatic with greater development of the {100} and {110} faces (Pupin, 1980). They are very common in rapidly crystallized, porphyritic, subvolcanic intrusions and in high level granites and gabbros (Corfu et al., 2003). The second group exhibits more equant forms with short prismatic and multifaceted pink crystals. They are classified in the Pupin diagram as pyramidal crystals with relatively greater development of the {211} and {101} face (Pupin, 1980). These are more common in deep- seated, slowly cooled intrusions (Corfu et al., 2003).

Twenty nine zircon grains were analized (Table 3, Fig. 10 A) resulting in concordant analyses indicating the Concordia age of **495 ± 4** Ma (MSWD= 0.95) which is considered, in this study, as the best estimate for the crystallization age of the El Niño Muerto dacites. One spot analysis defined the age of ca. 950 Ma indicating inheritance from older crust. On the other hand, IDTIMS analyses of this sample indicated a poorly defined younger age of 462 ± 29 Ma (Table 4, Fig. 10 B) which is probably caused by a combination of inheritance older zircon crystals and recent lead loss. The IDTIMS data, however, reveal strong inheritance

*Table 3: LA-ICPMS U-Pb isotopic data from the El Niño Muerto metadacites*

| Sample: | Shape* | ***Ratios*** | | | | | | ***Ages*** | | | | | | Disc (%) | rho |
|---|---|---|---|---|---|---|---|---|---|---|---|---|---|---|---|
| ***BNM 11*** | | $^{207}Pb/^{206}Pb$ | 2σ | $^{207}Pb/^{235}U$ | 2σ | $^{206}Pb/^{238}U$ | 2σ | $^{207}Pb/^{206}Pb$ | ± 2σ | $^{207}Pb/^{235}U$ | ± 2σ | $^{206}Pb/^{238}U$ | ± 2σ | 206/238 | |
| Grain N° | | | | | | | | | | | | | | | |
| 1 | *P* | 0.0571 | 0.000157 | 0.6255 | 0.017507 | 0.0800 | 0.002239 | 496.35 | 6 | 493.32 | 11 | 496.10 | 13 | 99.95 | 0.72 |
| 2 | *Pc* | 0.0581 | 0.000143 | 0.6830 | 0.025244 | 0.0860 | 0.003177 | 531.83 | 5 | 528.61 | 15 | 531.55 | 19 | 99.95 | 0.73 |
| 3 | *P* | 0.0576 | 0.000219 | 0.6603 | 0.039000 | 0.0832 | 0.004915 | 515.27 | 8 | 514.78 | 24 | 515.22 | 29 | 99.99 | 0.73 |
| 4 | *P* | 0.0569 | 0.000254 | 0.6171 | 0.022046 | 0.0786 | 0.002810 | 488.05 | 10 | 488.04 | 14 | 488.04 | 17 | 100.00 | 0.86 |
| 5 | *Pl* | 0.0574 | 0.000178 | 0.6454 | 0.039457 | 0.0820 | 0.005014 | 508.38 | 7 | 505.65 | 24 | 508.15 | 30 | 99.95 | 0.67 |
| 6 | *Pl* | 0.0574 | 0.000200 | 0.6400 | 0.028496 | 0.0817 | 0.003637 | 506.55 | 8 | 502.32 | 17 | 506.20 | 22 | 99.93 | 0.37 |
| 7 | *Pl* | 0.0576 | 0.000152 | 0.6473 | 0.033731 | 0.0828 | 0.004314 | 513.30 | 6 | 506.83 | 21 | 512.76 | 26 | 99.89 | 0.78 |
| 8 | *P* | 0.0574 | 0.000123 | 0.6408 | 0.016493 | 0.0817 | 0.002103 | 506.55 | 5 | 502.82 | 10 | 506.24 | 13 | 99.94 | 0.50 |
| 9 | *Pl* | 0.0578 | 0.000284 | 0.6711 | 0.020740 | 0.0841 | 0.002598 | 520.32 | 11 | 521.38 | 13 | 520.40 | 15 | 100.02 | 0.32 |
| 10 | *Pl* | 0.0575 | 0.000125 | 0.6477 | 0.017317 | 0.0825 | 0.002206 | 511.48 | 5 | 507.08 | 11 | 511.11 | 13 | 99.93 | 0.61 |
| 11 | *Pc* | 0.0577 | 0.000119 | 0.6614 | 0.022739 | 0.0839 | 0.002885 | 519.90 | 5 | 515.47 | 14 | 519.53 | 17 | 99.93 | 0.67 |
| 12 | *Pc* | 0.0577 | 0.000260 | 0.6609 | 0.047632 | 0.0840 | 0.006051 | 520.10 | 10 | 515.14 | 29 | 519.69 | 36 | 99.92 | 0.79 |
| 13 | *Pl* | 0.0572 | 0.000184 | 0.6314 | 0.062460 | 0.0804 | 0.007954 | 498.65 | 7 | 496.96 | 38 | 498.52 | 47 | 99.97 | 0.82 |
| 14 | *P* | 0.0573 | 0.000152 | 0.6371 | 0.028617 | 0.0811 | 0.003644 | 503.10 | 6 | 500.50 | 18 | 502.89 | 22 | 99.96 | 0.83 |
| 15 | *Pc* | 0.0569 | 0.000220 | 0.6168 | 0.030734 | 0.0784 | 0.003905 | 486.23 | 9 | 487.82 | 19 | 486.35 | 23 | 100.03 | 0.54 |
| 16 | *Pc* | 0.0571 | 0.000261 | 0.6211 | 0.018261 | 0.0798 | 0.002346 | 495.13 | 10 | 490.52 | 11 | 494.77 | 14 | 99.93 | 0.57 |
| 17 | *P* | 0.0566 | 0.000196 | 0.6011 | 0.028528 | 0.0766 | 0.003637 | 475.77 | 8 | 477.90 | 18 | 475.93 | 22 | 100.03 | 0.39 |
| 18 | *Pc* | 0.0568 | 0.000256 | 0.6098 | 0.029030 | 0.0778 | 0.003703 | 482.82 | 10 | 483.43 | 18 | 482.87 | 22 | 100.01 | 0.54 |
| 19 | *Pc* | 0.0571 | 0.000260 | 0.6172 | 0.027456 | 0.0798 | 0.003552 | 495.76 | 10 | 488.07 | 17 | 495.15 | 21 | 99.88 | 0.59 |
| 20 | *Pc* | 0.0570 | 0.000165 | 0.6181 | 0.023118 | 0.0790 | 0.002955 | 490.21 | 6 | 488.63 | 14 | 490.09 | 18 | 99.97 | 0.65 |
| 21 | *Pc* | 0.0566 | 0.000193 | 0.5998 | 0.046372 | 0.0766 | 0.005924 | 475.81 | 8 | 477.09 | 29 | 475.91 | 35 | 100.02 | 0.86 |
| 22 | *Pc* | 0.0566 | 0.000298 | 0.6028 | 0.026690 | 0.0766 | 0.003391 | 475.36 | 12 | 478.99 | 17 | 475.64 | 20 | 100.06 | 0.50 |
| 23 | *Pl* | 0.0566 | 0.000269 | 0.5963 | 0.015623 | 0.0768 | 0.002012 | 477.13 | 11 | 474.90 | 10 | 476.96 | 12 | 99.96 | 0.47 |
| 24 | *Pl* | 0.0571 | 0.000228 | 0.6193 | 0.017517 | 0.0795 | 0.002250 | 493.78 | 9 | 489.42 | 11 | 493.43 | 13 | 99.93 | 0.48 |
| 25 | *Pl* | 0.0572 | 0.000260 | 0.6281 | 0.058307 | 0.0802 | 0.007449 | 497.78 | 10 | 494.91 | 36 | 497.55 | 44 | 99.95 | 0.49 |
| 26 | *Pc* | 0.0568 | 0.000270 | 0.6222 | 0.027842 | 0.0781 | 0.003496 | 484.39 | 10 | 491.21 | 17 | 484.92 | 21 | 100.11 | 0.87 |
| 27 | *Pl* | 0.0571 | 0.000142 | 0.6295 | 0.023672 | 0.0802 | 0.003015 | 497.26 | 5 | 495.79 | 15 | 497.14 | 18 | 99.98 | 0.60 |
| 28 | *Pc* | 0.0572 | 0.000259 | 0.6269 | 0.027953 | 0.0804 | 0.003587 | 499.19 | 10 | 494.15 | 17 | 498.79 | 21 | 99.92 | 0.33 |
| 29 | *Pl* | 0.0572 | 0.000360 | 0.6277 | 0.041617 | 0.0807 | 0.005352 | 500.98 | 14 | 494.69 | 26 | 500.48 | 32 | 99.90 | 0.45 |

(*) *P* : prismatic crystals, *Pc* : short prismatic crystals and *Pl* : long prismatic crystals. Disc. (%) denotes percentage of discordance

*Table 4: Summary of ID-TIMS U-Pb data for metadacite of the El Niño Muerto*

| Fraction | Weight (mg) | U ppm | Pb ppm | $^{206}Pb/^{204}U$ | $^{207}Pb^*/^{235}U$ | (pct)[a] | $^{206}Pb/^{238}U$ | (pct)[b] | (rho) | $^{207}Pb^*/^{206}Pb$ | (pct)[c] | $^{206}Pb^*/^{238}U$ | $^{207}Pb^*/^{235}U$ | $^{207}Pb^*/^{206}Pb$ | (Ma)** |
|---|---|---|---|---|---|---|---|---|---|---|---|---|---|---|---|
| | | | | ***Ratios*** | | | | | | | | ***Age*** | | | |
| 1 | 0.023 | 288.29 | 22.6410 | 1702.30 | 0.6201 | 0.70 | 0.0773 | 0.66 | 0.94 | 0.058178 | 0.235 | 479.97 | 489.88 | 536.47 | 5.1 |
| 2 | 0.025 | 246.38 | 21.7820 | 3839.91 | 0.7358 | 0.69 | 0.0881 | 0.68 | 0.99 | 0.0605692 | 0.102 | 544.36 | 559.98 | 623.97 | 2.2 |
| 3 | 0.03 | 327.96 | 25.2850 | 3248.57 | 0.5995 | 0.57 | 0.0756 | 0.54 | 0.96 | 0.0575178 | 0.165 | 469.8 | 476.95 | 511.44 | 3.6 |
| 4 | 0.03 | 314.94 | 25.5480 | 1658.77 | 0.6420 | 0.92 | 0.0800 | 0.87 | 0.95 | 0.0581947 | 0.276 | 496.19 | 503.55 | 537.1 | 6 |
| 5 | 0.024 | 322.95 | 31.8500 | 1523.70 | 0.8996 | 0.76 | 0.1005 | 0.72 | 0.95 | 0.0649094 | 0.245 | 617.46 | 651.53 | 771.4 | 5.2 |
| 6 | 0.063 | 509.92 | 41.0610 | 3382.16 | 0.6707 | 0.59 | 0.0824 | 0.57 | 0.98 | 0.0590506 | 0.121 | 510.28 | 521.13 | 568.96 | 2.6 |
| 7 | 0.059 | 215.66 | 22.6020 | 875.44 | 0.9417 | 1.22 | 0.1020 | 0.99 | 0.82 | 0.0669922 | 0.698 | 625.84 | 673.78 | 837.53 | 15 |
| 8 | 0.059 | 316.49 | 25.6900 | 1708.17 | 0.6687 | 0.63 | 0.0808 | 0.61 | 0.96 | 0.0600526 | 0.175 | 500.62 | 519.89 | 605.47 | 3.8 |

(*) Common Pb corrected using measured $^{204}Pb$ (pct)[a]= Percentage of error of 207Pb*/U235; (pct)[b]= Percentaje of error of $^{206}Pb^*/^{238}U$; (pct)[c]= Percentage of error of $^{207}Pb^*/^{206}Pb$. (rho)= correlation coefficient of error between $^{207}Pb^*/U^{235}$ and $^{206}Pb/^{238}U$. (**) Millions years error for individual fraction.

from Mesoproterozoic ca. 1.16 Ga (Grenville?) sialic basement, which is not obvious from the LA-ICPMS data.

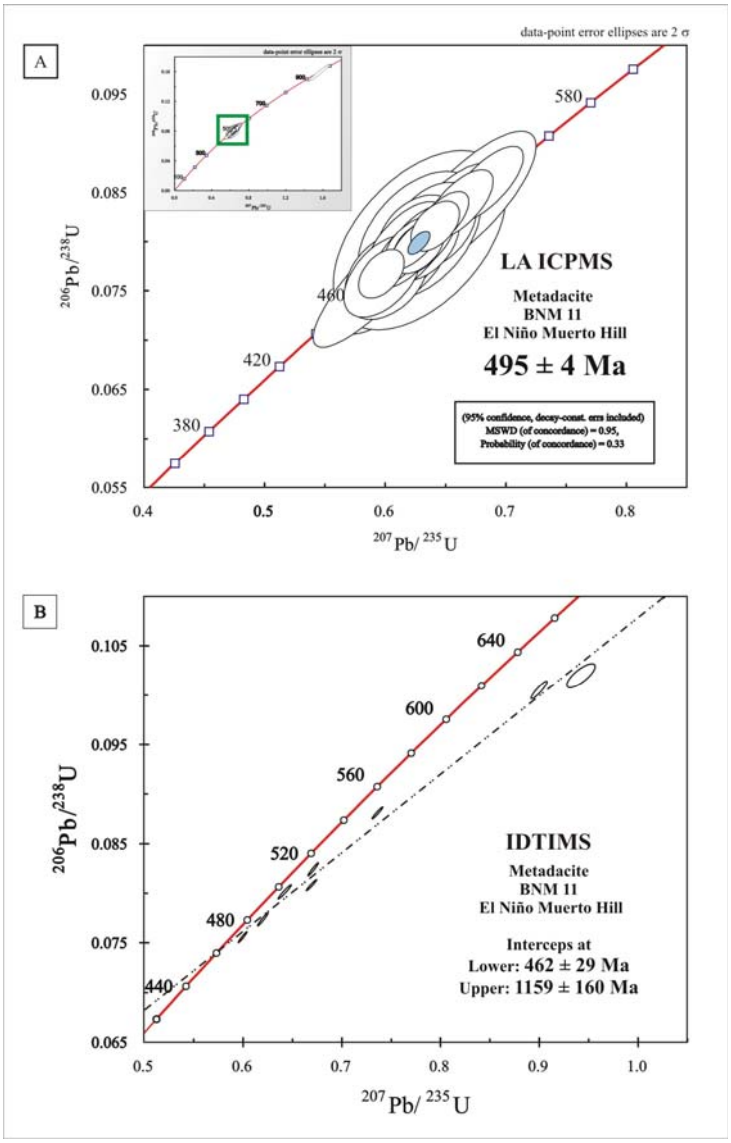


**Figure 10** Zircon U-Pb data for the El Nino Muerto Hill. A) LA-ICPMS Concórdia Age. B) ID-TIMS.

### 6.1.2. Río Blanco basalts (sample BRB 43)

Pink, transparent sub-rounded to prismatic zircon crystals up to 100 µm across are identified in this sample.

A total of seventy zircons were analyzed using Laser Ablation ICPMS (Table 5; Fig. 11) resulting in concordant analyses. On the basis of their distribution, two distinct groups of ages are recognized (Fig. 11): a younger age of 501 ± 9 Ma determined for four

*Table 5: LA-ICPMS U-Pb isotopic data from the Río Blanco volcanic rocks*

| Sample: ***BRB 43*** Grain N° | Shape* | ***Ratios*** | | | | | | ***Ages*** | | | | | | Disc (%) 206/238 | rho |
|---|---|---|---|---|---|---|---|---|---|---|---|---|---|---|---|
| | | $^{207}Pb/^{206}Pb$ | 2σ | $^{207}Pb/^{235}U$ | 2σ ind | $^{206}Pb/^{238}U$ | 2σ | $^{207}Pb/^{206}Pb$ | ± 2σ | $^{207}Pb/^{235}U$ | ± 2σ | $^{206}Pb/^{238}U$ | ± 2σ | | |
| 1 | *Psr* | 0.0671 | 0.000763 | 1.3545 | 0.082017 | 0.1397 | 0.008458 | 839.59 | 23 | 869.51 | 35 | 842.84 | 48 | 100.39 | 0.79 |
| 2 | *Psr* | 0.0583 | 0.000244 | 0.7369 | 0.021919 | 0.0880 | 0.002617 | 542.15 | 9 | 560.62 | 13 | 543.71 | 15 | 100.29 | 0.02 |
| 3 | *Psr* | 0.0586 | 0.000246 | 0.7548 | 0.022448 | 0.0899 | 0.002675 | 553.77 | 9 | 570.98 | 13 | 555.22 | 16 | 100.26 | 0.02 |
| 4 | *Psr* | 0.0582 | 0.000571 | 0.6926 | 0.025591 | 0.0866 | 0.003200 | 535.52 | 22 | 534.34 | 15 | 535.42 | 19 | 99.98 | 0.66 |
| 5 | *Psr* | 0.0569 | 0.000407 | 0.6479 | 0.043151 | 0.0790 | 0.005259 | 488.43 | 16 | 507.19 | 26 | 489.93 | 31 | 100.31 | 0.35 |
| 6 | *Psr* | 0.0575 | 0.000344 | 0.6423 | 0.022619 | 0.0822 | 0.002895 | 509.90 | 13 | 503.76 | 14 | 509.40 | 17 | 99.90 | 0.64 |
| 7 | *Psr* | 0.0585 | 0.000477 | 0.7100 | 0.054497 | 0.0890 | 0.006832 | 550.10 | 18 | 544.75 | 32 | 549.66 | 40 | 99.92 | 0.89 |
| 8 | *Psr* | 0.0575 | 0.000341 | 0.6435 | 0.034272 | 0.0824 | 0.004386 | 510.69 | 13 | 504.46 | 21 | 510.19 | 26 | 99.90 | 0.84 |
| 9 | *Psr* | 0.0586 | 0.000452 | 0.7207 | 0.030073 | 0.0896 | 0.003740 | 553.55 | 17 | 551.07 | 18 | 553.34 | 22 | 99.96 | 0.82 |
| 10 | *Psr* | 0.0568 | 0.000376 | 0.6432 | 0.028215 | 0.0784 | 0.003437 | 484.73 | 14 | 504.28 | 17 | 486.29 | 21 | 100.32 | 0.57 |
| 11 | *Psr* | 0.0617 | 0.000095 | 0.9304 | 0.031254 | 0.1085 | 0.003646 | 663.86 | 3 | 667.83 | 16 | 664.22 | 21 | 100.05 | 0.92 |
| 12 | *Psr* | 0.0592 | 0.000169 | 0.7702 | 0.030992 | 0.0931 | 0.003748 | 573.58 | 6 | 579.86 | 18 | 574.12 | 22 | 100.09 | 0.60 |
| 13 | *Psr* | 0.0597 | 0.000810 | 0.7837 | 0.061369 | 0.0963 | 0.007537 | 592.88 | 30 | 587.60 | 34 | 592.42 | 44 | 99.92 | 0.35 |
| 14 | *Psr* | 0.0593 | 0.000108 | 0.7738 | 0.028624 | 0.0939 | 0.003474 | 578.28 | 4 | 581.95 | 16 | 578.59 | 20 | 100.05 | 0.64 |
| 15 | *Psr* | 0.0598 | 0.000284 | 0.7957 | 0.033493 | 0.0970 | 0.004081 | 596.75 | 10 | 594.42 | 19 | 596.55 | 24 | 99.97 | 0.29 |
| 16 | *Psr* | 0.0591 | 0.000170 | 0.7553 | 0.031977 | 0.0927 | 0.003923 | 571.33 | 6 | 571.29 | 18 | 571.33 | 23 | 100.00 | 0.61 |
| 17 | *Psr* | 0.0614 | 0.000114 | 0.8879 | 0.024587 | 0.1066 | 0.002953 | 653.93 | 4 | 645.23 | 13 | 653.14 | 17 | 99.88 | 0.90 |
| 18 | *Psr* | 0.0589 | 0.000750 | 0.7775 | 0.217442 | 0.0917 | 0.025653 | 564.05 | 27 | 584.08 | 117 | 565.76 | 150 | 100.30 | 0.76 |
| 19 | *Psr* | 0.0565 | 0.001260 | 7.1717 | 0.307598 | 0.1309 | 0.005614 | 472.37 | 34 | 2133.00 | 38 | 792.93 | 32 | 167.86 | 0.95 |
| 20 | *Psr* | 0.0602 | 0.000195 | 0.8133 | 0.063000 | 0.0994 | 0.007699 | 611.50 | 7 | 604.33 | 35 | 610.87 | 45 | 99.90 | 0.92 |
| 21 | *Psr* | 0.0614 | 0.000947 | 1.2505 | 0.040131 | 0.1093 | 0.003507 | 651.60 | 30 | 823.61 | 18 | 668.61 | 20 | 102.61 | 0.60 |
| 22 | *Psr* | 0.0597 | 0.000114 | 0.7899 | 0.022773 | 0.0961 | 0.002769 | 591.34 | 4 | 591.13 | 13 | 591.32 | 16 | 100.00 | 0.74 |
| 23 | *Psr* | 0.0612 | 0.000148 | 0.8763 | 0.034411 | 0.1052 | 0.004131 | 645.44 | 5 | 638.97 | 18 | 644.85 | 24 | 99.91 | 0.36 |
| 24 | *Psr* | 0.0776 | 0.000230 | 2.4873 | 0.101772 | 0.1963 | 0.008032 | 1136.30 | 6 | 1268.35 | 29 | 1155.43 | 43 | 101.68 | 0.84 |
| 25 | *Psr* | 0.0595 | 0.000218 | 0.7937 | 0.024875 | 0.0951 | 0.002981 | 585.04 | 8 | 593.27 | 14 | 585.75 | 18 | 100.12 | 0.57 |
| 26 | *Psr* | 0.0598 | 0.000219 | 0.8067 | 0.025281 | 0.0972 | 0.003045 | 597.54 | 8 | 600.58 | 14 | 597.80 | 18 | 100.04 | 0.57 |
| 27 | *Psr* | 0.0599 | 0.000396 | 0.8004 | 0.058406 | 0.0976 | 0.007121 | 600.56 | 14 | 597.06 | 32 | 600.25 | 42 | 99.95 | 0.37 |

*(*) Psr: prismatic subrounded crystals*

concordant spot analysis and an older age of 581 ± 8 Ma for nine concordant zircon analyses. The age values ranging from ca. 580 to ca. 1200 Ma observed for the Rio Blanco basalts represent inherited zircons and agree with part of the age spectrum for the detrital zircons of the Puncoviscana Formation (Adams et al., 2006), suggesting contamination of the original magmas with these sediments. Adams et al. (2006) recognized, in Puncoviscana rocks, detrital zircons ages ranging from 580 to 1100 Ma, with two significant age groups at ca. 860-1100 and 580-760 Ma. Therefore zircon grains with ages between ca.580 and 1200 Ma in the Rio Blanco volcanics may be interpreted as inherited zircons from the Punillica phase (Adams et al., 2006) of the Pampean Ranges. The younger age of **501 ± 9 Ma** is interpreted in the present study, therefore, as the crystallization of the original basalts.

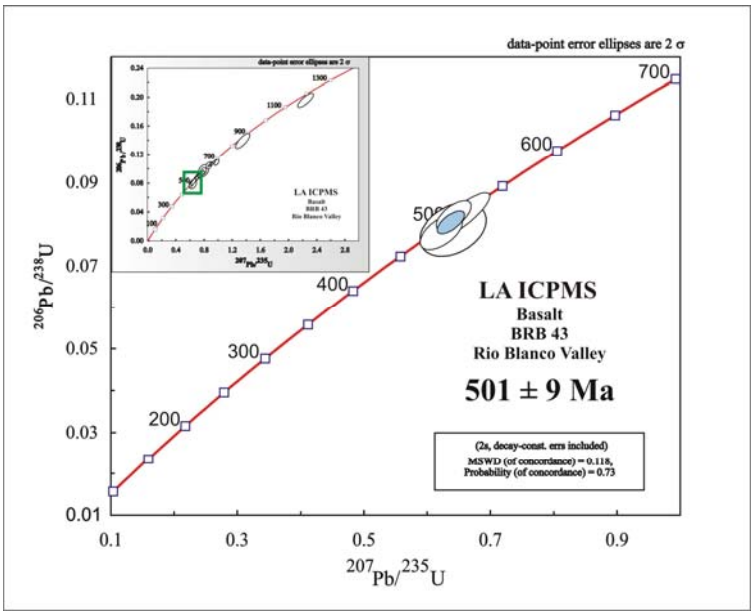


**Figure 11:** LA ICPMS Zircon U-Pb data for the Rio Blanco basalt

The presence of peperite deposits in the RB Valley indicates that the deposition of the turbidite sequence was contemporaneous with the extrusion of the RB Basalts, at approximately 500 Ma. Therefore, the sedimentary succession investigated here is

younger than the Puncoviscana Formation which has a minimum age of 530 Ma, being intruded by the Tastil granite at ca. 535 Ma (Bachmann et al., 1987). This is in agreement with the 527 Ma U-Pb age on detrital zircon found by Lork et al. (1990) in a similar turbidite sequence 30 km to the SW of the study area, indicating that this whole sedimentary succession can not be correlated with the Puncoviscana Formation**.**

## 6.2. Nd and Sr Isotopic Data

Fifteen representative samples of the El Niño Muerto Hill and the Rio Blanco igneous rocks were selected for whole-rock Nd isotope analyses. Sm and Nd elemental abundances were measured by isotope dilution following the method described by Gioia and Pimentel (2000). Only five whole-rock samples were selected for Sr isotope analyses. Rb and Sr concentrations were derived from ICPMS analyses. The isotopic data are listed in Table 6.

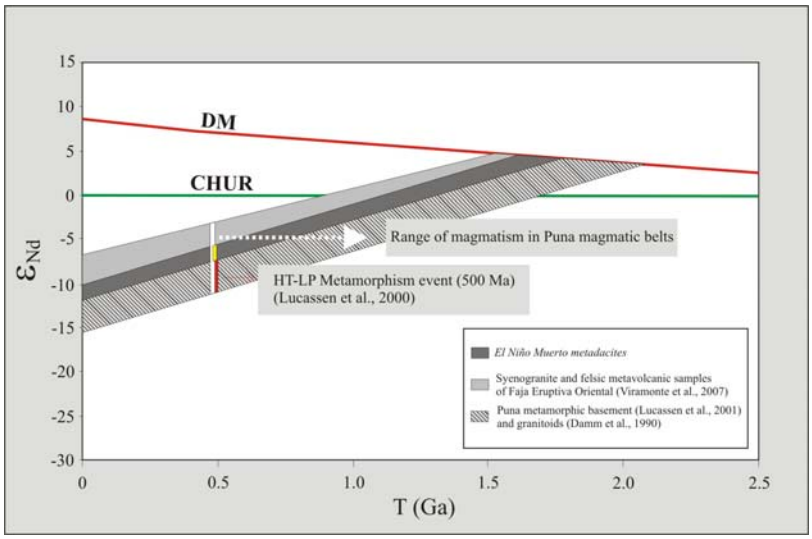


**Figure 12:** $\varepsilon_{Nd}$ versus age diagram for the El Niño Muerto metadacites. The Nd isotopic compositions of these rocks are similar to the felsic metavolcanic samples of Faja Eruptiva Oriental and the metamorphic and granitoids rocks of the basement of Puna.

Nd and Sr isotopic ratios for the El Niño Muerto Hill were re-calculated to **495** Ma. The analyzed samples have fairly homogeneous high initial $^{87}Sr/^{86}Sr$ ratios ranging between 0.71107 and 0.71180. All samples have negative $\varepsilon_{Nd}$ (t) values between -9.7 (BNM 16) and -5.9 (BNM 10) and their $T_{DM}$ model ages range between 1.62 and 1.79 Ga (Table 6). Nd and Sr isotopic data for the Rio Blanco basalts were corrected to **501** Ma. The initial $^{87}Sr/^{86}Sr$ isotopic ratios of three Rio Blanco samples vary between 0.70713 and 0.70942 (Table 5). All samples have positive initial $\varepsilon_{Nd}$ (t) values, between +2.5 (BRB 30) and +4.5 (BLC 95) with only one sample (BRB 25) showing a slightly negative $\varepsilon_{Nd}$ (t) value of -0.9. The $T_{DM}$ model ages for the Rio Blanco basalts vary from 0.84 to 1.12 Ga.

*Table 6: Sr-Nd isotopic data for volcanic rocks from the El Niño Muerto metadacites and Río Blanco basalts.*

| *Locality* | Sample | Rb(***) (ppm) | Sr (***) (ppm) | $^{87}(Rb/^{86}Sr)$ | $(^{87}Sr/^{86}Sr)_{meas}$ | $(^{87}Sr/^{86}Sr)t$ | Sm (ppm) | Nd (ppm) | $^{147}Sm/^{144}Nd$ | $(^{143}Nd/^{144}Nd)_{meas}$ | $(^{143}Nd/^{144}Nd)t$ | $\varepsilon_{Nd\,(t)}$ | $T_{DM}$ |
|---|---|---|---|---|---|---|---|---|---|---|---|---|---|
| | BMN 10 | | | | | | 7.79 | 37.17 | 0.1267 | 0.512108 (±10) | 0.511697 | -5.92 | 1.63 |
| | BMN 11 | 177.50 | 226.80 | 2.2690 | 0.72776 (±02) | 0.71179 | 6.17 | 28.15 | 0.1325 | 0.512086 (±13) | 0.511656 | -6.71 | 1.79 |
| ***El Niño Muerto*** | BMN 12 | | | | | | 6.189 | 30.10 | 0.1243 | 0.512091 (±06) | 0.511688 | -6.10 | 1.62 |
| ***(*)*** | BMN 14 | | | | | | 6.53 | 32.10 | 0.1230 | 0.512068 (±11) | 0.511669 | -6.46 | 1.63 |
| | BMN 15 | | | | | | 6.452 | 30.71 | 0.1270 | 0.512107 (±15) | 0.511695 | -5.96 | 1.64 |
| | BNM 16 | 158.40 | 161.70 | 2.8407 | 0.73111 (±05) | 0.71107 | 9.29 | 33.17 | 0.1693 | 0.512055 (±14) | 0.511506 | -9.65 | - |
| | BRB 22 | | | | | | 6.75 | 26.29 | 0.1552 | 0.512719 (±03) | 0.512210 | 4.24 | 0.85 |
| | BRB25 | 37.50 | 373.80 | 0.2903 | 0.71054 (±02) | 0.70847 | 13.15 | 39.20 | 0.2028 | 0.512612 (±09) | 0.511946 | -0.90 | - |
| | BRB 30 | | | | | | 6.13 | 24.38 | 0.1521 | 0.512618 (±15) | 0.512119 | 2.47 | 1.05 |
| | BRB 37 | 2.80 | 445.40 | 0.0182 | 0.70726 (±02) | 0.70714 | 8.26 | 30.44 | 0.1641 | 0.512696 (±10) | 0.512158 | 3.23 | 1.06 |
| ***Rio Blanco (**)*** | BRB 43 | 73.40 | 223.60 | 0.9505 | 0.71621 (±03) | 0.70942 | 8.362 | 34.31 | 0.1473 | 0.512677 (±15) | 0.512193 | 3.93 | 0.84 |
| | BRB 44 | | | | | | 4.06 | 15.20 | 0.1615 | 0.512715 (±12) | 0.512185 | 3.76 | 0.95 |
| | BRB 64 | | | | | | 6.88 | 25.92 | 0.1606 | 0.512649 (±18) | 0.512122 | 2.54 | 1.12 |
| | BRB 65 | | | | | | 4.11 | 16.79 | 0.1480 | 0.512639 (±14) | 0.512153 | 3.14 | 0.94 |
| | BRB 66 | | | | | | 4.25 | 17.28 | 0.1485 | 0.512665 (±13) | 0.512177 | 3.60 | 0.88 |

*Obs:*

Errors on measured isotope ratios are given in parenthesis as uncertainty in last digits (2s)

$\varepsilon_{Nd}$ (T) calculated relative to CHUR with present-day value of $^{143}Nd/^{144}Nd = 0.512638$. $T_{DM}$ values were calculated using DePaolo model (1981).

(*) $^{87}Sr/^{86}Sr$ and $^{143}Nd/^{144}Nd$ and $\varepsilon_{Nd(t)}$ calculate with an age of 495 ± 4 Ma

(**) $^{87}Sr/^{86}Sr$ and $^{143}Nd/^{144}Nd$ and $\varepsilon_{Nd(t)}$ calculate with an age of 501.0 Ma

(***) Elemental abundances of Rb and Sr are taken from ICP-MS analyses

In the $\varepsilon_{Nd}$ vs. time diagram (Fig. 12) the El Niño Muerto Hill dacites are compared with data for the Central Andean metamorphic-magmatic basement (Lucassen et al., 2000, 2001; Viramonte et al., 2007). The basement has a homogeneous distribution of Sm-Nd model ages ($T_{DM}$) between ca. 2.0 and 1.6 Ga (Lucassen et al., 2001). The El Niño Muerto dacites have very similar Nd isotopic characteristics compared to the metamorphic basement rocks of the Puna Plateau. They are also very similar isotopically and geochronologically to metadacites, metarhyolites and granitoids of the Faja Eruptiva de la Puna Oriental, either in the Salar Centenario area (485 ± 5 Ma**;** the Oire Igneous-Metamorphic Complex, Viramonte et al. 2007) or in the Calalaste Range (495 ± 3 Ma; Pinheiro et al., 2008), suggesting that the original magmas formed during a Late Cambrian-Early Ordovician magmatic event which reworked Mesoproterozoic or Paleoproterozoic continental crust.

## 7. Discussion and conclusions

The new petrographic, geochemical and isotopic data of the El Niño Muerto dacites (ENM) and the Rio Blanco basalts (RB) interlayered into the Lower paleozoic sediments of the Andean basement in NW Argentina are discussed below in order to constrain the magmatic evolution and tectonic setting of the study area.

### 7.1 El Niño Muerto metadacites

The new data for the ENM rocks indicate that they are high K calc-alkaline dacites. The calcalkaline, subduction-related, signature is also evident by the strong fractionation between LILE and HFSE and by the Nb-Ta negative anomaly.

The peraluminous character of the ENM rock suggests that they may have been generated by partial melting of sedimentary rocks or that they derived from a more primitive source but acquired the peraluminous nature by intense assimilation of high $Al_2O_3$ crustal material. Their high initial $^{87}Sr/^{86}Sr$ isotopic ratios and negative $\varepsilon_{Nd}$ (t) values (-5.2 to -9) confirm the involvement of older crustal material during the genesis of the original magmas. $T_{DM}$ model ages between 1.63 to 1.79 Ga of ENM rocks and the zircon inheritance pattern suggest participation of Mesoproterozoic continental crust which is in agreement with other basement data for the Central Andes (Lucassen et al., 2001, Viramonte et al., 2007).

## 7.2. Rio Blanco basalts

The RB submarine volcanic rocks have been affected by intense hydrothermal alteration that modifies the distribution of LIL elements and, for that reason, the application of major element oxides and large ion lithophile elements is not useful for identifying their paleotectonic setting. Therefore, the classification based on immobile elements (Winchester and Floyd 1977) is needed, and it shows that the RB rocks are transitional between subalkaline and alkali basalts (Fig. 8).

Concentrations of Th, Hf and Ta of the RB basalts are similar to either E-MORB or Within Plate Basalts (Fig. 13 A; Wood, 1980). Similarly, Zr, Ti and Y concentrations of most of the RB rocks are similar to those of within plate basalts (Fig. 13 B, Pearce and Cann, 1973). In the Zr-Nb-Y diagram (Meschede, 1986) (Figure 13 C) rock samples of the RB basalts seem to be transitional between AII (within plate alkali basalts) and B (plume-MORB). The RB basalts have low Zr/Nb ratios (~7), which is characteristic of rocks with E-MORB affinity or of oceanic island tholeiites (OIT) (Wood et al., 1979). They show moderate enrichment in the LREE and the lack of Eu anomaly suggests that contamination with older continental crust was not important, which is also supported by the generally positive values of $\varepsilon_{Nd}(t)$, although inherited zircon grains have been recognized. Negative Nb anomalies are not observed either. The slightly high Sr isotopic initial ratio, the enrichment in LILE elements and some of the Nd isotopic characteristics may reflect original features of the mantle source, combined with some degree of crustal assimilation.

The high $^{87}Sr/^{86}Sr$ isotopic ratio (0.70714-0.70942) and the positive $\varepsilon_{Nd}$ (t) values (from +2.47 to +4.24) suggest that these rocks are similar to OIB or E-MORB basalts, although the high $^{87}Sr/^{86}Sr$ isotopic ratio observed in many E-MORB or OIB are attributed to seawater-alteration effects.

## 7.3. Age and tectonic evolution

The **495 ± 4** Ma zircon age of the El Niño Muerto dacites places them into the initial stages of the Famatinian Cycle (Rapela et al., 1998). The ENM dacites, on the basis of the new field, geochemical, isotopic and geochronological data, are part of the Faja Eruptiva Oriental (Fig. 1) which is characterized by the presence of volcano-sedimentary sequences composed by metadacites and metarhyolites of similar age (ca. 485 to 475 Ma) and geochemical nature (e.g. Viramonte et al., 2007).

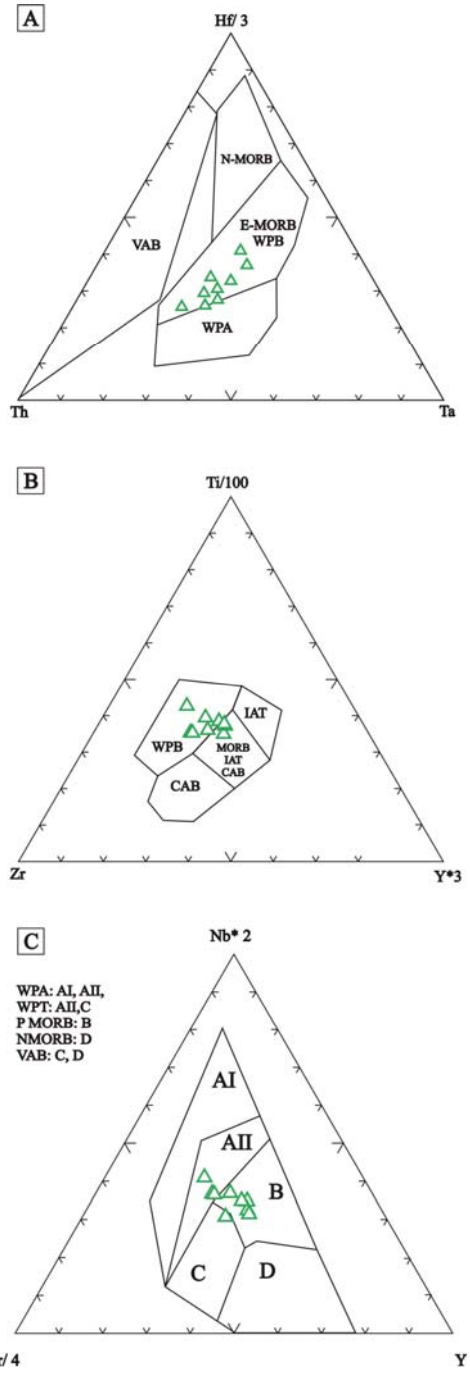


**Figure 13***:* Tectonic discriminant diagrams for the Rio Blanco basalts. A) Triangular discriminate Th-Hf/3-Ta diagram after Wood 1980. Abbreviations: N-MORB= normal mid-ocean ridge basalt, E-MORB and WPB= enriched mid-ocean ridge basalt and within plate basalt respectively, WPA= within plate alkali, VAB= volcanic arc basalt. B) Triangular discriminant diagram of Pearce and Cann (1973). Abbreviations: IAT= island-arc tholeiite, MORB= mid-ocean ridge basalt, CAB=calc-alkali basalt, WPB= within plate basalt. C) Triangular discriminant diagram of Meschede, 1986.

The **501 ± 9 Ma** U-Pb age of the RB basalts indicate that they are roughly synchronous with ENM arc dacites. Based on the field relationships as well as on the geochemical and isotopic E-MORB signature, the RB basalts may be interpreted as a remnant of a back-arc basin related with the Ordovician arc in NW Argentina. This model is in

agreement with that proposed by Miller and Sollner (2005) for the evolution of the Famatinian magmatic arc during the Ordovician.

***Acknowledgements***

The authors are CNPq and CONICET researchers and grateful for the research grant that allowed field and laboratory work and financing from the PROSUL programme. Sérgio Junges, Jorge Laux, Bárbara Lima and Sandrine Ferreira are acknowledged for technical assistance. This constitutes a new contribution of the Laboratorio de Geocronologia-UnB, from the Universidade de Brasilia.

## References

**Aceñolaza, F. G., Toselli, A. J., 1973.** Consideraciones estratigráficas y tectónicas sobre el Paleozoico inferior del Noroeste Argentino. Memorial del II Congreso Latinoamericano de Geología, Caracás. Ministerio de Minas e Hidrocarburos, Dirección de Geología, Caracás, 2, 755-764.

**Aceñolaza, E. G., Fernandez, R. I., Manca, N., 1982**. Caracteres bioestratigráficos y paleoambientales del Grupo Mesón (Cámbrico Medio-Superior), centro-oeste de América del Sur. Estudios Geológicos, 38, 385-392.

**Aceñolaza, E. G., Miller, H., Toselli, A. J., 1988.** The Puncoviscana Formation (Late Precambrian-Early Cambrian). Sedimentology, tectonometamorphic history and age of the oldest rocks of NW Argentina. In: Bahlburg, H., Breitkreuz, C., Giese, P (Eds.) The Southern Centra Andes: Contributions to Structure and Evolution of an Active Continental Margin. Lecturer Notes on Earth Sciences, **17**, Springer Verlag, Berlin, 25-38.

**Aceñolaza, E. G., Miller, H., Toselli, A. J., 1990**. El Ciclo Pampeano en el Noroeste Argentino **(Eds.)**.. Serie de Correlacion Geológica N 4. Universidad Nacional de Tucumán, 1-227.

**Adams, Ch., Miller, H., Toselli., A. J., 1990.** Nuevas Edades de Metamorfismo por el método k-Ar de la Formación Puncoviscana y equivalentes, NW Argentina. In: Aceñolaza, F. G; Millar, H; Toselli, A. J; (Eds.), El Ciclo Pampeano en el Noroeste Argentino. Serie de Correlación Geológica N 4. Universidad Nacional de Tucumán, 209-219.

**Adams, Ch.; Miller, H.; Toselli, A. J., 2006.** Maximum age and provenance area of the Puncoviscana Fm. Sediments (NW Argentina), based on detrital zircon geochronology-a pilot study. XI Congreso Geológico Chileno, 2006 Antofagasta, Chile. Actas, Vol. 1, 11-14.

**Bachmann, G., Grauert, B. Kramm, U., Lork, A., Miller, H., 1987** E1 magmatismo del Cámbrico Medio/Cámbrico superior en el basamento del noroeste Argentino: Investigaciones isotópicas y geocronológicas sobre los granitoides de los complejos intrusivos de Santa Rosa de Tastil y Cañani. X Congreso Geológico Argentino, Tucumán, Actas, 4, 125-127.

**Bahlburg, H., 1998.** The geochemistry and provenance of Ordovician turbidites in the Argentina Puna. In: Pankhurst, R. J. & Rapela, C. W. (Eds.), The Proto-Andean margin of Gondwana. Geological Society Special Publication, London N 142, 127-142.

**Blasco, G., Villar, L., Zappettini, E., 1996.** El Complejo Ofiolítico desmembrado de la Puna Argentina, provincias de Jujuy, Salta y Catamarca: XIII Congreso geológico Argentino y III Congreso de Exploración de Hidrocarburos, Actas, 3, 653-667.

**Bordonaro, O. L., 1992.** El Cámbrico de Sudamerica In: Gutiererz-Marco, J. G. Saavedra, J. and Rabano, I. (Eds.), Paleozoico Inferior de IberoAmerica. Universidad de Extremadura, Spain, 23-68.

**Buatois, L. A., Mángano, M. G. 2003.** La icnofauna de la formación Puncoviscana en el noroeste argentino: La colonización de fondos oceánicos y reconstrucción de paleoambientes y paleoecosistemas de la transición precámbrica-cámbrica. Ameghiniana 40 (1), 103–117.

**Busby-Spera, C. J., White, J. D. L., 1987** Variation in peperite textures associated with differing host sediment properties. Bull. Volcanol. 49, 765-775.

**Chayle, W., Coira, B., 1987**. Vulcanitas básicas a ultrabásicas y mesosilíceas de la Formación Puncovicana en el área del Cerro Alto de Minas-Departamento Tilcara-Jujuy, Argentina. X. Congr. Geol. Argentino, Tucumán, Actas 4**,** 292-295.

**Coira, B., Manca, N. y Chayle, W., 1990.** Registros volcánicos en la Formación Puncoviscana. In: Aceñolaza, F. G; Millar, H; Toselli, A. J; (Eds.), El Ciclo Pampeano en el Noroeste Argentino. Serie de Correlación Geológica N 4. Universidad de Tucumán, 53-60.

**Corfu, F., Hanchar, J.M., Hoskin, P.W.O., Kinny, P. (2003).** Atlas of zircon textures. In J.M. Hanchar & P.W.O. Hoskin, (Eds.) Zircon Rev. Mineral. Geochem**.** 53, 469-500.

**Dalziel, I. W. D., 1997.** Neoproterozoic - Paleozoic geography and tectonics, review, hypothesis, environmental speculation. Geological Society of America Bulletin, 109, 16-42.

**DePaolo, D.J., 1981**. A neodymium and strontium isotopic study of Mesozoic calc-alkaline granitic batholith of the Sierra Nevada and Peninsular Ranges. California. Journal Geophysical Research 86, 10470-10488.

**Do Campo M., Nieto, F., Omarini, R., 1998.** Mineralogía de arcillas y metamorfismo de la Formación Puncoviscana en localidades de la Cordillera Oriental y Puna, Argentina, Actas 10 Congreso Latinoamericano de Geología, Buenos Aires, Argentina Actas II, 217–223.

**Do Campo, M., Nieto, F., Omarini, R., Ostera, H., 1999.** Neoproterozoic K–Ar ages for the metamorphism of the Puncoviscana formation, Northwestern Argentina, 2 Simposio Sudamericano de Geología Isotópica, V. Carlos Paz, Argentina, Actas I, 48–53.

**Do Campo, M., 1999a.** Metamorfismo del basamento en la Cordillera Oriental y borde oriental de la Puna. In: Gonzalez Bonorino, G.,Omarini, R., Viramonte, J. (Eds.), Geología del Noroeste de Argentina, XIV Congreso Geológico Argentino, Salta, Tomo I, 41–51.

**Do Campo, M., 1999b.** Mineralogía, geoquímica y geocronología de la Formación Puncoviscana (Neoproterozoico) entre los 23° 30' y 25° 50' de Latitud Sur, Noroeste de Argentina. PhD thesis, Universidad de Buenos Aires, Argentina, 287 pp.

**Do Campo, M., Nieto, F., 2003.** Transmission electron microscopy study of the very low-grade metamorphic evolution in Neoproterozoic Pelites of the Puncoviscana formation (Cordillera Oriental, NW Argentina). Clay Minerals 38, 459–481.

**Do Campo, M., Riveiro Guevara, S., 2005.** Provenance and tectonic setting of late Neoproterozoic metasedimentary successions in NW Argentina. Journal of South American Earth Sciences 19, 143-153.

**Durant, F. R.; Aceñolaza, F. G. 1990.** Caracteres biofaunísticos, paleoecológicos y paleogeográficos de la Formación Puncoviscana (Precámbrico Superior-Cámbrico Inferior) del Noroeste Argentino. In: Aceñolaza, F. G; Millar, H; Toselli, A. J; (Eds.), El Ciclo Pampeano en el Noroeste Argentino. Serie de Correlación Geológica N 12. Universidad de Tucumán, 71-112.

**Durant, F. R., 1996.** La transición Precámbrico-Cámbrico en el sur de Sudamérica. In: Baldis, B., Aceñolaza, F. G. (Eds.), Early Paleozoic Evolution in NW Gondwana. Serie de Correlación Geológica, N **12.** Universidad Nacional de Tucumán, 195-205.

**Floyd, P. A., Winchester, J. A., 1978.** Identification and discrimination of altered and metamorphosed volcanic rocks using immobile elements. Chemical Geology, 21, 291-306.

**Gioia, S.M.C., Pimentel, M., 2000.** The Sm-Nd isotopic method in the Geochronology Laboratory of University of Brasilia. Anais da Academia Brasileira de Ciências, 72, 219-245.

**Gohrbrandt K. H. A., 1992.** Paleozoic paleogeographic and depositional developments on the proto-margin of Gondwana: their importance to hydrocarbon accumulation. Journal of South American Earth Sciences, 6, 267-287.

**Hanson, R. E., Wilson, T. J., 1993.** Large - scale rhyolitic peperites (Jurassic, southern Chile). J. Volcanol. Geotherm. Res. 54, 247-264.

**Hongn, F., Mon, R., Cuevas, J., Tubia, M., 1996.** Zones de cisaillement calédoniennes à hautes température dans la Quebrada Barranquilla (Puna Orientale, Argentine): donnés structurales et cinématiques. Compte Rendu Acaddmie des Sciences, 323, Ila, 809-815.

**Jezek, P., Willner, A. E., Aceñolaza, E. G., Miller, H., 1985**. The Puncoviscana trough a large basin of Late Precambrian to Early Cambrian age on the Pacific edge of the Brazilian shield. Geologische Rundsehau, *74,* 573-584.

**Jezek, P., Miller, H., 1986.** Deposition and facies distribution of turbiditic sediments of the Puncoviscana Formation (Upper Precambrian-Lower Cambrian) within the basement of the NW Argentine Andes. Zentralblatt fiir Geologie und Paltiontologie, Teil I, 9/10, 1235-1244.

**Jezek, P. 1990.** Análisis sedimentológico de la Formación Puncoviscana entre Tucumán y Salta. In: Aceñolaza, F. G; Millar, H; Toselli, A. J; (Eds.), El Ciclo Pampeano en el Noroeste Argentino. Serie de Correlación Geológica N 4. Universidad Nacional de Tucumán, 9-35.

**Keppie, J. D., Bahlburg, H. 1999.** Puncoviscana Formation of northwestern and central Argentina: Passive margin or foreland basin deposits? In*:* Ramos, V.A. & Keppie, J.D. (Eds.), Laurentia-Gondwana Connections before Pangaea. Geological Society of America Special Publications, 336, 139-144.

**Kleine, T., Mezger, K., Zimmerman, U., Münker, C., Bahlburg, H. 2004.** Crustal Evolution along the Early Ordovician Proto-Andean Margin of Gondwana: Trace Element and Isotope Evidence from the Complejo Igneo Pocitos (Northwest Argentina). Journal of Geology, 112, 503-520.

**Kohuskarsky, M., Quenardelle, S., Litvak, V., Maisonnave, E.B., Page, S., 2002.** Plutonismo del Ordovícico inferior en el sector Norte de la Sierra de Macón, provincia de Salta. Asociación Geológica Argentina, Revista 57 (2), 173-181.

**Kraemer, P. E., Escayola, M. P., Martino, R. D., 1995**. Hipótesis sobre la evolución neoproterozoica de las Sierras Pampeanas de Córdoba (30º40'–32º40' S) Argentina. Revista de la Asociación Geológica Argentina 50 (1–4), 47–59.

**Kumpa, M., Sanchez, T. M., 1988.** Geology and sedimentology of the Cambrian Grupo Mesón (NW Argentina). In: Bahlbur, G., H., Breitkreuz, C., Giese, P. (Eds.), The southern Central Andes: Contributions to Structure and Evolution of an Active Continental Margin. Lecturer Notes on Earth Sciences, 17, Springer Verlag, Berlín, 39-53.

**Le Maitre, R.W., Bateman, P., Dudek, A., Séller, J., Lamiere Le Bas, M.J., Sabine, P.A., Schmid, R., Sorensen, H., Streckeisen, A., Wolley, A.R., Zanettin, B., 1989**. A classification of igneous rocks and glossary of terms. Blackwell, Oxford.

**Llambías, E. J., Sato, A. M., Ortíz Suarez, A., Proxy, C. 1998.** The granitoids of the Sierra de San Luis. In: Pankhurst, R. J., Rapela, C. W. (Eds.), The Proto-Andean Margin of Gondwana. Geological Society, London, Special Publications, 142, 325-341.

**Lork, A., Miller, H. Kramm, U., Grauert, B., 1990**. Sistemática U-Pb de circones detríticos de la Fm. Puncoviscana y su significado para la edad máxima de sedimentación en la Sierra

de Cachy (prov. De Salta, Argentina). In: Aceñolaza, F. G; Millar, H; Toselli, A. J; (Eds.), El Ciclo Pampeano en el Noroeste Argentino. Serie de Correlación Geológica N 4. Universidad de Tucumán, 199-208.

**Lork, A., Bahlburg, H. 1993.** Precise U-Pb ages of monazite from the Faja Eruptiva de la Puna Oriental and the Cordillera Oriental, NW Argentina: XII Congreso Geológico Argentino y II Congreso de Exploración de Hidrocarburos Actas, 4, 1-6.

**Lucassen, F., Becchio, R., Wilke, H., Franz, G., Thirwall, M., Viramonte, J. G., Wemmer, K., 2000.** Proterozoic-Paleozoic development of the basement of the Central Andes (18-26º) a mobile belt of the South America craton. Journal of South America Earth Science, 13, 697-715.

**Lucassen, F., Becchio, R., Harmon, R., Kasemann, S., Franz, G., Trumbull, R., Wilke, H.-G., Romer, R.L., Dulski, P., 2001.** Composition and density model of the continental crust in an active continental margin —the Central Andes between 18° and 27°S. Tectonophysics, 341, 195–223.

**Lucassen F., Kramer W., Bartsch V., Wilke F. G., Franz G., Romer R. L., Dulski P., 2006.** Nd, Pb, and Sr isotope composition of juvenile magmatism in the Mesozoic large magmatic province of northern Chile (18–27°S): indications for a uniform subarc mantle. Contrib. Mineral. Petrol. 152, 571–589.

**Manca, N. Coira, B. Barber, E. Pérez, A. 1987**. Episodios magmáticos de los ciclos Pampeano y Famatiniano en el Río Yacoraite, Jujuy. X. Congr. Geol. Argentino, Tucumán, Actas, 4, 299-301.

**Méndez, V., Navarini, A., Plaza, D., Viera, O., 1973**. Faja Eruptiva de la Puna Oriental: 5° Congreso Geológico Argentino, Córdoba., Actas, 4: 89-100.

**Meschede, M., 1986.** A method of discriminating between different types of mid-ocean ridge basalts and continental tholeiites with the Nb–Zr–Y diagram. Chem Geol, 56, 207–218

**Miller, H., Sollner, E., 2005.** The Famatina complex (NW Argentina): back-docking of an island arc or terrane accretion? Early Palaeozoic geodynamics at the western Gondwana margin. In: Vaughan, P. T., Leat, P.T., Pankhurst, R. J., (Eds) Terrane Processes at the Margins of Gondwana. Geological Society, London, Special Publications, Vol. 246, 241-256.

**Mon, R. and Hongn, F., 1991**. The structure of the Precambrian and Lower Paleozoic basement of the Central Andes between 22º and 32 º Lat. Geologische Rundschau, 80, 745-758.

**Moya, M. C., Malanca, S., Hongn, F. D., Bahlburg, H., 1993.** El Tremadoc temprano en la Puna Occidental argentina. XII Congreso de Exploración de Hidrocarburos, Mendoza, Actas, 11, 20-30.

**Omarini, R. H., 1983.** Caracterización litológica, diferenciación y génesis de la Formación Puncoviscana entre el Valle de Lerma y la Faja Eruptiva de la Puna Oriental. PHD Tesis, Universidad Nacional de Salta, 202 pp.

**Omarini, R. H., Viramonte, J. G., Cordani, U., Salfity, J. A., Kawashita, K., 1984**. Estudio geocronológico Rb/Sr de la Faja de la Puna en el sector de San Antonio de los Cobres. Provincia de Salta, Argentina. IX Congreso Geológico Argentino, San Carlos de Bariloche, Actas 3, 146-158.

**Omarini R. H., Alonso N. R., 1987**. Lavas en la Formación Puncoviscana, Río Blanco, Salta, Argentina. X. Congreso Geológico Argentino, Tucumán, Actas, 4, 292-295.

**Omarini, R.H., Sureda, R.J., Götze, H.J., Seilacher, A., Plüger, F., 1999**. The Puncoviscana folded belt: a testimony of Late Proterozoic Rodinia fragmentation and the collisional pre-Gondwanic episodes. Int Journ. Earth Sciences 88 (1), 76-97.

**Omarini R.H., Sureda R.J., Escayola M.P., Pimentel, M., Matteini M., 2005.** Datos preliminares (Sm-Nd) en lavas de la fm. Puncoviscana, Provincias de Salta y Jujuy, Republica Argentina. XVI Congreso geológico Argentino, La Plata 1, 181-184.

**Palma, M. A., Parica, P. D., Ramos, V. A., 1986.** El granito Archibarca: su edad y significado tectónico, provincia de Catamarca. Revista de la Asociación Geológica Argentina, 41, 414-419.

**Pankhurst, R. J., Rapela, C. W., Fanning, C. M., 2000.** Age and origen of coeval TTG, I- and S-type granites in the Famatinian belt of NW Argentina. Transactions of the Royal Society of Edinburgh: Earth Sciences, 91, 151-168.

**Pearce, J. A., Cann, J. R., 1973.** Tectonic setting of basic volcanic rocks determined using trace element analyses. Earth and Planetary Science Letters, 19, 290-300.

**Peccerillo, A., Taylor, S. R., 1976.** Geochemistry of Eocene calc-alkaline volcanic rocks from the Kastamonu area, Northern Turkey. Contribution to Mineralogy and Petrology, 58, 189-202.

**Pinheiro G.M., Pimentel, M.M. and Schalamuk, A., 2008.** Unpublished. LA-ICPMS U-Pb and Sm-Nd data for Cambrian/Ordovician rocks of the Calalaste Range, NW Argentina. VI Symposio Sudamerican de Geología Isotópica, San Carlos de Bariloche, Argentina (submitted).

**Pupin, J. P., 1980.** Zircon and granite petrology. Contribution to Mineralogy and Petrology, 73, 207-220

**Ramos, V.A., 1988**. Late Proterozoic–early Paleozoic of South America: a collisional history. Episodes 2, 168–174.

**Ramos, V. A., Basei, M., 1997.** The basement of Chilenia: an exotic continental terrane to Gondwana during the early Paleozoic. In: Bradshaw, J. D., Weaver, S. D. (Eds.) Terrane Dynamics International Conference on Terrane Geology, Christchurch, New Zealand, Abstracts, 140-143.

**Rapela C. W., Coira B., Toselli, A. Saavedra J., 1992**. El magmatismo del Paleozóico en el sudoeste de Gondwana. In: Gutiérrez Marco J.G., Saavedra, J. Rabano, I. (Eds.) Paleozóico Inferior de Ibero-América, Universidad de Extremadura, Spain, 21-68.

**Rapela, C. W., Pankhurst, R. J., Casquet, C., Baldo, E., Saavedra, J., Galindo, C., Fanning, C. M., 1998.** The Pampean Orogeny of the southern proto-Andes: Cambrian continental collision in the Sierras de Cordoba. In: Pankhurst, R.J. & Rapela, C.W. (Eds.), The Proto-Andean Margin of Gondwana. Geological Society, London, Special Publications, 142, 181-217.

**Rapela, C. W., Casquet, C., Baldo, E., Dahlquist, J., Pankhurst, R. J., Galindo, C., Saavedra J., 2001a**. Las Orogénesis del Paleozoico Inferior en el margen proto-andino de America del Sur , Sierras pampeanas, Argentina. Journal of Iberian Geology, **27**, 23-41.

**Rapela C. W., Pankhurst R. J., Baldo E., Casquet C., Galindo C., Fanning C. M., Saavedra J., 2001b**. Ordovician metamorphism in the Sierras Pampeanas: New U-Pb SHRIMP ages in central east Valle Fertil and the Velasco batholith. 3rd South American Symposium on Isotope Geology, Pucon, Actas (CD).

**Rossi, J. N., Toselli, A. J., Durand, F. R., 1992.** Metamorfismo de baja presion, su relación con el desarrollo de la cuenca Puncoviscana, plutonismo y regimen tectónico. Estudios geológicos, **48**, 279-287.

**Salfity J. A., Omarini, R. H., Baldis, B., Gutierrez, W. 1975.** Consideraciones sobre la evolución geológica del Precámbrico y Paleozoico del norte argentino. 2nd Congreso Iberoamericano de Geología Económica, Buenos Aires, 4, 341-361.

**Salfity, J. A., 1985.** Lineamientos transversales al rumbo andino en noroeste argentino. IV Congreso Geológico de Chile, Antofagasta, Actas II: 119 137.

**Shand, S. J., 1929.** Eruptive rocks, D. Von Nostrand, Company. New York. 360 pp.

**Sun, S., McDonough, W. F., 1989**. Chemical and isotopic systematic of ocean basalts: implication for mantle, composition and processes. In: Sounders A. D., Norry, M.J. (Eds.), Magmatism in ocean basins. Geol. Soc. London. Spec. Pub. 42, 313-345.

**Toselli, A.J., Aceñolaza, F.G., 1984.** Presencia de eruptivas basálticas en los afloramientos de la Formación Puncoviscana, en Coraya, departamento Humahuaca, Jujuy. Revista de la Asociación Geológica Argentina, 39 (1-2), 158-159.

**Toselli, A.J. 1990.** Metamorfismo del ciclo Pampeano. In: Aceñolaza, F. G; Millar, H; Toselli, A. J; (Eds.), El Ciclo Pampeano en el Noroeste Argentino. Serie de Correlación Geológica N 4. Universidad Nacional de Tucumán, 181-197.

**Turner, J. C. M. 1960.** Estratigrafía de la Sierra de Santa Victoria y adyacencias Academia Nacional de Ciencias Boletín 41, Córdoba, 163-196.

**Viramonte, J. G., Galliski, M. A., Araña Saavedra, V., Aparicio, A., García, L., Martín Escorza, C., 1984.** El finivolcanismo básico de la depresión de Arizaro, provincia de Salta, República Argentina. IX Congreso Geológico Argentino, Actas III: 234-254.

**Viramonte, J. M., Becchio, R., Viramonte, J. G., Pimentel, M. M., Martino, R. D., 2007**. Ordovician igneous and metamorphic units in southeastern Puna: New U-Pb and Sm-Nd data and implications for the evolution of northwestern Argentina. Journal of South American Earth Sciences, 24, 167-183.

**Willner, A.R, Miller, H., Jezek, P., 1990.** Composición geoquímica del basamento sedimentario/ metamórfico de los Andes del NW Argentino (Precámbrico Superior/Cánbrico Inferior). In: Aceñolaza, F. G; Millar, H; Toselli, A. J; (Eds.), El Ciclo Pampeano en el Noroeste Argentino. Serie de Correlación Geológica N 4. Universidad Nacional de Tucumán, 161-179.

**Winchester, J. A., Floyd, P. A., 1977.** Geochemical discrimination of different magma series and their differentiation products using immobile elements. Chemical Geology, 20: 325–343.

**Wood, D. A., Tarney, J., Saunders, A. D., Bougault, H., Joron J. L., Treuilet, M., Cann, J. R., 1979.** Geochemistry of basalts drilled in the north Atlantic by IPOD Leg. 49: implications for mantle heterogeneity. Earth Planet. Sci. Lett. 42, 77-97.

**Wood, D. A., 1980.** The application of a Th-Hf-Ta diagram to problems of the tectonomagmatic classification and to establishing the nature of crustal contamination of basaltic lavas of the British Tertiary Volcanic Province. Earth and Planetary Science Letters, 50, 11-30.

**Zimmermann, U., 2005.** Provenance studies of very low-to low grade metasedimentary rocks of the Puncoviscana complex, northwest Argentina. In Vaughan, A.P.M.; Leat, P.T., Pankhrust, R.J; (Eds.) Terrane processes at the margins of Gondwana. Geological Society, London, Special Publications, Vol. 246: p. 381-416.

# CAPÍTULO IV

## 4.1. Conclusões

Os novos dados de campo, geoquímicos e isotópicos obtidos para as rochas vulcânicas do embasamento do Noroeste Argentino permitiram as seguintes conclusões.

*Setor Norte: Vale do Río Grande*

1) Com base na composição dos minerais e na geoquímica de rocha total, os diques alojados na Formação Puncoviscana no Vale do Río Grande, são re-classificados como *ocellar analcima monchiquites***.** Estes são uma variedade de lamprófiro alcalino sem feldspato ou plagioclásio, caracterizados pela presença de diopsídio, biotita/flogopita, estas últimas ricas em Ti, pargasita titanífera e olivina forsterítica como fenocristais em uma matriz de composição semelhante, porém sem olivina. A nomenclatura dessas rochas foi baseada na presença de analcima e carbonato nas abundantes estruturas globulares presentes.

2) A idade K-Ar de 163 ± 8 Ma obtida em biotitas e os diagramas discriminantes de ambientes que indicam ambiente de intraplaca para essas rochas permitiram associar os lamprófiros do Vale de Río Grande com a etapa de pré-rift do Rift de Salta, desenvolvido durante o Cretáceo no noroeste argentino.

3) As altas razões iniciais de $^{87}Sr/^{86}Sr$ e os valores positivos de $\varepsilon_{Nd(t)}$, em conjunto com as características observadas durante o estudo petroquímico sugerem que o manto do qual estas rochas derivam é um manto metassomatizado. Altos conteúdos em SrO no carbonato presente nas estruturas globulares, na matriz e em alguns xenólitos indicam que ele é de origem magmática. Isto pode ser compatível com a participação de fluidos carbonatiticos durante metassomatismo.

4) As $T_{DM}$ destas rochas, entre 0.64 e 0.25 Ga, indicam, bem como os dados da literatura, que o evento de metassomatismo possivelmente ocorreu durante a Orogenia Famatiniana (460 Ma).

5) Pode-se concluir que as rochas deste setor não estão associadas aos orógenos paleozóicos da Plataforma Sulamericana.

*Setor Central e Sul: Serra de El Niño Muerto e Vale de* Río *Blanco*

1) As rochas fésicas da Serra de El Niño Muerto são classificadas como dacitos calci-alcalinos de alto-K e são relacionadas a ambientes de subduccção. Seu caráter peraluminoso indica que elas possivelmente derivam da fusão parcial de rochas sedimentares ou que rochas sedimentares foram assimiladas pelos magmas mais primitivos. O alto fracionamento de LILE e HFSE, as anomalias negativas em Nb-Ta, as altas relações iniciais de $^{87}Sr/^{86}Sr$ e os valores negativos de $\varepsilon_{Nd(t)}$ sugerem que os dacitos de El Niño Muerto foram alojados em um ambiente de arco continental. Em sua gênese houve participação de crosta continental possivelmente mesoproterozóica, como é indicam as idades modelo em torno 1.70 Ga.

2) Com base em elementos imóveis, as rochas de Río Blanco possuem características intermediárias entre basaltos subalcalinos e basaltos alcalinos. Os diagramas discriminantes indicam que elas foram alojadas em ambiente de intraplaca, ou seja, em ambiente de E-MORB. Razões iniciais de $^{87}Sr/^{86}Sr$ intermediárias e $\varepsilon_{Nd(t)}$ positivos indicam que a fonte dos magmas era mantélica e levemente enriquecida.

3) As análises U-Pb dos dacitos de El Niño Muerto fornecem idade de **495 ± 4** Ma. Assim, eles estão relacionados aos estágios iniciais do magmatismo do Ciclo Famatiniano, desenvolvido durante o Ordoviciano no centro-noroeste da Argentina. Pela localização, estes pertencem ao arco mais interno, conhecido na literatura como Faixa Eruptiva da Puna Oriental.

4) As análises U-Pb dos basaltos de Río Blanco fornecem idade de **501 ± 8** Ma, o que indicaria que estes são contemporâneos aos dacitos de El Niño Muerto. As características de campo, geoquímicas e isotópicas mostram afinidades E-MORB e permitem interpretar os basaltos de Río Blanco como possíveis remanescentes de um back-arc desenvolvido a leste do arco Famatiniano, no noroeste de Argentina.

*Os resultados obtidos com base em dados geológicos do noroeste da Argentina permitem acrescentar e esclarecer os processos ocorridos durante o Paleozóico Inf*erior*. Por outro lado levantam novos problemas geológicos e novos pontos de vista sobre a evolução da margem oeste de Gondwana requerendo, portanto, estudos mais detalhados neste setor dos Andes Centrais.*

## References

**Aceñolaza, F. G., Toselli, A. J., 1973.** Consideraciones estratigráficas y tectónicas sobre el Paleozoico inferior del Noroeste Argentino. Memorial del II Congreso Latinoamericano de Geología, Caracás. Ministerio de Minas e Hidrocarburos, Dirección de Geologia, Caracás, 2, 755-764.

**Aceñolaza, E. G., Miller, H., Toselli, A. J., 1990**. El Ciclo Pampeano en el Noroeste Argentino **(Eds.)**.. Serie de Correlacion Geológica N 4. Universidad Nacional de Tucumán, 1-227.

**Alonso, R., Gutierrez, R., Viramonte, J. G., 1984.** Puna austral-Bases para el subprovincialismo geológico de la Puna Argentina. IX Congreso Geológico Argentino, San carlos de Bariloche, Actas, 1, 43-63.

**Bachmann, G., Grauert, B. Kramm, U., Lork, A., Miller, H., 1987** E1 magmatismo del Cámbrico Medio/Cámbrico superior en el basamento del noroeste Argentino: Investigaciones isotópicas y geocronológicas sobre los granitoides de los complejos intrusivos de Santa Rosa de Tastil y Cañani. X Congreso Geológico Argentino, Tucumán, Actas, 4, 125-127.

**Baldis, B. A., Gorroño, A., Ploszkiewicz, J. V., Sarudiansky, R. M., 1976.** Geotectónica de la Cordillera Oriental, Sierras Subandinas y áreas adyacentes. VI Congreso Geológico Argentino, Buenos Aires Actas, 1, 3-22.

**Bonarelli, G., 1913, 1915**. Epirogenia y paleogeografia de Suramerica. Physics I, 5, 221-240 and I, 8, 499-522.

**Brachkebusch, L., 1883.** Estudio sobre la Formacion Petrolífera de Jujuy. Academia nacional de Ciencias Córdoba, Boletin 5, 137-252

**Brachkebusch, L., 1892.**Die Kordillerenpaese zwischen der Argentinischen Republik und Chile, von 22º-35º S. Br. Zeitschrift Deutsche Gesellschaft fur Erdkunde XXVII, Berlin, 250-348.

**Caminos, R., 1979.**Cordillera Frontal. In: Turner J. C. M. (Ed.) Geología Regional Argentina, Academia Nacional de Ciencias, Córdoba, 2 do Simposio I, 397-453.

**Coira, B., Manca, N. y Chayle, W., 1990.** Registros volcánicos en la Formación Puncoviscana. In: Aceñolaza, F. G; Millar, H; Toselli, A. J; (Eds.), El Ciclo Pampeano en el Noroeste Argentino. Serie de Correlación Geológica N 4. Universidad de Tucumán, 53-60.

**Do Campo, M., Riveiro Guevara, S., 2005.** Provenance and tectonic setting of late Neoproterozoic metasedimentary successions in NW Argentina. Journal of South American Earth Sciences 19, 143-153.

**Groeber, P., 1938.** Mineralogia y Geología Espasa-Calpe, Argentina, Buenos Aires, 1-492.

**Jezek, P. 1990.** Análisis sedimentológico de la Formación Puncoviscana entre Tucumán y Salta. In: Aceñolaza, F. G; Millar, H; Toselli, A. J; (Eds.), El Ciclo Pampeano en el Noroeste Argentino. Serie de Correlación Geológica N 4. Universidad Nacional de Tucumán, 9-35.

**Keidel, J., 1925.** Sobre el desarrollo paleogeografico de las grandes unidades geológicas de la Argentina. Sociedad Argentina de Estudios Geográficos GAEA, Anales, 4, 251-312.

**Keidel, J., 1927.** Sobre las realciones geológicas entre la Puna y la Cordillera Principal o Cordillera de los Andes. Academia Nacional de Ciencias, Córdoba, Boletin 30, 295-307

**Keidel, J., 1943.** El ordovícico inferior en los Andes del Norte argentino y sus depóstos marinos-glaciales. Academia nacional de Ciencias, Cordoba, Boletin 36, 140-229.

**Lucassen, F., Becchio, R., Wilke, H., Franz, G., Thirwall, M., Viramonte, J. G., Wemmer, K., 2000.** Proterozoic-Paleozoic development of the basement of the Central Andes (18-26º) a mobile belt of the South America craton. Journal of South America Earth Science, 13, 697-715.

**Lucassen F., Kramer W., Bartsch V., Wilke F. G., Franz G., Romer R. L., Dulski P., 2006.** Nd, Pb, and Sr isotope composition of juvenile magmatism in the Mesozoic large magmatic province of northern Chile (18–27°S): indications for a uniform subarc mantle. Contrib. Mineral. Petrol. 152, 571–589.

**Méndez, V., Navarini, A., Plaza, D., Viera, O., 1973**. Faja Eruptiva de la Puna Oriental: 5° Congreso Geológico Argentino, Córdoba., Actas, 4: 89-100.

**Miller, H., Sollner, E., 2005.** The Famatina complex (NW Argentina): back-docking of an island arc or terrane accretion? Early Palaeozoic geodynamics at the western Gondwana margin. In: Vaughan, P. T., Leat, P.T., Pankhurst, R. J., (Eds) Terrane Processes at the Margins of Gondwana. Geological Society, London, Special Publications, Vol. 246, 241-256.

**Mon, R. and Hongn, F., 1991**. The structure of the Precambrian and Lower Paleozoic basement of the Central Andes between 22º and 32 º Lat. Geologische Rundschau, 80, 745-758.

**Omarini, R. H., Viramonte, J. G., Cordani, U., Salfity, J. A., Kawashita, K., 1984**. Estudio geocronológico Rb/Sr de la Faja de la Puna en el sector de San Antonio de los Cobres. Provincia de Salta, Argentina. IX Congreso Geológico Argentino, San Carlos de Bariloche, Actas 3, 146-158.

**Omarini, R.H., Sureda, R.J., Götze, H.J., Seilacher, A., Plüger, F., 1999.** The Puncoviscana folded belt: a testimony of Late Proterozoic Rodinia fragmentation and the collisional pre-Gondwanic episodes. Int Journ. Earth Sciences 88 (1), 76-97.

**Palma, M. A., Parica, P. D., Ramos, V. A., 1986.** El granito Archibarca: su edad y significado tectónico, provincia de Catamarca. Revista de la Asociación Geológica Argentina, 41, 414-419.

**Pankhurst, R., Rapela, C. W., 1998 (Eds.).** The protomargin of Gondwana: an introduction. In: Pankhurst, R. J. & Rapela, C. W. (Eds.), The Proto-Andean margin of Gondwana. Geological Society Special Publication, London N 142, 1-9.

**Ramos, V.A., 1988**. Late Proterozoic–early Paleozoic of South America: a collisional history. Episodes 2, 168–174.

**Ramos, V. A., Palma, M. A., 1996.** Tectónica. In: Archangelsky, S. (Ed.) El sistema Pérmico n la República Argentina y en la República Oriental del Uruguay. Academia Nacional de Ciencias, Córdoba, 239-254.

**Rapela, C. W., Pankhurst, R. J., Casquet, C., Baldo, E., Saavedra, J., Galindo, C., Fanning, C. M., 1998.** The Pampean Orogeny of the southern proto-Andes: Cambrian continental collision in the Sierras de Cordoba. In: Pankhurst, R.J. & Rapela, C.W. (Eds.), he Proto-Andean Margin of Gondwana. Geological Society, London, Special Publications, 142, 181-217.

**Rapela, C. W., Casquet, C., Baldo, E., Dahlquist, J., Pankhurst, R. J., Galindo, C., Saavedra J., 2001a**. Las Orogénesis del Paleozoico Inferior en el margen proto-andino de America del Sur , Sierras pampeanas, Argentina. Journal of Iberian Geology, **27**, 23-41.

**Rapela C. W., Pankhurst R. J., Baldo E., Casquet C., Galindo C., Fanning C. M., Saavedra J., 2001b**. Ordovician metamorphism in the Sierras Pampeanas: New U-Pb SHRIMP ages in central east Valle Fertil and the Velasco batholith. 3rd South American Symposium on Isotope Geology, Pucon, Actas (CD).

**Roeder, 1988.** Andean age structure of Eastern Cordillera, (Province of la Paz, Bolivia). Tectonics, 7 (1) 23-40

**Salfity J. A., Omarini, R. H., Baldis, B., Gutierrez, W. 1975.** Consideraciones sobre la evolución geológica del Precámbrico y Paleozoico del norte argentino. 2nd Congreso Iberoamericano de Geología Económica, Buenos Aires, 4, 341-361.

**Salfity, J. A., Marquillas, R. A., 1981.** Las unidades estratigráficas cretácicas del Norte de la República Argentina. In: Volkheimer, W., Musacchio, E. (Eds.) Cuencas sedimentarias del Jurásico y Cretácico de América del Sur. Comité del Jurásico y Cretácico, 1, 303-317.

**Salfity, J. A., Marquillas, R. A., 1994.** Tectonic and sedimentary evolution of the Cretaceous-Eocene Salta Group basin, Argentina. In: Salfity J. A. (Ed.) Cretaceous Tectonics of the Andes Vieweged, 266-315.

**Sollner, E., Brodtkorb, M. K., Miller, H.,Pezzutti, N., Fernandez, R. E., 2000.** Dataciones U-Pb en circones de rocas metavolcánicas de la Sierra de San Luís. Revista de la Asociaci6n Geol6gica Argentina, 55, 15-22.

**Toselli, A.J., Aceñolaza, F.G., 1984.** Presencia de eruptivas basálticas en los afloramientos de la Formación Puncoviscana, en Coraya, departamento Humahuaca, Jujuy. Revista de la Asociación Geológica Argentina, 39 (1-2), 158-159.

**Turner, J. C. M. 1960.** Estratigrafía de la Sierra de Santa Victoria y adyacencias Academia Nacional de Ciencias Boletín 41, Córdoba, 163-196.

**Turner, J. C. M., 1970. (**Ed.) Geologia regional Argentina. Academia Nacional de Ciencias, Córdoba, Segundo Simposio I, 1-869, II, 879-1717.

**Viramonte, J. M., Becchio, R., Viramonte, J. G., Pimentel, M. M., Martino, R. D., 2007**. Ordovician igneous and metamorphic units in southeastern Puna: New U-Pb and Sm-Nd data and implications for the evolution of northwestern Argentina. Journal of South American Earth Sciences, 24, 167-183.

# ANEXO I:
# DIFRATOMETRIA DE RAIOS-X

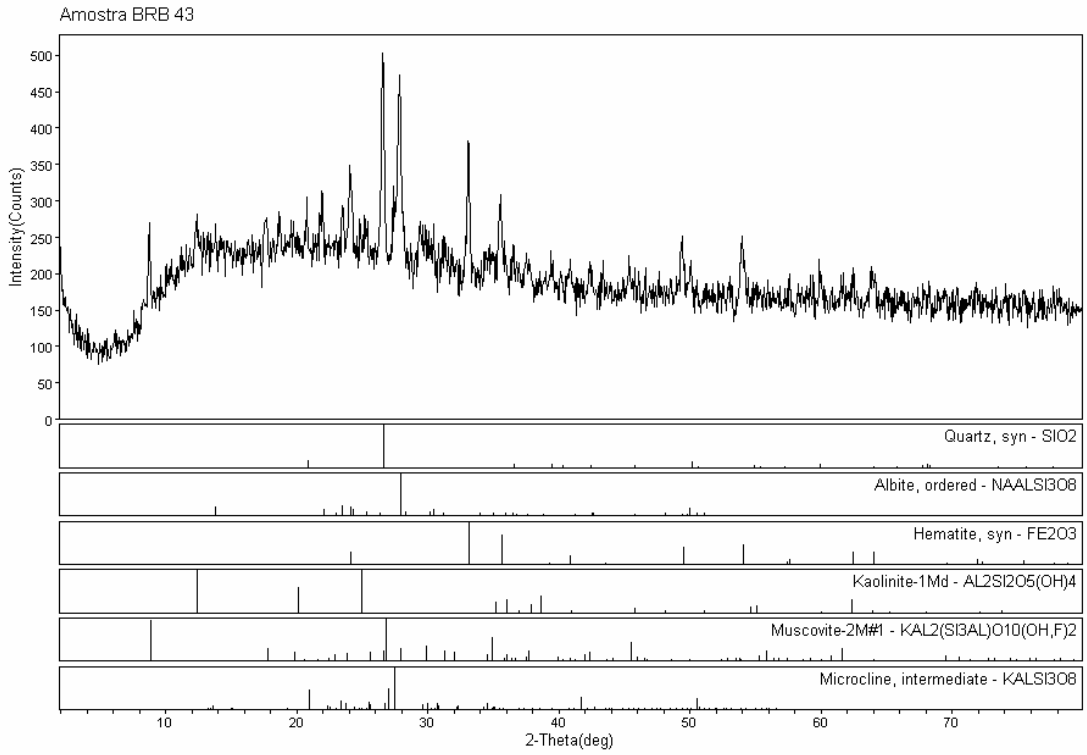


Laboratorio de DRX - IG/UnB

<d:\natali~1>

# ANEXO II:
## ANALISES DE MICROSONDA

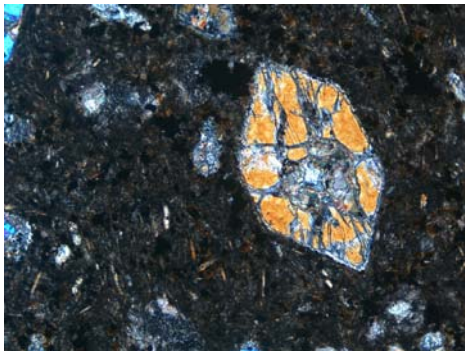

OLIVINA

**ANEXO:** Análises de microsonda de cristais de olivina da amostra BYA 124a, lamprofiros de Río Grande

| | *AMOSTRA BYA 124A* | | | | |
|---|---|---|---|---|---|
| | Phenocristais | | | Xenolitos | |
| | 1 | 2 | 3 | 4 | 5 |
| *Amostra* | BYA124A.10.OLV.214 | BYA124A.7.OLV.266 | BYA124A.5.OLV.280 | BYA124A.4.OLVXEN.236 | BYA124A.4.OLVXEN.238 |
| $SiO_2$ | 40.37 | 38.06 | 39.49 | 39.98 | 39.60 |
| $TiO_2$ | 0.00 | 0.03 | 0.02 | 0.04 | 0.03 |
| $Al_2O_3$ | 0.03 | 0.02 | 0.01 | 0.04 | 0.07 |
| $FeO_{(t)}$ | 17.40 | 21.96 | 17.04 | 17.80 | 14.28 |
| *MnO* | 0.13 | 0.31 | 0.22 | 0.20 | 0.19 |
| *MgO* | 42.51 | 39.05 | 42.86 | 42.45 | 44.50 |
| *CaO* | 0.19 | 0.13 | 0.31 | 0.19 | 0.21 |
| $Cr_2O_3$ | 0.03 | 0.01 | 0.01 | 0.03 | 0.03 |
| *NiO* | 0.12 | 0.18 | 0.29 | 0.21 | 0.30 |
| $K_2O$ | 0.01 | 0.00 | 0.01 | 0.01 | 0.00 |
| *Total* | 100.77 | 99.75 | 100.25 | 100.95 | 99.20 |
| ***FO*** | 81.42 | 75.89 | 81.92 | 80.99 | 84.82 |
| ***FA*** | 18.70 | 23.94 | 18.28 | 19.05 | 15.27 |
| ***mg#*** | 0.71 | 0.64 | 0.72 | 0.70 | 0.76 |

**ANEXO:** Análises de microsonda de cristais de olivina da amostra BYA 127, lamprofiros de Río Grande

*AMOSTRA BYA 127*

| | Bordas | | | | | | | | Intermedios | | Núcleos | | | | | | | | |
|---|---|---|---|---|---|---|---|---|---|---|---|---|---|---|---|---|---|---|---|
| | 1 | 2 | 3 | ***4*** | ***5*** | 6 | ***7*** | 8 | ***2*** | 4 | ***1*** | 2 | ***3*** | 4 | ***5*** | 6 | ***7*** | 8 | ***9*** |
| *Amostra* | BYA127.5 .OLVRIM. 478 | BYA127.3 B.OLVRIM .481 | BYA127.1 A.OLVRIM .501 | BYA127.1 B.OLVRI M.505 | BYA127.2 B.OLVRI M.508 | BYA127.2 A.OLVRIM .519 | BYA127.6 A.OLVRIM .545 | BYA127.6 .OLVRIM. 557 | BYA127.3B .OLVINTER .482 | BYA127.1 B.OLVCOR E.503 | BYA127.5. OLVCORE .479 | BYA127.3B. OLVINTCOR E.483 | BYA127. 1A.OLV. 500 | BYA127.1B.O LVMORECOR E.504 | BYA127.2B .OLVCORE .509 | BYA127.2 A.OLVCOR E.518 | BYA127.6 A.OLVCOR E.543 | BYA127.6. OLVCORE .556 | BYA127.1. OLVCORE 506 |
| $SiO_2$ | 39.52 | 40.32 | 40.66 | 39.47 | 40.11 | 39.95 | 39.52 | 39.44 | 40.21 | 39.59 | 39.38 | 40.22 | 40.22 | 39.66 | 40.43 | 40.37 | 39.64 | 39.87 | 39.01 |
| $TiO_2$ | 0.00 | 0.05 | 0.02 | 0.07 | 0.04 | 0.05 | 0.06 | 0.08 | 0.01 | 0.01 | 0.05 | 0.02 | 0.00 | 0.01 | 0.03 | 0.03 | 0.07 | 0.00 | 0.01 |
| $Al_2O_3$ | 0.02 | 0.08 | 0.02 | 0.01 | 0.05 | 0.53 | 0.03 | 0.04 | 0.02 | 0.03 | 0.06 | 0.05 | 0.06 | 0.05 | 0.07 | 0.05 | 0.02 | 0.03 | 0.07 |
| $FeO_{(t)}$ | 15.03 | 15.00 | 12.60 | 15.08 | 14.60 | 14.93 | 14.84 | 14.93 | 13.05 | 14.11 | 19.14 | 13.20 | 12.90 | 13.10 | 13.36 | 12.96 | 13.40 | 12.81 | 13.87 |
| *MnO* | 0.26 | 0.22 | 0.14 | 0.25 | 0.24 | 0.17 | 0.27 | 0.27 | 0.15 | 0.12 | 0.24 | 0.18 | 0.15 | 0.12 | 0.14 | 0.11 | 0.12 | 0.11 | 0.15 |
| *MgO* | 43.70 | 44.02 | 46.84 | 44.12 | 44.50 | 43.98 | 44.16 | 43.92 | 45.56 | 44.79 | 41.16 | 45.21 | 45.41 | 45.68 | 46.17 | 45.88 | 44.88 | 45.83 | 45.20 |
| *CaO* | 0.38 | 0.42 | 0.19 | 0.40 | 0.30 | 0.34 | 0.43 | 0.41 | 0.21 | 0.26 | 0.11 | 0.24 | 0.18 | 0.23 | 0.22 | 0.24 | 0.22 | 0.16 | 0.23 |
| $Cr_2O_3$ | 0.05 | 0.08 | 0.07 | 0.09 | 0.02 | 0.02 | 0.09 | 0.07 | 0.04 | 0.04 | 0.01 | 0.03 | 0.03 | 0.07 | 0.00 | 0.07 | 0.01 | 0.03 | 0.04 |
| *NiO* | 0.20 | 0.19 | 0.37 | 0.15 | 0.20 | 0.15 | 0.15 | 0.17 | 0.32 | 0.21 | 0.16 | 0.31 | 0.26 | 0.20 | 0.23 | 0.42 | 0.20 | 0.46 | 0.29 |
| $K_2O$ | 0.01 | 0.00 | 0.01 | 0.00 | 0.02 | 0.09 | 0.00 | 0.00 | 0.01 | 0.01 | 0.00 | 0.01 | 0.00 | 0.01 | 0.00 | 0.02 | 0.00 | 0.00 | 0.00 |
| *Total* | 99.16 | 100.38 | 100.91 | 99.63 | 100.06 | 100.21 | 99.53 | 99.32 | 99.58 | 99.17 | 100.30 | 99.46 | 99.21 | 99.13 | 100.65 | 100.15 | 98.56 | 99.30 | 98.87 |
| ***FO*** | 84.03 | 84.24 | 86.98 | 84.14 | 84.58 | 84.24 | 84.39 | 84.22 | 86.27 | 85.18 | 79.22 | 86.04 | 86.32 | 86.30 | 86.16 | 86.49 | 85.80 | 86.53 | 85.43 |
| ***FA*** | 16.21 | 16.11 | 13.13 | 16.13 | 15.57 | 16.04 | 15.91 | 16.06 | 13.86 | 15.05 | 20.67 | 14.10 | 13.76 | 13.88 | 13.99 | 13.71 | 14.37 | 13.57 | 14.71 |
| ***mg#*** | 0.74 | 0.75 | 0.79 | 0.75 | 0.75 | 0.75 | 0.75 | 0.75 | 0.78 | 0.76 | 0.68 | 0.77 | 0.78 | 0.78 | 0.78 | 0.78 | 0.77 | 0.78 | 0.77 |

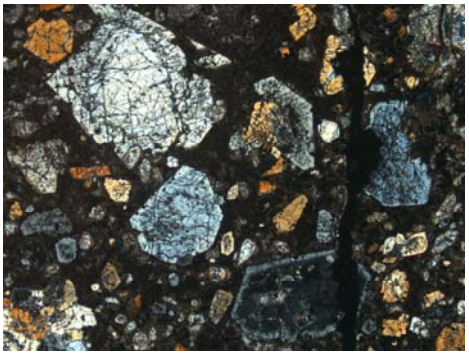

CLINOPIROXÊNIO

**ANEXO:** Análises de microsonda de cristais de clinopiroxênio da amostra P8, lamprofiros de Río Grande

| | ***Fenocristais brancos*** | | | | | | | | | | | | | |
|---|---|---|---|---|---|---|---|---|---|---|---|---|---|---|
| | Bordas | | | | | | | Núcleos | | | | | | |
| | 1 | 2 | 3 | 4 | 5 | 6 | 7 | 1 | 2 | 3 | 4 | 5 | 6 | 7 |
| *Amostra* | P8A.5.CPX BORDE.A | P8A.13.CPX RIM.18 | P8A.13.CPX RIM.25 | P8G.4.CPX RIM.712 | P8G.9.CPX RIM.719 | P8H.7.CPX RIMXENOXX .668 | P8H.4.CPX RIM.617 | P8A.5.CPX CORE.B | P8A.13.CPX CORE.17 | P8A.13.CPX CORE.24 | P8G.4.CPX CORE.711 | P8G.9.CPX CORE.718 | P8H.7.CPX. XENOXX.667 | P8H.4.CPX. CORE.616 |
| $SiO_2$ | 46.85 | 47.85 | 50.13 | 48.26 | 49.32 | 49.47 | 49.69 | 50.81 | 50.04 | 49.19 | 52.10 | 49.67 | 48.36 | 49.03 |
| $TiO_2$ | 2.34 | 1.50 | 1.42 | 1.60 | 1.54 | 1.31 | 1.27 | 1.09 | 1.12 | 1.45 | 0.87 | 1.34 | 1.19 | 1.36 |
| $Al_2O_3$ | 6.73 | 7.08 | 5.25 | 4.80 | 4.82 | 5.29 | 5.23 | 5.68 | 5.14 | 5.37 | 3.96 | 5.07 | 5.51 | 5.98 |
| $FeO_{(t)}$ | 7.82 | 5.57 | 8.34 | 7.79 | 7.93 | 7.86 | 7.41 | 6.73 | 5.36 | 8.07 | 6.80 | 9.39 | 7.70 | 7.03 |
| *MnO* | 0.20 | 0.09 | 0.16 | 0.16 | 0.14 | 0.13 | 0.12 | 0.12 | 0.09 | 0.19 | 0.15 | 0.23 | 0.10 | 0.16 |
| *MgO* | 11.95 | 13.30 | 11.87 | 12.73 | 13.27 | 12.65 | 12.84 | 13.53 | 14.85 | 11.93 | 14.15 | 11.84 | 12.74 | 12.45 |
| *CaO* | 22.66 | 21.28 | 20.67 | 22.64 | 22.58 | 20.68 | 21.42 | 20.71 | 21.66 | 20.99 | 20.94 | 19.96 | 20.70 | 21.54 |
| $Cr_2O_3$ | 0.05 | 0.67 | 0.02 | 0.01 | 0.00 | 0.03 | 0.10 | 0.30 | 0.48 | 0.02 | 0.55 | 0.00 | 0.08 | 0.12 |
| $Na_2O$ | 0.89 | 0.80 | 1.66 | 0.53 | 0.80 | 1.49 | 1.49 | 1.37 | 0.35 | 1.60 | 1.24 | 2.07 | 1.32 | 1.46 |
| $K_2O$ | 0.02 | 0.02 | 0.01 | 0.00 | 0.00 | 0.00 | 0.03 | 0.02 | 0.02 | 0.01 | 0.00 | 0.04 | 0.02 | 0.01 |
| *Total* | 100.07 | 98.41 | 99.82 | 98.83 | 100.93 | 99.31 | 100.08 | 100.58 | 99.15 | 99.32 | 100.95 | 100.28 | 98.21 | 99.61 |
| **Fórmula estrutural baseada em 6 oxigênios** | | | | | | | | | | | | | | |
| **Si** | 1.75 | 1.79 | 1.86 | 1.82 | 1.82 | 1.84 | 1.84 | 1.86 | 1.85 | 1.84 | 1.90 | 1.84 | 1.82 | 1.82 |
| **$Al^{IV}$** | 0.25 | 0.21 | 0.14 | 0.18 | 0.18 | 0.16 | 0.16 | 0.14 | 0.15 | 0.16 | 0.10 | 0.16 | 0.18 | 0.18 |
| **$Fe^{3+}$** | 0.00 | 0.00 | 0.00 | 0.00 | 0.00 | 0.00 | 0.00 | 0.00 | 0.00 | 0.00 | 0.00 | 0.00 | 0.00 | 0.00 |
| ***Sitio T*** | 2.00 | 2.00 | 2.00 | 2.00 | 2.00 | 2.00 | 2.00 | 2.00 | 2.00 | 2.00 | 2.00 | 2.00 | 2.00 | 2.00 |
| **$Al^{VI}$** | 0.05 | 0.10 | 0.09 | 0.03 | 0.03 | 0.08 | 0.07 | 0.10 | 0.08 | 0.08 | 0.07 | 0.06 | 0.07 | 0.08 |
| **Ti** | 0.07 | 0.04 | 0.04 | 0.05 | 0.04 | 0.04 | 0.04 | 0.03 | 0.03 | 0.04 | 0.02 | 0.04 | 0.03 | 0.04 |
| **$Fe^{3+}$** | 0.14 | 0.06 | 0.08 | 0.09 | 0.12 | 0.11 | 0.13 | 0.07 | 0.02 | 0.12 | 0.05 | 0.17 | 0.14 | 0.12 |
| **$Fe^{2+}$** | 0.11 | 0.12 | 0.18 | 0.15 | 0.12 | 0.13 | 0.10 | 0.14 | 0.15 | 0.14 | 0.16 | 0.12 | 0.11 | 0.10 |
| **Mn** | 0.01 | 0.00 | 0.01 | 0.01 | 0.00 | 0.00 | 0.00 | 0.00 | 0.00 | 0.01 | 0.00 | 0.01 | 0.00 | 0.00 |
| **Mg** | 0.67 | 0.74 | 0.66 | 0.72 | 0.73 | 0.70 | 0.71 | 0.74 | 0.82 | 0.67 | 0.77 | 0.66 | 0.72 | 0.69 |
| **Cr** | 0.00 | 0.02 | 0.00 | 0.00 | 0.00 | 0.00 | 0.00 | 0.01 | 0.01 | 0.00 | 0.02 | 0.00 | 0.00 | 0.00 |
| ***Sitio O*** | 1.03 | 1.09 | 1.06 | 1.05 | 1.05 | 1.07 | 1.04 | 1.09 | 1.11 | 1.04 | 1.09 | 1.06 | 1.07 | 1.04 |
| **Ca** | 0.91 | 0.85 | 0.82 | 0.92 | 0.89 | 0.83 | 0.85 | 0.81 | 0.86 | 0.84 | 0.82 | 0.79 | 0.84 | 0.86 |
| **Na** | 0.06 | 0.06 | 0.12 | 0.04 | 0.06 | 0.11 | 0.11 | 0.10 | 0.03 | 0.12 | 0.09 | 0.15 | 0.10 | 0.10 |
| **K** | 0.00 | 0.00 | 0.00 | 0.00 | 0.00 | 0.00 | 0.00 | 0.00 | 0.00 | 0.00 | 0.00 | 0.00 | 0.00 | 0.00 |
| ***Sitio C*** | 0.97 | 0.91 | 0.94 | 0.95 | 0.95 | 0.93 | 0.96 | 0.91 | 0.89 | 0.96 | 0.91 | 0.94 | 0.93 | 0.96 |
| ***Wo*** | 49.92 | 48.21 | 47.29 | 48.76 | 47.81 | 46.56 | 47.53 | 46.23 | 46.57 | 47.83 | 45.58 | 45.60 | 46.59 | 48.55 |
| ***En*** | 36.63 | 41.95 | 37.81 | 38.15 | 39.08 | 39.63 | 39.65 | 42.04 | 44.44 | 37.83 | 42.86 | 37.66 | 39.89 | 39.07 |
| ***Fs*** | 13.45 | 9.84 | 14.90 | 13.09 | 13.10 | 13.81 | 12.83 | 11.72 | 8.99 | 14.35 | 11.56 | 16.74 | 13.52 | 12.38 |
| **mg#*** | 73.14 | 80.99 | 71.73 | 74.45 | 74.89 | 74.16 | 75.55 | 78.20 | 83.18 | 72.50 | 78.76 | 69.22 | 74.68 | 75.94 |

*mg# =100*Mg/(Mg+Fetot)

**ANEXO:** Análises de microsonda de cristais de clinopiroxênio da amostra P8, lamprofiros de Río Grande

| | ***Meso e microfenocristais brancos*** | | | | | | | | | | | |
|---|---|---|---|---|---|---|---|---|---|---|---|---|
| | 8 | 9 | 10 | 11 | 12 | 13 | 14 | 15 | 16 | 17 | 18 | 19 |
| *Amostra* | P8A.5.CPXCORE.12 | P8A.13.CPXRIM.19 | P8D.2.CPX.432 | P8D.4.CPX.440 | P8D.3.CPX.443 | P8D.3.CPX.444 | P8E.1A.CPX.300 | P8E.3.CPX.312 | P8E.7.CPXCORE.344 | P8E.13.CPXCORE.36 c | P8G.1Y2.CPX.698 | P8G.1Y2.CPX.699 |
| $SiO_2$ | 46.59 | 49.55 | 49.54 | 50.23 | 50.59 | 50.22 | 53.49 | 51.26 | 51.86 | 48.32 | 53.27 | 51.41 |
| $TiO_2$ | 2.25 | 1.26 | 1.55 | 1.32 | 1.14 | 0.86 | 0.18 | 1.08 | 0.66 | 1.70 | 0.25 | 0.42 |
| $Al_2O_3$ | 8.05 | 5.33 | 6.80 | 5.71 | 4.78 | 3.25 | 0.98 | 4.63 | 3.14 | 8.30 | 1.36 | 4.54 |
| $FeO_{(t)}$ | 5.99 | 5.41 | 8.25 | 7.29 | 6.96 | 6.71 | 8.78 | 6.77 | 8.98 | 6.38 | 7.63 | 7.86 |
| *MnO* | 0.02 | 0.04 | 0.11 | 0.14 | 0.11 | 0.18 | 0.33 | 0.16 | 0.24 | 0.12 | 0.21 | 0.16 |
| *MgO* | 12.57 | 14.55 | 11.67 | 13.07 | 12.95 | 13.66 | 13.88 | 13.47 | 11.32 | 12.73 | 13.43 | 12.65 |
| *CaO* | 21.65 | 21.65 | 20.64 | 21.17 | 21.35 | 22.97 | 20.43 | 21.73 | 19.99 | 20.31 | 20.90 | 21.60 |
| $Cr_2O_3$ | 0.51 | 0.33 | 0.05 | 0.08 | 0.16 | 0.00 | 0.01 | 0.12 | 0.13 | 0.21 | 0.20 | 0.00 |
| $Na_2O$ | 0.80 | 0.63 | 1.74 | 1.25 | 1.41 | 0.66 | 1.67 | 1.02 | 2.52 | 1.38 | 2.06 | 1.15 |
| $K_2O$ | 0.00 | 0.01 | 0.02 | 0.03 | 0.00 | 0.01 | 0.01 | 0.00 | 0.00 | 0.00 | 0.02 | 0.00 |
| *Total* | 98.66 | 98.96 | 100.70 | 100.58 | 99.78 | 98.84 | 100.15 | 100.42 | 99.27 | 99.69 | 99.81 | 100.02 |
| | | | | | | | | | | | | |
| **Fórmula estrutural baseada em 6 oxigênios** | | | | | | | | | | | | |
| **Si** | 1.75 | 1.84 | 1.82 | 1.85 | 1.87 | 1.88 | 1.98 | 1.89 | 1.94 | 1.78 | 1.97 | 1.90 |
| **Al $^{IV}$** | 0.25 | 0.16 | 0.18 | 0.15 | 0.13 | 0.12 | 0.02 | 0.11 | 0.06 | 0.22 | 0.03 | 0.10 |
| **$Fe^{3+}$** | 0.00 | 0.00 | 0.00 | 0.00 | 0.00 | 0.00 | 0.00 | 0.00 | 0.00 | 0.00 | 0.00 | 0.00 |
| ***Sitio T*** | 2.00 | 2.00 | 2.00 | 2.00 | 2.00 | 2.00 | 2.00 | 2.00 | 2.00 | 2.00 | 2.00 | 2.00 |
| | | | | | | | | | | | | |
| **Al $^{VI}$** | 0.10 | 0.07 | 0.12 | 0.09 | 0.08 | 0.03 | 0.02 | 0.09 | 0.08 | 0.14 | 0.03 | 0.10 |
| **Ti** | 0.06 | 0.04 | 0.04 | 0.04 | 0.03 | 0.02 | 0.00 | 0.03 | 0.02 | 0.05 | 0.01 | 0.01 |
| **$Fe^{3+}$** | 0.07 | 0.05 | 0.10 | 0.08 | 0.08 | 0.09 | 0.11 | 0.04 | 0.13 | 0.07 | 0.13 | 0.05 |
| **$Fe^{2+}$** | 0.12 | 0.11 | 0.16 | 0.15 | 0.14 | 0.12 | 0.16 | 0.17 | 0.15 | 0.13 | 0.10 | 0.19 |
| **Mn** | 0.00 | 0.00 | 0.00 | 0.00 | 0.00 | 0.01 | 0.01 | 0.01 | 0.01 | 0.00 | 0.01 | 0.00 |
| **Mg** | 0.70 | 0.81 | 0.64 | 0.72 | 0.71 | 0.76 | 0.76 | 0.74 | 0.63 | 0.70 | 0.74 | 0.70 |
| **Cr** | 0.02 | 0.01 | 0.00 | 0.00 | 0.00 | 0.00 | 0.00 | 0.00 | 0.00 | 0.01 | 0.01 | 0.00 |
| ***Sitio O*** | 1.07 | 1.09 | 1.06 | 1.08 | 1.05 | 1.03 | 1.07 | 1.07 | 1.02 | 1.10 | 1.02 | 1.06 |
| | | | | | | | | | | | | |
| **Ca** | 0.87 | 0.86 | 0.81 | 0.83 | 0.85 | 0.92 | 0.81 | 0.86 | 0.80 | 0.80 | 0.83 | 0.86 |
| **Na** | 0.06 | 0.05 | 0.12 | 0.09 | 0.10 | 0.05 | 0.12 | 0.07 | 0.18 | 0.10 | 0.15 | 0.08 |
| **K** | 0.00 | 0.00 | 0.00 | 0.00 | 0.00 | 0.00 | 0.00 | 0.00 | 0.00 | 0.00 | 0.00 | 0.00 |
| ***Sitio C*** | 0.93 | 0.91 | 0.94 | 0.92 | 0.95 | 0.97 | 0.93 | 0.93 | 0.98 | 0.90 | 0.98 | 0.94 |
| | | | | | | | | | | | | |
| ***Wo*** | 49.41 | 46.94 | 47.65 | 47.00 | 47.65 | 48.65 | 43.85 | 47.50 | 46.76 | 47.23 | 45.89 | 47.65 |
| ***En*** | 39.92 | 43.90 | 37.48 | 40.37 | 40.22 | 40.25 | 41.44 | 40.96 | 36.84 | 41.19 | 41.04 | 38.82 |
| ***Fs*** | 10.67 | 9.16 | 14.87 | 12.63 | 12.13 | 11.09 | 14.70 | 11.54 | 16.40 | 11.58 | 13.08 | 13.53 |
| **mg#*** | 78.91 | 82.74 | 71.60 | 76.17 | 76.83 | 78.40 | 73.81 | 78.01 | 69.19 | 78.05 | 75.83 | 74.15 |

*mg# =100*Mg/(Mg+Fetot)

**ANEXO:** Analises de microsonda de cristais de clinopiroxênio verdes da amostra P8, lamprofiros de Río Grand

## *Fenocristais verdes*

| | Bordas | | | Núcleos | | |
|---|---|---|---|---|---|---|
| | 1 | 2 | 3 | 1 | 2 | 3 |
| *Amostra* | P8D.7.CPX RIM.437 | P8E.4.CPX RIM.316 | P8E.10.CPX RIM.362 | P8D.CPX CORE.438 | P8E.4.CPX. CORE315 | P8E.10.CPX CORE.363 |
| $SiO_2$ | 47.36 | 46.44 | 48.00 | 50.72 | 51.34 | 51.91 |
| $TiO_2$ | 2.31 | 3.06 | 1.52 | 1.20 | 0.80 | 0.54 |
| $Al_2O_3$ | 6.68 | 6.84 | 5.50 | 4.20 | 3.21 | 3.27 |
| $FeO_{(t)}$ | 7.75 | 6.37 | 7.67 | 10.71 | 10.24 | 9.53 |
| *MnO* | 0.11 | 0.06 | 0.14 | 0.17 | 0.22 | 0.19 |
| *MgO* | 12.14 | 13.13 | 12.46 | 10.89 | 11.12 | 11.21 |
| *CaO* | 22.64 | 23.92 | 22.81 | 19.47 | 20.30 | 20.06 |
| $Cr_2O_3$ | 0.00 | 0.00 | 0.02 | 0.03 | 0.03 | 0.00 |
| $Na_2O$ | 1.09 | 0.44 | 0.82 | 2.38 | 2.35 | 2.51 |
| $K_2O$ | 0.00 | 0.01 | 0.00 | 0.01 | 0.02 | 0.00 |
| *Total* | 100.62 | 100.77 | 99.41 | 100.29 | 100.19 | 99.80 |
| **Fórmula estrutural baseada em 6 oxigênios** | | | | | | |
| **Si** | 1.75 | 1.72 | 1.80 | 1.89 | 1.91 | 1.93 |
| **$Al^{IV}$** | 0.25 | 0.28 | 0.20 | 0.11 | 0.09 | 0.07 |
| **$Fe^{3+}$** | 0.00 | 0.00 | 0.00 | 0.00 | 0.00 | 0.00 |
| ***Sitio T*** | 2.00 | 2.00 | 2.00 | 2.00 | 2.00 | 2.00 |
| **$Al^{VI}$** | 0.05 | 0.01 | 0.04 | 0.07 | 0.05 | 0.08 |
| **Ti** | 0.06 | 0.09 | 0.04 | 0.03 | 0.02 | 0.02 |
| **$Fe^{3+}$** | 0.15 | 0.13 | 0.13 | 0.14 | 0.16 | 0.14 |
| **$Fe^{2+}$** | 0.09 | 0.07 | 0.11 | 0.19 | 0.16 | 0.16 |
| **Mn** | 0.00 | 0.00 | 0.00 | 0.01 | 0.01 | 0.01 |
| **Mg** | 0.67 | 0.72 | 0.70 | 0.60 | 0.62 | 0.62 |
| **Cr** | 0.00 | 0.00 | 0.00 | 0.00 | 0.00 | 0.00 |
| ***Sitio O*** | 1.02 | 1.02 | 1.03 | 1.05 | 1.02 | 1.02 |
| **Ca** | 0.90 | 0.95 | 0.92 | 0.78 | 0.81 | 0.80 |
| **Na** | 0.08 | 0.03 | 0.06 | 0.17 | 0.17 | 0.18 |
| **K** | 0.00 | 0.00 | 0.00 | 0.00 | 0.00 | 0.00 |
| ***Sitio C*** | 0.98 | 0.98 | 0.97 | 0.95 | 0.98 | 0.98 |
| ***Wo*** | 49.66 | 50.72 | 49.44 | 45.29 | 46.38 | 46.54 |
| ***En*** | 37.06 | 38.74 | 37.59 | 35.26 | 35.37 | 36.19 |
| ***Fs*** | 13.27 | 10.55 | 12.97 | 19.45 | 18.26 | 17.27 |
| **mg#*** | 73.63 | 78.60 | 74.35 | 64.45 | 65.95 | 67.70 |

*mg# =100*Mg/(Mg+Fetot)

**ANEXO:** Análises de microsonda de cristais e megacristais de clinopiroxênio da amostra BYA 123, lamprofiros de Río Grande

| | ***Fenocristais*** | | | | | | | | | | | | | | | | | |
|---|---|---|---|---|---|---|---|---|---|---|---|---|---|---|---|---|---|---|
| | Bordas Externas | | Bordas Internas | | | | | | Intermedios | | | Núcleos | | | | | | |
| | **2** | **3** | **1** | **2** | **3** | **4** | **5** | **6** | **1** | **2** | **4** | **1** | **2** | **3** | **4** | **5** | **6** | |
| *Amostra* | BYA123.1.CPX RIMEXT.372 | BYA123.2.CPX RIMEXT.395 | BYA123.1.CPX RIM.371 | BYA123.1.CPX RIM.373 | BYA123.2.CPX RIM.394 | BYA123.2.CPX RIM.398 | BYA123.2.CPX RIM.409 | BYA123.4D.CPX. 427 | BYA123.1.CPX INTERM.370 | BYA123.1.CPXI NTER.374 | BYA123.2.CPX INTERM.400 | BYA123.1.CPX CORE.369 | BYA123.1.CPX CORE.376 | BYA123.2.CPX CORE.396 | BYA123.2.CPX CORE.401 | BYA123.2.CPX CORE.408 | BYA123.4D.CPX CORE.429 | |
| $SiO_2$ | 46.36 | 44.21 | 48.23 | 45.83 | 46.21 | 46.43 | 45.96 | 49.81 | 49.45 | 48.33 | 47.71 | 47.12 | 47.09 | 51.92 | 48.67 | 49.69 | 45.53 | |
| $TiO_2$ | 2.76 | 3.54 | 2.18 | 2.83 | 2.45 | 2.12 | 2.54 | 1.40 | 1.41 | 1.83 | 1.95 | 2.16 | 2.25 | 0.59 | 1.50 | 1.23 | 2.86 | |
| $Al_2O_3$ | 6.06 | 8.73 | 5.26 | 8.39 | 7.72 | 6.55 | 6.25 | 4.57 | 5.25 | 6.11 | 6.27 | 8.45 | 8.30 | 2.55 | 6.12 | 5.80 | 8.44 | |
| $FeO_{(t)}$ | 7.36 | 7.16 | 6.59 | 7.06 | 6.85 | 6.33 | 7.39 | 5.44 | 5.07 | 5.36 | 6.04 | 6.02 | 6.50 | 8.04 | 5.19 | 5.92 | 6.74 | |
| *MnO* | 0.08 | 0.11 | 0.10 | 0.05 | 0.09 | 0.04 | 0.11 | 0.15 | 0.09 | 0.07 | 0.04 | 0.10 | 0.10 | 0.16 | 0.06 | 0.06 | 0.06 | |
| *MgO* | 12.82 | 11.77 | 13.50 | 12.40 | 12.57 | 13.59 | 12.75 | 14.64 | 14.14 | 13.66 | 13.67 | 12.67 | 12.92 | 14.16 | 14.35 | 14.55 | 12.25 | |
| *CaO* | 23.65 | 23.82 | 23.59 | 23.05 | 23.27 | 23.33 | 23.56 | 22.76 | 23.25 | 23.25 | 23.40 | 22.71 | 22.61 | 21.50 | 22.78 | 21.31 | 21.24 | |
| $Cr_2O_3$ | 0.08 | 0.35 | 0.15 | 0.28 | 0.34 | 0.74 | 0.07 | 0.56 | 0.79 | 0.87 | 0.45 | 0.21 | 0.01 | 0.00 | 0.94 | 0.20 | 0.46 | |
| $Na_2O$ | 0.16 | 0.53 | 0.53 | 0.50 | 0.38 | 0.58 | 0.50 | 0.74 | 0.74 | 0.50 | 0.67 | 0.56 | 0.64 | 0.94 | 0.79 | 0.59 | 0.61 | |
| $K_2O$ | 0.01 | 0.02 | 0.03 | 0.00 | 0.02 | 0.03 | 0.02 | 0.01 | 0.01 | 0.01 | 0.02 | 0.00 | 0.01 | 0.00 | 0.00 | 0.01 | 0.01 | |
| *Total* | 99.73 | 100.90 | 100.60 | 100.85 | 100.27 | 100.45 | 99.81 | 100.45 | 100.60 | 100.32 | 100.77 | 100.21 | 100.83 | 100.22 | 100.91 | 99.51 | 98.47 | |
| **Fórmula estrutural baseada em 6 oxigênios** | | | | | | | | | | | | | | | | | | |
| **Si** | 1.74 | 1.64 | 1.78 | 1.69 | 1.72 | 1.72 | 1.72 | 1.83 | 1.81 | 1.78 | 1.75 | 1.74 | 1.73 | 1.92 | 1.78 | 1.84 | 1.72 | |
| **$Al^{IV}$** | 0.26 | 0.36 | 0.22 | 0.31 | 0.28 | 0.28 | 0.28 | 0.17 | 0.19 | 0.22 | 0.25 | 0.26 | 0.27 | 0.08 | 0.22 | 0.16 | 0.28 | |
| **$Fe^{3+}$** | 0.00 | 0.00 | 0.00 | 0.00 | 0.00 | 0.00 | 0.00 | 0.00 | 0.00 | 0.00 | 0.00 | 0.00 | 0.00 | 0.00 | 0.00 | 0.00 | 0.00 | |
| ***Sitio T*** | 2.00 | 2.00 | 2.00 | 2.00 | 2.00 | 2.00 | 2.00 | 2.00 | 2.00 | 2.00 | 2.00 | 2.00 | 2.00 | 2.00 | 2.00 | 2.00 | 2.00 | |
| **$Al^{VI}$** | 0.01 | 0.03 | 0.01 | 0.06 | 0.05 | 0.00 | 0.00 | 0.03 | 0.04 | 0.05 | 0.03 | 0.11 | 0.09 | 0.03 | 0.04 | 0.09 | 0.10 | |
| **Ti** | 0.08 | 0.10 | 0.06 | 0.08 | 0.07 | 0.06 | 0.07 | 0.04 | 0.04 | 0.05 | 0.05 | 0.06 | 0.06 | 0.02 | 0.04 | 0.03 | 0.08 | |
| **$Fe^{3+}$** | 0.11 | 0.16 | 0.12 | 0.12 | 0.11 | 0.18 | 0.17 | 0.11 | 0.10 | 0.08 | 0.15 | 0.07 | 0.10 | 0.08 | 0.13 | 0.05 | 0.05 | |
| **$Fe^{2+}$** | 0.12 | 0.06 | 0.08 | 0.10 | 0.10 | 0.02 | 0.06 | 0.06 | 0.06 | 0.09 | 0.04 | 0.12 | 0.10 | 0.16 | 0.03 | 0.14 | 0.16 | |
| **Mn** | 0.00 | 0.00 | 0.00 | 0.00 | 0.00 | 0.00 | 0.00 | 0.00 | 0.00 | 0.00 | 0.00 | 0.00 | 0.00 | 0.01 | 0.00 | 0.00 | 0.00 | |
| **Mg** | 0.72 | 0.65 | 0.74 | 0.68 | 0.70 | 0.75 | 0.71 | 0.80 | 0.77 | 0.75 | 0.75 | 0.70 | 0.71 | 0.78 | 0.78 | 0.80 | 0.69 | |
| **Cr** | 0.00 | 0.01 | 0.00 | 0.01 | 0.01 | 0.02 | 0.00 | 0.02 | 0.02 | 0.03 | 0.01 | 0.01 | 0.00 | 0.00 | 0.03 | 0.01 | 0.01 | |
| ***Sitio O*** | 1.04 | 1.01 | 1.03 | 1.05 | 1.05 | 1.03 | 1.02 | 1.05 | 1.03 | 1.04 | 1.03 | 1.06 | 1.06 | 1.08 | 1.05 | 1.11 | 1.09 | |
| **Ca** | 0.95 | 0.95 | 0.93 | 0.91 | 0.93 | 0.93 | 0.95 | 0.89 | 0.91 | 0.92 | 0.92 | 0.90 | 0.89 | 0.85 | 0.89 | 0.84 | 0.86 | |
| **Na** | 0.01 | 0.04 | 0.04 | 0.04 | 0.03 | 0.04 | 0.04 | 0.05 | 0.05 | 0.04 | 0.05 | 0.04 | 0.05 | 0.07 | 0.06 | 0.04 | 0.04 | |
| **K** | 0.00 | 0.00 | 0.00 | 0.00 | 0.00 | 0.00 | 0.00 | 0.00 | 0.00 | 0.00 | 0.00 | 0.00 | 0.00 | 0.00 | 0.00 | 0.00 | 0.00 | |
| ***Sitio C*** | 0.96 | 0.99 | 0.97 | 0.95 | 0.95 | 0.97 | 0.98 | 0.95 | 0.97 | 0.96 | 0.97 | 0.94 | 0.94 | 0.92 | 0.95 | 0.89 | 0.91 | |
| ***Wo*** | **50.06** | **52.01** | **49.64** | **50.30** | **50.46** | **49.45** | **50.05** | **48.05** | **49.59** | **50.06** | **49.65** | **50.42** | **49.51** | **45.28** | **48.68** | **46.15** | **48.78** | |
| ***En*** | **37.77** | **35.78** | **39.54** | **37.66** | **37.94** | **40.08** | **37.69** | **42.99** | **41.98** | **40.92** | **40.35** | **39.14** | **39.38** | **41.51** | **42.66** | **43.84** | **39.14** | |
| ***Fs*** | **12.17** | **12.21** | **10.82** | **12.03** | **11.60** | **10.47** | **12.26** | **8.96** | **8.43** | **9.02** | **10.01** | **10.43** | **11.10** | **13.21** | **8.66** | **10.00** | **12.08** | |
| **mg#*** | **75.63** | **74.56** | **78.52** | **75.78** | **76.58** | **79.28** | **75.45** | **82.75** | **83.27** | **81.94** | **80.12** | **78.96** | **78.01** | **75.85** | **83.13** | **81.42** | **76.42** | |

*mg# =100*Mg/(Mg+Fetot)

**ANEXO:** Análises de microsonda de cristais e megacristais de clinopiroxênio da amostra BYA 123, lamprofiros de Rio Grande

| | ***Microfenocristais*** | | | | |
|---|---|---|---|---|---|
| | Cristais na matriz | | | | Inclusão |
| | **1** | **2** | **3** | **4** | **5** |
| *Amostra* | BYA123.1.CPXMZ. 391 | BYA123.2.CPXMZ. 397 | BYA123.2.CPXMZ ACIC.403 | BYA123.2.CPXMZ ACI.404 | BYA123.1.INCLIN CPXGRANDE.377 |
| $SiO_2$ | 48.09 | 40.91 | 44.14 | 46.86 | 45.26 |
| $TiO_2$ | 2.17 | 4.62 | 3.00 | 2.44 | 2.77 |
| $Al_2O_3$ | 5.38 | 10.10 | 9.69 | 5.50 | 8.24 |
| $FeO_{(t)}$ | 6.62 | 8.60 | 8.51 | 7.29 | 6.47 |
| *MnO* | 0.11 | 0.10 | 0.07 | 0.05 | 0.07 |
| *MgO* | 13.61 | 10.36 | 12.36 | 12.77 | 12.06 |
| *CaO* | 23.33 | 23.11 | 20.64 | 23.22 | 22.98 |
| $Cr_2O_3$ | 0.17 | 0.00 | 0.00 | 0.00 | 0.47 |
| $Na_2O$ | 0.41 | 0.35 | 0.68 | 0.51 | 0.53 |
| $K_2O$ | 0.02 | 0.04 | 0.47 | 0.03 | 0.02 |
| *Total* | 100.32 | 98.84 | 100.31 | 99.16 | 99.38 |
| **Fórmula estrutural baseada em 6 oxigênios** | | | | | |
| **Si** | 1.78 | 1.57 | 1.64 | 1.76 | 1.70 |
| **$Al^{IV}$** | 0.22 | 0.43 | 0.36 | 0.24 | 0.30 |
| **$Fe^{3+}$** | 0.00 | 0.00 | 0.00 | 0.00 | 0.00 |
| ***Sitio T*** | 2.00 | 2.00 | 2.00 | 2.00 | 2.00 |
| **$Al^{VI}$** | 0.02 | 0.02 | 0.07 | 0.01 | 0.06 |
| **Ti** | 0.06 | 0.13 | 0.08 | 0.07 | 0.08 |
| **$Fe^{3+}$** | 0.10 | 0.18 | 0.19 | 0.13 | 0.11 |
| **$Fe^{2+}$** | 0.10 | 0.10 | 0.07 | 0.10 | 0.10 |
| **Mn** | 0.00 | 0.00 | 0.00 | 0.00 | 0.00 |
| **Mg** | 0.75 | 0.59 | 0.69 | 0.72 | 0.67 |
| **Cr** | 0.00 | 0.00 | 0.00 | 0.00 | 0.01 |
| ***Sitio O*** | 1.04 | 1.02 | 1.11 | 1.02 | 1.04 |
| **Ca** | 0.93 | 0.95 | 0.82 | 0.94 | 0.92 |
| **Na** | 0.03 | 0.03 | 0.05 | 0.04 | 0.04 |
| **K** | 0.00 | 0.00 | 0.02 | 0.00 | 0.00 |
| ***Sitio C*** | 0.96 | 0.98 | 0.89 | 0.98 | 0.96 |
| ***Wo*** | 49.19 | 52.24 | 46.40 | 49.75 | 51.29 |
| ***En*** | 39.92 | 32.58 | 38.67 | 38.06 | 37.44 |
| ***Fs*** | 10.89 | 15.18 | 14.93 | 12.18 | 11.27 |
| **mg#*** | 78.57 | 68.22 | 72.14 | 75.75 | 76.87 |

*mg# =100*Mg/(Mg+Fetot)

**ANEXO:** Análises de microsonda de cristais e megacristais de clinopiroxênio da amostra BYA 124a, lamprofiros de Río Grande

| | ***Fenocristais*** | | | | | | | | | | | | | | | | | |
|---|---|---|---|---|---|---|---|---|---|---|---|---|---|---|---|---|---|---|
| | Bordas Externas | | | Bordas Internas | | | | | | Intermedios | | | Núcleos | | | | | |
| | **2** | **4** | **5** | **1** | **2** | **3** | **4** | **5** | **6** | **2** | **4** | **5** | **1** | **2** | **3** | **4** | **5** | |
| *Amostra* | BYA124A.9B. CPXRIMEXT.246 | BYA124A.9A. CPXRIMEXT.263 | BYA124A.5A. CPXRIMEXT.273 | BYA124A.10 .CPXRIM.220 | BYA124A.9B. CPXRIM.251 | BYA124A.9C .CPXRIM.254 | BYA124A.9A .CPXRIM.262 | BYA124A.5A. CPXRIM.274 | BYA124A.7. CPXRIM.271 | BYA124A.9B. CPXINTER.247 | BYA124A.9A.C PXINTER.261 | BYA124A.5A. CPXINTER.275 | BYA124A.10. CPXCORE.221 | BYA124A.9B. CPXCORE.249 | BYA124A.9C. CPXCORE.258 | BYA124A.9A. CPXCORE.259 | BYA124A.5. CPXCORE.276 | |
| $SiO_2$ | 46.73 | 46.95 | 51.47 | 43.63 | 51.33 | 47.53 | 46.71 | 46.90 | 40.80 | 50.78 | 51.83 | 52.21 | 48.64 | 51.88 | 51.77 | 51.25 | 52.75 | |
| $TiO_2$ | 2.15 | 2.75 | 0.70 | 4.11 | 0.49 | 2.46 | 2.51 | 2.68 | 4.33 | 0.59 | 0.84 | 0.34 | 2.28 | 0.65 | 0.55 | 0.94 | 0.41 | |
| $Al_2O_3$ | 6.78 | 5.46 | 4.61 | 9.06 | 4.33 | 5.18 | 6.22 | 5.39 | 10.66 | 5.04 | 4.46 | 4.32 | 6.06 | 4.59 | 4.25 | 4.08 | 4.24 | |
| $FeO_{(t)}$ | 6.46 | 6.64 | 5.36 | 7.41 | 5.65 | 6.69 | 6.58 | 6.67 | 8.62 | 5.51 | 7.21 | 5.47 | 6.35 | 5.53 | 5.73 | 7.30 | 5.34 | |
| *MnO* | 0.06 | 0.10 | 0.09 | 0.11 | 0.11 | 0.13 | 0.10 | 0.13 | 0.07 | 0.13 | 0.14 | 0.15 | 0.08 | 0.07 | 0.20 | 0.13 | 0.14 | |
| *MgO* | 12.70 | 13.13 | 16.44 | 11.24 | 17.20 | 13.40 | 12.98 | 12.75 | 10.20 | 16.84 | 14.09 | 17.02 | 13.63 | 17.29 | 17.58 | 13.99 | 17.33 | |
| *CaO* | 22.71 | 23.09 | 19.51 | 23.18 | 18.42 | 23.49 | 23.42 | 23.50 | 22.03 | 18.86 | 19.85 | 18.42 | 23.08 | 18.81 | 17.95 | 19.88 | 18.56 | |
| $Cr_2O_3$ | 0.25 | 0.02 | 0.35 | 0.02 | 0.35 | 0.02 | 0.00 | 0.00 | 0.02 | 0.37 | 0.21 | 0.52 | 0.04 | 0.29 | 0.25 | 0.11 | 0.49 | |
| $Na_2O$ | 0.85 | 0.62 | 0.76 | 0.52 | 0.96 | 0.36 | 0.36 | 0.30 | 0.69 | 0.94 | 1.83 | 0.90 | 0.34 | 1.05 | 0.77 | 1.49 | 0.78 | |
| $K_2O$ | 0.01 | 0.01 | 0.02 | 0.01 | 0.01 | 0.00 | 0.03 | 0.00 | 0.02 | 0.00 | 0.02 | 0.02 | 0.01 | 0.03 | 0.02 | 0.00 | 0.00 | |
| *Total* | 99.26 | 99.21 | 99.50 | 99.79 | 99.18 | 99.64 | 99.31 | 98.59 | 98.16 | 99.39 | 100.89 | 99.55 | 100.74 | 100.52 | 99.29 | 99.51 | 100.13 | |
| **Fórmula estrutural baseada em 6 oxigênios** | | | | | | | | | | | | | | | | | | |
| **Si** | 1.75 | 1.76 | 1.89 | 1.64 | 1.88 | 1.78 | 1.75 | 1.77 | 1.57 | 1.86 | 1.89 | 1.91 | 1.79 | 1.88 | 1.89 | 1.90 | 1.91 | |
| **Al $^{IV}$** | 0.25 | 0.24 | 0.11 | 0.36 | 0.12 | 0.22 | 0.25 | 0.23 | 0.43 | 0.14 | 0.11 | 0.09 | 0.21 | 0.12 | 0.11 | 0.10 | 0.09 | |
| **$Fe^{3+}$** | 0.00 | 0.00 | 0.00 | 0.00 | 0.00 | 0.00 | 0.00 | 0.00 | 0.00 | 0.00 | 0.00 | 0.00 | 0.00 | 0.00 | 0.00 | 0.00 | 0.00 | |
| ***Sitio T*** | 2.00 | 2.00 | 2.00 | 2.00 | 2.00 | 2.00 | 2.00 | 2.00 | 2.00 | 2.00 | 2.00 | 2.00 | 2.00 | 2.00 | 2.00 | 2.00 | 2.00 | |
| **Al $^{VI}$** | 0.05 | 0.00 | 0.08 | 0.04 | 0.07 | 0.00 | 0.03 | 0.01 | 0.05 | 0.08 | 0.08 | 0.09 | 0.05 | 0.07 | 0.08 | 0.07 | 0.09 | |
| **Ti** | 0.06 | 0.08 | 0.02 | 0.12 | 0.01 | 0.07 | 0.07 | 0.08 | 0.13 | 0.02 | 0.02 | 0.01 | 0.06 | 0.02 | 0.02 | 0.03 | 0.01 | |
| **$Fe^{3+}$** | 0.14 | 0.13 | 0.03 | 0.12 | 0.08 | 0.11 | 0.11 | 0.08 | 0.18 | 0.09 | 0.11 | 0.03 | 0.05 | 0.09 | 0.05 | 0.08 | 0.01 | |
| **$Fe^{2+}$** | 0.06 | 0.08 | 0.13 | 0.11 | 0.09 | 0.10 | 0.10 | 0.13 | 0.09 | 0.08 | 0.11 | 0.13 | 0.14 | 0.08 | 0.13 | 0.14 | 0.15 | |
| **Mn** | 0.00 | 0.00 | 0.00 | 0.00 | 0.00 | 0.00 | 0.00 | 0.00 | 0.00 | 0.00 | 0.00 | 0.00 | 0.00 | 0.00 | 0.01 | 0.00 | 0.00 | |
| **Mg** | 0.71 | 0.73 | 0.90 | 0.63 | 0.94 | 0.75 | 0.73 | 0.72 | 0.58 | 0.92 | 0.76 | 0.93 | 0.75 | 0.93 | 0.96 | 0.77 | 0.94 | |
| **Cr** | 0.01 | 0.00 | 0.01 | 0.00 | 0.01 | 0.00 | 0.00 | 0.00 | 0.00 | 0.01 | 0.01 | 0.02 | 0.00 | 0.01 | 0.01 | 0.00 | 0.01 | |
| ***Sitio O*** | 1.03 | 1.03 | 1.18 | 1.03 | 1.21 | 1.03 | 1.03 | 1.03 | 1.04 | 1.19 | 1.10 | 1.21 | 1.06 | 1.20 | 1.24 | 1.10 | 1.22 | |
| **Ca** | 0.91 | 0.93 | 0.77 | 0.93 | 0.72 | 0.94 | 0.94 | 0.95 | 0.91 | 0.74 | 0.77 | 0.72 | 0.91 | 0.73 | 0.70 | 0.79 | 0.72 | |
| **Na** | 0.06 | 0.05 | 0.05 | 0.04 | 0.07 | 0.03 | 0.03 | 0.02 | 0.05 | 0.07 | 0.13 | 0.06 | 0.02 | 0.07 | 0.05 | 0.11 | 0.05 | |
| **K** | 0.00 | 0.00 | 0.00 | 0.00 | 0.00 | 0.00 | 0.00 | 0.00 | 0.00 | 0.00 | 0.00 | 0.00 | 0.00 | 0.00 | 0.00 | 0.00 | 0.00 | |
| ***Sitio C*** | 0.97 | 0.97 | 0.82 | 0.97 | 0.79 | 0.97 | 0.97 | 0.97 | 0.96 | 0.81 | 0.90 | 0.79 | 0.94 | 0.80 | 0.76 | 0.90 | 0.78 | |
| ***Wo*** | 49.99 | 49.61 | 41.89 | 51.97 | 39.40 | 49.60 | 50.24 | 50.59 | 51.28 | 40.48 | 44.04 | 39.72 | 49.10 | 39.87 | 38.29 | 44.14 | 39.62 | |
| ***En*** | 38.91 | 39.25 | 49.13 | 35.07 | 51.17 | 39.38 | 38.74 | 38.20 | 33.05 | 50.29 | 43.48 | 51.07 | 40.36 | 50.99 | 52.17 | 43.21 | 51.49 | |
| ***Fs*** | 11.11 | 11.14 | 8.98 | 12.96 | 9.43 | 11.02 | 11.02 | 11.20 | 15.67 | 9.23 | 12.48 | 9.21 | 10.54 | 9.14 | 9.55 | 12.64 | 8.89 | |
| **mg#*** | 77.79 | 77.89 | 84.54 | 73.02 | 84.43 | 78.13 | 77.86 | 77.32 | 67.83 | 84.50 | 77.70 | 84.72 | 79.29 | 84.80 | 84.53 | 77.36 | 85.27 | |

*mg# =100*Mg/(Mg+Fetot)

**ANEXO:** Análises de microsonda de cristais e megacristais de clinopiroxênio da amostra BYA 124a, lamprofiros de Río Grande

| | ***Mesofenocristais*** | | | |
|---|---|---|---|---|
| | **1** | **2** | **3** | **4** |
| *Amostra* | BYA124A.1.CPX.201 | BYA124A.2.CPX.207 | BYA124A.4.CPX.231 | BYA124A.4.CPX.239 |
| $SiO_2$ | 50.83 | 46.12 | 51.40 | 49.39 |
| $TiO_2$ | 1.25 | 3.29 | 0.85 | 1.38 |
| $Al_2O_3$ | 6.16 | 7.48 | 5.69 | 7.22 |
| $FeO_{(t)}$ | 8.05 | 7.09 | 5.17 | 5.14 |
| *MnO* | 0.06 | 0.08 | 0.07 | 0.03 |
| *MgO* | 13.45 | 12.54 | 15.87 | 14.51 |
| *CaO* | 18.88 | 23.30 | 18.92 | 20.50 |
| $Cr_2O_3$ | 0.04 | 0.03 | 0.72 | 0.36 |
| $Na_2O$ | 1.51 | 0.58 | 0.94 | 1.14 |
| $K_2O$ | 0.01 | 0.02 | 0.02 | 0.00 |
| *Total* | 100.43 | 100.97 | 99.70 | 100.03 |
| **Fórmula estrutural baseada em 6 oxigênios** | | | | |
| **Si** | 1.86 | 1.70 | 1.88 | 1.81 |
| **$Al^{IV}$** | 0.14 | 0.30 | 0.12 | 0.19 |
| **$Fe^{3+}$** | 0.00 | 0.00 | 0.00 | 0.00 |
| ***Sitio T*** | 2.00 | 2.00 | 2.00 | 2.00 |
| **$Al^{VI}$** | 0.13 | 0.03 | 0.12 | 0.12 |
| **Ti** | 0.03 | 0.09 | 0.02 | 0.04 |
| **$Fe^{3+}$** | 0.04 | 0.12 | 0.00 | 0.07 |
| **$Fe^{2+}$** | 0.20 | 0.09 | 0.16 | 0.09 |
| **Mn** | 0.00 | 0.00 | 0.00 | 0.00 |
| **Mg** | 0.74 | 0.69 | 0.86 | 0.79 |
| **Cr** | 0.00 | 0.00 | 0.02 | 0.01 |
| ***Sitio O*** | 1.15 | 1.04 | 1.19 | 1.12 |
| **Ca** | 0.74 | 0.92 | 0.74 | 0.80 |
| **Na** | 0.11 | 0.04 | 0.07 | 0.08 |
| **K** | 0.00 | 0.00 | 0.00 | 0.00 |
| ***Sitio C*** | 0.85 | 0.96 | 0.81 | 0.88 |
| ***Wo*** | **43.03** | **50.34** | **42.00** | **45.87** |
| ***En*** | **42.65** | **37.71** | **49.05** | **45.16** |
| ***Fs*** | **14.32** | **11.95** | **8.96** | **8.97** |
| **mg#*** | **74.86** | **75.93** | **84.56** | **83.43** |

*mg# =100*Mg/(Mg+Fetot)

**ANEXO:** Análises de microsonda de cristais de clinopiroxênio da amostra BYA 127, lamprofiros de Río Grande

| | ***Microfenocristais*** | | | | | | | ***Ocellas*** | | | ***Matriz*** | | | | | | | |
|---|---|---|---|---|---|---|---|---|---|---|---|---|---|---|---|---|---|---|
| | Bordas | | | Intermedio | Núcleos | | | | | | | | | | | | | |
| | **1** | **2** | **3** | **1** | **1** | **2** | **3** | **4** | **5** | **6** | **7** | **8** | **9** | **10** | **11** | **12** | **13** | **14** |
| *Amostra* | BYA127.6A.CPXRIMMZ.552 | BYA127.6.CPXRIMMZ.569 | BYA127.4.CPXRIM.572 | BYA127.6A.CPXRIM.551 | BYA127.6A.CPXCOREMZ.550 | BYA127.6.CPXCOREMZ.568 | BYA127.4.CPXCORE.571 | BYA127.5I.CPXOCEL.466 | BYA127.5I.CPXOCEL.474 | BYA127.5I.CPXOCEL.475 | BYA127.4.CPXMICRO.589 | BYA127.5.CPXMZ.461 | BYA127.5.CPXMZ.480 | BYA127.3B.CPXMZ.487 | BYA127.6A.CPXMZ.549 | BYA127.6.CPXMZ.565 | BYA127.6.CPXMZ.566 | BYA127.6.CPXMZ.567 |
| $SiO_2$ | 45.38 | 46.03 | 47.44 | 43.49 | 44.55 | 45.73 | 46.38 | 52.05 | 53.34 | 52.17 | 46.15 | 46.36 | 40.28 | 46.66 | 46.41 | 45.74 | 46.26 | 42.39 |
| $TiO_2$ | 3.42 | 3.06 | 2.81 | 6.20 | 3.17 | 3.15 | 3.01 | 1.44 | 0.52 | 1.14 | 2.93 | 3.06 | 5.54 | 2.91 | 2.94 | 3.10 | 2.99 | 4.24 |
| $Al_2O_3$ | 6.73 | 5.75 | 5.56 | 6.14 | 6.63 | 5.82 | 5.85 | 2.06 | 0.85 | 1.25 | 5.66 | 5.66 | 10.00 | 5.65 | 5.51 | 5.70 | 5.53 | 8.36 |
| $FeO_{(t)}$ | 7.41 | 7.19 | 6.55 | 7.18 | 7.55 | 6.94 | 7.15 | 6.41 | 5.47 | 5.72 | 6.88 | 7.10 | 8.53 | 6.78 | 7.07 | 7.08 | 6.82 | 7.75 |
| *MnO* | 0.04 | 0.08 | 0.14 | 0.02 | 0.12 | 0.10 | 0.10 | 0.15 | 0.15 | 0.05 | 0.05 | 0.13 | 0.13 | 0.10 | 0.08 | 0.08 | 0.11 | 0.05 |
| *MgO* | 12.49 | 13.00 | 13.37 | 12.91 | 12.88 | 12.80 | 13.06 | 14.03 | 15.26 | 14.53 | 13.22 | 12.87 | 10.00 | 13.16 | 12.95 | 12.96 | 13.07 | 11.53 |
| *CaO* | 24.11 | 24.19 | 24.13 | 21.86 | 22.36 | 23.99 | 23.61 | 23.56 | 23.38 | 23.29 | 23.66 | 24.05 | 23.01 | 24.04 | 24.15 | 24.18 | 23.84 | 23.78 |
| $Cr_2O_3$ | 0.00 | 0.01 | 0.00 | 0.00 | 0.01 | 0.00 | 0.03 | 0.02 | 0.02 | 0.00 | 0.05 | 0.03 | 0.02 | 0.00 | 0.01 | 0.04 | 0.00 | 0.00 |
| $Na_2O$ | 0.23 | 0.50 | 0.26 | 0.47 | 0.38 | 0.23 | 0.26 | 0.67 | 0.52 | 0.76 | 0.44 | 0.45 | 0.84 | 0.46 | 0.44 | 0.28 | 0.44 | 0.29 |
| $K_2O$ | 0.01 | 0.04 | 0.01 | 0.26 | 0.05 | 0.01 | 0.02 | 0.01 | 0.03 | 0.03 | 0.04 | 0.01 | 0.05 | 0.04 | 0.01 | 0.02 | 0.00 | 0.04 |
| *Total* | 100.37 | 100.56 | 100.65 | 98.96 | 98.25 | 99.24 | 99.96 | 100.55 | 99.69 | 99.21 | 99.63 | 100.30 | 99.18 | 100.37 | 100.15 | 99.73 | 99.60 | 99.07 |
| **Fórmula estrutural baseada em 6 oxigênios** | | | | | | | | | | | | | | | | | | |
| **Si** | 1.70 | 1.71 | 1.76 | 1.65 | 1.70 | 1.72 | 1.73 | 1.92 | 1.97 | 1.94 | 1.73 | 1.73 | 1.54 | 1.73 | 1.73 | 1.72 | 1.73 | 1.61 |
| **Al $^{IV}$** | 0.30 | 0.25 | 0.24 | 0.27 | 0.30 | 0.26 | 0.26 | 0.08 | 0.03 | 0.05 | 0.25 | 0.25 | 0.45 | 0.25 | 0.24 | 0.25 | 0.24 | 0.37 |
| **$Fe^{3+}$** | 0.01 | 0.04 | 0.00 | 0.07 | 0.01 | 0.02 | 0.01 | 0.00 | 0.00 | 0.00 | 0.02 | 0.02 | 0.01 | 0.02 | 0.03 | 0.03 | 0.02 | 0.01 |
| ***Sitio T*** | 2.00 | 2.00 | 2.00 | 2.00 | 2.00 | 2.00 | 2.00 | 2.00 | 2.00 | 2.00 | 2.00 | 2.00 | 2.00 | 2.00 | 2.00 | 2.00 | 2.00 | 2.00 |
| **Al $^{VI}$** | 0.00 | 0.00 | 0.00 | 0.00 | 0.00 | 0.00 | 0.00 | 0.01 | 0.01 | 0.00 | 0.00 | 0.00 | 0.00 | 0.00 | 0.00 | 0.00 | 0.00 | 0.00 |
| **Ti** | 0.10 | 0.09 | 0.08 | 0.18 | 0.09 | 0.09 | 0.08 | 0.04 | 0.01 | 0.03 | 0.08 | 0.09 | 0.16 | 0.08 | 0.08 | 0.09 | 0.08 | 0.12 |
| **$Fe^{3+}$** | 0.13 | 0.15 | 0.11 | 0.04 | 0.15 | 0.11 | 0.11 | 0.04 | 0.03 | 0.05 | 0.14 | 0.13 | 0.21 | 0.14 | 0.13 | 0.13 | 0.13 | 0.17 |
| **$Fe^{2+}$** | 0.09 | 0.03 | 0.10 | 0.11 | 0.08 | 0.09 | 0.10 | 0.16 | 0.14 | 0.12 | 0.05 | 0.07 | 0.05 | 0.06 | 0.06 | 0.06 | 0.06 | 0.06 |
| **Mn** | 0.00 | 0.00 | 0.00 | 0.00 | 0.00 | 0.00 | 0.00 | 0.00 | 0.00 | 0.00 | 0.00 | 0.00 | 0.00 | 0.00 | 0.00 | 0.00 | 0.00 | 0.00 |
| **Mg** | 0.70 | 0.72 | 0.74 | 0.73 | 0.73 | 0.72 | 0.73 | 0.77 | 0.84 | 0.81 | 0.74 | 0.72 | 0.57 | 0.73 | 0.72 | 0.72 | 0.73 | 0.65 |
| **Cr** | 0.00 | 0.00 | 0.00 | 0.00 | 0.00 | 0.00 | 0.00 | 0.00 | 0.00 | 0.00 | 0.00 | 0.00 | 0.00 | 0.00 | 0.00 | 0.00 | 0.00 | 0.00 |
| ***Sitio O*** | 1.02 | 1.00 | 1.02 | 1.06 | 1.06 | 1.01 | 1.03 | 1.02 | 1.04 | 1.01 | 1.02 | 1.01 | 0.99 | 1.01 | 1.00 | 1.01 | 1.01 | 1.01 |
| **Ca** | 0.97 | 0.96 | 0.96 | 0.89 | 0.91 | 0.97 | 0.95 | 0.93 | 0.93 | 0.93 | 0.95 | 0.96 | 0.94 | 0.96 | 0.97 | 0.97 | 0.96 | 0.97 |
| **Na** | 0.02 | 0.04 | 0.02 | 0.03 | 0.03 | 0.02 | 0.02 | 0.05 | 0.04 | 0.06 | 0.03 | 0.03 | 0.06 | 0.03 | 0.03 | 0.02 | 0.03 | 0.02 |
| **K** | 0.00 | 0.00 | 0.00 | 0.01 | 0.00 | 0.00 | 0.00 | 0.00 | 0.00 | 0.00 | 0.00 | 0.00 | 0.00 | 0.00 | 0.00 | 0.00 | 0.00 | 0.00 |
| ***Sitio C*** | 0.98 | 1.00 | 0.98 | 0.94 | 0.94 | 0.99 | 0.97 | 0.98 | 0.96 | 0.99 | 0.98 | 0.99 | 1.01 | 0.99 | 1.00 | 0.99 | 0.99 | 0.99 |
| ***Wo*** | 50.99 | 50.51 | 50.44 | 48.12 | 48.43 | 50.81 | 49.86 | 49.00 | 47.82 | 48.56 | 49.89 | 50.63 | 52.79 | 50.46 | 50.65 | 50.65 | 50.36 | 51.83 |
| ***En*** | 36.77 | 37.78 | 38.87 | 39.55 | 38.81 | 37.73 | 38.37 | 40.60 | 43.44 | 42.14 | 38.79 | 37.71 | 31.94 | 38.43 | 37.78 | 37.77 | 38.40 | 34.98 |
| ***Fs*** | 12.23 | 11.71 | 10.69 | 12.33 | 12.76 | 11.47 | 11.78 | 10.41 | 8.74 | 9.30 | 11.32 | 11.66 | 15.27 | 11.11 | 11.57 | 11.58 | 11.24 | 13.19 |
| **mg#*** | 75.04 | 76.34 | 78.44 | 76.24 | 75.26 | 76.69 | 76.51 | 79.59 | 83.26 | 81.92 | 77.41 | 76.38 | 67.65 | 77.58 | 76.55 | 76.54 | 77.36 | 72.62 |

**ANEXO:** Análises de microsonda de cristais de clinopiroxênio da amostra BHU 131, lamprofiros de Río Grande

| | ***Mesofenocristais*** | | | | | | | | | | | | | |
|---|---|---|---|---|---|---|---|---|---|---|---|---|---|---|
| | Bordas | | | | | | Intermedios | | Núcleos | | | | | |
| | **1** | **2** | **3** | **4** | **5** | **6** | **4** | **5** | **1** | **2** | **3** | **4** | **5** | **6** |
| *Amostra* | BHU131.5A.CPX RIM.65 | BHU131.5A.CPX RIM.67 | BHU131.12.CPX RIM.74 | BHU131.12.CP XRIM.75 | BHU131.1.CPX MZRIM.105 | BHU131.9.CPX RIM.128 | BHU131.12.CPX INTER.76 | BHU131.1.CP XINTER.106 | BHU131.5A. CPXCORE.64 | BHU131.5A.CP XCORE.68 | BHU131.12.CP XCORE.73 | BHU131.12.C PXCORE.77 | BHU131.1.CP XCORE.108 | BHU131.9.CPX .127 |
| $SiO_2$ | 49.03 | 47.44 | 44.80 | 44.21 | 47.98 | 40.55 | 50.03 | 44.97 | 46.46 | 46.89 | 45.10 | 49.42 | 48.17 | 46.37 |
| $TiO_2$ | 1.71 | 2.60 | 3.60 | 4.43 | 2.78 | 5.51 | 1.86 | 3.49 | 2.96 | 2.67 | 3.44 | 1.75 | 2.73 | 3.20 |
| $Al_2O_3$ | 3.35 | 4.55 | 7.09 | 8.04 | 4.63 | 9.92 | 3.36 | 6.97 | 6.00 | 5.64 | 6.80 | 3.45 | 4.59 | 5.88 |
| $FeO_{(t)}$ | 5.43 | 6.71 | 7.43 | 7.48 | 6.79 | 8.46 | 5.56 | 7.14 | 6.33 | 6.12 | 6.87 | 5.91 | 6.81 | 6.50 |
| *MnO* | 0.12 | 0.14 | 0.11 | 0.03 | 0.08 | 0.09 | 0.11 | 0.10 | 0.07 | 0.08 | 0.08 | 0.07 | 0.10 | 0.09 |
| *MgO* | 14.25 | 13.34 | 12.21 | 11.98 | 13.42 | 10.51 | 14.41 | 12.08 | 12.78 | 12.93 | 12.42 | 14.36 | 13.76 | 12.98 |
| *CaO* | 23.36 | 23.70 | 23.46 | 23.39 | 23.91 | 22.75 | 23.59 | 23.35 | 23.15 | 23.40 | 22.79 | 22.94 | 23.63 | 23.10 |
| $Cr_2O_3$ | 0.39 | 0.00 | 0.02 | 0.34 | 0.01 | 0.02 | 0.47 | 0.18 | 0.63 | 0.60 | 0.17 | 0.24 | 0.13 | 0.39 |
| $Na_2O$ | 0.42 | 0.48 | 0.32 | 0.54 | 0.72 | 0.80 | 0.40 | 0.25 | 0.22 | 0.43 | 0.34 | 0.48 | 0.39 | 0.42 |
| $K_2O$ | 0.00 | 0.00 | 0.02 | 0.02 | 0.01 | 0.01 | 0.00 | 0.01 | 0.01 | 0.00 | 0.00 | 0.02 | 0.01 | 0.00 |
| *Total* | 98.37 | 99.45 | 99.51 | 100.99 | 100.90 | 99.37 | 100.02 | 98.88 | 98.84 | 99.06 | 98.31 | 98.95 | 100.72 | 99.26 |
| **Fórmula estrutural baseada em 6 oxigênios** | | | | | | | | | | | | | | |
| **Si** | 1.84 | 1.78 | 1.69 | 1.64 | 1.77 | 1.54 | 1.85 | 1.70 | 1.75 | 1.76 | 1.71 | 1.85 | 1.78 | 1.74 |
| **Al $^{IV}$** | 0.15 | 0.20 | 0.31 | 0.35 | 0.20 | 0.44 | 0.15 | 0.30 | 0.25 | 0.24 | 0.29 | 0.15 | 0.20 | 0.26 |
| **$Fe^{3+}$** | 0.01 | 0.02 | 0.00 | 0.00 | 0.03 | 0.01 | 0.00 | 0.00 | 0.00 | 0.00 | 0.00 | 0.00 | 0.02 | 0.00 |
| ***Sitio T*** | 2.00 | 2.00 | 2.00 | 2.00 | 2.00 | 2.00 | 2.00 | 2.00 | 2.00 | 2.00 | 2.00 | 2.00 | 2.00 | 2.00 |
| **Al $^{VI}$** | 0.00 | 0.00 | 0.00 | 0.00 | 0.00 | 0.00 | 0.00 | 0.02 | 0.02 | 0.01 | 0.02 | 0.00 | 0.00 | 0.00 |
| **Ti** | 0.05 | 0.07 | 0.10 | 0.12 | 0.08 | 0.16 | 0.05 | 0.10 | 0.08 | 0.08 | 0.10 | 0.05 | 0.08 | 0.09 |
| **$Fe^{3+}$** | 0.08 | 0.11 | 0.13 | 0.14 | 0.12 | 0.20 | 0.06 | 0.09 | 0.05 | 0.09 | 0.09 | 0.08 | 0.09 | 0.09 |
| **$Fe^{2+}$** | 0.09 | 0.08 | 0.10 | 0.09 | 0.06 | 0.05 | 0.11 | 0.13 | 0.15 | 0.11 | 0.13 | 0.10 | 0.10 | 0.11 |
| **Mn** | 0.00 | 0.00 | 0.00 | 0.00 | 0.00 | 0.00 | 0.00 | 0.00 | 0.00 | 0.00 | 0.00 | 0.00 | 0.00 | 0.00 |
| **Mg** | 0.80 | 0.75 | 0.69 | 0.66 | 0.74 | 0.60 | 0.80 | 0.68 | 0.72 | 0.72 | 0.70 | 0.80 | 0.76 | 0.73 |
| **Cr** | 0.01 | 0.00 | 0.00 | 0.01 | 0.00 | 0.00 | 0.01 | 0.01 | 0.02 | 0.02 | 0.01 | 0.01 | 0.00 | 0.01 |
| ***Sitio O*** | 1.03 | 1.01 | 1.03 | 1.03 | 1.00 | 1.01 | 1.04 | 1.03 | 1.05 | 1.03 | 1.05 | 1.05 | 1.03 | 1.04 |
| **Ca** | 0.94 | 0.95 | 0.95 | 0.93 | 0.95 | 0.93 | 0.94 | 0.95 | 0.94 | 0.94 | 0.93 | 0.92 | 0.94 | 0.93 |
| **Na** | 0.03 | 0.03 | 0.02 | 0.04 | 0.05 | 0.06 | 0.03 | 0.02 | 0.02 | 0.03 | 0.02 | 0.03 | 0.03 | 0.03 |
| **K** | 0.00 | 0.00 | 0.00 | 0.00 | 0.00 | 0.00 | 0.00 | 0.00 | 0.00 | 0.00 | 0.00 | 0.00 | 0.00 | 0.00 |
| ***Sitio C*** | 0.97 | 0.99 | 0.97 | 0.97 | 1.00 | 0.99 | 0.96 | 0.97 | 0.95 | 0.97 | 0.95 | 0.95 | 0.97 | 0.96 |
| ***Wo*** | 49.26 | 49.89 | 50.72 | 50.96 | 49.93 | 51.73 | 49.16 | 51.06 | 50.46 | 50.69 | 50.15 | 48.25 | 49.12 | 49.95 |
| ***En*** | 41.81 | 39.08 | 36.74 | 36.33 | 39.00 | 33.25 | 41.79 | 36.76 | 38.78 | 38.97 | 38.05 | 42.04 | 39.82 | 39.07 |
| ***Fs*** | 8.93 | 11.03 | 12.53 | 12.71 | 11.07 | 15.01 | 9.05 | 12.18 | 10.77 | 10.34 | 11.80 | 9.71 | 11.06 | 10.97 |
| **mg#*** | 82.39 | 77.99 | 74.57 | 74.08 | 77.90 | 68.90 | 82.20 | 75.11 | 78.27 | 79.03 | 76.33 | 81.24 | 78.27 | 78.07 |

*mg# =100*Mg/(Mg+Fetot)

**ANEXO:** Análises de microsonda de microcristais de clinopiroxênio da amostra BHU 131, lamprofiros de Río Grande.

| | *Matriz* | | | | | | *Glomerófiro* |
|---|---|---|---|---|---|---|---|
| | **5** | **6** | **7** | **8** | **9** | **10** | **11** |
| *Amostra* | BHU131.11.CPXMZ. 143 | BHU131.6.CPXMZ. 72 | BHU131.8.CPXMZ. 121 | BHU131.5A.CPX. 66 | BHU131.1.CPXMZ. 104 | BHU131.5A.CPXRIM. 69 | BHU131.4.CPXGLOME. 117 |
| $SiO_2$ | 45.36 | 49.04 | 47.94 | 46.80 | 45.30 | 44.21 | 47.62 |
| $TiO_2$ | 2.96 | 2.09 | 2.19 | 2.75 | 3.64 | 4.15 | 2.42 |
| $Al_2O_3$ | 6.24 | 4.17 | 3.98 | 4.59 | 7.22 | 7.48 | 5.03 |
| $FeO_{(t)}$ | 6.66 | 6.24 | 6.10 | 6.63 | 7.57 | 7.62 | 6.77 |
| *MnO* | 0.03 | 0.09 | 0.11 | 0.10 | 0.10 | 0.11 | 0.15 |
| *MgO* | 12.33 | 14.04 | 13.85 | 13.28 | 11.94 | 12.06 | 13.39 |
| *CaO* | 23.24 | 23.41 | 23.17 | 23.34 | 22.74 | 23.00 | 22.75 |
| $Cr_2O_3$ | 0.38 | 0.03 | 0.36 | 0.27 | 0.10 | 0.25 | 0.11 |
| $Na_2O$ | 0.42 | 0.31 | 0.20 | 0.51 | 0.30 | 0.62 | 0.49 |
| $K_2O$ | 0.00 | 0.01 | 0.00 | 0.01 | 0.00 | 0.03 | 0.05 |
| *Total* | 98.01 | 99.67 | 98.14 | 98.77 | 99.11 | 100.14 | 99.16 |
| **Fórmula estrutural baseada em 6 oxigênios** | | | | | | | |
| **Si** | 1.73 | 1.83 | 1.82 | 1.77 | 1.71 | 1.66 | 1.79 |
| **$Al^{IV}$** | 0.27 | 0.17 | 0.18 | 0.20 | 0.29 | 0.33 | 0.21 |
| **$Fe^{3+}$** | 0.00 | 0.00 | 0.01 | 0.03 | 0.00 | 0.01 | 0.00 |
| ***Sitio T*** | 2.00 | 2.00 | 2.00 | 2.00 | 2.00 | 2.00 | 2.00 |
| **$Al^{VI}$** | 0.01 | 0.01 | 0.00 | 0.00 | 0.03 | 0.00 | 0.01 |
| **Ti** | 0.08 | 0.06 | 0.06 | 0.08 | 0.10 | 0.12 | 0.07 |
| **$Fe^{3+}$** | 0.11 | 0.07 | 0.06 | 0.11 | 0.06 | 0.15 | 0.10 |
| **$Fe^{2+}$** | 0.10 | 0.12 | 0.12 | 0.07 | 0.18 | 0.08 | 0.11 |
| **Mn** | 0.00 | 0.00 | 0.00 | 0.00 | 0.00 | 0.00 | 0.00 |
| **Mg** | 0.70 | 0.78 | 0.78 | 0.75 | 0.67 | 0.67 | 0.75 |
| **Cr** | 0.01 | 0.00 | 0.01 | 0.01 | 0.00 | 0.01 | 0.00 |
| ***Sitio O*** | 1.02 | 1.04 | 1.05 | 1.02 | 1.06 | 1.03 | 1.05 |
| **Ca** | 0.95 | 0.93 | 0.94 | 0.94 | 0.92 | 0.92 | 0.91 |
| **Na** | 0.03 | 0.02 | 0.01 | 0.04 | 0.02 | 0.05 | 0.04 |
| **K** | 0.00 | 0.00 | 0.00 | 0.00 | 0.00 | 0.00 | 0.00 |
| ***Sitio C*** | 0.98 | 0.96 | 0.95 | 0.98 | 0.94 | 0.97 | 0.95 |
| ***Wo*** | 50.98 | 48.96 | 49.09 | 49.66 | 50.24 | 50.31 | 48.75 |
| ***En*** | 37.62 | 40.86 | 40.83 | 39.33 | 36.71 | 36.69 | 39.93 |
| ***Fs*** | 11.40 | 10.18 | 10.08 | 11.02 | 13.05 | 13.00 | 11.33 |
| **mg#*** | 76.75 | 80.05 | 80.20 | 78.12 | 73.77 | 73.83 | 77.90 |

*mg# =100*Mg/(Mg+Fetot)

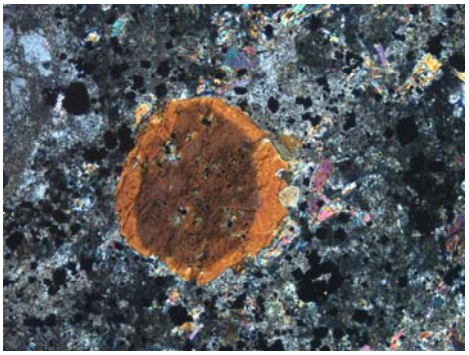

ANFIBÓLIO

Anexo : Análises de microsonda em anfibólios marrones e verdes da amostra P8, lamprofiros de Río Grande.

***ANFIBÓLIOS MARRONES***

| | Bordas | | | | | | | | Intermedios | | Núcleos | | | | | | | |
|---|---|---|---|---|---|---|---|---|---|---|---|---|---|---|---|---|---|---|
| | 1 | 2 | 3 | 4 | 5 | 6 | 7 | 9 | 5 | 7 | 1 | 2 | 3 | 4 | 5 | 6 | 7 | 9 |
| *Amostra* | P8A.13.AMPRIM.13 | P8A.6.AMPRIM.26 | P8A.12.AMPRIM.45 | P8C.6.AMPRIM.183 | P8D.3.AMPRIM.447 | P8G.1Y2.AMPRIM.705 | P8G.6.AMPCPXRIM.714 | P8G.7.AMPRIM.746 | P8D.3.AMPINTER.446 | P8G.6.AMPINTER.715 | P8A.13.AMPCORE.14 | P8A.6.AMPCORE.27 | P8A.12.AMPCORE.44 | P8C.6.AMPCORE.185 | P8D.3.AMPCore.448 | P8G.1Y2.AMPCORE.706 | P8G.6.AMPCORE.716 | P8G.8.AMPCORE.745 |
| $SiO_2$ | 41.22 | 40.30 | 40.40 | 41.42 | 46.80 | 40.34 | 40.42 | 39.92 | 47.59 | 39.81 | 40.75 | 40.99 | 40.97 | 43.76 | 40.92 | 40.52 | 40.18 | 40.61 |
| $TiO_2$ | 2.84 | 3.90 | 3.93 | 3.54 | 2.03 | 3.39 | 4.00 | 3.73 | 2.08 | 4.38 | 3.99 | 4.15 | 4.06 | 2.85 | 3.27 | 4.24 | 4.33 | 4.15 |
| $Al_2O_3$ | 12.07 | 13.16 | 12.64 | 13.18 | 7.29 | 12.33 | 12.83 | 12.92 | 7.97 | 13.56 | 12.62 | 12.45 | 12.81 | 11.17 | 12.61 | 12.49 | 12.96 | 12.13 |
| $Fe_2O_3$ | 1.33 | 0.06 | 0.26 | 0.45 | 1.52 | 0.45 | 0.00 | 0.64 | 1.86 | 0.20 | 0.47 | 0.82 | 0.31 | 1.02 | 1.86 | 0.81 | 0.23 | 0.54 |
| *FeO* | 8.84 | 10.38 | 10.15 | 10.07 | 9.22 | 10.24 | 9.69 | 9.77 | 8.62 | 8.48 | 11.74 | 12.61 | 11.43 | 9.79 | 10.22 | 12.19 | 11.89 | 12.66 |
| $Cr_2O_3$ | 0.00 | 0.03 | 0.00 | 0.00 | 0.16 | 0.05 | 0.03 | 0.00 | 0.11 | 0.14 | 0.07 | 0.00 | 0.00 | 0.14 | 0.06 | 0.00 | 0.00 | 0.00 |
| *MnO* | 0.17 | 0.14 | 0.08 | 0.10 | 0.15 | 0.13 | 0.04 | 0.10 | 0.14 | 0.02 | 0.13 | 0.17 | 0.17 | 0.19 | 0.14 | 0.14 | 0.12 | 0.13 |
| *MgO* | 14.57 | 13.41 | 13.20 | 13.65 | 15.28 | 13.46 | 13.85 | 13.63 | 15.90 | 14.20 | 12.19 | 11.67 | 12.34 | 13.91 | 13.05 | 12.06 | 11.81 | 11.68 |
| *CaO* | 11.90 | 11.99 | 11.42 | 11.86 | 9.00 | 11.65 | 11.81 | 11.94 | 8.99 | 11.75 | 10.64 | 10.58 | 11.16 | 10.47 | 10.62 | 10.72 | 10.73 | 10.26 |
| $Na_2O$ | 2.74 | 2.29 | 2.25 | 2.21 | 4.96 | 2.63 | 2.67 | 2.10 | 4.63 | 2.20 | 2.80 | 2.70 | 2.19 | 3.33 | 3.06 | 2.73 | 2.56 | 3.26 |
| $K_2O$ | 1.42 | 1.99 | 1.98 | 2.00 | 1.00 | 1.88 | 1.83 | 2.00 | 0.98 | 2.16 | 2.11 | 2.00 | 2.16 | 1.14 | 1.50 | 2.13 | 2.10 | 2.06 |
| *Total* | 97.08 | 97.65 | 96.32 | 98.50 | 97.41 | 96.54 | 97.16 | 96.75 | 98.87 | 96.90 | 97.50 | 98.15 | 97.59 | 97.75 | 97.31 | 98.03 | 96.90 | 97.48 |
| **Fórmula estrutural baseada em 23 oxigênios** | | | | | | | | | | | | | | | | | | |
| **Si** | 6.11 | 5.98 | 6.06 | 6.07 | 6.85 | 6.06 | 6.01 | 5.97 | 6.82 | 5.91 | 6.09 | 6.10 | 6.10 | 6.41 | 6.09 | 6.04 | 6.04 | 6.10 |
| **AlIV** | 1.89 | 2.02 | 1.94 | 1.93 | 1.15 | 1.94 | 1.99 | 2.03 | 1.18 | 2.09 | 1.91 | 1.90 | 1.90 | 1.59 | 1.91 | 1.96 | 1.96 | 1.90 |
| **Sum T** | **8.00** | **8.00** | **8.00** | **8.00** | **8.00** | **8.00** | **8.00** | **8.00** | **8.00** | **8.00** | **8.00** | **8.00** | **8.00** | **8.00** | **8.00** | **8.00** | **8.00** | **8.00** |
| **AlVI** | 0.22 | 0.28 | 0.30 | 0.34 | 0.11 | 0.24 | 0.26 | 0.25 | 0.17 | 0.28 | 0.31 | 0.29 | 0.34 | 0.33 | 0.30 | 0.24 | 0.34 | 0.25 |
| **Fe3+** | 0.15 | 0.01 | 0.03 | 0.05 | 0.17 | 0.05 | 0.00 | 0.07 | 0.20 | 0.02 | 0.05 | 0.09 | 0.03 | 0.11 | 0.21 | 0.09 | 0.03 | 0.06 |
| **Ti** | 0.32 | 0.44 | 0.44 | 0.39 | 0.22 | 0.38 | 0.45 | 0.42 | 0.22 | 0.49 | 0.45 | 0.46 | 0.45 | 0.31 | 0.37 | 0.48 | 0.49 | 0.47 |
| **Cr** | 0.00 | 0.00 | 0.00 | 0.00 | 0.02 | 0.01 | 0.00 | 0.00 | 0.01 | 0.02 | 0.01 | 0.00 | 0.00 | 0.02 | 0.01 | 0.00 | 0.00 | 0.00 |
| **Mg** | 3.22 | 2.97 | 2.95 | 2.98 | 3.33 | 3.01 | 3.07 | 3.04 | 3.40 | 3.14 | 2.72 | 2.59 | 2.74 | 3.03 | 2.89 | 2.68 | 2.65 | 2.62 |
| **Fe2+** | 1.09 | 1.29 | 1.27 | 1.23 | 1.13 | 1.29 | 1.20 | 1.21 | 0.99 | 1.05 | 1.47 | 1.57 | 1.42 | 1.19 | 1.23 | 1.51 | 1.50 | 1.59 |
| **Zn** | 0.00 | 0.00 | 0.00 | 0.00 | 0.00 | 0.00 | 0.00 | 0.00 | 0.00 | 0.00 | 0.00 | 0.00 | 0.00 | 0.00 | 0.00 | 0.00 | 0.00 | 0.00 |
| **Mn** | 0.00 | 0.02 | 0.00 | 0.00 | 0.02 | 0.02 | 0.00 | 0.00 | 0.00 | 0.00 | 0.00 | 0.00 | 0.01 | 0.00 | 0.00 | 0.00 | 0.01 | 0.01 |
| **Sum C** | **5.00** | **5.00** | **5.00** | **5.00** | **5.00** | **5.00** | **4.98** | **5.00** | **5.00** | **5.00** | **5.00** | **5.00** | **5.00** | **5.00** | **5.00** | **5.00** | **5.00** | **5.00** |
| **Mg** | 0.00 | 0.00 | 0.00 | 0.00 | 0.00 | 0.00 | 0.00 | 0.00 | 0.00 | 0.00 | 0.00 | 0.00 | 0.00 | 0.00 | 0.00 | 0.00 | 0.00 | 0.00 |
| **Fe2+** | 0.00 | 0.00 | 0.00 | 0.00 | 0.00 | 0.00 | 0.00 | 0.01 | 0.04 | 0.00 | 0.00 | 0.00 | 0.00 | 0.01 | 0.04 | 0.01 | 0.00 | 0.00 |
| **Zn** | 0.00 | 0.00 | 0.00 | 0.00 | 0.00 | 0.00 | 0.00 | 0.00 | 0.00 | 0.00 | 0.00 | 0.00 | 0.00 | 0.00 | 0.00 | 0.00 | 0.00 | 0.00 |
| **Mn** | 0.02 | 0.00 | 0.01 | 0.01 | 0.00 | 0.00 | 0.00 | 0.01 | 0.02 | 0.00 | 0.01 | 0.02 | 0.01 | 0.02 | 0.02 | 0.02 | 0.01 | 0.00 |
| **Ca** | 1.89 | 1.91 | 1.84 | 1.86 | 1.41 | 1.87 | 1.88 | 1.91 | 1.38 | 1.87 | 1.70 | 1.69 | 1.78 | 1.64 | 1.69 | 1.71 | 1.73 | 1.65 |
| **Na** | 0.09 | 0.09 | 0.16 | 0.12 | 0.59 | 0.13 | 0.12 | 0.06 | 0.56 | 0.12 | 0.28 | 0.29 | 0.21 | 0.33 | 0.25 | 0.26 | 0.26 | 0.35 |
| **Sum B** | **2.00** | **2.00** | **2.00** | **2.00** | **2.00** | **2.00** | **2.00** | **2.00** | **2.00** | **2.00** | **2.00** | **2.00** | **2.00** | **2.00** | **2.00** | **2.00** | **2.00** | **2.00** |
| **Na** | 0.70 | 0.57 | 0.50 | 0.50 | 0.82 | 0.64 | 0.65 | 0.54 | 0.73 | 0.51 | 0.53 | 0.49 | 0.42 | 0.62 | 0.63 | 0.53 | 0.48 | 0.60 |
| **K** | 0.27 | 0.38 | 0.38 | 0.37 | 0.19 | 0.36 | 0.35 | 0.38 | 0.18 | 0.41 | 0.40 | 0.38 | 0.41 | 0.21 | 0.29 | 0.41 | 0.40 | 0.39 |
| **Sum A** | **0.97** | **0.95** | **0.88** | **0.88** | **1.00** | **1.00** | **1.00** | **0.93** | **0.90** | **0.92** | **0.93** | **0.87** | **0.83** | **0.83** | **0.92** | **0.94** | **0.88** | **1.00** |
| | | | | | | | | | | | | | | | | | | |
| ***(Ca+Na)B*** | **1.98** | **2.00** | **1.99** | **1.99** | **2.00** | **2.00** | **2.00** | **1.98** | **1.94** | **1.99** | **1.99** | **1.97** | **1.99** | **1.97** | **1.94** | **1.97** | **1.99** | **2.00** |
| ***NaB*** | **0.09** | **0.09** | **0.16** | **0.12** | **0.59** | **0.13** | **0.12** | **0.06** | **0.56** | **0.12** | **0.28** | **0.29** | **0.21** | **0.33** | **0.25** | **0.26** | **0.26** | **0.35** |
| ***CaB*** | **1.89** | **1.91** | **1.84** | **1.86** | **1.41** | **1.87** | **1.88** | **1.91** | **1.38** | **1.87** | **1.70** | **1.69** | **1.78** | **1.64** | **1.69** | **1.71** | **1.73** | **1.65** |
| ***(Na+K)A*** | **0.97** | **0.95** | **0.88** | **0.88** | **1.00** | **1.00** | **1.00** | **0.93** | **0.90** | **0.92** | **0.93** | **0.87** | **0.83** | **0.83** | **0.92** | **0.94** | **0.88** | **1.00** |
| ***Si*** | **6.11** | **5.98** | **6.06** | **6.07** | **6.85** | **6.06** | **6.01** | **5.97** | **6.82** | **5.91** | **6.09** | **6.10** | **6.10** | **6.41** | **6.09** | **6.04** | **6.04** | **6.10** |
| ***Mg/(Mg+Fe2+)*** | **0.75** | **0.70** | **0.70** | **0.71** | **0.75** | **0.70** | **0.72** | **0.71** | **0.77** | **0.75** | **0.65** | **0.62** | **0.66** | **0.72** | **0.69** | **0.64** | **0.64** | **0.62** |

Anexo : Análises de microsonda em anfibólios verdes da amostra P8, lamprofiros de Río Grande.

| | ***ANFIBÓLIOS VERDES*** | | | | | | | ***Incl*** |
|---|---|---|---|---|---|---|---|---|
| | Bordas | | | Intermedios | Núcleos | | | |
| | 10 | 11 | 12 | 11 | 10 | 11 | 12 | 8 |
| *Amostra* | P8A.13.AMPRIM.16 | P8A.8D.AMPRIM.31 | P8A.12.AMPRIM.53 | P8A.8D.AMPINTER.32 | P8A.13.AMPCORE.15 | P8A.8D.AMPCORE.33 | P8A.12.AMPCORE.54 | P8G.8.INCAMP.732 |
| $SiO_2$ | 40.13 | 41.49 | 40.67 | 41.30 | 41.01 | 42.77 | 42.46 | 39.47 |
| $TiO_2$ | 3.96 | 3.46 | 3.50 | 1.22 | 1.24 | 1.40 | 1.70 | 3.79 |
| $Al_2O_3$ | 12.97 | 11.28 | 12.91 | 14.12 | 14.45 | 13.38 | 12.41 | 13.24 |
| $Fe_2O_3$ | 0.56 | 0.31 | 0.59 | 3.12 | 3.07 | 2.52 | 3.18 | 1.06 |
| *FeO* | 10.09 | 13.37 | 9.54 | 8.92 | 10.70 | 9.46 | 9.52 | 8.59 |
| $Cr_2O_3$ | 0.01 | 0.07 | 0.04 | 0.01 | 0.00 | 0.00 | 0.02 | 0.09 |
| *MnO* | 0.14 | 0.24 | 0.11 | 0.23 | 0.25 | 0.30 | 0.25 | 0.12 |
| *MgO* | 13.69 | 11.48 | 13.91 | 12.54 | 11.13 | 12.80 | 12.73 | 14.11 |
| *CaO* | 11.94 | 11.24 | 12.00 | 10.14 | 9.63 | 9.76 | 9.57 | 11.73 |
| $Na_2O$ | 2.50 | 3.13 | 2.60 | 3.74 | 4.02 | 3.98 | 4.29 | 2.30 |
| $K_2O$ | 1.90 | 1.86 | 1.99 | 1.29 | 1.06 | 1.33 | 0.96 | 2.01 |
| *Total* | 97.89 | 97.94 | 97.84 | 96.60 | 96.55 | 97.69 | 97.08 | 96.52 |
| **Fórmula estrutural baseada em 23 oxigênios** | | | | | | | | |
| **Si** | 5.95 | 6.22 | 6.01 | 6.15 | 6.14 | 6.28 | 6.29 | 5.90 |
| **AlIV** | 2.05 | 1.78 | 1.99 | 1.85 | 1.86 | 1.72 | 1.71 | 2.10 |
| **Sum T** | **8.00** | **8.00** | **8.00** | **8.00** | **8.00** | **8.00** | **8.00** | **8.00** |
| **AlVI** | 0.21 | 0.22 | 0.26 | 0.62 | 0.69 | 0.60 | 0.46 | 0.24 |
| **Fe3+** | 0.06 | 0.04 | 0.07 | 0.35 | 0.35 | 0.28 | 0.35 | 0.12 |
| **Ti** | 0.44 | 0.39 | 0.39 | 0.14 | 0.14 | 0.15 | 0.19 | 0.43 |
| **Cr** | 0.00 | 0.01 | 0.00 | 0.00 | 0.00 | 0.00 | 0.00 | 0.01 |
| **Mg** | 3.03 | 2.57 | 3.07 | 2.78 | 2.49 | 2.80 | 2.81 | 3.15 |
| **Fe2+** | 1.25 | 1.68 | 1.18 | 1.11 | 1.33 | 1.16 | 1.18 | 1.06 |
| **Zn** | 0.00 | 0.00 | 0.00 | 0.00 | 0.00 | 0.00 | 0.00 | 0.00 |
| **Mn** | 0.01 | 0.03 | 0.01 | 0.00 | 0.00 | 0.00 | 0.00 | 0.00 |
| **Sum C** | **5.00** | **4.93** | **4.98** | **5.00** | **5.00** | **5.00** | **5.00** | **5.00** |
| **Mg** | 0.00 | 0.00 | 0.00 | 0.00 | 0.00 | 0.00 | 0.00 | 0.00 |
| **Fe2+** | 0.00 | 0.00 | 0.00 | 0.00 | 0.01 | 0.00 | 0.00 | 0.02 |
| **Zn** | 0.00 | 0.00 | 0.00 | 0.00 | 0.00 | 0.00 | 0.00 | 0.00 |
| **Mn** | 0.01 | 0.00 | 0.00 | 0.03 | 0.03 | 0.04 | 0.03 | 0.02 |
| **Ca** | 1.90 | 1.81 | 1.90 | 1.62 | 1.54 | 1.54 | 1.52 | 1.88 |
| **Na** | 0.09 | 0.19 | 0.10 | 0.36 | 0.42 | 0.43 | 0.45 | 0.09 |
| **Sum B** | **2.00** | **2.00** | **2.00** | **2.00** | **2.00** | **2.00** | **2.00** | **2.00** |
| **Na** | 0.63 | 0.72 | 0.65 | 0.72 | 0.75 | 0.71 | 0.78 | 0.58 |
| **K** | 0.36 | 0.36 | 0.38 | 0.24 | 0.20 | 0.25 | 0.18 | 0.38 |
| **Sum A** | **0.99** | **1.07** | **1.02** | **0.97** | **0.95** | **0.96** | **0.96** | **0.96** |
| | | | | | | | | |
| ***(Ca+Na)B*** | **1.99** | **2.00** | **2.00** | **1.97** | **1.96** | **1.96** | **1.97** | **1.97** |
| ***NaB*** | **0.09** | **0.19** | **0.10** | **0.36** | **0.42** | **0.43** | **0.45** | **0.09** |
| ***CaB*** | **1.90** | **1.81** | **1.90** | **1.62** | **1.54** | **1.54** | **1.52** | **1.88** |
| ***(Na+K)A*** | **0.99** | **1.07** | **1.02** | **0.97** | **0.95** | **0.96** | **0.96** | **0.96** |
| ***Si*** | **5.95** | **6.22** | **6.01** | **6.15** | **6.14** | **6.28** | **6.29** | **5.90** |
| ***Mg/(Mg+Fe2+)*** | **0.71** | **0.60** | **0.72** | **0.71** | **0.65** | **0.71** | **0.70** | **0.75** |

ANEXO: Análises de microsonda em anfibólios (amostra P8) presentes em xenólitos, lamprofiros de Río Gran

| | P8C.9.CORONA.157 | P8C.11.AMP.197 | P8E.9.INCLBLUEXEN.336 | P8E.9.AMPXEN.337 | P8D.5.AMPBLUEXEN.339 | P8D.5.AMPCONSEC.340 | P8E.7.AMPGREEN.348 | P8E.7.AMPHRIM.349 | P8E.14.AMPCORE.353 | P8H.8.AMPGREEN.604 | P8H.5.AMPXEN.642 | P8H.6.AMPXEN.662 | P8H.6.AMPXEN.664 | P8G.1Y2.AMPCORE.701 | P8G.1Y2.AMPRIM.702 | P8G.8.AMPCORE.727 | P8G.8.AMPRIM.728 |
|---|---|---|---|---|---|---|---|---|---|---|---|---|---|---|---|---|---|
| $SiO_2$ | 41.85 | 41.33 | 44.01 | 41.42 | 40.88 | 40.98 | 41.51 | 41.37 | 42.44 | 42.22 | 43.53 | 44.24 | 44.82 | 41.43 | 41.01 | 41.15 | 40.84 |
| $TiO_2$ | 0.01 | 1.68 | 2.90 | 3.80 | 4.05 | 4.13 | 0.89 | 3.73 | 1.31 | 1.47 | 2.97 | 2.33 | 2.22 | 1.51 | 3.54 | 3.97 | 3.83 |
| $Al_2O_3$ | 19.61 | 17.95 | 10.19 | 12.81 | 12.24 | 12.34 | 15.17 | 12.43 | 14.71 | 12.65 | 11.57 | 10.11 | 9.18 | 13.83 | 12.79 | 11.93 | 13.07 |
| $Fe_2O_3$ | 4.35 | 1.58 | 1.17 | 0.00 | 0.41 | 0.00 | 3.35 | 0.00 | 2.15 | 2.58 | 0.19 | 2.04 | 2.74 | 1.67 | 1.13 | 1.23 | 0.22 |
| $FeO$ | 4.23 | 7.01 | 8.16 | 8.91 | 14.66 | 15.25 | 9.49 | 10.32 | 9.91 | 11.48 | 8.47 | 10.45 | 9.62 | 10.57 | 9.76 | 11.68 | 9.16 |
| $Cr_2O_3$ | 0.00 | 0.00 | 0.10 | 0.05 | 0.02 | 0.04 | 0.01 | 0.04 | 0.04 | 0.00 | 0.47 | 0.21 | 0.25 | 0.04 | 0.04 | 0.04 | 0.09 |
| $MnO$ | 0.09 | 0.09 | 0.10 | 0.11 | 0.21 | 0.13 | 0.22 | 0.11 | 0.34 | 0.23 | 0.10 | 0.20 | 0.15 | 0.20 | 0.11 | 0.14 | 0.11 |
| $MgO$ | 14.44 | 13.24 | 15.51 | 14.22 | 10.38 | 10.09 | 11.69 | 13.95 | 12.60 | 11.44 | 15.27 | 13.79 | 14.52 | 12.19 | 14.01 | 12.31 | 14.35 |
| $CaO$ | 10.54 | 10.98 | 10.64 | 11.41 | 10.43 | 10.39 | 9.86 | 12.43 | 10.42 | 9.34 | 11.39 | 10.10 | 10.01 | 10.55 | 11.75 | 10.40 | 11.84 |
| $Na_2O$ | 3.78 | 3.01 | 3.30 | 2.71 | 2.89 | 3.32 | 4.31 | 2.14 | 3.78 | 4.04 | 3.29 | 4.20 | 4.26 | 3.45 | 2.56 | 2.78 | 2.58 |
| $K_2O$ | 0.24 | 1.04 | 1.40 | 1.94 | 1.84 | 1.84 | 1.25 | 1.88 | 1.03 | 1.24 | 1.25 | 1.15 | 1.10 | 1.37 | 1.93 | 2.00 | 1.99 |
| *Total* | 99.13 | 97.89 | 97.46 | 97.37 | 98.01 | 98.51 | 97.73 | 98.40 | 98.72 | 96.70 | 98.51 | 98.82 | 98.86 | 96.80 | 98.64 | 97.63 | 98.05 |
| **Fórmula estrutural baseada em 23 oxigênios** | | | | | | | | | | | | | | | | | |
| **Si** | 5.89 | 5.95 | 6.43 | 6.10 | 6.14 | 6.14 | 6.12 | 6.08 | 6.17 | 6.33 | 6.30 | 6.46 | 6.53 | 6.18 | 6.02 | 6.14 | 6.00 |
| **AlIV** | 2.11 | 2.05 | 1.57 | 1.90 | 1.86 | 1.86 | 1.88 | 1.92 | 1.83 | 1.67 | 1.70 | 1.54 | 1.47 | 1.82 | 1.98 | 1.86 | 2.00 |
| **Sum T** | **8.00** | **8.00** | **8.00** | **8.00** | **8.00** | **8.00** | **8.00** | **8.00** | **8.00** | **8.00** | **8.00** | **8.00** | **8.00** | **8.00** | **8.00** | **8.00** | **8.00** |
| **AlVI** | 1.14 | 1.00 | 0.19 | 0.33 | 0.31 | 0.32 | 0.75 | 0.23 | 0.69 | 0.56 | 0.28 | 0.20 | 0.10 | 0.61 | 0.23 | 0.24 | 0.27 |
| **Fe3+** | 0.46 | 0.17 | 0.13 | 0.00 | 0.05 | 0.00 | 0.37 | 0.00 | 0.24 | 0.29 | 0.02 | 0.22 | 0.30 | 0.19 | 0.13 | 0.14 | 0.02 |
| **Ti** | 0.00 | 0.18 | 0.32 | 0.42 | 0.46 | 0.47 | 0.10 | 0.41 | 0.14 | 0.17 | 0.32 | 0.26 | 0.24 | 0.17 | 0.39 | 0.45 | 0.42 |
| **Cr** | 0.00 | 0.00 | 0.01 | 0.01 | 0.00 | 0.00 | 0.00 | 0.00 | 0.00 | 0.00 | 0.05 | 0.02 | 0.03 | 0.00 | 0.00 | 0.01 | 0.01 |
| **Mg** | 3.03 | 2.84 | 3.38 | 3.12 | 2.33 | 2.25 | 2.57 | 3.06 | 2.73 | 2.56 | 3.29 | 3.00 | 3.15 | 2.71 | 3.07 | 2.74 | 3.14 |
| **Fe2+** | 0.38 | 0.81 | 0.97 | 1.10 | 1.84 | 1.91 | 1.17 | 1.27 | 1.19 | 1.43 | 1.03 | 1.28 | 1.17 | 1.32 | 1.18 | 1.44 | 1.13 |
| **Zn** | 0.00 | 0.00 | 0.00 | 0.00 | 0.00 | 0.00 | 0.00 | 0.00 | 0.00 | 0.00 | 0.00 | 0.00 | 0.00 | 0.00 | 0.00 | 0.00 | 0.00 |
| **Mn** | 0.00 | 0.00 | 0.00 | 0.01 | 0.01 | 0.02 | 0.03 | 0.01 | 0.00 | 0.00 | 0.01 | 0.02 | 0.00 | 0.00 | 0.00 | 0.00 | 0.01 |
| **Sum C** | **5.00** | **5.00** | **5.00** | **4.99** | **5.00** | **4.97** | **4.99** | **4.99** | **5.00** | **5.00** | **5.00** | **5.00** | **5.00** | **5.00** | **5.00** | **5.00** | **5.00** |
| **Mg** | 0.00 | 0.00 | 0.00 | 0.00 | 0.00 | 0.00 | 0.00 | 0.00 | 0.00 | 0.00 | 0.00 | 0.00 | 0.00 | 0.00 | 0.00 | 0.00 | 0.00 |
| **Fe2+** | 0.12 | 0.04 | 0.02 | 0.00 | 0.00 | 0.00 | 0.00 | 0.00 | 0.01 | 0.01 | 0.00 | 0.00 | 0.00 | 0.00 | 0.01 | 0.02 | 0.00 |
| **Zn** | 0.00 | 0.00 | 0.00 | 0.00 | 0.00 | 0.00 | 0.00 | 0.00 | 0.00 | 0.00 | 0.00 | 0.00 | 0.00 | 0.00 | 0.00 | 0.00 | 0.00 |
| **Mn** | 0.01 | 0.01 | 0.01 | 0.00 | 0.01 | 0.00 | 0.00 | 0.00 | 0.04 | 0.03 | 0.01 | 0.01 | 0.01 | 0.02 | 0.01 | 0.02 | 0.01 |
| **Ca** | 1.59 | 1.69 | 1.67 | 1.80 | 1.68 | 1.67 | 1.56 | 1.96 | 1.62 | 1.50 | 1.77 | 1.58 | 1.56 | 1.69 | 1.85 | 1.66 | 1.86 |
| **Na** | 0.28 | 0.26 | 0.30 | 0.20 | 0.31 | 0.33 | 0.44 | 0.04 | 0.32 | 0.46 | 0.23 | 0.41 | 0.42 | 0.29 | 0.12 | 0.30 | 0.13 |
| **Sum B** | **2.00** | **2.00** | **2.00** | **2.00** | **2.00** | **2.00** | **2.00** | **2.00** | **2.00** | **2.00** | **2.00** | **2.00** | **2.00** | **2.00** | **2.00** | **2.00** | **2.00** |
| **Na** | 0.75 | 0.58 | 0.64 | 0.57 | 0.53 | 0.63 | 0.79 | 0.57 | 0.74 | 0.71 | 0.70 | 0.78 | 0.78 | 0.71 | 0.60 | 0.51 | 0.61 |
| **K** | 0.04 | 0.19 | 0.26 | 0.36 | 0.35 | 0.35 | 0.23 | 0.35 | 0.19 | 0.24 | 0.23 | 0.21 | 0.20 | 0.26 | 0.36 | 0.38 | 0.37 |
| **Sum A** | **0.79** | **0.77** | **0.90** | **0.94** | **0.89** | **0.99** | **1.02** | **0.92** | **0.93** | **0.95** | **0.93** | **0.99** | **0.98** | **0.97** | **0.97** | **0.89** | **0.98** |
| | | | | | | | | | | | | | | | | | |
| ***(Ca+Na)B*** | **1.87** | **1.95** | **1.96** | **2.00** | **1.99** | **2.00** | **2.00** | **2.00** | **1.95** | **1.96** | **1.99** | **1.99** | **1.99** | **1.98** | **1.97** | **1.96** | **1.99** |
| ***NaB*** | **0.28** | **0.26** | **0.30** | **0.20** | **0.31** | **0.33** | **0.44** | **0.04** | **0.32** | **0.46** | **0.23** | **0.41** | **0.42** | **0.29** | **0.12** | **0.30** | **0.13** |
| ***CaB*** | **1.59** | **1.69** | **1.67** | **1.80** | **1.68** | **1.67** | **1.56** | **1.96** | **1.62** | **1.50** | **1.77** | **1.58** | **1.56** | **1.69** | **1.85** | **1.66** | **1.86** |
| ***(Na+K)A*** | **0.79** | **0.77** | **0.90** | **0.94** | **0.89** | **0.99** | **1.02** | **0.92** | **0.93** | **0.95** | **0.93** | **0.99** | **0.98** | **0.97** | **0.97** | **0.89** | **0.98** |
| ***Si*** | **5.89** | **5.95** | **6.43** | **6.10** | **6.14** | **6.14** | **6.12** | **6.08** | **6.17** | **6.33** | **6.30** | **6.46** | **6.53** | **6.18** | **6.02** | **6.14** | **6.00** |
| ***Mg/(Mg+Fe2+)*** | **0.86** | **0.77** | **0.77** | **0.74** | **0.56** | **0.54** | **0.69** | **0.71** | **0.69** | **0.64** | **0.76** | **0.70** | **0.73** | **0.67** | **0.72** | **0.65** | **0.74** |

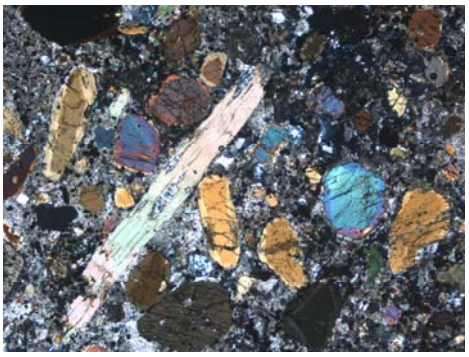

BIOTITA

**ANEXO:** Análises de microsonda de cristais de biotita da amostra P8, lamprofiros de Río Grande

| | ***Cristais*** | | | | | | | | | |
|---|---|---|---|---|---|---|---|---|---|---|
| | Bordas | | | | Intermedio | | Núcleos | | | |
| | **1** | **2** | **3** | **4** | **3** | **4** | **1** | **2** | **3** | **4** |
| *Amostra* | P8A.2.RIM.A | P8G.BTRIM.723 | P8G.8.BTRIM.724 | P8G.8.BTRIM.729 | P8G.8.BTINTER.72 5 | P8G.8.BTINTER.730 | P8A.2.BTCORE.B | P8G.BTCORE.722 | P8G.8.BTCORE.726 | P8G.8.BTCORE.731 |
| $SiO_2$ | 37.61 | 37.39 | 35.80 | 41.94 | 36.17 | 39.97 | 36.57 | 36.69 | 36.10 | 40.15 |
| $TiO_2$ | 3.24 | 3.60 | 6.06 | 1.89 | 6.29 | 2.17 | 5.23 | 3.71 | 6.16 | 2.02 |
| $Al_2O_3$ | 14.99 | 15.03 | 15.24 | 12.64 | 15.27 | 12.49 | 14.83 | 14.56 | 15.31 | 12.29 |
| *FeO* | 7.06 | 7.20 | 13.62 | 10.69 | 13.82 | 11.08 | 13.21 | 13.29 | 13.78 | 11.16 |
| $Fe_2O_3$ | 0.00 | 0.00 | 0.00 | 0.00 | 0.00 | 0.00 | 0.00 | 0.00 | 0.00 | 0.00 |
| $Cr_2O_3$ | 0.00 | 0.00 | 0.00 | 0.00 | 0.00 | 0.00 | 0.00 | 0.00 | 0.00 | 0.00 |
| *MnO* | 0.22 | 0.23 | 0.10 | 0.10 | 0.11 | 0.13 | 0.04 | 0.17 | 0.10 | 0.10 |
| *MgO* | 20.67 | 21.36 | 14.62 | 19.19 | 14.30 | 20.32 | 15.29 | 15.97 | 14.71 | 20.12 |
| *CaO* | 0.04 | 0.03 | 0.00 | 0.07 | 0.01 | 0.04 | 0.03 | 0.02 | 0.03 | 0.02 |
| $Na_2O$ | 0.40 | 0.78 | 0.60 | 1.01 | 0.72 | 1.26 | 0.82 | 1.84 | 0.60 | 1.32 |
| $K_2O$ | 9.12 | 9.09 | 9.16 | 7.68 | 9.19 | 8.24 | 9.23 | 7.98 | 9.24 | 8.28 |
| *BaO* | 1.14 | 1.02 | 0.00 | 0.00 | 0.00 | 0.00 | 0.28 | 0.27 | 0.16 | 0.00 |
| *Cl* | 0.00 | 0.01 | 0.02 | 0.01 | 0.02 | 0.02 | 0.03 | 0.03 | 0.02 | 0.02 |
| $H_2O$ | 4.09 | 4.13 | 4.00 | 4.15 | 4.03 | 4.11 | 4.01 | | 4.04 | 4.10 |
| *Total* | 98.57 | 99.87 | 99.23 | 99.36 | 99.92 | 99.83 | 99.57 | 94.53 | 100.26 | 99.55 |
| **Fórmula estrutural baseada em 22 oxigênios** | | | | | | | | | | |
| **Si** | 5.51 | 5.42 | 5.34 | 6.04 | 5.36 | 5.80 | 5.44 | 5.50 | 5.34 | 5.85 |
| **$Al^{IV}$** | 2.49 | 2.57 | 2.66 | 1.96 | 2.64 | 2.14 | 2.56 | 2.50 | 2.66 | 2.11 |
| **$Fe^{+3}$** | 0.00 | 0.01 | 0.00 | 0.00 | 0.00 | 0.06 | 0.00 | 0.00 | 0.00 | 0.04 |
| **Sum T** | **8.00** | **8.00** | **8.00** | **8.00** | **8.00** | **8.00** | **8.00** | **8.00** | **8.00** | **8.00** |
| **$Al^{VI}$** | 0.10 | 0.00 | 0.03 | 0.19 | 0.03 | 0.00 | 0.04 | 0.07 | 0.01 | 0.00 |
| **$Fe^{+2}_t$** | 0.86 | 0.86 | 1.70 | 1.29 | 1.71 | 1.29 | 1.64 | 1.67 | 1.71 | 1.32 |
| **$Fe^{+3}$** | 4.51 | 4.61 | 3.25 | 4.12 | 3.16 | 4.40 | 3.39 | 3.57 | 3.25 | 4.37 |
| **Ti** | 0.03 | 0.03 | 0.01 | 0.01 | 0.01 | 0.02 | 0.01 | 0.02 | 0.01 | 0.01 |
| **Mg** | 0.36 | 0.39 | 0.68 | 0.20 | 0.70 | 0.24 | 0.59 | 0.42 | 0.69 | 0.22 |
| **Mn** | 0.00 | 0.00 | 0.00 | 0.00 | 0.00 | 0.00 | 0.00 | 0.00 | 0.00 | 0.00 |
| **Sum O** | **5.86** | **5.89** | **5.67** | **5.82** | **5.62** | **5.94** | **5.66** | **5.74** | **5.66** | **5.92** |
| **Ca** | 0.01 | 0.00 | 0.00 | 0.01 | 0.00 | 0.01 | 0.00 | 0.00 | 0.00 | 0.00 |
| **Na** | 0.11 | 0.22 | 0.17 | 0.28 | 0.21 | 0.36 | 0.24 | 0.53 | 0.17 | 0.37 |
| **K** | 0.85 | 0.84 | 0.87 | 0.71 | 0.87 | 0.76 | 0.88 | 0.76 | 0.87 | 0.77 |
| **Ba** | 0.13 | 0.12 | 0.00 | 0.00 | 0.00 | 0.00 | 0.03 | 0.03 | 0.02 | 0.00 |
| **Sum A** | **1.10** | **1.18** | **1.05** | **1.00** | **1.08** | **1.12** | **1.15** | **1.33** | **1.07** | **1.14** |
| ***Cations*** | **14.96** | **15.07** | **14.72** | **14.82** | **14.70** | **15.06** | **14.81** | **15.08** | **14.73** | **15.06** |
| ***$Mg/(Mg+Fe^{+2})$*** | 0.84 | 0.84 | 0.66 | 0.76 | 0.65 | 0.77 | 0.67 | 0.68 | 0.66 | 0.77 |
| ***$Fe^{+2}/(Fe^{+2}+Mg)$*** | 0.16 | 0.16 | 0.34 | 0.24 | 0.35 | 0.23 | 0.33 | 0.32 | 0.34 | 0.23 |

*Obs: $H_2O$ recalculated by stequiometrie. $Fe_2O_3$ only recalculated for samples with deficiency in tetraedric site.*

**ANEXO:** Análises de microsonda de cristais de biotita da amostra P8, lamprofiros de Río Grande

| | Mesofenocristais | | | | | | | Matriz | | Inclusões | | | Borda de anfibólio |
|---|---|---|---|---|---|---|---|---|---|---|---|---|---|
| | **1** | **2** | **3** | **4** | **5** | **6** | **7** | **8** | **9** | **10** | **11** | **12** | **13** |
| *Amostra* | P8G.8.BTCORE.733 | P8A.2.MZBTC | P8A.5.BTMZ.E | P8A.13.BT.23 | P8A.12.BT.47 | P8E.1A.BT.301 | P8G.1Y2.BTCORE.708 | P8H.10.BT.689 | P8H.1.BT.621 | P8E.10.BTMZ.364 | P8A.8D.INCLUSIONBT.34 | P8D.BTINCAMP.442 | P8H.10.BTRIM.685 |
| $SiO_2$ | 36.23 | 38.24 | 37.47 | 39.27 | 40.81 | 39.83 | 40.10 | 38.79 | 37.88 | 36.47 | 40.77 | 38.89 | 37.41 |
| $TiO_2$ | 6.10 | 2.87 | 3.19 | 2.68 | 1.43 | 2.59 | 1.35 | 2.51 | 2.42 | 3.42 | 1.33 | 3.13 | 3.16 |
| $Al_2O_3$ | 15.28 | 14.06 | 14.30 | 14.76 | 11.96 | 12.91 | 12.54 | 14.44 | 14.15 | 15.05 | 14.23 | 14.16 | 14.86 |
| $FeO$ | 13.48 | 7.29 | 7.42 | 6.61 | 5.61 | 10.14 | 7.82 | 6.83 | 7.03 | 10.65 | 11.84 | 11.90 | 7.16 |
| $Fe_2O_3$ | 0.00 | 0.00 | 0.00 | 0.00 | 0.00 | 0.00 | 0.00 | 0.00 | 0.00 | 0.00 | 0.00 | 0.00 | 0.00 |
| $Cr_2O_3$ | 0.00 | 0.00 | 0.00 | 0.00 | 0.00 | 0.00 | 0.00 | 0.00 | 0.00 | 0.00 | 0.00 | 0.00 | 0.00 |
| $MnO$ | 0.03 | 0.17 | 0.15 | 0.19 | 0.21 | 0.08 | 0.12 | 0.21 | 0.16 | 0.15 | 0.23 | 0.12 | 0.16 |
| $MgO$ | 14.98 | 21.12 | 20.80 | 21.21 | 24.21 | 20.32 | 22.10 | 22.56 | 22.44 | 20.26 | 13.02 | 18.85 | 20.97 |
| $CaO$ | 0.01 | 0.08 | 0.04 | 0.11 | 0.11 | 0.09 | 0.04 | 0.10 | 0.10 | 0.12 | 10.15 | 0.01 | 0.07 |
| $Na_2O$ | 0.65 | 0.61 | 0.68 | 0.89 | 1.25 | 0.95 | 1.12 | 0.91 | 0.40 | 0.13 | 2.88 | 1.36 | 0.74 |
| $K_2O$ | 9.16 | 9.37 | 9.26 | 9.04 | 8.58 | 8.45 | 8.83 | 9.00 | 9.10 | 9.01 | 2.12 | 8.31 | 8.92 |
| $BaO$ | 0.00 | 1.17 | 1.03 | 0.74 | 0.24 | 0.47 | 0.22 | 0.49 | 0.41 | 0.78 | 0.00 | 0.00 | 1.57 |
| $Cl$ | 0.03 | 0.00 | 0.01 | 0.00 | 0.00 | 0.04 | 0.03 | 0.01 | 0.01 | 0.02 | 0.00 | 0.02 | 0.00 |
| $H_2O$ | 4.04 | 4.09 | 4.05 | 4.16 | 4.15 | 4.11 | 4.09 | 4.17 | 4.09 | 4.08 | 4.17 | 4.13 | 4.09 |
| *Total* | 99.98 | 99.07 | 98.37 | 99.67 | 98.55 | 99.99 | 98.36 | 100.03 | 98.19 | 100.14 | 100.74 | 100.89 | 99.11 |
| **Fórmula estrutural baseada em 22 oxigênios** | | | | | | | | | | | | | |
| **Si** | 5.36 | 5.59 | 5.52 | 5.65 | 5.88 | 5.77 | 5.85 | 5.57 | 5.54 | 5.34 | 5.85 | 5.62 | 5.48 |
| **$Al^{IV}$** | 2.64 | 2.41 | 2.48 | 2.35 | 2.03 | 2.20 | 2.15 | 2.43 | 2.44 | 2.60 | 2.15 | 2.38 | 2.52 |
| **$Fe^{+3}$** | 0.00 | 0.00 | 0.00 | 0.00 | 0.09 | 0.03 | 0.00 | 0.00 | 0.02 | 0.06 | 0.00 | 0.00 | 0.00 |
| **Sum T** | **8.00** | **8.00** | **8.00** | **8.00** | **8.00** | **8.00** | **8.00** | **8.00** | **8.00** | **8.00** | **8.00** | **8.00** | **8.00** |
| **$Al^{VI}$** | 0.02 | 0.01 | 0.00 | 0.15 | 0.00 | 0.00 | 0.00 | 0.01 | 0.00 | 0.00 | 0.26 | 0.03 | 0.04 |
| **$Fe^{+2}_t$** | 1.67 | 0.89 | 0.91 | 0.79 | 0.58 | 1.20 | 0.95 | 0.82 | 0.84 | 1.24 | 1.42 | 1.44 | 0.88 |
| **$Fe^{+3}$** | 3.30 | 4.60 | 4.57 | 4.55 | 5.20 | 4.39 | 4.81 | 4.83 | 4.90 | 4.42 | 2.79 | 4.06 | 4.57 |
| **Ti** | 0.00 | 0.02 | 0.02 | 0.02 | 0.03 | 0.01 | 0.01 | 0.03 | 0.02 | 0.02 | 0.03 | 0.01 | 0.02 |
| **Mg** | 0.68 | 0.32 | 0.35 | 0.29 | 0.15 | 0.28 | 0.15 | 0.27 | 0.27 | 0.38 | 0.14 | 0.34 | 0.35 |
| **Mn** | 0.00 | 0.00 | 0.00 | 0.00 | 0.00 | 0.00 | 0.00 | 0.00 | 0.00 | 0.00 | 0.00 | 0.00 | 0.00 |
| **Sum O** | **5.67** | **5.84** | **5.85** | **5.80** | **5.96** | **5.88** | **5.92** | **5.95** | **6.02** | **6.06** | **4.64** | **5.88** | **5.86** |
| **Ca** | 0.00 | 0.01 | 0.01 | 0.02 | 0.02 | 0.01 | 0.01 | 0.01 | 0.02 | 0.02 | 1.56 | 0.00 | 0.01 |
| **Na** | 0.19 | 0.17 | 0.19 | 0.25 | 0.35 | 0.27 | 0.32 | 0.25 | 0.11 | 0.04 | 0.80 | 0.38 | 0.21 |
| **K** | 0.86 | 0.87 | 0.87 | 0.83 | 0.79 | 0.78 | 0.82 | 0.82 | 0.85 | 0.84 | 0.19 | 0.77 | 0.83 |
| **Ba** | 0.00 | 0.13 | 0.12 | 0.08 | 0.03 | 0.05 | 0.02 | 0.05 | 0.05 | 0.09 | 0.00 | 0.00 | 0.18 |
| **Sum A** | **1.05** | **1.19** | **1.19** | **1.18** | **1.18** | **1.12** | **1.17** | **1.15** | **1.03** | **0.99** | **2.56** | **1.15** | **1.23** |
| ***Cations*** | **14.72** | **15.04** | **15.04** | **14.98** | **15.14** | **15.00** | **15.09** | **15.10** | **15.05** | **15.05** | **15.20** | **15.03** | **15.09** |
| ***Mg/(Mg+$Fe^{+2}$)*** | 0.66 | 0.84 | 0.83 | 0.85 | 0.90 | 0.78 | 0.83 | 0.85 | 0.85 | 0.78 | 0.66 | 0.74 | 0.84 |
| ***$Fe^{+2}$/($Fe^{+2}$+Mg)*** | 0.34 | 0.16 | 0.17 | 0.15 | 0.10 | 0.22 | 0.17 | 0.15 | 0.15 | 0.22 | 0.34 | 0.26 | 0.16 |

*Obs: $H_2O$ recalculated by stequiometrie. $Fe_2O_3$ only recalculated for samples with deficiency in tetraedric site.*

**ANEXO:** Análises de microsonda de cristais de biotita em ocelli e segregados (amostra BHU 131), lamprofiros de Río Grande

| | em ocelli | | | | | | em segregados | | Matriz |
|---|---|---|---|---|---|---|---|---|---|
| | **1** | **2** | **3** | **4** | **5** | **6** | **7** | **8** | **9** |
| *Amostra* | BHU131.3.BTANAL.61 | BHU131.3.BTANAL.62 | BHU131.12.BTCOREOCELLUS.80 | BHU131.12.BTRIMOCELLUS.81 | BHU131.1.BTOCELLA.93 | BHU131.11.BTTG.140 | BHU131.1.BTMZCLARA.96 | BHU131.11.BTMZRICAEN.149 | BHU131.6.BT.71 |
| $SiO_2$ | 34.35 | 34.01 | 34.25 | 35.49 | 34.29 | 33.78 | 34.74 | 34.25 | 34.93 |
| $TiO_2$ | 7.21 | 7.43 | 7.88 | 6.82 | 7.71 | 7.56 | 6.04 | 7.85 | 6.83 |
| $Al_2O_3$ | 15.18 | 15.58 | 15.51 | 14.79 | 15.35 | 15.37 | 15.80 | 15.33 | 15.61 |
| $FeO$ | 13.54 | 13.62 | 12.10 | 12.38 | 15.29 | 11.77 | 13.42 | 13.23 | 14.56 |
| $Fe_2O_3$ | 0.00 | 0.00 | 0.00 | 0.00 | 0.00 | 0.00 | 0.00 | 0.00 | 0.00 |
| $Cr_2O_3$ | 0.00 | 0.00 | 0.00 | 0.00 | 0.00 | 0.00 | 0.00 | 0.00 | 0.00 |
| $MnO$ | 0.15 | 0.16 | 0.10 | 0.10 | 0.14 | 0.14 | 0.17 | 0.06 | 0.14 |
| $MgO$ | 13.37 | 13.32 | 14.86 | 14.96 | 13.64 | 15.01 | 14.60 | 13.38 | 13.85 |
| $CaO$ | 0.04 | 0.09 | 0.05 | 0.11 | 0.18 | 0.03 | 0.05 | 0.12 | 0.04 |
| $Na_2O$ | 0.52 | 0.61 | 0.46 | 0.38 | 0.60 | 0.44 | 0.34 | 0.75 | 0.72 |
| $K_2O$ | 8.68 | 8.56 | 8.71 | 8.64 | 8.67 | 8.51 | 8.43 | 8.47 | 8.35 |
| $BaO$ | 1.91 | 1.52 | 2.00 | 0.98 | 1.18 | 1.49 | 1.40 | 1.39 | 1.75 |
| $Cl$ | 0.01 | 0.00 | 0.00 | 0.02 | 0.03 | 0.00 | 0.01 | 0.02 | 0.01 |
| $H_2O$ | 3.93 | 3.94 | 4.02 | 3.98 | 3.99 | 3.94 | 3.97 | 3.95 | 4.01 |
| *Total* | 98.89 | 98.83 | 99.93 | 98.63 | 101.05 | 98.04 | 98.96 | 98.79 | 100.78 |
| **Fórmula estrutural baseada em 22 oxigênios** | | | | | | | | | |
| **Si** | 5.23 | 5.17 | 5.13 | 5.33 | 5.12 | 5.13 | 5.24 | 5.19 | 5.21 |
| **$Al^{IV}$** | 2.72 | 2.79 | 2.74 | 2.62 | 2.70 | 2.75 | 2.76 | 2.74 | 2.74 |
| **$Fe^{+3}$** | 0.05 | 0.05 | 0.14 | 0.05 | 0.18 | 0.12 | 0.00 | 0.08 | 0.04 |
| **Sum T** | **8.00** | **8.00** | **8.00** | **8.00** | **8.00** | **8.00** | **8.00** | **8.00** | **8.00** |
| **$Al^{VI}$** | 0.00 | 0.00 | 0.00 | 0.00 | 0.00 | 0.00 | 0.04 | 0.00 | 0.00 |
| **$Fe^{+2}_t$** | 1.67 | 1.68 | 1.38 | 1.50 | 1.73 | 1.37 | 1.69 | 1.60 | 1.77 |
| **$Fe^{+3}$** | 3.03 | 3.02 | 3.32 | 3.35 | 3.04 | 3.40 | 3.28 | 3.02 | 3.08 |
| **Ti** | 0.02 | 0.02 | 0.01 | 0.01 | 0.02 | 0.02 | 0.02 | 0.01 | 0.02 |
| **Mg** | 0.83 | 0.85 | 0.89 | 0.77 | 0.87 | 0.86 | 0.68 | 0.89 | 0.77 |
| **Mn** | 0.00 | 0.00 | 0.00 | 0.00 | 0.00 | 0.00 | 0.00 | 0.00 | 0.00 |
| **Sum O** | **5.55** | **5.57** | **5.60** | **5.63** | **5.65** | **5.65** | **5.72** | **5.52** | **5.64** |
| **Ca** | 0.01 | 0.01 | 0.01 | 0.02 | 0.03 | 0.00 | 0.01 | 0.02 | 0.01 |
| **Na** | 0.15 | 0.18 | 0.13 | 0.11 | 0.17 | 0.13 | 0.10 | 0.22 | 0.21 |
| **K** | 0.84 | 0.83 | 0.83 | 0.83 | 0.83 | 0.82 | 0.81 | 0.82 | 0.79 |
| **Ba** | 0.23 | 0.18 | 0.23 | 0.12 | 0.14 | 0.18 | 0.17 | 0.17 | 0.20 |
| **Sum A** | **1.23** | **1.20** | **1.21** | **1.07** | **1.16** | **1.14** | **1.08** | **1.22** | **1.21** |
| ***Cations*** | **14.78** | **14.77** | **14.80** | **14.70** | **14.82** | **14.79** | **14.81** | **14.74** | **14.85** |
| ***$Mg/(Mg+Fe^{+2})$*** | 0.64 | 0.64 | 0.71 | 0.69 | 0.64 | 0.71 | 0.66 | 0.65 | 0.63 |
| ***$Fe^{+2}/(Fe^{+2}+Mg)$*** | 0.36 | 0.36 | 0.29 | 0.31 | 0.36 | 0.29 | 0.34 | 0.35 | 0.37 |

*Obs: $H_2O$ recalculated by stequiometrie. $Fe_2O_3$ only recalculated for samples with deficiency in tetraedric site.*

**ANEXO:** Análises de microsonda de cristais de biotita em ocelli e segregados (amostras BYA123 e BYA127), lamprofiros de R. Grande

| | 1 | 2 | 3 | 3 | 3 | 6 |
|---|---|---|---|---|---|---|
| *Amostra* | BYA123.3D.BTOCEL.417 | BYA127.2.BTGLO.527 | BYA127.4.BTCOREGLO.577 | BYA127.4.BTRIMGLO.578 | BYA127.7.BTCARBO.591 | BYA127.6A.COREOLV.546 |
| $SiO_2$ | 34.67 | 34.62 | 36.96 | 37.19 | 33.61 | 39.48 |
| $TiO_2$ | 5.76 | 5.57 | 3.68 | 2.58 | 5.59 | 0.50 |
| $Al_2O_3$ | 15.52 | 8.71 | 10.11 | 10.78 | 14.51 | 11.79 |
| *FeO* | 13.37 | 32.04 | 26.65 | 22.72 | 14.36 | 13.33 |
| $Fe_2O_3$ | 0.00 | 0.00 | 0.00 | 0.00 | 0.00 | 0.00 |
| $Cr_2O_3$ | 0.00 | 0.00 | 0.00 | 0.00 | 0.00 | 0.00 |
| *MnO* | 0.11 | 0.52 | 0.43 | 0.50 | 0.25 | 0.33 |
| *MgO* | 15.63 | 4.46 | 9.37 | 12.38 | 14.14 | 20.21 |
| *CaO* | 0.08 | 0.24 | 0.21 | 0.47 | 0.29 | 0.04 |
| $Na_2O$ | 0.35 | 0.00 | 0.00 | 0.00 | 0.27 | 0.81 |
| $K_2O$ | 9.22 | 9.03 | 9.49 | 9.59 | 9.10 | 8.56 |
| *BaO* | 0.43 | 0.00 | 0.00 | 0.00 | 2.08 | 0.20 |
| *Cl* | 0.02 | 0.00 | 0.02 | 0.01 | 0.01 | 0.01 |
| $H_2O$ | 3.98 | 3.61 | 3.81 | 3.85 | 3.85 | 4.04 |
| *Total* | 99.12 | 98.81 | 100.72 | 100.06 | 98.04 | 99.29 |
| | | | | | | |
| **Fórmula estrutural baseada em 22 oxigênios** | | | | | | |
| **Si** | 5.21 | 5.73 | 5.80 | 5.77 | 5.22 | 5.85 |
| **$Al^{IV}$** | 2.75 | 1.70 | 1.87 | 1.97 | 2.65 | 2.06 |
| **$Fe^{+3}$** | 0.05 | 0.57 | 0.33 | 0.26 | 0.13 | 0.09 |
| **Sum T** | **8.00** | **8.00** | **8.00** | **8.00** | **8.00** | **8.00** |
| **$Al^{VI}$** | 0.00 | 0.00 | 0.00 | 0.00 | 0.00 | 0.00 |
| **$Fe^{+2}_t$** | 1.63 | 3.86 | 3.16 | 2.69 | 1.73 | 1.56 |
| **$Fe^{+3}$** | 3.50 | 1.10 | 2.19 | 2.86 | 3.27 | 4.46 |
| **Ti** | 0.01 | 0.07 | 0.06 | 0.07 | 0.03 | 0.04 |
| **Mg** | 0.65 | 0.69 | 0.43 | 0.30 | 0.65 | 0.06 |
| **Mn** | 0.00 | 0.00 | 0.00 | 0.00 | 0.00 | 0.00 |
| **Sum O** | **5.80** | **5.73** | **5.85** | **5.92** | **5.69** | **6.12** |
| **Ca** | 0.01 | 0.04 | 0.04 | 0.08 | 0.05 | 0.01 |
| **Na** | 0.10 | 0.00 | 0.00 | 0.00 | 0.08 | 0.23 |
| **K** | 0.88 | 0.95 | 0.95 | 0.95 | 0.90 | 0.81 |
| **Ba** | 0.05 | 0.00 | 0.00 | 0.00 | 0.25 | 0.02 |
| **Sum A** | **1.05** | **1.00** | **0.98** | **1.03** | **1.28** | **1.07** |
| ***Cations*** | **14.84** | **14.73** | **14.83** | **14.94** | **14.97** | **15.19** |
| | | | | | | |
| ***$Mg/(Mg+Fe^{+2})$*** | 0.68 | 0.22 | 0.41 | 0.52 | 0.65 | 0.74 |
| ***$Fe^{+2}/(Fe^{+2}+Mg)$*** | 0.32 | 0.78 | 0.59 | 0.48 | 0.35 | 0.26 |

*Obs: $H_2O$ recalculated by stequiometrie. $Fe_2O_3$ only recalculated for samples with deficiency in tetraedric site.*

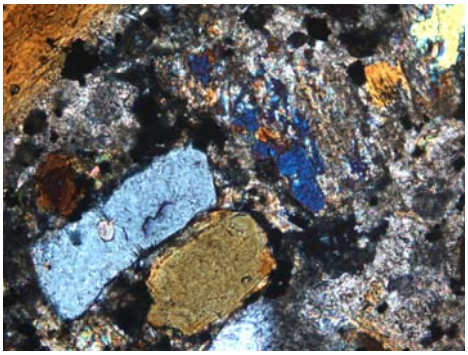

APATITA

**ANEXO:** Análises de microsonda de cristais de apatita, lamprofiros de Río Grande

| | *Fenocristal* | *em fenocristal de augite* | |
|---|---|---|---|
| | *1* | 2 | 3 |
| $SiO_2$ | 0.00 | 0.13 | 0.12 |
| $Al_2O_3$ | 0.00 | 0.00 | 0.01 |
| *MgO* | 0.14 | 0.38 | 0.34 |
| $Fe_2O_3$ | 0.34 | 0.34 | 0.32 |
| *CaO* | 53.31 | 53.83 | 54.50 |
| $Na_2O$ | 0.35 | 0.06 | 0.12 |
| $K_2O$ | 0.00 | 0.01 | 0.03 |
| $P_2O_5$ | 41.67 | 40.14 | 40.51 |
| *Cl* | 0.24 | 0.13 | 0.11 |
| *SrO* | 1.08 | 0.43 | 0.31 |
| *BaO* | 0.01 | 0.00 | 0.00 |
| $H_2O_3$ | 1.70 | 1.69 | 1.72 |
| *Total* | 98.83 | 97.14 | 98.07 |
| | | | |
| **Cations por fórmula unidad** | | | |
| Na | 0.12 | 0.02 | 0.04 |
| Si | 0.00 | 0.02 | 0.02 |
| Al | 0.00 | 0.00 | 0.00 |
| Mg | 0.04 | 0.10 | 0.09 |
| K | 0.00 | 0.00 | 0.01 |
| P | 6.02 | 5.90 | 5.90 |
| Ca | 9.74 | 10.02 | 10.04 |
| Cl | -0.05 | -0.03 | -0.02 |
| Sr | 0.11 | 0.04 | 0.03 |
| Fe | 0.05 | 0.05 | 0.05 |
| Ba | 0.00 | 0.00 | 0.00 |
| H | 0.56 | 0.57 | 0.57 |
| ***Cations*** | 16.57 | 16.69 | 16.71 |

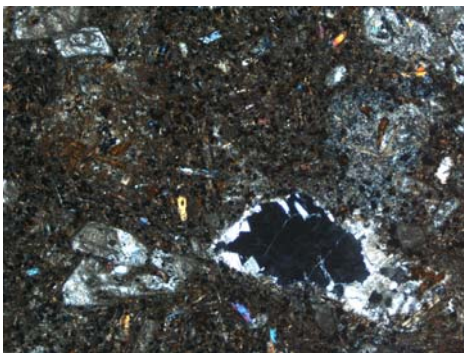

ANALCIMA

**ANEXO:** Análises de microsonda de cristais de analcima, lamprofiros de Río Grande

| | *Borda de anfibólio* | *em Ocelli* | | | | | | | *em segragdos ricos em biotita* | *Microfenocristais* | | |
|---|---|---|---|---|---|---|---|---|---|---|---|---|
| | 1 | 2 | 3 | 4 | 5 | 6 | 7 | 8 | 9 | 10 | 11 | 12 |
| $SiO_2$ | 55.51 | 57.23 | 53.20 | 55.76 | 52.18 | 54.66 | 59.20 | 61.92 | 58.02 | 62.77 | 50.61 | 52.08 |
| $Al_2O_3$ | 24.57 | 24.63 | 23.73 | 21.17 | 24.92 | 25.46 | 24.85 | 22.71 | 24.91 | 22.47 | 22.72 | 23.19 |
| *FeO* | 0.14 | 0.01 | 0.07 | 0.09 | 0.63 | 0.51 | 0.13 | 0.18 | 0.16 | 0.26 | 0.04 | 1.23 |
| *CaO* | 0.16 | 0.00 | 0.30 | 0.11 | 0.63 | 0.69 | 0.05 | 0.01 | 0.13 | 0.08 | 0.29 | 0.32 |
| $Na_2O$ | 12.94 | 13.26 | 12.93 | 13.96 | 10.92 | 10.46 | 13.58 | 12.18 | 12.24 | 10.91 | 11.46 | 11.85 |
| $K_2O$ | 0.12 | 0.04 | 0.25 | 0.12 | 0.34 | 0.20 | 0.08 | 0.08 | 0.05 | 0.09 | 0.27 | 0.55 |
| *Total* | 93.43 | 95.28 | 90.49 | 91.30 | 89.62 | 91.99 | 97.90 | 97.08 | 95.50 | 96.69 | 85.42 | 89.23 |
| **Cations recalculados em base a 7 oxigênios** | | | | | | | | | | | | |
| **Si** | 2.20 | 2.39 | 2.23 | 2.33 | 2.18 | 2.29 | 2.48 | 2.59 | 2.43 | 2.63 | 2.12 | 2.18 |
| **Al** | 1.15 | 1.21 | 1.17 | 1.04 | 1.23 | 1.26 | 1.22 | 1.12 | 1.23 | 1.11 | 1.12 | 1.14 |
| **Sum T** | **3.35** | **3.61** | **3.39** | **3.38** | **3.41** | **3.54** | **3.70** | **3.71** | **3.65** | **3.73** | **3.24** | **3.32** |
| $\mathbf{Fe^{+2}_t}$ | 0.00 | 0.00 | 0.00 | 0.00 | 0.02 | 0.02 | 0.00 | 0.01 | 0.01 | 0.01 | 0.00 | 0.04 |
| **Ca** | 0.01 | 0.00 | 0.01 | 0.01 | 0.03 | 0.03 | 0.00 | 0.00 | 0.01 | 0.00 | 0.01 | 0.01 |
| **Na** | 1.00 | 1.08 | 1.05 | 1.13 | 0.89 | 0.85 | 1.10 | 0.99 | 0.99 | 0.88 | 0.93 | 0.96 |
| **K** | 0.01 | 0.00 | 0.01 | 0.01 | 0.02 | 0.01 | 0.00 | 0.00 | 0.00 | 0.00 | 0.01 | 0.03 |
| **Sum A** | **1.01** | **1.08** | **1.08** | **1.15** | **0.95** | **0.91** | **1.11** | **1.00** | **1.01** | **0.90** | **0.96** | **1.05** |
| ***Cations*** | *4.36* | *4.69* | *4.47* | *4.52* | *4.37* | *4.45* | *4.81* | *4.71* | *4.66* | *4.64* | *4.20* | *4.37* |

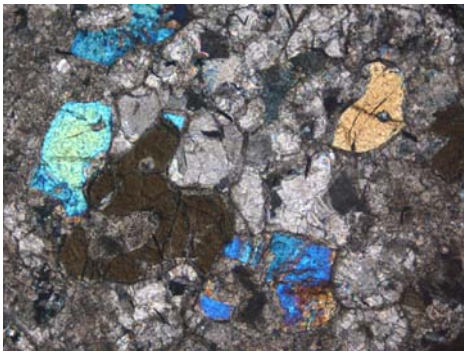

CARBONATO

**ANEXO:** Análises de microsonda de cristais de carbonato da amostra P8, lamprofiros de Río Grande

| | *Em Ocelli tipo-I* | | | | | | | | *Segregados* | *Matriz* | | | | | *Carbonato do xenolito* | | *Borda de anfibólio* |
|---|---|---|---|---|---|---|---|---|---|---|---|---|---|---|---|---|---|
| | *1* | *2* | *3* | *4* | *5* | *6* | *7* | | | 1 | 2 | 3 | 4 | 5 | 6 | 7 | |
| $FeCO_3$ | 12.70 | 9.69 | 7.08 | 12.12 | 8.62 | 15.77 | 17.70 | 15.87 | 45.15 | 13.02 | 16.01 | 14.05 | 12.85 | 14.68 | 11.77 | 9.21 | 9.84 |
| $MnCO_3$ | 0.56 | 0.68 | 0.75 | 0.57 | 1.12 | 0.91 | 0.96 | 1.16 | 0.13 | 1.09 | 1.36 | 1.10 | 0.73 | 1.82 | 0.22 | 0.37 | 0.80 |
| $MgCO_3$ | 30.73 | 34.43 | 33.91 | 33.86 | 30.92 | 30.07 | 28.63 | 30.19 | 51.40 | 28.35 | 26.32 | 30.73 | 33.19 | 28.74 | 29.77 | 35.41 | 35.26 |
| $CaCO_3$ | 51.20 | 52.15 | 55.63 | 52.19 | 57.30 | 50.81 | 50.39 | 51.67 | 2.07 | 54.75 | 52.64 | 51.35 | 51.11 | 51.77 | 53.32 | 51.89 | 51.58 |
| $Sr_2CO_3$ | 2.06 | 0.80 | 0.45 | 0.15 | 0.04 | 0.45 | 0.47 | 0.62 | 0.02 | 0.96 | 0.71 | 0.48 | 0.39 | 1.13 | 3.09 | 2.50 | 0.33 |
| $BaCO_3$ | 0.00 | 0.00 | 0.18 | 0.00 | 0.00 | 0.00 | 0.00 | 0.00 | 0.05 | 0.00 | 0.00 | 0.00 | 0.00 | 0.05 | 0.22 | 0.07 | 0.02 |
| *TOTAL* | 98.57 | 99.10 | 99.34 | 100.25 | 99.35 | 99.35 | 99.47 | 100.88 | 100.16 | 99.50 | 98.35 | 99.05 | 99.61 | 99.52 | 99.72 | 100.80 | 99.18 |
| | | | | | | | | | | | | | | | | | |
| Ca | 1.02 | 1.02 | 1.08 | 0.95 | 1.07 | 1.00 | 1.00 | 1.01 | 0.04 | 1.05 | 1.05 | 0.52 | 1.00 | 1.03 | 1.05 | 1.00 | 0.97 |
| Mg | 0.73 | 0.80 | 0.78 | 0.73 | 0.68 | 0.71 | 0.67 | 0.70 | 1.09 | 0.65 | 0.63 | 0.37 | 0.77 | 0.68 | 0.70 | 0.81 | 0.79 |
| Fe | 0.22 | 0.16 | 0.12 | 0.19 | 0.14 | 0.27 | 0.30 | 0.27 | 0.70 | 0.22 | 0.28 | 0.12 | 0.22 | 0.25 | 0.20 | 0.15 | 0.16 |
| Ba | 0.00 | 0.00 | 0.00 | 0.00 | 0.00 | 0.00 | 0.00 | 0.00 | 0.00 | 0.00 | 0.00 | 0.00 | 0.00 | 0.00 | 0.00 | 0.00 | 0.00 |
| Sr | 0.03 | 0.01 | 0.01 | 0.00 | 0.00 | 0.01 | 0.01 | 0.01 | 0.00 | 0.01 | 0.01 | 0.00 | 0.01 | 0.02 | 0.04 | 0.03 | 0.00 |
| Mn | 0.01 | 0.01 | 0.01 | 0.01 | 0.02 | 0.02 | 0.02 | 0.02 | 0.00 | 0.02 | 0.02 | 0.01 | 0.01 | 0.03 | 0.00 | 0.01 | 0.01 |
| ***Cations*** | 2.00 | 2.00 | 2.00 | 2.00 | 2.00 | 2.00 | 2.00 | 2.00 | 2.00 | 2.00 | 2.00 | 2.00 | 2.00 | 2.00 | 2.00 | 2.00 | 2.00 |

# ANEXO III:
## COORDENADAS AMOSTRAS

| Amostras | *Coordenadas geográficas* | | | | |
|---|---|---|---|---|---|
| **Dacitos de El Niño Muerto** | | | | | |
| BNM-08 | 23 44 16.43 | S | 66 10 39.34 | W | |
| BNM-09 | 23 44 16.43 | S | 66 10 39.34 | W | |
| BNM-10 | 23 44 16.43 | S | 66 10 39.34 | W | |
| BNM-11 | 23 44 16.48 | S | 66 12 59.10 | W | |
| BNM-12 | 23 44 16.48 | S | 66 12 59.10 | W | |
| BNM-13 | 23 44 16.48 | S | 66 12 57.79 | W | |
| BNM-14 | 23 44 16.48 | S | 66 12 57.79 | W | |
| BNM-15 | 23 44 49.87 | S | 66 13 18.71 | W | |
| BNM-16 | 23 44 56.89 | S | 66 13 17.74 | W | |
| BNM-17 | 23 50 02.47 | S | 66 15 14.05 | W | |
| BNM-18 | 24 14 32.06 | S | 66 20 09.52 | W | |
| **Basaltos de Río Blanco** | | | | | |
| BRB-19 | 25 48 41.79 | S | 65 41 19.42 | W | |
| BRB-20 | 26 01 22.28 | S | 65 49 41.24 | W | |
| BRB-21 | 24 57 30.11 | S | 65 49 46.88 | W | |
| BRB-22 | 24 57 30.11 | S | 65 49 46.88 | W | |
| BRB-23 | 24 57 23.03 | S | 65 57 47.79 | W | |
| BRB-24 | 24 57 24.98 | S | 65 57 30.75 | W | |
| BRB-25 | 24 57 24.98 | S | 65 57 30.75 | W | |
| BRB-26 | 24 57 26.76 | S | 65 57 29.14 | W | |
| BRB-27 | 24 57 30.37 | S | 65 57 29.60 | W | |
| BRB-28 | 24 57 30.37 | S | 65 57 29.60 | W | |
| BRB-29 | 24 57 33.20 | S | 65 57 30.67 | W | |
| BRB-30 | 24 57 33.20 | S | 65 57 30.67 | W | |
| BRB-31 | 24 57 24.62 | S | 65 57 33.71 | W | |
| BRB-32 | 24 57 27.02 | S | 65 57 29.32 | W | |
| BRB-33A | 24 57 27.02 | S | 65 57 29.32 | W | |
| BRB-33B | 24 57 27.02 | S | 65 57 29.32 | W | |
| BRB-34 | 24 57 36.77 | S | 65 57 28.14 | W | |
| BRB-35 | 24 57 46.79 | S | 65 57 35.62 | W | |
| BRB-36 | 24 57 50.49 | S | 65 57 36.59 | W | |
| BRB-37 | 24 57 52.99 | S | 65 57 33.77 | W | |
| BRB-38 | 24 57 51.79 | S | 65 57 31.91 | W | |
| BRB-39 | 24 57 51.79 | S | 65 57 31.91 | W | |
| BRB-40 | 24 57 51.79 | S | 65 57 31.91 | W | |
| BRB-41 | 24 57 30.34 | S | 65 57 29.39 | W | |
| BRB-42 | 24 57 30.34 | S | 65 57 29.39 | W | |
| BRB-43 | 24 57 26.76 | S | 65 57 29.14 | W | |
| BRB-44 | 25 08 18.40 | S | 66 10 05.00 | W | |
| BRB-45 | 25 08 18.40 | S | 66 10 05.00 | W | |
| BRB-46 | 25 08 18.40 | S | 66 10 05.00 | W | |
| BRB-47 | 25 19 23.19 | S | 66 14 08.12 | W | |

| Amostras | *Coordenadas geográficas* | | | | |
|---|---|---|---|---|---|
| BRB-47B | 25 19 23.19 | S | 66 14 08.12 | W | |
| BRB-64 | 24 57 20.51 | S | 65 58 45.50 | W | |
| BRB-65 | 24 57 20.51 | S | 65 58 45.50 | W | |
| BRB-66 | 24 57 20.51 | S | 65 58 45.50 | W | |
| BRB-67 | 24 57 18.29 | S | 65 40 59.74 | W | |
| BRB-68 | 24 57 13.76 | S | 66 05 04.23 | W | |
| **Lamprofiros de Coraya** | | | | | |
| BCOY-49A | 23 10 03.74 | S | 65 26 29.89 | W | |
| BCOY-49B | 23 10 03.74 | S | 65 26 29.89 | W | |
| BCOY-50 | 23 10 03.74 | S | 65 26 29.89 | W | |
| BCOY-51A | 23 10 05.96 | S | 65 26 32.24 | W | |
| BCOY-51B | 23 10 05.96 | S | 65 26 32.24 | W | |
| BCOY-52 | 23 10 09.58 | S | 65 26 34.40 | W | |
| BCOY-53 | 23 10 13.91 | S | 65 26 37.02 | W | |
| BCOY-54 | 23 10 13.98 | S | 65 26 55.94 | W | |
| BCOY-55 | 23 10 13.98 | S | 65 26 55.94 | W | |
| **Lamprofiros do Vale de Yacoraite** | | | | | |
| BYA-121A | 23 20 13.3 | S | 65 25 43.4 | W | |
| BYA-121B | 23 20 13.0 | S | 65 25 43.4 | W | |
| BYA-122 | 23 20 13.3 | S | 65 25 43.4 | W | |
| BYA-123 | 23 20 13.3 | S | 65 25 43.4 | W | |
| BYA-124A | 23 20 13.3 | S | 65 25 43.4 | W | |
| BYA-124B | 23 20 13.3 | S | 65 25 43.4 | W | |
| BYA-125 | 23 19 58.8 | S | 65 26 12.5 | W | |
| BYA-126 | 23 19 58.8 | S | 65 26 12.5 | W | |
| BYA-127 | 23 19 55.8 | S | 65 26 36.1 | W | |
| BYA-128 | 23 19 55.8 | S | 65 26 36.1 | W | |
| **Lamprofiros do Vale de Huichaira** | | | | | |
| BHUI-131 | 23 33 51.1 | S | 65 27 32.8 | W | |
| BHUI-132 | 23 33 51.1 | S | 65 27 32.8 | W | |